Springer Theses
Recognizing Outstanding Ph.D. Research

Matthew J. Simpson

Two Studies in Gas-Phase Ion Spectroscopy

Vacuum-Ultraviolet Negative Photoion Spectroscopy and Ion-Molecule Reaction Kinetics

Springer

Springer Theses

Recognizing Outstanding Ph.D. Research

For further volumes:
http://www.springer.com/series/8790

Aims and Scope

The series "Springer Theses" brings together a selection of the very best Ph.D. theses from around the world and across the physical sciences. Nominated and endorsed by two recognized specialists, each published volume has been selected for its scientific excellence and the high impact of its contents for the pertinent field of research. For greater accessibility to non-specialists, the published versions include an extended introduction, as well as a foreword by the student's supervisor explaining the special relevance of the work for the field. As a whole, the series will provide a valuable resource both for newcomers to the research fields described, and for other scientists seeking detailed background information on special questions. Finally, it provides an accredited documentation of the valuable contributions made by today's younger generation of scientists.

Theses are accepted into the series by invited nomination only and must fulfill all of the following criteria

- They must be written in good English.
- The topic should fall within the confines of Chemistry, Physics and related interdisciplinary fields such as Materials, Nanoscience, Chemical Engineering, Complex Systems and Biophysics.
- The work reported in the thesis must represent a significant scientific advance.
- If the thesis includes previously published material, permission to reproduce this must be gained from the respective copyright holder.
- They must have been examined and passed during the 12 months prior to nomination.
- Each thesis should include a foreword by the supervisor outlining the significance of its content.
- The theses should have a clearly defined structure including an introduction accessible to scientists not expert in that particular field.

Matthew J. Simpson

Two Studies in Gas-Phase Ion Spectroscopy

Vacuum-Ultraviolet Negative Photoion Spectroscopy and Ion-Molecule Reaction Kinetics

Doctoral Thesis accepted by
University of Birmingham, UK

Springer

Author
Dr. Matthew J. Simpson
Science Department
King Edward's High School for Girls
Birmingham
B15 2UB
UK
e-mail: m.j.simpson@live.com

Supervisor
Prof. Dr. Richard P. Tuckett
School of Chemistry
University of Birmingham
Edgbaston, Birmingham
B15 2TT
UK
e-mail: r.p.tuckett@bham.ac.uk

ISSN 2190-5053
ISBN 978-3-642-23128-5
DOI 10.1007/978-3-642-23129-2
Springer Heidelberg Dordrecht London New York

e-ISSN 2190-5061
e-ISBN 978-3-642-23129-2

Library of Congress Control Number: 2011937631

Printed on acid-free paper

Springer is part of Springer Science+Business Media (www.springer.com)

Parts of this thesis have been published in the following journal articles

[1] M.J. Simpson and R.P. Tuckett, *Vacuum-UV negative photoion spectroscopy of polyatomic molecules*, *International Reviews of Physical Chemistry* **30**, 197–273 (2011). *Reproduced with permission.

[2] M.J. Simpson and R.P. Tuckett, *Vacuum-UV negative photoion spectroscopy of SF_5Cl*, *Journal of Physical Chemistry A* **114**, 8043–8048 (2010). *Reproduced with permission.

[3] M.J. Simpson, R.P. Tuckett, K.F. Dunn, C.A. Hunniford, and C.J. Latimer, *Vacuum-UV negative photoion spectroscopy of CF_3Cl, CF_3Br and CF_3I*, *Journal of Chemical Physics* **130**, 194302,1–194302,11 (2009). *Reproduced with permission.

[4] M.J. Simpson, R.P. Tuckett, K.F. Dunn, C.A. Hunniford, C.J. Latimer, and S.W.J. Scully, *Vacuum-UV negative photoion spectroscopy of SF_5CF_3*, *Journal of Chemical Physics* **128**, 124315,1–124315,10 (2008). *Reproduced with permission.

[5] N.J. Rogers, M.J. Simpson, R.P. Tuckett, K.F. Dunn, and C.J. Latimer, *Vacuum-UV negative photoion spectroscopy of CH_4*, *Molecular Physics* **108**, 895–904 (2010). *Reproduced with permission.

[6] N.J. Rogers, M.J. Simpson, R.P. Tuckett, K.F. Dunn, and C.J. Latimer, *Vacuum-UV negative photoion spectroscopy of CH_3F, CH_3Cl and CH_3Br*, *Physical Chemistry Chemical Physics* **12**, 10971–10980 (2010). *Reproduced with permission.

[7] M.A. Parkes, S. Ali, M.J. Simpson, R.P. Tuckett, and A.E.R. Malins, *Threshold photoelectron photoion coincidence spectroscopy of trichloroethene and tetrachloroethene: the effect of Cl substitution in the series $C_2H_xCl_{4-x}$*, *Molecular Physics* **106**, 1739–1749 (2008). *Reproduced with permission.

[8] V.A. Mikhailov, M.A. Parkes, M.J. Simpson, R.P. Tuckett, and C.A. Mayhew, *Selected ion flow tube ion-molecule reactions of monochloroethene, trichloroethene and tetrachloroethene: comparison with TPEPICO data*, *Journal of Physical Chemistry A* **112**, 9012–9022 (2008). *Reproduced with permission.

I was the principal author of [2–4], made major contributions to [1, 5] and [6], and minor contributions to [7] and [8]. The data of Chaps. 7–9 of this Springer Thesis have yet to be published.

Since my thesis was examined and submitted to the University of Birmingham in November 2010, the review article, reference [1], was submitted and subsequently published in the *International Reviews of Physical Chemistry* in June 2011. Parts of chapter 1.A of this Springer Thesis have therefore been modified, and in addition Table 4.2 and Appendix III are greatly expanded from their version in my original Ph.D. thesis. I am grateful to my supervisor, Professor Richard Tuckett, for his major contribution to these modifications.

Supervisor's Foreword

The research described in Matthew Simpson's Ph.D. Thesis involves two aspects of the spectroscopy and reaction kinetics of gas-phase ions. First, the observation and analysis of negative ions following vacuum-ultraviolet excitation of polyatomic molecules using tunable radiation from a synchrotron source. Second, the determination of rate coefficients and branching ratios of either cations or anions reacting with polyatomic molecules in a Selected Ion Flow Tube at 298 K. This thesis will lead to *ca.* ten papers plus one review in the international peer-reviewed literature.

Using tunable vacuum-ultraviolet radiation from a synchrotron, negative ions have been detected following photoexcitation of 24 gaseous molecules. The molecules studied were CF_4, SF_6 and CH_4; the CF_3X series where X = Cl, Br, I; the CH_3Y series where Y = F, Cl, Br; and SF_5Z where Z = CF_3, Cl. Spectra and raw data only are reported for other members of the CH_xF_y, CH_xCl_y including CCl_4, and CF_xCl_y series where $(x+y) = 4$; and saturated and unsaturated members of the C_mH_n and C_mF_n series up to $m = 3$. Product anions resulting from unimolecular ion-pair dissociation reactions were detected, and their ion yields recorded in the range 8–35 eV at a resolution down to 0.02 eV. Absolute cross sections for ion-pair formation and resulting quantum yields were calculated. This vast collection of data is summarised and ion-pair formation from polyatomic molecules is reviewed.

Selected Ion Flow Tube mass spectrometry has been used to study the reactions of cations and anions with ethene, monofluoroethene, 1,1-difluoroethene, trifluoroethene and tetrafluoroethene. Calculated collisional reaction rate coefficients are compared to those measured by the experiment. The product ions from these reactions have been detected and their branching ratios measured. Many of these results have been explained with arrow-pushing mechanisms which are used by organic chemists. Perhaps more than many papers and reviews on ion-molecule reactions, this work tries to explain *why* certain products are formed preferentially over other products at a microscopic level of understanding.

The work reported in this Thesis will be of primary relevance to those involved in experimental studies of the spectroscopy and kinetics of gas-phase ions,

especially those working in the under-studied area of *negative anions*. The data reported in Chap. 6 forms the most comprehensive set of vacuum-ultraviolet excitation spectra forming anions in the scientific literature to date.

Birmingham, September 2011 Prof. Richard P. Tuckett

Acknowledgments

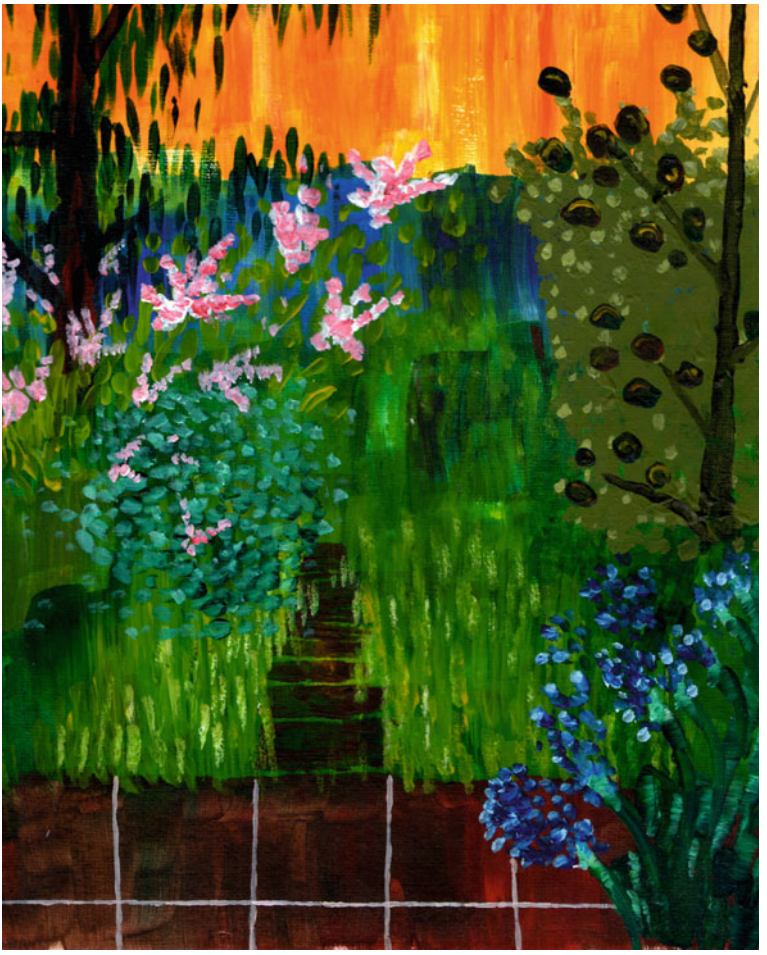

The Garden at 21 King Edward

Thank you for all your help to: Sahangir Ali, Liam Cox, Ken Dunn, Jonelle Harvey, David Holland, Adam Hunniford, Colin Latimer, Chris Mayhew, Victor Mikhailov, Mike Parkes, Nicola Rogers, David Shaw and Richard Tuckett.

Contents

Chapter 1
Introduction and Background Information

1.1 Ion-Pair Formation

The first part of this thesis reports and discusses results collected from an experiment designed to investigate the formation of ion pairs following the vacuum ultraviolet photoexcitation of a gas-phase molecule. The experiment is described in Chap. 2, and the results are discussed in Chaps. 3–6 and Appendix II. The majority of this work has been published including a review [1–4]. Two other papers, for which I am *not* the lead author, have also been published in the primary literature [5, 6].

The production of an anion–cation pair of fragments following unimolecular dissociation of an isolated gas-phase molecule is often called 'ion-pair formation'. For a diatomic molecule, AB, this reaction can generally be described as:

$$AB + h\nu \rightarrow A^- + B^+ \tag{1.1}$$

For a polyatomic molecule, ABC, the ion-pair reaction may also produce neutral fragments,

$$ABC + h\nu \rightarrow A^- + BC^+ \tag{1.2}$$

or

$$ABC + h\nu \rightarrow A^- + B^+ + C \tag{1.3}$$

This thesis is concerned exclusively with polyatomic molecules, so from henceforth we will use reactions (1.2) or (1.3) to describe a generic ion-pair reaction. In these studies, it is usually the anion, A^-, that is detected as a function of the photon energy. Anions formed in this way can either form *directly* or *indirectly*. An anion–cation pair may be formed by direct excitation to the ion-pair state, or indirectly via predissociation of an initially-excited neutral state of ABC. Indirect formation is by far the more common mechanism, the excited neutral states are nearly always Rydberg in character, and so our experiments relate

M. J. Simpson, *Two Studies in Gas-Phase Ion Spectroscopy*, Springer Theses,
DOI: 10.1007/978-3-642-23129-2_1, © Springer-Verlag Berlin Heidelberg 2012

closely to the vacuum-UV absorption spectroscopy of Rydberg states of polyatomic molecules.

A^- can also be produced above the ionisation energy of the parent molecule by the alternative mechanism of dissociative electron attachment:

$$ABC + h\nu \rightarrow ABC^+ + e^-$$

$$\text{followed by } ABC + e^- \rightarrow A^- + BC \textit{ or } A^- + B + C \qquad (1.4)$$

A more accurate description of this type of study is therefore 'negative photoion spectroscopy', and one should regard ion-pair formation in a polyatomic molecule (1.2) or (1.3), as a special case of negative photoion spectroscopy in which a cation is produced simultaneously. Furthermore, with ion-pair formation the signal of A^- increases *linearly* with the concentration or pressure of ABC, as only one molecule of parent is needed to produce one anion. By contrast, if A^- is produced by dissociative electron attachment (1.4), then the A^- signal should increase *quadratically* with the concentration of ABC since two molecules of ABC are needed to produce one anion; at the very least, the rate of change of A^- signal will increase as the concentration of parent molecule increases. Whilst the formation of A^- by reaction (1.4) is also a multi-step indirect process, we will always describe this method of anion production as two-step dissociative electron attachment. This will avoid confusion with the indirect ion-pair reaction described above for production of an anion–cation pair by predissociation of a Rydberg state of ABC.

Typically, these unimolecular reactions are endothermic by between 8 and 25 eV, ca. 150 nm, with this energy increasing as the extent of fragmentation of the polyatomic molecule increases. Therefore, a photon in the vacuum-ultraviolet (VUV) region of the electromagnetic spectrum must be absorbed by the molecule (Fig. 1.1), and it is no surprise that the majority of negative photoion studies of polyatomic molecules use tunable VUV radiation from a synchrotron as the source of electromagnetic radiation. For spectroscopic studies, the relatively poor resolution of such sources, compared to other sources such as VUV lasers, is more than compensated by the ease which the photon energy can be tuned. For dynamical studies, radiation from a synchrotron can operate either as a source of linearly- *or* circularly-polarised radiation, but such properties have received little attention to date in negative photoion or ion-pair studies.

For reaction (1.2), the appearance energy of the anion, $AE(A^-)$ is constrained to the energetic relationship:

$$AE(A^-) \geq D^o(A - BC) + IE(BC) - EA(A) \qquad (1.5)$$

where D^o is a dissociation energy, IE an ionisation energy and EA an electron affinity. If experiments are performed at 298 K, then we can write:

$$AE_{298}(A^-) \geq D^o_{298}(A - BC) + IE(BC) - EA(A) \qquad (1.6)$$

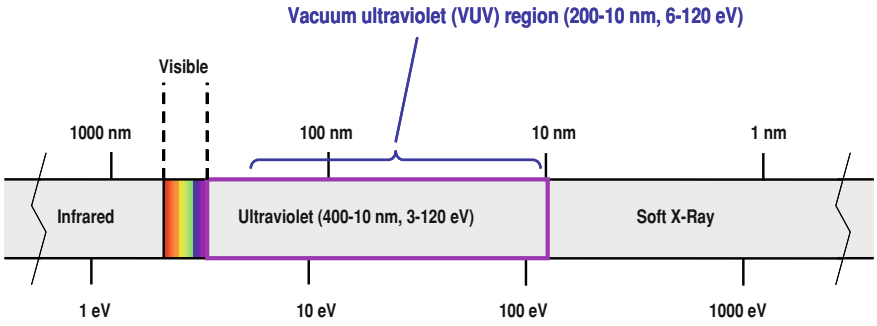

Fig. 1.1 Part of the electromagnetic spectrum, showing the vacuum ultraviolet region

To avoid confusion about signs, we note that whilst the *IE* of a molecule is always positive (i.e. the reaction $ABC \rightarrow ABC^+ + e^-$ is always endothermic), we use the convention used by most chemical physicists that a positive *EA* corresponds to the energy of A^- lying below that of A (i.e. the reaction $A + e^- \rightarrow A^-$ is exothermic). As stated earlier, ion-pair production can either occur directly into the ion-pair continuum, or indirectly following predissociation of an initially-excited Rydberg electronic state into the continuum. On Franck–Condon grounds the latter process is more common [7], so the detection of ion pairs provides information on the electronic structure of a molecule and the decay dynamics of its excited states.

An alternative way to express the inequality of Eq. 1.1 is to write:

$$AE(A^-) \geq IE(ABC) + D^o(A - BC^+) - EA(A)$$

or

$$AE_{298}(A^-) \geq IE(ABC) + D^o_{298}(A - BC^+) - EA(A) \tag{1.7}$$

Thus, ion-pair formation may occur at energies below the adiabatic *IE* of ABC if the electron affinity of A exceeds the dissociation energy of $A - BC^+$. Anions are then being detected in the absence of photoelectrons, facilitating the experiment. This condition is met for all the thallium halide diatomic molecules [8]. Furthermore, for TlBr and TlI the threshold for ion-pair formation occurs above the VUV onset of 200 nm, or below ca. 6 eV, making the detection of anions with conventional UV lamp sources relatively easy. Thus the study of the negative photoion spectroscopy of these molecules started as early as the 1930s. The halogen and inter-halogen diatomic molecules provide a rich source of ion-pair states, due to the relatively high *EA* value of all the halogen atoms. These molecules, reviewed in [9], could be studied by VUV and UV lasers operating in the wavelength range of ca. 150–250 nm (or 5–8 eV), and were complemented by synchrotron studies using VUV radiation from the second generation of these sources.

The first studies on *polyatomic* molecules in the 1960s, mostly from the National Bureau of Standards in Washington DC, USA, used the continuum

sources from discharge lamps coupled with mass spectrometric detection of the anion, but these studies rarely accessed wavelengths below 100 nm, or photon energies above 12.4 eV [10, 11]. The first set of dedicated experiments on polyatomic molecules using VUV radiation from a synchrotron were made in the early 1990s by Mitsuke et al. [12–16] at the Institute of Molecular Sciences in Okasaki, Japan, and a range of molecules were studied including CH_4 and larger hydrocarbons, CF_4, SF_6 and CH_3X (X = F,Cl,Br). The state of knowledge of ion-pair states in diatomic and polyatomic molecules up to 1996 was reviewed by Berkowitz [7]. A more recent project using a pulsed time-of-flight reflectron mass spectrometer to detect anions has been initiated by Tian et al. [17, 18] at the National Synchrotron Radiation Laboratory in Hefei, China. Starting in the 1990s, the development of imaging techniques opened a new window into ion-pair spectroscopy. Coupled with linearly-polarised VUV lasers, the dynamics of ion-pair dissociation via molecular Rydberg states started to be investigated, with detailed studies on CH_3Cl and CH_3Br being reported [19, 20]. Simultaneously, the development of threshold ion pair production spectroscopy [21, 22] applied to diatomic and some hydride triatomic molecules meant that the full potential of laser-based coherent VUV sources at high resolution could be applied to ion-pair formation. These studies up to 2006 were reviewed by Suits and Hepburn [23].

In the work reported in this thesis, we have exploited the increased sensitivity of modern mass spectrometers and the wide tunability and availability of synchrotron sources over the energy range 10–30 eV to study anion formation from a wide range of polyatomic molecules. The systems studied include CH_4, CF_4, SF_6, CH_3X (X = F,Cl,Br), CF_3Y (Y = Cl,Br,I), SF_5Z (Z = Cl,CF_3), CH_xF_y ($x + y = 4$), CH_aCl_b ($a + b = 4$), CF_cCl_d ($c + d = 4$), C_mH_n and C_mF_n ($m = 1,2,3$). For common molecules studied, a much wider range of anions are observed than those observed by Mitsuke et al., and a generic methodology has been developed to determine *absolute* cross sections and quantum yields for anion formation; this has never been done before for such a wide range of molecules. The data form the most comprehensive collection of information on ion-pair formation in polyatomic molecules since the Berkowitz review [7]. In addition, attempts are made to explain *why* some anions form in preference to others. Since many of our studies involve fluorinated molecules, it is perhaps not surprising that phenomena such as the electronegativity of the departing anion and the perfluoro effect [24] can explain some of the observations. However, certainly for indirect ion-pair formation, it is the *dynamics* of the crossing between the Rydberg and the ion-pair state which determine predominantly the product anions that are formed.

1.1.1 Direct and Indirect Ion-Pair Formation, Rydberg States

In their review on halogen diatomic molecules, Lawley and Donovan [9] suggest a model for the potential energy function of an ion-pair state, incorporating an exponential repulsion term with a long-range Coulombic attractive interation,

$$V(r) = A\exp(-\alpha r) - \frac{e^2}{4\pi\varepsilon_0 r} + E_{\text{ip}} \tag{1.8}$$

$V(r)$ is the potential energy, r the bond distance along the reaction coordinate, A and α are constants, and E_{ip} is the energy needed to place $V(r)$ onto an absolute scale. For reaction (1.1), $E_{ip} = D^o(\text{A}-\text{B}) + IE(\text{B}) - EA(\text{A})$. This model assumes both pure ionic behaviour and the equilibrium bond distance of the ion-pair state at equilibrium being large.

As stated in Sect. 1.1, anion–cation pair may be formed by direct excitation to the ion-pair state, or indirectly via predissociation of an initially-excited neutral state. Figure 1.2 shows these two processes for the generic polyatomic molecule ABC dissociating into $A^- + BC^+$. Direct ion-pair formation involves excitation to the repulsive inner wall of the potential energy surface above the asymptotic dissociation energy. Consequently, the transition may have very small Franck–Condon factor at threshold, and vibrational states of the ion-pair potential curve cannot be probed. However, given the necessary sensitivity in the experiment, unless the Franck–Condon factor is truly zero at threshold one would expect the signal of A^- to turn on at its thermochemical energy. By contrast, for the indirect process the restricting factor is not this Franck–Condon overlap, but rather the degree of coupling between the initially-excited neutral state and the ion-pair state. In addition, vibrational levels within the neutral excited state can be probed. Although it is not shown as such in Fig. 1.2b, there is now no reason why the signal of A^- should turn on at its thermochemical threshold, because the initially-excited neutral state may lie higher in energy than the $A^- + BC^+$ threshold. This explains the inequality in the energetics of Eqs. 1.5–1.7. Nevertheless, regardless of which process leads to the formation of ion pairs, competing processes can result in products other than $A^- + BC^+$ being formed. These processes include neutral dissociation, molecular ionisation, or fluorescence. The measurement of quantum yields for these different exit channels is notoriously difficult, especially in the VUV region of the spectrum where absolute standards can be difficult to obtain. However, the general acceptance is that the quantum yield for ion-pair formation in polyatomic molecules is small, typically 10^{-3} or less, with the value decreasing as the size of the molecule increases [7, 23, 25].

Rydberg states are commonly identified as the initially-excited intermediate involved in indirect ion-pair formation (i.e. ABC* in Fig. 1.2b) [7, 25]. A molecular Rydberg state is a high-lying electronic state of the neutral molecule where an electron is excited such that it observes the molecule as a distant positively-charged core. The Rydberg electron resides in an atomic-like orbital which is very large compared to the size of the molecule. Series of Rydberg states converge to ionisation limits and generally obey the Rydberg formula [25, 26]:

$$E_n = IE - \left[\frac{R_\infty}{(n-\delta)^2}\right] \tag{1.9}$$

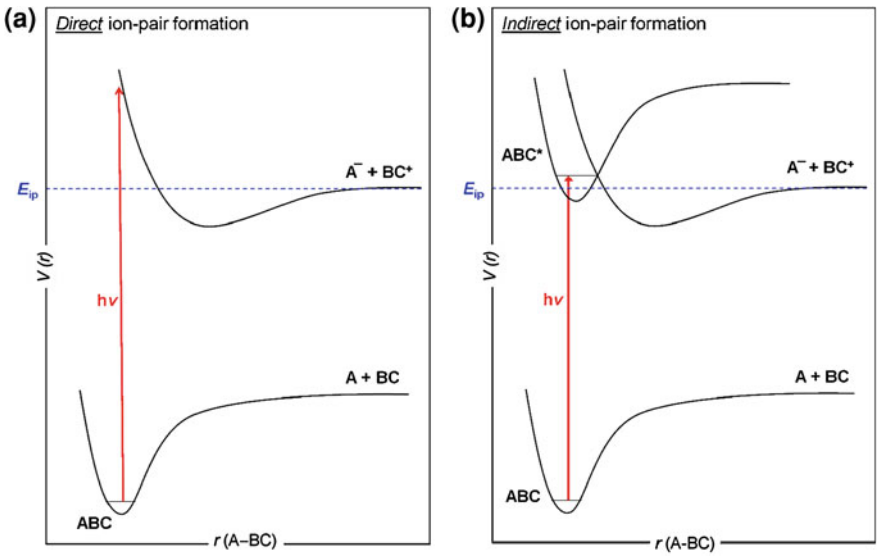

Fig. 1.2 **a** Potential energy (V) as a function of bond distance (r) showing *direct* ion-pair formation process for the generic reaction $ABC + h\nu \rightarrow A^- + BC^+$. E_{ip} represents the asymptotic ion-pair dissociation energy. **b** Potential energy (V) as a function of bond distance (r) showing *indirect* ion-pair formation process via predissociation of a neutral excited state (ABC^*), i.e. $ABC + h\nu \rightarrow (ABC^*) \rightarrow A^- + BC^+$

where E_n is the energy of the nth Rydberg state, *IE* is the ionisation energy to which the Rydberg series converges, R_∞ is the Rydberg constant (109737.32 cm^{-1} *or* 13.6059 eV, the *IE* of atomic hydrogen), n is the principal quantum number of the Rydberg orbital, and δ is the quantum defect. $(E_n - IE)$ is called the *term value*. The angular momentum quantum number, l, of the Rydberg orbital is identified by δ. For example, the value of δ will be the same for each member of an *ns* (or *np* or *nd*… etc.) Rydberg series. Typical values of δ for period 1 and 2 elements of the periodic table are: for *ns* series, 0.9–1.2; for *np* series, 0.3–0.6; for *nd* series, <0.1 [26]. In addition, δ values increase with increasing period number. Thus, an *np* Rydberg orbital in Cl will have a larger quantum defect than an *np* Rydberg orbital in F. δ therefore represents an arbitrary, dimensionless number, the magnitude of which reflects the degree of orbital-core penetration, including the shielding effects of 'core' electrons on the Rydberg electron. The Rydberg formula originated from the analysis of the spectrum of atomic hydrogen, a single-electron system with no requirement to define δ; in Eq. 1.9, for atomic H $\delta = 0$. The quantum defect is introduced for many-electron systems to account for electron–electron interactions. Thus, the smaller the value of δ, the more the system behaves like a hydrogen atom and the more diffuse the Rydberg orbital becomes.

Peaks in a spectrum (providing a value for E_n) may be assigned to a Rydberg orbital using the Rydberg formula if the value for the *IE* is known. In practice, it is

common that several assignments exist for the same value of E_n because of many possible combinations for *IE*, n and δ. Assignments presented later are therefore given with a degree of uncertainty, reflecting the moderate resolution at which the negative photoion spectra are recorded. One particular difficulty in assigning *molecular* Rydberg orbitals is that only quantum defect values for atomic systems are well known. In this work the tabulations by Theodosiou et al. [27] were used as a guide to identify appropriate quantum defect values. More confident assignments require E_n to be known more accurately from higher-resolution spectra, or several peaks to be fitted to the same Rydberg series; the latter is more likely to be possible from total photoabsorption or atomic spectroscopy.

1.1.2 Thermochemical Aspects of Ion-Pair Formation

The standard enthalpy of a unimolecular reaction, $\Delta_r H°$, can be calculated if the standard enthalpies of formation ($\Delta_f H°$) for each individual reactant and product species are known. All our experiments are performed at 298 K, and thus the following relationship can be used:

$$\Delta_r H°_{298} = \sum \Delta_f H°_{298}\,(products) - \sum \Delta_f H°_{298}\,(reactants) \tag{1.10}$$

The $\Delta_f H°_{298}$ values used to calculate these enthalpies of reaction are taken from standard sources [28, 29], although more recent and accurate data may be available for some of the ion-pair products we observe. In reality, however, it is the change in standard Gibbs energy of the reaction, $\Delta_r G°$, and not the change in standard enthalpy, which determines the thermodynamic feasibility of a reaction. The relationship between $\Delta_r G°$ and $\Delta_r H°$ is given by:

$$\Delta_r G° = \Delta_r H° - T\Delta_r S° \tag{1.11}$$

where T is the temperature in K and $\Delta_r S°$ is the standard entropy of reaction. Thus, the effects of entropy in a reaction are ignored when using enthalpy, and not free energy, values. For most ion-pair reactions needing the input of a vacuum-UV photon (e.g. 10 eV $\equiv$ ca. 965 kJ mol^{-1}), the $T\Delta_r S°$ term is small compared to the magnitude of $\Delta_r G°$ or $\Delta_r H°$, even though Δn, the number of product minus the number of reactant species, for reactions (1.1)–(1.3) is always positive and never zero. We therefore believe that the use of $\Delta_r H°$, the endothermicity of the reaction, instead of $\Delta_r G°$ is justified, provided this fact is acknowledged. However, in the very few cases where $\Delta_r H°$ is very small and $\Delta_r S°$ is very large, this approximation may not be applicable. Note that for *bimolecular* reactions involving cations or anions, which are considered in the second half of this thesis, $\Delta_r H°$ values can be much smaller, and the magnitude of $T\Delta_r S°$ may sometimes lie within the uncertainty of the calculated $\Delta_r H°$ value. Then entropic effects may be significant.

It has already been seen that the asymptotic ion-pair formation energy, E_{ip}, from a generic polyatomic molecule ABC can be expressed using either of the two equations:

$$E_{ip}(\mathrm{A}^- + \mathrm{BC}^+) = D^o(\mathrm{A}-\mathrm{BC}) + IE(\mathrm{BC}) - EA(\mathrm{A})$$

or

$$E_{ip}(\mathrm{A}^- + \mathrm{BC}^+) = IE(\mathrm{ABC}) + D^o(\mathrm{A}-\mathrm{BC}^+) - EA(\mathrm{A}) \tag{1.12}$$

As seen earlier, one advantage of using the second of these two equations is to identify that ion-pair formation can occur at an energy below the onset to ionisation: $E_{\mathrm{ip}} < IE$ when $EA(\mathrm{A}) > D^o(\mathrm{A} - \mathrm{BC}^+)$. This is often the case when A is a halogen atom because their *EA* values are relatively large. Below the *IE, any* ion formed must arise as a result of an ion-pair reaction, and positive or negative species can be detected with relative ease. Above the *IE*, however, in addition to anions, cations and free electrons are produced often in huge excess, which provide additional experimental challenges.

In practice, the value of E_{ip} is often not known or cannot be measured, and it is more convenient to use the experimental appearance energy instead. Although there are several definitions of the appearance energy in the literature, at the relatively modest resolution of our experiments, ca. 0.05–0.20 eV (see Chap. 2), we believe it most appropriate to define the AE_T at the temperature of the experiment, T (which is usually 298 K), as the lowest energy at which ion-pair formation is detected; that is, the photon energy at which an anion signal is first observed above the background noise. This can be considered as the value for hv shown earlier in Fig. 1.2a and b. The two equations of (1.12) may then be rewritten as the inequalities shown earlier in Eqs. 1.5–1.7. These inequalities can be used to calculate an upper limit to the value of either a bond dissociation energy or an ionisation energy, or a lower limit to the value of an electron affinity, whichever has the least well-known value [7, 30].

The anion is detected is identified by its mass (Chap. 2). However, the positive ion and any neutral fragments produced by the ion-pair reaction are not known. The enthalpy change for a unimolecular ion-pair reaction may be calculated using Eq. 1.10 and compared with onsets to features in a spectrum. Previous experimental results from Mitsuke et al. showed that an experimental AE_T value commonly occurs at, or slightly higher in energy than the calculated thermochemical threshold (i.e. the value for E_{ip} calculated from Eq. 1.12). Assigning an AE_T value to a particular reaction is often straightforward, because usually only one ion-pair dissociation is energetically possible; for the lowest-energy ion-pair process only one bond is broken and no neutral fragments are produced. Assigning a reaction to features in a spectrum at higher energy is often more difficult because many different ion-pair dissociation channels become energetically open.

The values calculated from the right-hand side of Eq. 1.10 are *enthalpy* changes. Before proceeding further, *energy* and *enthalpy* must be distinguished. Consider one molecule of an ideal gas interacting with a photon to produce a

negative–positive pair of ions. The enthalpy change, $\Delta_r H^o$, does not allow for the fact that some internal energy is transferred to the surroundings as an increase in volume and/or pressure; the number of gaseous species increases due to the unimolecular dissociation reaction, $\Delta n > 0$, and the products are produced with translational momentum. The enthalpy change of a gas-phase reaction where all the species behave as ideal gases is defined by:

$$\Delta_r H^o = \Delta_r U^o + RT\Delta n \tag{1.13}$$

where U is the internal energy and R the universal gas constant. Energy and enthalpy are only equivalent quantities when $T = 0$ or $\Delta n = 0$. Corrections to AE_T values, so that they may be compared to those for $\Delta_r H^o_T$, have been outlined by Traeger and McLoughlin for photoionisation reactions [31]. For the generic ion-pair reaction $ABC + h\nu \rightarrow A^- + BC^+$ at 298 K, their methods can be modified to show that

$$\Delta_r H^o_{298} \leq AE_{298}(A^-) + \int_0^{298} c_{p,m}(A^-).dT + \int_0^{298} c_{p,m}(BC^+).dT - \frac{5}{2}RT \tag{1.14}$$

where $c_{p,m}$ is a molar specific heat capacity at constant pressure. The upper limit for $\Delta_r H^o_{298}$ arises because the appearance energy of A^- defines an upper limit to the thermochemical energy of $A^- + BC^+$. The inequality arises in the presence of a kinetic shift and/or a barrier in the exit channel, the equality holds if both effects are insignificant. Considering the second and third terms in the right-hand side of Eq. 1.14,

$$\int_0^{298} c_{p,m}\ (A^- \textit{ or } BC^+).dT = H^o_{298} - H^o_0 \tag{1.15}$$

For both anion and cation, this term may contain contributions from translational ($2.5RT$), rotational (up to $1.5RT$) and vibrational ($N_A h\nu / [\exp(h\nu / k_B T) - 1]$ per mode) motion evaluated at $T = 298$ K. For many neutral molecules where all its vibrational frequencies are known, values of $H^o_{298} - H^o_0$ are tabulated [28]. For some anions and cations, ab initio calculations of vibrational frequencies may be necessary. In practice, however, unless the products of the reaction are large polyatomic species with many low-frequency vibrational modes contributing to their vibrational partition functions, the difference between $\Delta_r H^o_{298}$ and AE_{298} is relatively small, typically <0.1 eV or 10 kJ mol^{-1}. This correction falls within the combination of uncertainties in the calculated $\Delta_r H^\circ_T$ and AE_T values determined in this work. In this thesis, therefore, the thermal correction is ignored: experimental *energy* values are compared like-for-like with calculated *enthalpy* change.

1.2 Ion–Molecule Reactions

The second part of this thesis reports and discusses the results collected from an experiment designed to investigate the gas-phase reactions of ions with neutral molecules. A variety of cations and anions have been reacted with ethene and some fluorine-substituted ethenes. The experiment is described in Chap. 2 and the results are discussed in Chaps. 7–9. Additional data is presented in Appendix IV and V. None of this work is yet published, but it will be written up for publication in the primary literature over the next year.

The primary aim is to measure the rate coefficient and product ions of a generic ion-molecule reaction in the gas phase,

$$A^{+}\text{or } A^{-} + BC \rightarrow \text{product cations or anions} + \text{neutral species} \quad (1.16)$$

All reactions are measured at 298 K in a selected ion flow tube (SIFT) apparatus. These experiments are more mature than the negative ion spectroscopic experiments, the SIFT apparatus used is over 25 years old, and it has been described in many detailed reviews [32, 33]. A much smaller Introduction to this part of the thesis is therefore given. However, particular emphasis is given here to the different mechanisms that can describe the dynamics of how the reaction between a cation/anion with a neutral molecule can occur.

1.2.1 Cation-Molecule Reactions

Charge transfer is important in the reaction between a cation and a neutral molecule. If the energy gained by the cation recombining with an electron [its *Recombination Energy* (*RE*)] exceeds the energy required to remove an electron from the neutral molecule [its *Ionisation Energy* (*IE*)], then charge transfer may occur:

$$A^{+} + BC \rightarrow A + BC^{+} \quad (1.17)$$

The *RE* of the cation A^{+} is the same as the *IE* of neutral A, and takes a positive value. If the *RE* $(A^{+}) \gg$ *IE* (BC), several eV for example, the resulting excess energy may fragment the newly formed cation:

$$A^{+} + BC \rightarrow A + (BC^{+})^{*} \rightarrow A + B + C^{+} \quad (1.18)$$

$$or\ A^{+} + BC \rightarrow A + (BC^{+})^{*} \rightarrow A + B^{+} + C \quad (1.19)$$

Dissociative and non-dissociative charge transfer has been observed from a variety of different cation-molecule reactions. Results have shown that in most cases, if charge transfer is energetically allowed, it will occur and is usually the dominant

reaction channel [34–45]. The same experiments have shown that some cations and molecules do not react when the energetics do not allow for charge transfer. In these instances for a reaction to happen, the two species must engage 'intimately', and steric effects become important in addition to energetics. The term *intimate* is used to describe a reaction where the two species interact at close proximity, and bonds are formed and/or broken.

1.2.2 Anion-Molecule Reactions

Consider the generic anion-molecule reaction below:

$$A^- + BC \rightarrow \text{products} \tag{1.20}$$

For an electron to transfer from A^- to BC, the *Electron Affinity* (*EA*) of BC must be greater than the *EA* of A. This is not the case for many anion-molecule reactions because usually the *EA* (A) > *EA* (BC). Indeed when charge transfer *has* been observed, the *EA* of the neutral reactant molecule is large; dissociative and non-dissociative charge transfer has been identified in some reactions of O_2^-, O^-, CF_3^-, OH^- and F^- with SF_6 (*EA* = 1.1 eV), SeF_6 (*EA* = 2.9 eV), and TeF_6 (*EA* = 3.3 eV) [46]. To put these values into context, the *EA* values of O_2, O, CF_3, OH and F are 0.45, 1.46, 1.82, 1.83, and 3.40 eV, respectively [47].

Such charge transfer is not common, and anions are more likely to react intimately with molecules. Anion-molecule reactions have been shown to commonly occur by abstraction (e.g. H^+ abstraction), or addition–elimination/substitution (e.g. F^- elimination) mechanisms [48–50].

1.2.3 Collisional Rate Coefficients

In bimolecular reactions a *collisional* rate, also known as a *capture* rate, represents an upper limit which assumes every collision leads to a reaction. The efficiency of a reaction can be determined by comparing the maximum rate with that measured by experiment. The ratio of an experimentally measured rate coefficient, k_{exp}, to a calculated collisional value, k_c, represents the reaction efficiency. Bimolecular collisional rate coefficients for ion-molecule reactions are typically in the order of 10^{-9} cm^3 molecule^{-1} s^{-1}.

The values for k_c given in this work use the model formulated by Chesnavich et al. [51], and further modified by Su and Chesnavich [52–54]. It assumes the potential energy interaction between the reactant ion and molecule takes the form:

$$V(r,\theta) = -\frac{\alpha' q^2}{8\pi\varepsilon_0 r^4} - \frac{q\mu_D}{4\pi\varepsilon_0 r^2}\cos\theta \tag{1.21}$$

where V is the potential energy of interaction in J, α' is the polarisability volume of the neutral molecule in m^3, q is the charge on the ion in C, ε_0 is the permittivity of free space (8.85419×10^{-12} C^2 m^{-1} J^{-1}), r is the distance between the centres of mass of the ion and neutral molecule in m, μ_D is the dipole moment of the neutral molecule in C m, and θ is the angle between the direction of the dipole with respect to r. The resulting expression for the collisional rate constant is:

$$k_c = k_L K_c \tag{1.22}$$

where k_c and k_L are defined here in units of m^3 $molecule^{-1}$ s^{-1}, and K_c is dimensionless. k_L is the *Langevin* rate coefficient, named after the scientist who first modelled the dynamics of ion–molecule interactions [55], and formulated by Gioumousis and Stevenson [56]:

$$k_L = \left(\frac{\pi \alpha' q^2}{\varepsilon_0 \mu}\right)^{\frac{1}{2}} \tag{1.23}$$

where μ is the reduced mass of the colliding species in kilogram. The other term in Eq. 1.21, K_c, is defined as follows [54]:

$$K_c = \begin{cases} \dfrac{(x + 0.5090)^2}{10.526} + 0.9754; & x \leq 2 \\ 0.4767x + 0.6200; & 2 \leq x \leq 3 \\ 0.5781x + 0.3165; & 3 \leq x \leq 35 \\ 0.6201x - 1.153; & 35 \leq x \leq 60 \\ 0.6347x - 2.029; & x \geq 60 \end{cases} \tag{1.24}$$

$$x = \left(\frac{\mu_D^2}{8\pi\varepsilon_0 \alpha' k_B T}\right)^{\frac{1}{2}} \tag{1.25}$$

where k_B is the Boltzmann constant in J K^{-1}, and T is the temperature in K.

It should be acknowledged that Eqs. 1.21–1.25 are expressed in *International Standard* (SI) units, and so may differ to those in older scientific literature where *centimetre-gram-second* (cgs) units are commonly used. The first difference to note is that a *polarisability* in cgs units of cm^3 is often expressed as α, whereas in SI units the equivalent quantity is referred to as the *polarisability volume* in m^3 with the symbol α'. In SI units the polarisability, α, has units of C^2 m^2 J^{-1} and is related to the polarisability volume, α', by the following expression:

$$\alpha' = \frac{\alpha}{4\pi\varepsilon_0} \tag{1.26}$$

The second difference to note is how the unit of 'charge' is expressed. Charge in cgs units ($cm^{3/2}$ $g^{1/2}$ s^{-1}) can be converted to SI units (C or A s) by using the relationship below:

Table 1.1 Polarisability volumes and dipole moments for ethene and the fluorinated ethenes

Molecule	C_2H_4	C_2H_3F	CH_2CF_2	C_2HF_3	C_2F_4
$\alpha'/Å^{3a}$	4.25[c]	3.99[d]	5.01[c]	4.16[d]	4.35[d]
μ_D/D^b	–	1.47[c]	1.39[c]	1.32[c]	–

[a] The polarisability volume, α'. For simplicity, units of α' are often given in $Å^3$ where 1 $Å^3 = 10^{-24}$ $cm^3 = 10^{-30}$ m^3

[b] The dipole moment, μ_D. Values of μ_D are commonly expressed in units of debyes (D), where 1 D = 3.336×10^{-30} C m (SI units)

[c] Value taken from the CRC handbook of Chemistry and Physics [58]

[d] Value calculated using the method developed by Miller [57]

$$charge(\mathbf{cgs}) = charge(\mathbf{SI}) \times \left(\frac{1}{4\pi\varepsilon_0}\right)^{\frac{1}{2}} \tag{1.27}$$

This is relevant in the equations above to the terms q and μ_D which have SI units of C and C m, respectively.

In order to calculate k_c for a reaction, the polarisability volume and dipole moment (if applicable) of the neutral molecule are required. The values used in this thesis, and their sources, are given in Table 1.1. While dipole moments of molecules are not difficult to find in the scientific literature, molecular polarisabilities often are. However, a very successful method to calculate polarisability volumes has been developed by Miller [57]:

$$\alpha'(ahc) = \left(\frac{4}{N}\right)\left[\sum_A \tau_A(ahc)\right]^2 \tag{1.28}$$

where N is the total number of electrons in the molecule and τ_A is an atomic hybrid component (ahc) for each atom A in a given state of hybridisation.

References

1. Simpson MJ, Tuckett RP, Dunn KF, Hunniford CA, Latimer CJ, Scully SWJ (2008) J Chem Phys 128:124315
2. Simpson MJ, Tuckett RP, Dunn KF, Hunniford CA, Latimer CJ (2009) J Chem Phys 130:194302
3. Simpson MJ, Tuckett RP (2010) J Phys Chem A 114:8043
4. Simpson MJ, Tuckett RP (2011) Int Rev Phys Chem 30:197
5. Rogers NJ, Simpson MJ, Tuckett RP, Dunn KF, Latimer CJ (2010) Mol Phys 108:895
6. Rogers NJ, Simpson MJ, Tuckett RP, Dunn KF, Latimer CJ (2010) PCCP 12:10971
7. Berkowitz J (1996) VUV and Soft x-ray photoionisation. In: Becker U, Shirley DA (eds) Chap. 8, Plenum, New York, ISBN: 0306450380
8. Terenin A, Popov B (1932) Phys Z. Sowjetunion 2:299
9. Lawley KP, Donovan RJ (1993) J Chem Soc Faraday Trans 89:1885
10. Dibeler VH, Walker JA (1965) J Chem Phys 43:1842
11. Krauss M, Walker JA, Dibeler VH (1968) J Res Nat Bureau Stand 72A:281
12. Mitsuke K, Suzuki S, Imamura T, Koyano I (1991) J Chem Phys 94:6003
13. Mitsuke K, Hattori H, Yoshida H (1993) J Chem Phys 99:6642

14. Mitsuke K, Suzuki S, Imamura T, Koyano I (1991) J Chem Phys 95:2398
15. Mitsuke K, Suzuki S, Imamura T, Koyano I (1990) J Chem Phys 93:8717
16. Suzuki S, Mitsuke K, Imamura T, Koyano I (1992) J Chem Phys 96:7500
17. Tian SX, Lu YF, Wang YF, Feng Q, Chen LL, Sun JD, Liu FY, Shan XB, Sheng LS (2010) Chem Phys Lett 496:254
18. Chen LL, Xu YF, Feng Q, Tian SX, Liu FY, Shan XB, and Sheng LS (2011) J Phys Chem A 115:4248
19. Suto K, Sato Y, Reed CL, Skorokhodov V, Matsumi Y, Kawasaki M (1997) J Phys Chem A 101:1222
20. Xu DD, Huang J, Price RJ, Jackson WM (2004) J Phys Chem A 108:9916
21. Martin JDD, Hepburn JW (1997) Phys Rev Lett 79:3154
22. Shiell RC, Hu XK, Hu QJ, Hepburn JW (2000) J Phys Chem A 104:4339
23. Suits AG, Hepburn JW (2006) Annu Rev Phys Chem 57:431
24. Brundle CR, Basch H, Robin MB, Keubler NA (1972) J Am Chem Soc 94:1451
25. Berkowitz J (1979) Photoabsorption photoionisation and photoelectron spectroscopy. Academic, London ISBN: 0120916509
26. Sandorfy C (1999) The role of Rydberg states in spectroscopy and photochemistry. Sandorfy C (ed) Kluwer Academic Publishers, London, p 1. ISBN: 0792355334
27. Theodosiou CE, Inokuti M, Manson S (1986) At Data Nucl Data Tables 35:473
28. Chase MW (1998) J Phys Chem Ref Data Monograph 17:1 ISBN: 1563968312
29. Lias SG, Bartmess JE, Liebman JF, Holmes JL, Levin RD, Mallard WG (1988) J Phys Chem Ref Data 17:1 ISBN: 0883185628
30. Shaw DA, Holland DMP, Walker IC (2006) J Phys B: At Mol Opt Phys 39:3549
31. Traeger JC, McLoughlin RG (1981) J Am Chem Soc 103:3647
32. Smith D, Adams N (1988) Adv At Mol Phys 24:1
33. Bohme DK (2000) Int J Mass Spectrom 200:97
34. Mayhew CA (1992) J Phys B 25:1865
35. Smith D, Spanel P, Mayhew CA (1992) Int J Mass Spectrom Ion Processes 117:457
36. Jarvis GK, Mayhew CA, Tuckett RP (1996) J Phys Chem 100:17166
37. Jarvis GK, Kennedy RA, Mayhew CA, Tuckett RP (2000) Int J Mass Spectrom 202:323
38. Atterbury C, Kennedy RA, Mayhew CA, Tuckett RP (2001) PCCP 3:1949
39. Atterbury C, Critchley A, Kennedy RA, Mayhew CA, Tuckett RP (2002) PCCP 4:2206
40. Mayhew CA, Thomas R, Watts P (2003) Int J Mass Spectrom 223:91
41. Critchley A, Howle CR, Mayhew CA, Tuckett RP (2004) Chem Phys 303:235
42. Howle CR, Mayhew CA, Tuckett RP (2005) J Phys Chem A 109:3626
43. Parkes MA, Chim RYL, Mayhew CA, Mikhailov V, Tuckett RP (2006) Mol Phys 104:263
44. Parkes MA, Ali S, Tuckett RP, Mikhailov V, Mayhew CA (2006) PCCP 8:3643
45. Mikhailov V, Parkes MA, Simpson MJ, Tuckett RP, Mayhew CA (2008) J Phys Chem A 112:9012
46. Kennedy RA, Mayhew CA (2001) PCCP 3:5511
47. Rienstra-Kiracofe JC, Tschumper GS, Schaefer HF, Nandi S, Ellison B (2002) Chem Rev 102:231
48. Kennedy RA, Mayhew CA, Peverall R, Watts P (2000) PCCP 2:3145
49. Lee EPF, Dyke JM, Mayhew CA (1998) J Phys Chem A 102:8349
50. Arnold ST, Miller TM, Viggiano AA, Mayhew CA (2003) Int J Mass Spectrom 223:403
51. Chesnavich WJ, Su T, Bowers MT (1980) J Chem Phys 72:2641
52. Su T, Chesnavich WJ (1982) J Chem Phys 76:5183
53. Su T (1988) J Chem Phys 88:4102
54. Su T (1988) J Chem Phys 89:5355
55. Langevin PM (1905) Annales de Chimie et de Physique 5:245
56. Gioumousis G, Stevenson DP (1958) J Chem Phys 29:294
57. Miller KJ (1990) J Am Chem Soc 112:8533
58. Lide DR (2008) Handb of Chem Phys, 89th edn. Taylor and Francis, London Sections 9 and 10

Chapter 2
The Experiments

2.1 Negative Photoion Spectroscopy

2.1.1 The Synchrotron Radiation Source

Energy must be absorbed by a molecule in order for ion-pair dissociation to occur. *Synchrotron radiation* is ideal for such experiments because it provides a bright, monochromated and tunable energy source across the entire electromagnetic spectrum [1]. Synchrotron radiation sources accelerate electrons at relativistic velocities in a circular orbit using magnets; this takes place in a *storage ring*, tens of metres in diameter. The accelerating charges emit collimated light tangentially to the orbital path. Collected from the storage ring at a *beamline*, the light is optically focused into a monochromator prior to entering the experimental end station. The experiments described in Chaps. 3–6 utilised vacuum ultraviolet (VUV) radiation from beamline 3.1 at the UK Daresbury Synchrotron Radiation Source (SRS).

The Wadsworth monochromator, focal length 1 m, installed on beamline 3.1 is designed to provide the user with a high flux beam, albeit at the expense of wavelength resolution; it does not have an entrance slit limiting the amount of light hitting the *diffraction grating*, as is common in many other designs [2]. A diffraction grating consists of a large number of equally spaced parallel grooves cut into a reflective surface. The angle of the grating relative to the incident light determines which wavelengths will interfere constructively when reflected from the surface. It can be observed from Fig. 2.1 that for constructive interference of light to occur, the difference between distances x_1 and x_2 when divisible by an integer must equal the wavelength, λ; note that angles i and θ are both measured relative to the same normal reference, one angle taking a positive value, the other a negative value. Distance d represents the spacing between grooves on the surface of the grating. The relationship between the relative position of the grating (with respect to angles i and θ), d and λ can be written as follows:

M. J. Simpson, *Two Studies in Gas-Phase Ion Spectroscopy*, Springer Theses,
DOI: 10.1007/978-3-642-23129-2_2, © Springer-Verlag Berlin Heidelberg 2012

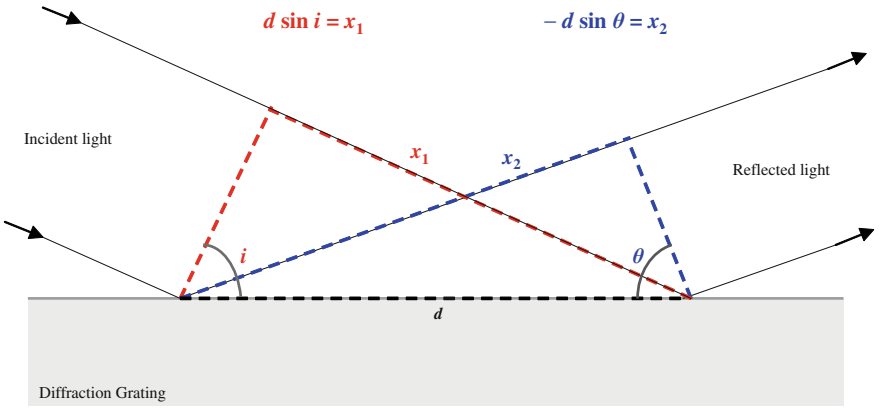

Fig. 2.1 A simple diagram to show how a diffraction grating works. Distances x_1 and x_2 represent the side of a right angle triangle 'opposite' to the angles i and θ, respectively. Distance d represents the spacing between grooves on the surface of the grating

$$m\lambda = d(\sin i + \sin \theta) \tag{2.1}$$

where m represents an integer value. When angles i and θ are equal and opposite, all wavelengths of light are constructively reflected and m takes the value of zero: hence the term *zero-order* radiation. During scanning experiments, however, *first-order* radiation is used ($m = 1$). Higher-orders of radiation become a problem when the desired energy of radiation is relatively low, i.e. between 8 and 16 eV. For example, a first-order spectrum at 10 eV may contain unwanted contributions from second-order radiation at 20 eV. In such cases, a lithium fluoride window may be placed in the path of the beam; LiF absorbs all radiation above 11.7 eV, thus eliminating contributions from higher orders.

Two different diffraction gratings are installed within the beamline 3.1 monochromator. The medium energy grating (MEG) is efficient in the range 8–18 eV and the high energy grating (HEG) from 12 to 35 eV. The beam of light reflected from the diffraction grating is directed through a manually controlled slit, known as the *exit slit*, before passing into the experimental endstation. A reduced slit width provides a higher resolution of light for the experiment, but the total flux is reduced; likewise a larger slit provides higher flux for the experiment, but at the expense of resolution.

A few experiments discussed in Chap. 6 used the 5 m focal length McPherson monochromator installed on beamline 3.2 at the SRS. This monochromator provides superior resolution for a given exit slit width compared to 3.1 due to the longer focal length, but the principles of operation are exactly the same as described above.

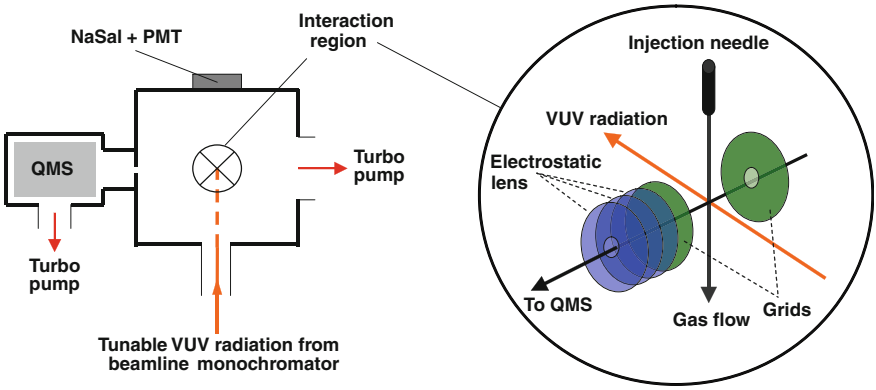

Fig. 2.2 A simple diagram of the experimental endstation used for detecting negative photoions

2.1.2 The Experimental Endstation

A simple diagram showing the main components and setup of the experimental end station is presented in Fig. 2.2, and should be referred to when reading the description below.

A 2 mm diameter, 300 mm long capillary light guide connecting the experimental apparatus to the beamline directs the monochromatised light to the interaction region. The gas under study is injected via a needle generating an effusive directed jet (with no internal cooling) which bisects orthogonally the incident photon beam. The crossing point, which dictates the centre of the interaction region, is positioned in the middle of two grids on the third orthogonal axis. A three-element electrostatic lens for focusing, and into a Hiden Analytical HAL IV triple quadrupole mass spectrometer (QMS) for mass selection. Detection is achieved by a channeltron electron multiplier. Sensitivity is considerably enhanced by differential pumping which reduces the number of free electrons and secondary collisions in the QMS. Spectra in which the monochromator is scanned are flux normalised using a sodium salicylate (NaSal) window and visible photomultiplier tube (PMT) combination, which has a constant response over the energy range of the experiments. The apparatus and QMS, connected via a 1 mm diameter aperture, are pumped separately by turbo pumps which are backed by a common rotary pump, and the base pressure of the apparatus is approximately 10^{-7} mbar. With sample gas running, the typical pressure in the chamber is raised to 10^{-5} mbar. The pressure inside the chamber is measured using an ionisation gauge, the sensitivity of which to the sample gas under study is calibrated in a separate experiment relative to N_2 gas using a capacitance manometer (Dunn 2009 private communication) [3].

Mass spectra are recorded to observe all anions produced from photo absorption of the sample gas by exposure to white light (i.e. zero-order radiation). The mass-to-charge ratio (m/z) of each peak in the mass spectrum is then fixed and the signal

recorded as a function of photon energy, typically over the range 8–35 eV. In addition, for each anion, its signal is recorded at a fixed photon energy (usually the energy of a peak observed in the spectrum) as a function of sample gas pressure over the typical range (0.5–5.0) $\times$ 10^{-5} mbar. Anions which show a non-linear dependence with pressure cannot be assigned as ion-pair products, and their signal is most likely influenced by secondary processes. Anions which show a linear dependence of signal with pressure can be attributed to ion-pair formation; being a unimolecular process, the rate of formation of ion pairs is expected to obey first-order kinetics. Full details of the pressure dependencies are given in Chaps. 3–6.

2.1.3 The Determination of Absolute Ion-Pair Cross Sections

Anion spectra resulting from ion-pair formation are presented as cross sections, σ, in absolute units of cm^2. The value of σ at a given photon energy hv is calculated as follows:

$$\sigma(hv) = k\left(\frac{SM}{frp}\right) \tag{2.2}$$

where S is the detected signal in counts s^{-1}, M is the relative mass sensitivity of the QMS, f is the relative photon flux (effectively a measure of the grating efficiency), r is the storage ring current, p is the sample gas pressure corrected for ionisation gauge sensitivity and k is a normalisation constant. Normalisation to f, r and p is straight forward, but this is not the case for M. An extensive set of experiments was performed to determine M as a function of m/z, described below in Sect. 2.1.5.

The corrected signal (to M, f, r and p) for F^- from SF_6 is normalised to the known cross section at 14.3 eV of (7 $\pm$ 2) $\times$ 10^{-21} cm^2 [4]. Likewise, the corrected signal for F^- from CF_4 is normalised to its value at 13.9 eV of (1.25 $\pm$ 0.25) $\times$ 10^{-21} cm^2 [5]. (It is noted that these known cross section values are not strictly absolute, but are obtained from calibrated measurements of O^- yields from O_2 [6]). Thus, normalisation factors $k(SF_6)$ and $k(CF_4)$ are determined. An average of these two k values is then used in Eq. 2.2 to determine cross section values for anions from other gases. In theory, these two values should be the same. In practice, they vary by a factor ranging from 1.2 to 1.7. These measurements were made at every visit to the SRS, and the appropriate average value of k was used.

2.1.4 The Determination of Quantum Yields

The ion-pair cross section from a molecule, calculated as described above in Sect. 2.1.3, can be divided by the *total* photoabsorption cross section for that molecule (absolute values are taken from the literature, where available, and are referenced

where appropriate in Chaps. 3–6) to provide an ion-pair formation quantum yield, Φ. Thus, the value for Φ represents the probability that the absorption of a photon will lead to ion-pair formation. Individual values for Φ are quoted with the photon energy at which the ion-pair and total photoabsorption cross section values are taken.

2.1.5 Considerations When Detecting Ions with the QMS

All quadrupole mass spectrometers exhibit an element of mass discrimination, with a tendency to transmit heavier ions less efficiently [7]. To correct for this effect the mass factor, M, has been determined by comparing the cation mass spectra of many polyatomic molecules in the QMS, following 70 eV electron impact ionisation, to 'true' mass spectra published in the electronic NIST database [8]. The values for M used in Eq. 2.2 are taken from the plot shown in Fig. 2.3. It can be seen that as m/z increases, the detection efficiency of the QMS decreases and a higher M value is required to correct this effect.

The zero-blast effect arises because *all* ions entering the QMS may be transmitted when the applied potentials are set to detect m/z values close to zero [7]. This becomes important when studying hydrogen-containing molecules; the tail of the zero-blast peak in the mass spectrum overlaps with m/z 1. Therefore, H^- spectra can only be trusted where there is no resemblance to other anion spectra recorded from the same molecule. Examples where this has caused problems include H^- detected from CH_3X molecules (X = F, Cl, Br), where the H^- spectra can mimic the X^- spectra [9]. By contrast, H^- detected from CH_4 is an example where this is not an issue because the H^- signal is dominant [10].

2.2 Ion–Molecule Reactions

2.2.1 The Selected Ion Flow Tube

The Selected Ion Flow Tube (SIFT) is an experimental apparatus used to study gas-phase ion–molecule reactions. An experimental rate coefficient can be measured and the ionic product species for the reaction can be identified. The relative branching ratios (BRs) for the detected products can also be determined. The SIFT technique has been described in detail in several review papers [11–13]. A description of the experiment, and how rate coefficients and BRs are determined, is also presented here.

The SIFT is vacuum sealed, and consists of three distinct sections. First is the ion source, where cations and/or anions are produced from a neutral precursor molecule by electron impact ionisation. Second is the flow tube, where helium

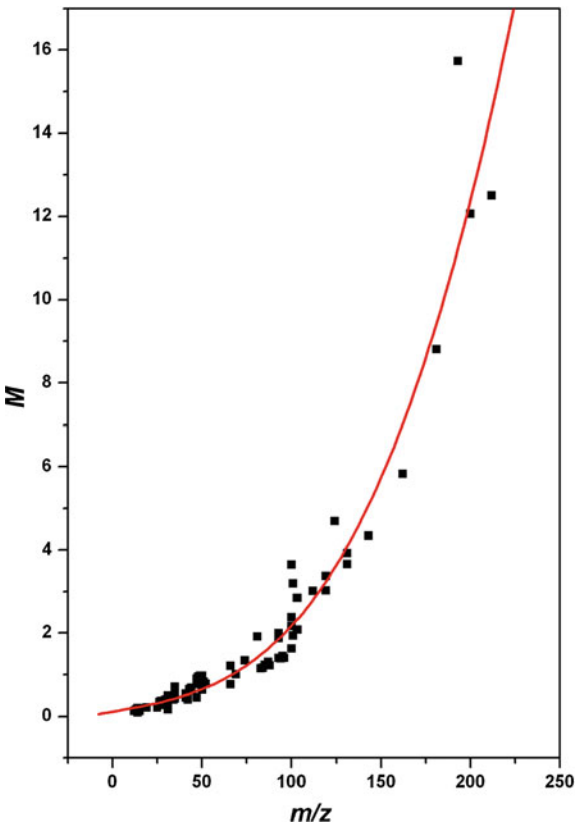

Fig. 2.3 Graph to determine the relative mass sensitivity, *M*, of the Hiden Analytical HAL IV quadrupole mass spectrometer (QMS) as a function of *m/z*. Sample gases include CF_4, SF_6, SF_5CF_3, CH_3F, CH_3Cl, CH_3Br, CH_2Cl_2, CF_2Cl_2, $CFCl_3$, C_2H_4, C_2H_6, C_3H_8, C_2F_4, C_2F_6, C_3F_8, 2-C_4F_8, *c*-C_4F_8, *c*-C_5F_8. The mass spectrum of each sample was measured with 70 eV electron impact ionisation, and compared with the NIST spectrum [8]. At each *m/z* value, the percentage yield from NIST is divided by the percentage yield from the QMS spectrum, and the data are normalised to unity at *m/z* 69 (*i.e.* CF_3^+). The *squares* show data points, the *solid* line shows the best fit to a third-order polynomial

buffer gas carries the ions downstream to a point where the neutral reactant is injected, and the reaction may occur. Third is the detection region, where the product ions are mass filtered and detected. Figure 2.4 presents a basic schematic of the SIFT, showing how these three sections relate to one another.

The ion source consists of a small closed chamber containing a tungsten filament and a series of electrostatic lenses. A simple cartoon of the ion source, showing the example of selecting $C_2F_4^+$ ions from C_3F_8 source gas, is presented in Fig. 2.5. When no gas is flowing a diffusion pump, backed by a common rotary pump, achieves a vacuum pressure of ca. 10^{-6} mbar. During operation, a neutral source gas is introduced into the chamber such that a relatively high pressure is maintained, ca. 10^{-4} mbar. Molecules from the source gas are ionised by 70 eV electrons; the filament emits electrons which are subsequently accelerated by an applied potential difference. This process may produce many different cation and anion species. For example, C_2F_6 may be used to produce the ions F^+, CF^+, CF_2^+, CF_3^+, F^- and CF_3^-. The reactant ions used in this work and their corresponding source gases are listed in Table 2.1. For the ions to enter the flow tube they must first pass through the electrostatic lenses and then through a quadrupole mass filter.

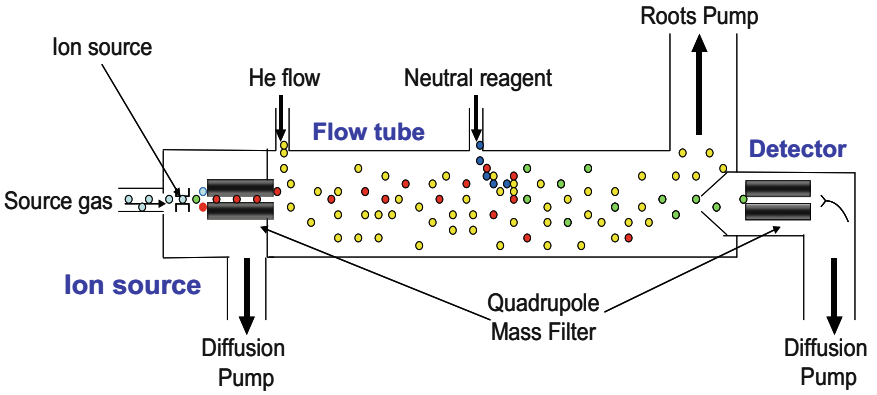

Fig. 2.4 A basic schematic of the Selected Ion Flow Tube apparatus. The *red* circles represent the ions generated in the ion source, the *yellow* circles represent the helium buffer gas, the *blue* circles represent the neutral reactant gas, and the *green* circles represent the product species

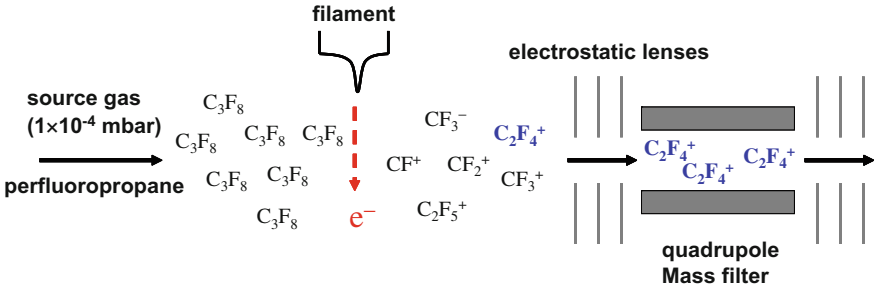

Fig. 2.5 A simple cartoon of the ion source in the Selected Ion Flow Tube, showing the example of selecting $C_2F_4^+$ ions using perfluoropropane source gas

Table 2.1 Source gases used to produce reactant cations and anions in the ion source

Ion	Source gas	Process
CF^+	$CF_4/C_2F_6/C_3F_8$	Single electron impact
CF_2^+	$CF_4/C_2F_6/C_3F_8$	Single electron impact
CF_3^+	$CF_4/C_2F_6/C_3F_8$	Single electron impact
$C_2F_4^+$	C_3F_8	Single electron impact
O_2^-	$N_2 + O_2$ mixture	Collisionally stabilised electron attachment
O^-	N_2O	Dissociative electron attachment
OH^-	$N_2O + CH_4$ mixture	Dissociative electron attachment forming O^-, followed by H abstraction from CH_4
F^-	C_2F_6	Dissociative electron attachment
CF_3^-	C_2F_6	Dissociative electron attachment

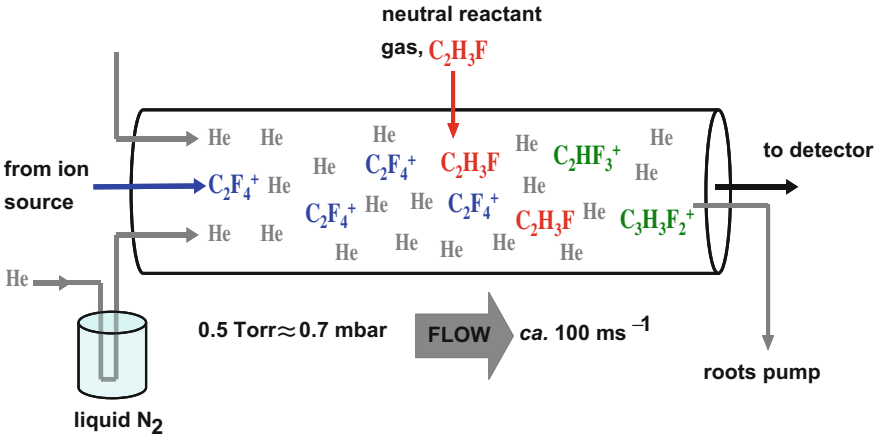

Fig. 2.6 A simple cartoon showing the flow tube part of the Selected Ion Flow Tube apparatus. The example of the reaction between $C_2F_4^+$ with C_2H_3F is used. The helium buffer gas is shown in *grey*, the reactant ion in *blue*, the reactant neutral in *red*, and the product ions in *green*

The quadrupole can be set to a desired mass-to-charge ratio (*m*/*z*) value with one atomic mass unit (a.m.u) resolution, such that only the desired reactant ion is selected. The ion signal is then maximised by monitoring the signal at the detection region (discussed below) by tuning the electrostatic lenses. The lens settings in the ion source are significantly different for positive or negative ions. For example, if the signal is maximised to transmit CF_3^+ ions (detection region set to positive mode) then CF_3^- anions produced will be repelled by the lens system, and not reach the mass filter. In addition, altering the pressure in the ion source can have an effect on the resultant ion signal.

The selected ions enter the flow tube along with helium (99.997% purity) buffer gas. The helium gas is passed through liquid nitrogen to increase its purity, and injected into the flow tube in a way which is designed to minimise back streaming of helium into the ion source [11]. The flow tube is 1 m in length and 8 cm in diameter. During operation it is filled with 0.5 Torr of buffer gas, which is drawn downstream at a velocity of ca. 100 m s^{-1} by an Edwards EH 2600 roots pump, backed by an Edwards E1M176 rotary pump. The conditions inside the flow tube are thermal, and the measurements in this work are all reported at 298 K. Any excited ions produced in the ion source are expected to be collisionally cooled by the buffer gas. At a known distance along the flow tube the neutral reactant gas is introduced. A simple cartoon of the flow tube is shown in Fig. 2.6, using the example of $C_2F_4^+$ ions reacting with C_2H_3F. All species, including helium, reactants and products, will then continue down the flow tube towards the detection region of the apparatus.

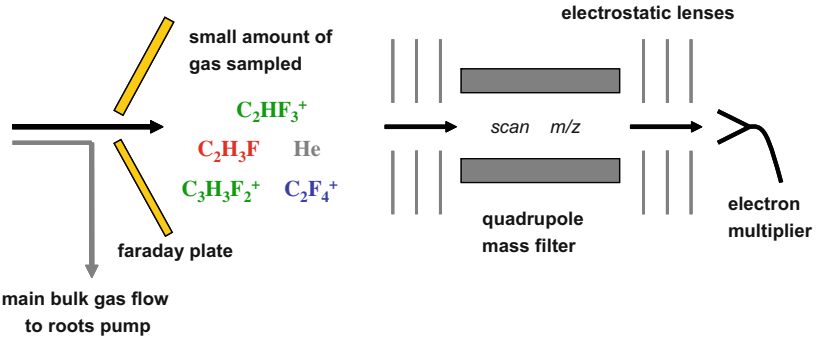

Fig. 2.7 A simple cartoon showing the detection region of the Selected Ion Flow Tube apparatus showing the example of reacting $C_2F_4^+$ with C_2H_3F

A simple cartoon of the detection region of the SIFT apparatus is shown in Fig. 2.7. At the end of the flow tube is a cone shaped end plate, with a 1 mm diameter hole at the centre. It is this orifice which samples the gas from the flow tube, and is the only connection to the detection region. The main bulk gas flow is drawn away by the roots pump as shown in Figs. 2.6 and 2.7. The detection region is differentially pumped by a diffusion pump backed by a common rotary pump; the base pressure in this region is ca. 10^{-6} mbar (compared to 0.7 mbar in the flow tube) and during operation the small amount of sampled gas through the end plate raises the pressure to ca. 10^{-5} mbar. The end plate not only samples the gas, but also acts as a Faraday plate. It has a floating voltage applied (being electrically isolated from the rest of the system), and the current produced is proportional to the number of ions hitting it.

Measurement of the current is therefore useful to tune the ion signal from the ion source, as discussed above. In addition, when reacting anions in the SIFT, a drop in the ion current can indicate a reaction is ejecting electrons; an electron is much lighter than an atomic or molecular anion, and so hits the wall of the flow tube rather than reaching the Faraday plate, which results in the total ion current decreasing. Ions are drawn into the quadrupole mass filter by electrostatic lenses, and then towards a channeltron electron multiplier which records the resultant ion signal. The ion signal is recorded as a function of *m*/*z*, and a mass spectrum is obtained.

2.2.2 The Determination of the Reaction Rate Coefficient

In the reactions performed in the SIFT the concentration of the reactant neutral molecule is much greater than the concentration of the reactant ion. This allows pseudo first-order kinetics to be applied, and if we consider the generic

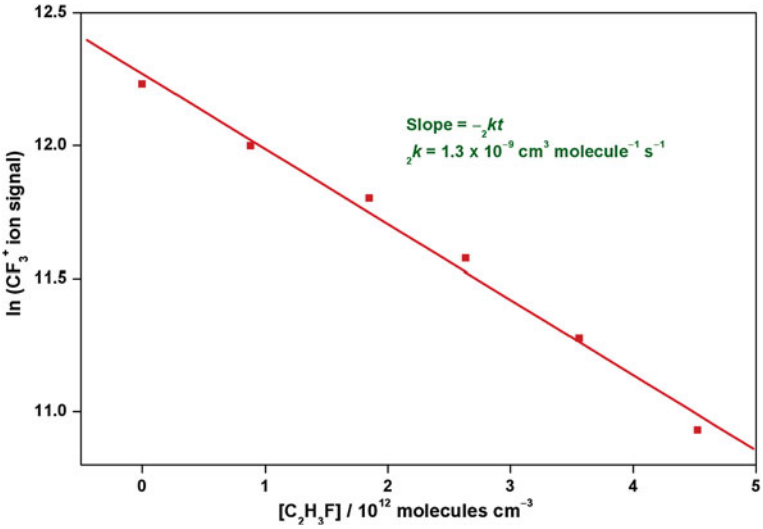

Fig. 2.8 A rate coefficient plot for the reaction between CF_3^+ and C_2H_3F. Computer software fits the data points to a straight line. The reaction time in s, t, is also calculated by the data analysis software, and a value for the bimolecular rate coefficient, $_2k$, is given in units of cm^3 $molecule^{-1}$ s^{-1}

ion–molecule reaction as being $A^+ + B$, then the integrated rate equation can be given as:

$$\frac{\ln[A^+]_{rel}}{[B]} = -_2kt \tag{2.3}$$

where $[A^+]_{rel}$ is the relative ion concentration (this is simply the ion count recorded by the mass spectrometer), [B] is the neutral reactant concentration (the absolute concentration of B (in molecules cm^{-3}) measured during the experiment as described in Appendix IV), $_2k$ is the bimolecular rate coefficient, and t is the reaction time. Equation 2.3 shows that the gradient of a linear plot of $\ln[A^+]_{rel}$ vs. [B] will be equal to $-\ _2kt$. An example of such a plot, for the reaction between CF_3^+ and C_2H_3F, is shown in Fig. 2.8.

The reaction time cannot be measured independently, but can be calculated by dividing the reaction length, z, by the ion flow velocity, v_i. The reaction length is a known value defined by the point along the flow tube where the neutral reactant enters, and Smith and Adams have given a detailed account of how v_i can be measured [11]. An experimental value for $_2k$ (in cm^3 $molecule^{-1}$ s^{-1}) can therefore be calculated. Such measurements are repeated several times until a consistent result is achieved, and the estimated uncertainty in the value' obtained is ca. ±20%. Experimentally-measured bimolecular rate coefficients are referred to as k_{exp}.

In some reactions performed in the SIFT, an association product is observed. These reactions are pressure dependent due to the involvement of a third body, M, and so the rate equation includes a third-order rate coefficient, ${}_3k$:

$$A^+ + B + M \rightarrow AB^+ + M \tag{2.4}$$

$$rate = {}_3k\,[M][A^+][B] \tag{2.5}$$

where the square brackets represent concentrations of the respective species in molecule cm^{-3}, ${}_3k$ has units of cm^6 molecule^{-2} s^{-1}, and the *rate* has units of molecule cm^{-3} s^{-1}. In the SIFT M is most likely to be helium, and in Eq. 2.5 $[M]$ can be considered constant. A bimolecular rate coefficient is still measured for association reactions, as described above and shown in Fig. 2.8, but in these cases it is a *pseudo* second-order rate coefficient, ${}_2k'$. This value can be related to ${}_3k$ if the concentration of M is known:

$${}_2k' = {}_3k\,[M] \tag{2.6}$$

In association reactions discussed in this report the value for ${}_2k'$ is quoted because it can then be compared with other bimolecular rate coefficients. However, the rate coefficient of an association reaction is only valid at a given pressure of M, and so where ${}_2k'$ is quoted the pressure of helium recorded at the time is also given. Knowing the pressure of M allows $[M]$ to be calculated in much the same way as [B] is calculated, as described in Appendix IV.

2.2.3 The Determination of the Product Branching Ratios

Product branching ratios (BRs) are recorded in much the same way as the rate coefficient is measured, however, rather than the reactant ion signal, it is the *product* ion signals which are recorded as a function of neutral reactant concentration.

The individual product ion counts are converted into a percentage of the total product ion counts, and plotted using data analysis software. A line through the data points is added using a polynomial fit, and the %BR values are taken by extrapolating to zero neutral reactant concentration, which aims to eliminate any contributions from secondary reactions. An example of such a plot is provided in Fig. 2.9 for the reaction between CF_3^+ and C_2H_3F. The mass spectrum recorded for this reaction showed product peaks at m/z 27 ($C_2H_3^+$), 47 ($C_2H_4F^+$), 51 (CHF_2^+) and 53 ($CH_2F_2.H^+$). For the products at m/z 47 and 53 a BR of 0% is determined, indicating these are secondary products. The primary products for this reaction are m/z 27 ($C_2H_3^+$) and m/z 51 (CHF_2^+) with BRs of 75 and 25%, respectively.

The reported BR values have a ±20% uncertainty. This error is an estimate based on the variation in experimentally detected relative ion signals and the

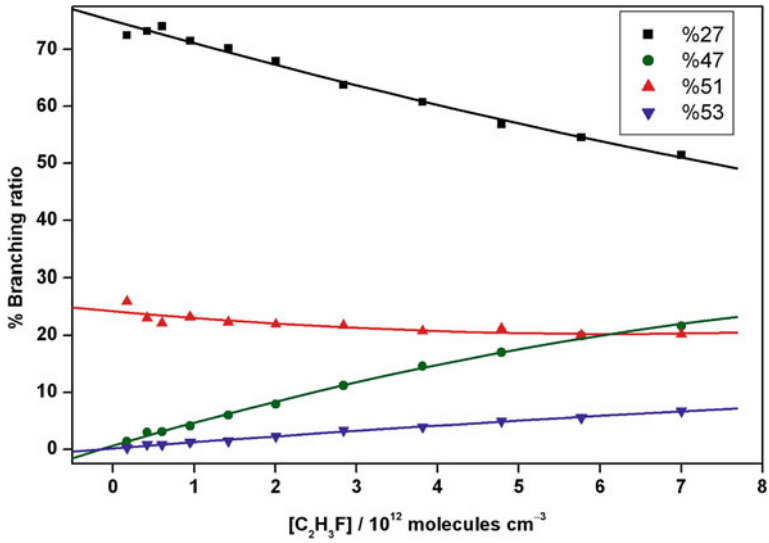

Fig. 2.9 A branching ratio (BR) plot for the products detected from the reaction between CF_3^+ and C_2H_3F. The products are indicated by their *m/z* values shown in the *top right* corner of the graph. At zero C_2H_3F concentration the BRs are 75 and 25% for the primary products $C_2H_3^+$ (*m/z* 27 in *black*) and CHF_2^+ (*m/z* 51 in *red*), respectively. The plots corresponding to *m/z* 47 (*green*) and *m/z* 53 (*blue*) show a BR of 0%, indicating they are secondary products

polynomial data fitting; it is noteworthy that ±20% is a modest estimate for the example data provided in Fig. 2.9.

References

1. Hulbert SL, Williams GP (2000) In: Samson JA, Ederer DL (eds) Vacuum ultraviolet spectroscopy. Academic, London
2. Howle CR, Ali S, Tuckett RP, Shaw DA, West JB (2005) Nucl Instrum Methods Phys Res Sect B 237:656
3. Simpson MJ, Tuckett RP (2011) Int Rev Phys Chem 30:197
4. Mitsuke K, Suzuki S, Imamura T, Koyano I (1990) J Chem Phys 93:8717
5. Mitsuke K, Suzuki S, Imamura T, Koyano I (1991) J Chem Phys 95:2398
6. Dehmer PM, Chupka WA (1975) J Chem Phys 62:4525
7. Dawson PH (1995) Quadrupole mass spectrometry and its applications. American Institute of Physics, NY
8. National Institute of Standards and Technology website (http://webbook.nist.gov/chemistry/)
9. Rogers NJ, Simpson MJ, Tuckett RP, Dunn KF, Latimer CJ (2010) PCCP 12:10971
10. Rogers NJ, Simpson MJ, Tuckett RP, Dunn KF, Latimer CJ (2010) Mol Phys 108:895
11. Smith D, Adams N (1988) Adv At Mo Phys 24:1
12. Graul ST, Squires RR (1988) Mass Spectrom Rev 7:263
13. Bohme DK (2000) Int J Mass Spectrom 200:97

Chapter 3
Vacuum Ultraviolet Negative Photoion Spectroscopy of SF_6, CF_4 and SF_5CF_3

This chapter focuses on the original data collected for trifluoromethyl sulphur pentafluoride (SF_5CF_3), however, the discussion extends to include the data also collected for the related molecules sulphur hexafluoride (SF_6) and tetrafluoromethane (CF_4). These results were collected in September 2006 at the Daresbury synchrotron radiation source on beamline 3.1. Although the majority of the data collection and analysis was performed by myself, it would not have been possible without the help from Richard Tuckett, Colin Latimer, Ken Dunn, Adam Hunniford, Michael Parkes, and David Shaw. This work was published in the *Journal of Chemical Physics* in 2008 [1]. The ion-pair cross section values reported in this chapter use the *correct* value for *M* (see Sects. 2.1.3 and 2.1.5), and they update the data given in this original publication.

3.1 Background Information

The presence of the super greenhouse gas trifluoromethyl sulphur pentafluoride, SF_5CF_3, in the atmosphere was first reported in 2000 by Sturges et al. [2]. Although the known atmospheric concentrations of SF_5CF_3 are very low, its lifetime is in the region of 1,000 years [3], and it is thought to have a Global Warming Potential 18,000 times greater than CO_2, absorbing strongly in the infrared between 750 and 1,250 cm^{-1} [4]. Of anthropogenic origin, SF_5CF_3 has been linked to SF_6 production and the manufacture of fluorochemicals [2], but in truth the main source of this potent greenhouse gas has not yet unambiguously been identified. Since its discovery, SF_5CF_3 has been the focus of numerous studies aimed to understand better its spectroscopic properties and reactivity. Laboratory experiments have confirmed the original estimates on the severity of SF_5CF_3 as a greenhouse gas [4–7], yet more work is required to gather a more comprehensive understanding of its sources and sinks. The original suggestion that SF_5 and CF_3 radicals combine to produce SF_5CF_3 in high voltage equipment [2]

M. J. Simpson, *Two Studies in Gas-Phase Ion Spectroscopy*, Springer Theses,
DOI: 10.1007/978-3-642-23129-2_3, © Springer-Verlag Berlin Heidelberg 2012

has since been disputed [8]; reactions mimicking these conditions showed no evidence of SF_5CF_3 production, although small amounts were detected when SF_6 reacted with some hydrofluorocarbons in a spark discharge [8]. Low energy electron attachment to SF_5CF_3 is dissociative [9–12] (Hotop (2007) private communication) and may provide a mechanism for atmospheric removal, but stratospheric UV photolysis is unlikely to contribute due to the absence of photoabsorption by SF_5CF_3 below 8 eV [5] and the high value of the SF_5–CF_3 bond dissociation energy (4.06 ± 0.45 eV at 0 K) [13, 14]. Following a new measurement of the ionisation energy of the CF_3 radical [15], this bond strength has since been refined to 3.86 ± 0.45 eV [16].

The surprisingly high value of the S–C bond has spurred investigations into the sink routes for SF_5CF_3 that might occur at higher altitudes in the mesosphere or ionosphere: ion–molecule reactions, electron attachment, and vacuum ultraviolet (VUV) photodissociation. Ion–molecule reaction studies have shown that both cations [17, 18] and anions [19] react rapidly with SF_5CF_3 and may therefore remove it from the upper atmosphere. However, the concentration of atmospherically-relevant ions (e.g. O^+, O_2^+, N^+, N_2^+) is so low that the pseudo-first-order rate constant for ion–molecule reactions, $\Sigma\, k_{ion}$[ion], is too small for this channel to contribute to any significant extent [16]. Low-energy electron attachment to SF_5CF_3 is relatively fast, 8.0×10^{-8} cm^3 molecule^{-1} s^{-1} at 298 K [12], and the absorption cross section at the Lyman-α wavelength (121.6 nm) is surprisingly high, ca. 10^{-17} cm^2 [3, 20]. By comparison with equivalent data for SF_6, it was shown that the electron attachment process is responsible for ∼99% of the removal of SF_5CF_3 in the mesosphere, VUV photodissociation ∼1% [3]. However, the long lifetime of SF_5CF_3 in the earth's atmosphere, ∼1,000 years, is not determined by these *microscopic* chemical processes that occur in the mesosphere, but by the much slower *macroscopic* meteorology that transports the pollutant from the earth's surface up into the mesosphere [3]. Advances made to 2006 to understand the chemical physics properties and environmental impact of SF_5CF_3 since its discovery in 2000 have been reviewed [16].

One of the possible products following VUV photoexcitation of SF_5CF_3 at 121.6 nm is ion-pair formation, e.g. $CF_3^+ + SF_5^-$. This chapter describes an experiment to detect anions following VUV excitation as a means to study the dynamics of electronically excited states of SF_5CF_3. Absolute cross sections for anion production and, using photoabsorption data [20], quantum yields have been evaluated for all the anion products observed. In addition to SF_5CF_3, the closely-related molecules SF_6 and CF_4 have also been investigated. The photoion-pair formation of SF_6 into $SF_5^+ + F^-$ and CF_4 into $CF_3^+ + F^-$ has been studied previously by Mitsuke et al. [21, 22] and Scully et al. [23]. The results presented here have seen a much larger number of anions than observed by these groups, and the data of Mitsuke et al. has allowed the SF_5CF_3 data to be put on an *absolute* scale (as outlined in Sect. 2.1.3).

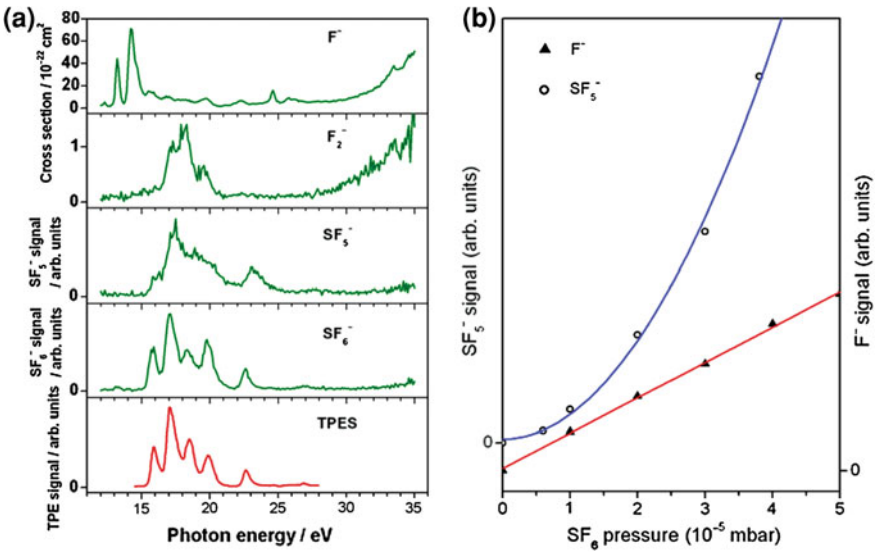

Fig. 3.1 **a** Cross sections for anion production following photoexcitation of SF_6. Note that the SF_5^- and SF_6^- spectra are not on an absolute scale. Ion yields were recorded as a function of photon energy between 12 and 35 eV with a step size of 0.1 eV and a wavelength resolution of 6 Å. This resolution is equivalent to 0.07 eV at 12 eV, 0.6 eV at 35 eV. The ion yields are compared with the threshold photoelectron spectrum of SF_6 [24]. **b** Pressure dependence of F^- and SF_5^- anion signals from SF_6. A linear pressure dependence indicates the anion arises from unimolecular ion-pair dissociation. A non-linear pressure dependence suggests a secondary process is involved in the anion formation

3.2 Sulphur Hexafluoride (SF_6)

The white light negative ion mass spectrum for SF_6 shows eight peaks corresponding to the anions F^- (100%), F_2^- (1%), SF^- (<1%), SF_2^- (<1%), SF_3^- (<1%), SF_4^- (<1%), SF_5^- (2%), and SF_6^- (67%). The relative signal strengths are shown in parentheses.

All anion signals from SF_6 recorded as a function of photon energy are presented in Fig. 3.1a, whilst Table 3.1 shows appearance energy (*AE*) values of the anions, their cross sections and quantum yields. For comparative purposes, Fig. 3.1a includes the threshold photoelectron spectrum (TPES) of SF_6 [24]. Poor signal strengths prevented ion yields for SF^-, SF_2^-, SF_3^-, and SF_4^- from being recorded. The F^- and F_2^- signals increase linearly with pressure, those of SF_5^- and SF_6^- non-linearly with the rate of change increasing as pressure increases. Figure 3.1b shows the plot of anion signal vs SF_6 pressure, with the example of F^- compared with SF_5^-. The linear dependence of the F^- and F_2^- anion signals suggest they result from unimolecular ion-pair dissociation, whereas the SF_5^- and SF_6^- signals are formed by a secondary process.

Table 3.1 Appearance energies, cross sections, and quantum yields for anions observed from photoexcitation of SF_6, CF_4, and SF_5CF_3

Molecule (IE[a]/eV)	Anion	AE[b]/eV	Cross section[c]/cm^2	Energy[d]/eV	Quantum yield[e]
SF_6	F^-	12.7	7.1×10^{-21}	14.2	2.4×10^{-4}
[15.1]	F_2^-	16.3	1.4×10^{-22}	18.3	1.9×10^{-6}
	SF_5^-	15.1	–[f]	17.5	–[g]
	SF_6^-	15.1	–[f]	17.1	–[g]
CF_4	F^-	13.0	1.4×10^{-21}	14.0	2.8×10^{-5}
[15.4]	F_2^-	20.1	4.0×10^{-23}	21.6	5.6×10^{-7}
SF_5CF_3	F^-	11.05	3.4×10^{-20}	16.9	3.4×10^{-4}
[12.9]	F_2^-	16.1	1.2×10^{-21}	17.9	1.1×10^{-5}
	SF^-	24.0	2.8×10^{-22}	28.8	2.4×10^{-6}
	SF_2^-	20.2	3.9×10^{-22}	24.2	2.5×10^{-6}
	SF_3^-	15.4	1.0×10^{-20}	17.6	1.0×10^{-4}
	SF_4^-	13.0	1.3×10^{-20}	14.1	1.7×10^{-4}
	SF_5^-	13.0	–[f]	17.0	–[g]

[a] Adiabatic ionisation energy. Values are taken from the observed onset of ionisation for SF_6 [26], CF_4 [24] and SF_5CF_3 [13]

[b] Observed appearance energy (AE) from this work. The error is estimated to be ±0.2 eV (except for F^- from SF_5CF_3 for which the error is ±0.05 eV), based on the resolution and step size used when recording ion yields

[c] Cross section for anion production following photoexcitation of the parent molecule

[d] Energy of strongest peak. It is at this energy, where appropriate, where cross section and quantum yield measurements are taken

[e] Quantum yields for anion production, obtained by dividing cross sections for anions (column 4) by total photoabsorption cross sections. The latter values are given for SF_6 [28], CF_4 [3] and SF_5CF_3 [20]

[f] Normalisation of the signal strength to determine an effective cross section is not possible because of the non-linear dependence of signal with pressure

[g] Quantum yield cannot be determined because the cross section is not defined

Previous ion pair experiments have also observed SF_5^- and SF_6^- from SF_6, their formation being attributed to electron attachment processes [21, 23]:

$$SF_6 + h\nu \rightarrow SF_6^+ + e^- \tag{3.1}$$

$$SF_6 + e^- \rightarrow SF_6^- \tag{3.2}$$

$$SF_6 + e^- \rightarrow SF_5^- + F \tag{3.3}$$

There can be little argument that reaction (3.2) must be responsible for the appearance of SF_6^-, and certainly SF_6 is a well-known electron scavenger, the rate coefficient at 300 K being $(2.38 \pm 0.15) \times 10^{-7}$ cm^3 s^{-1} [12], which attaches zero-energy electrons with a very large cross section [25]. Furthermore, Fig. 3.1a highlights the striking similarities between the SF_6^- spectrum and the SF_6 TPES. The only significant difference between the two is the peak at 19.9 eV, which appears stronger in the SF_6^- spectrum. The same comparison has been discussed by Yencha et al. [26] who compared their TPES of SF_6 with the ion yield of SF_6^- produced from SF_6 reported by Mitsuke et al. [21]; the same discrepancy in

relative signal strengths between the bands at 19.9 eV was observed. It is noted that the cross section for non-dissociative electron attachment to SF_6 peaks at very low energy characteristic of *s*-wave capture [25], but SF_6^- anions observed from reaction (3.2) will arise from *all* electrons integrated under the cross section vs electron energy distribution. By contrast, the TPES arises only from low-energy electrons detected within the bandpass of the threshold analyser, ca. 4 meV [24]. In practice, the experimentally-observed resolution will depend upon a convolution of the electron energy distribution and the resolution of the photon source. In both experiments the monochromator resolution, ca. 0.4 nm or 130 meV at 19.9 eV, will probably dominate. Notwithstanding this point, there is no reason why the intensities of the TPES and SF_6^- spectra in Fig. 3.1a should be *exactly* the same, and this may explain the small differences that have been observed both by us and by Yencha et al. [26]. We also note that this difference may not be a particular property of SF_6, because a similar inconsistency in intensities in the threshold photoelectron and parent anion yields has been observed with another polyatomic molecule which attaches electrons very rapidly, *cyclic*-C_5F_8 [27].

There are two observations from this work which provide evidence for SF_5^- arising predominantly from reaction (3.3). First, the SF_5^- signal increases non-linearly when recorded as a function of pressure, consistent with the two-step mechanism represented by reactions (3.1) and (3.3); an anion signal arising from ion-pair formation, $SF_6 + h\nu \rightarrow F^+ + SF_5^-$, would increase linearly with pressure. This is illustrated in Fig. 3.1b which shows clearly the contrast between the signal for the ion-pair product, F^-, and that for SF_5^-. Second, the SF_5^- ion yield shows many similarities to the TPES of SF_6 whereas that of F^- does not. However, these arguments do not exclude the possibility that a small amount of SF_5^- is produced via the ion-pair reaction above.

The following ion-pair reactions are suggested as mechanisms for F^- and F_2^- formation:

$$SF_6 \rightarrow F^- + SF_x^+ + (5-x)\,F \quad (x \leq 5) \tag{3.4}$$

$$SF_6 \rightarrow F_2^- + SF_x^+ + (4-x)\,F \quad (x \leq 4) \tag{3.5}$$

The calculated enthalpy changes for reaction (3.4) are 10.4, 14.9, 15.5, 19.7 and 23.7 eV for $x = 5$–1, respectively. For reaction (3.5) they are 13.6, 14.1, 18.4 and 22.4 eV for $x = 4$–1, respectively. F^- produced from reaction (3.4) has been observed before in the photon energy range 11 − 31 eV and a detailed analysis performed [21]. Below 14.9 eV the associated cation can only be SF_5^+, and the present work, Fig. 3.1a, is in very good agreement with this earlier study. Scully et al. have observed the ion-pair products F^- and F_2^- from SF_6 in the photon energy range 20–205 eV [23]. Both fragment ions show broad bands centred at 35.5 eV. Although not photoexciting SF_6 above 35 eV, this study clearly shows the onsets to these features.

The F_2^- spectrum in Fig. 3.1a shows features in the photon energy range 16–21 eV which have not been observed before. Below 18.4 eV it is not possible to say whether the associated cation is SF_4^+ or SF_3^+. The low F_2^- cross section is

reflected in its low signal strength, resulting in a poor signal-to-noise ratio. Three peaks are identified centered at 17.2, 18.2, and 19.7 eV. They most likely reflect the presence of Rydberg states which couple effectively to the ion-pair state, the peak energies therefore representing Rydberg transitions. Mitsuke et al. found that the most prominent features in the F^- ion yield at 13.2 and 14.3 eV were due to Rydberg transitions [21]. The peaks in the F_2^- ion yield at 17.2, 18.2, and 19.7 eV approximately match with peaks in the TPES of SF_6 at 17.1, 18.5, and 19.9 eV, respectively. A similar observation is made in the F_2^- ion yield from SF_5CF_3 (Sect. 3.4).

3.3 Tetrafluoromethane (CF_4)

The white light negative ion mass spectrum for CF_4 shows three peaks corresponding to the anions F^- (100%), CF^- (1%) and F_2^- (3%). The F^- and F_2^- signals were recorded as a function of photon energy and are shown in Fig. 3.2a, along with the TPES of CF_4 which is included for comparative purposes [24]. The corresponding data is shown in Table 3.1. The ion yield of CF^- was not obtained due to the poor signal strength. CF_4 has T_d symmetry, and the outer-valence electronic configuration is $\ldots(4a_1)^2\,(3t_2)^6\,(1e)^4\,(4t_2)^6\,(1t_1)^6$.

The F^- and F_2^- signals both increase linearly with pressure and the following ion-pair reactions are suggested as mechanisms for their formation:

$$CF_4 \rightarrow F^- + CF_x^+ + (3-x)\,F \quad (x \leq 3) \tag{3.6}$$

$$CF_4 \rightarrow F_2^- + CF_x^+ + (2-x)\,F \quad (x \leq 2) \tag{3.7}$$

The calculated enthalpy changes for reaction (3.6) are 11.3, 17.7 and 20.7 eV for $x = 3$–1, respectively; for (3.7) they are 16.3 and 19.3 eV for $x = 2$ and 1, respectively. The F^- ion yield recorded here is in good agreement with a previous study in the photon energy range 12–31 eV reported by Mitsuke et al. [22]. The F^- and F_2^- yields are also in good agreement with those reported by Scully [29] at higher resolution in the photon range 20–35 eV (Fig. 3.2a), but *absolute* cross sections were not determined in this earlier work.

It is immediately obvious from Fig. 3.2a that the F^- and F_2^- yields share a similar feature between 20 and 23 eV. Mitsuke et al. assigned this feature in the F^- yield to three Rydberg transitions ($3t_2 \rightarrow np$ where $n = 4$, 5 and 6 at energies 20.96, 21.16 and 21.45 eV, respectively) converging on the third excited valence state of CF_4^+ ($\tilde{C}^2T_2$) [22]. The Rydberg states excited at these energies would then couple to an ion-pair state which dissociates to F^-, the corresponding cation, and any neutral fragments. The presence of Rydberg states in this energy region has also been observed in a high resolution threshold photoelectron study of CF_4 by Yencha et al. [30]. Autoionising structure is observed from 20.3 to 21.6 eV, preceding the onset of the $\tilde{C}^2T_2$ state of CF_4^+. This can be observed in the TPES in

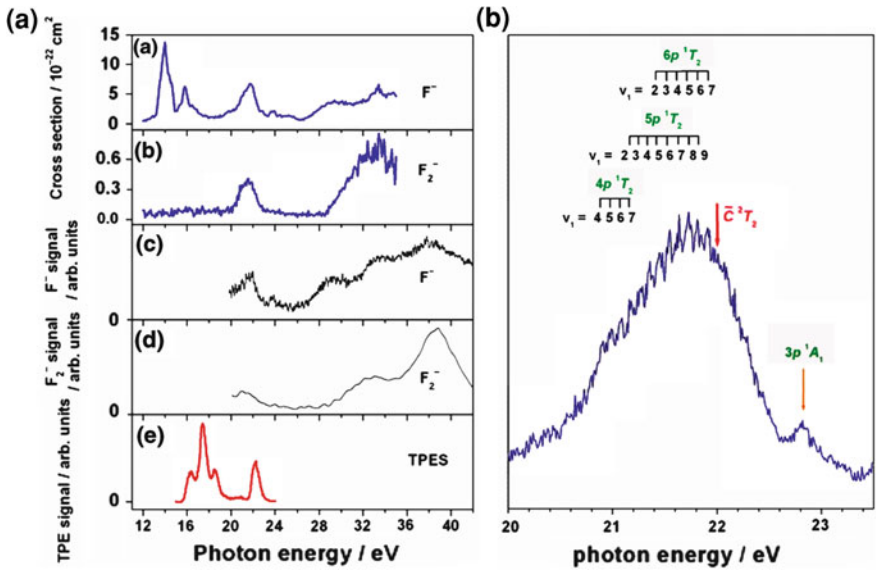

Fig. 3.2 **a** Cross sections for anion production following photoexcitation of CF_4. (*a*) and (*b*) F^- and $F_2{}^-$ ion yields recorded as a function of photon energy between 12 and 35 eV with a step size of 0.1 eV and a wavelength resolution of 6 Å (this work). This resolution is equivalent to 0.07 eV at 12 eV, 0.6 eV at 35 eV. The cross sections are on an absolute scale. (*c*) and (*d*) F^- and $F_2{}^-$ ion yields from Scully [29] recorded over a narrower energy range at a higher resolution of 0.5 and 2.0 Å, respectively. The cross sections are now on a relative scale. (*e*) Threshold photoelectron spectrum of CF_4 for comparison [24]. **b** F^- anion signal from CF_4 in the photon energy range 20–23.5 eV with a step size of 0.01 eV and a wavelength resolution of 2 Å. This resolution is equivalent to 0.1 eV at 22 eV. Vibrational progressions of the ν_1 totally symmetric stretching mode in CF_4^* *n*p Rydberg states converging on the $CF_4{}^+$ ($\tilde{C}^2T_2$) state are shown by *black* ticks [22]. The vertical ionisation energy for $CF_4{}^+$ ($\tilde{C}^2T_2$) is 22.04 eV [31], shown here by a *red* arrow. A new feature is observed at 22.82 eV which is assigned to a Rydberg state converging to $CF_4{}^+$ ($\tilde{D}^2A_1$), shown by the *orange* arrow

Fig. 3.2a as a slight rise above the baseline in the same energy range. It is therefore proposed that Rydberg states converging to $CF_4^+\tilde{C}^2T_2$ couple to ion-pair states which dissociate to both F^- *and* $F_2{}^-$. At 21.8 eV the F^- cross section is ca. 16 times larger than that for $F_2{}^-$. This may reflect the degree of coupling between states and/or the steric disadvantage on forming an extra bond to produce $F_2{}^-$.

The feature between 20 and 23.5 eV in the F^- ion yield has been recorded with better resolution, and is shown in Fig. 3.2b. It shows the CF_4^* 4, 5, and 6p overlapping Rydberg states converging on the $CF_4^+\tilde{C}^2T_2$ state. Fine structure is also observed in the spectrum which shows the ν_1 totally symmetric stretching mode in CF_4^*. These progressions have been observed before in the ion-pair study by Mitsuke et al., and Table 3.2 compares the two sets of data, listing energy positions, the resulting energy spacings, and the vibrational quantum number assignments. The assignments for these Rydberg transitions and for the vibrational progressions are taken directly

Table 3.2 Peak positions and energy spacings, in eV, for the vibrational states observed in the F^- ion yield from CF_4 in the photon energy range 20.9–22.1 eV

$3t_2 \rightarrow 4p^1T_2$					$3t_2 \rightarrow 5p^1T_2$					$3t_2 \rightarrow 6p^1T_2$				
ΔE^a	E^b		E^c	ΔE^d	ΔE^a	E^b		E^c	ΔE^d	ΔE^a	E^b		E^c	ΔE^d
		$(\upsilon_1, 0, 0, 0)^e$												
		υ_1 =												
	20.90	4	20.87											
0.09				0.09										
	20.99	5	20.96											
0.09				0.11										
	21.08	6	21.07				$(\upsilon_1, 0, 0, 0)^e$							
0.1				0.09			υ_1 =							
	21.18	7	21.16			21.18	2	21.16						
					0.09				0.07					
						21.27	3	21.23						
					0.09				0.11					
						21.36	4	21.34				$(\upsilon_1, 0, 0, 0)^e$		
					0.09	*21.38*			0.11			υ_1 =		
						21.45	5	21.45			21.45	2	21.45	
					0.10	*21.48*			0.09	0.10	*21.48*			0.09
						21.53					*21.53*			
						21.55	6	21.54			21.55	3	21.54	
					0.09				0.10	0.09				0.10
						21.64	7	21.64			21.64	4	21.64	
					0.09				0.07	0.09				0.07
						21.73	8	21.71			21.73	5	21.71	
					0.08	*21.75*			0.11	0.08	*21.75*			0.11
						21.81	9	21.82			21.81	6	21.82	

(continued)

Table 3.2 (continued)

$3t_2 \rightarrow 4p^1T_2$				$3t_2 \rightarrow 5p^1T_2$				$3t_2 \rightarrow 6p^1T_2$				
ΔE^a	E^b		E^c	ΔE^d	ΔE^a	E^b	E^c	ΔE^d	ΔE^a	E^b		E^c	ΔE^d
						21.85			0.10	*21.85*			0.09
										21.91	7	21.91	
													0.09
											8	22.00	
													0.08
											9	22.08	

[a] Energy spacing between vibrational states, in eV, taken from this work
[b] Energy of peak maximum, in eV, taken from this work. Values in italics show energy positions of weak shoulder features
[c] Energy of peak maximum, in eV, taken from the work by Mitsuke et al. [22]
[d] Energy spacing between vibrational states, in eV, taken from the work of Mitsuke et al. [22]
[e] Assignments for the vibrational quantum number in the ν_1 mode of CF_4*. These assignments are taken from the ion-pair study of Mitsuke et al. [22] and the photoabsorption study of Lee et al. [32]

from the work of Mitsuke et al. [22], who performed a quantum defect analysis, such that the resulting quantum defect is almost exactly the same for all three vibronic assignments, a value close to 0.60. This analysis also agrees with the photoabsorption study of Lee et al. [32]. Photoelectron spectroscopy shows a vibrational progression in the band representing the $\tilde{C}^2T_2$ state of CF_4^+ with a spacing of about 90 meV, assigned to the ν_1 mode [30, 31]. The vibrational spacing of the progressions observed in the *np* Rydberg states in the F^- ion yield converging to this same ionic state are also about 90 meV, as expected.

Figure 3.2b shows an additional feature at 22.82 eV which has not been seen in the previous study. It is assigned here as the $4a_1 \rightarrow 3p$ valence-Rydberg transition. This assignment uses the vertical ionisation energy of 25.11 eV for the fourth excited state of CF_4^+ $\tilde{D}^2A_1$ [31], and the peak position of the observed feature as 22.82 eV. The resulting term value of 2.29 leads to a quantum defect value of 0.56. This assignment is consistent with the observation of features in the F^- ion yield at 24.0 and 24.45 eV, which Mitsuke et al. assign as $4a_1 \rightarrow 4p$ and $4a_1 \rightarrow 5p$ Rydberg transitions respectively [22], the next two members of this *p* Rydberg series.

The highest outer-valence electronic state of CF_4^+ is the $\tilde{D}^2A_1$ state at 25.1 eV, whereas the next discrete state in the photoelectron spectrum corresponding to ionisation of the $2t_2$ inner-valence electron is the $\tilde{E}^2T_2$ state at 40.3 eV [24, 31]. Both the F^- and F_2^- yields increase above 25 eV, and the spectral features at higher energies are more clearly observed in the work of Scully [29] which extends up to 110 eV.

3.4 Trifluoromethyl Sulphur Pentafluoride (SF_5CF_3)

The white light negative ion mass spectrum for SF_5CF_3 shows eight peaks corresponding to the anions F^- (100%), CF^- (1%), F_2^- (2%), SF^- (1%), SF_2^- (1%), SF_3^- (1%), SF_4^- (2%) and SF_5^- (14%). With the exception of SF_5^-, all of the anion signals increase linearly with pressure. SF_5^- formed following photoexcitation of SF_5CF_3 shows a similar pressure behaviour to SF_5^- formation from SF_6, which is discussed in more detail in Sect. 3.2.

Ion yields for the anions resulting from ion-pair formation are presented in Fig. 3.3, the data in Table 3.1. The quantum yields are all in the range 10^{-6}–10^{-4}, consistent with those expected for a large polyatomic molecule [33, 34]. The ion yield of F^- below 12 eV was recorded with a LiF window in place to display the threshold region more clearly, and an appearance energy (*AE*) value of 11.05 ± 0.05 eV is determined.

The following reactions are suggested as the main sources of formation of the anions:

$$SF_5CF_3 \rightarrow F^- + CF_3^+ + SF_4 \tag{3.8}$$

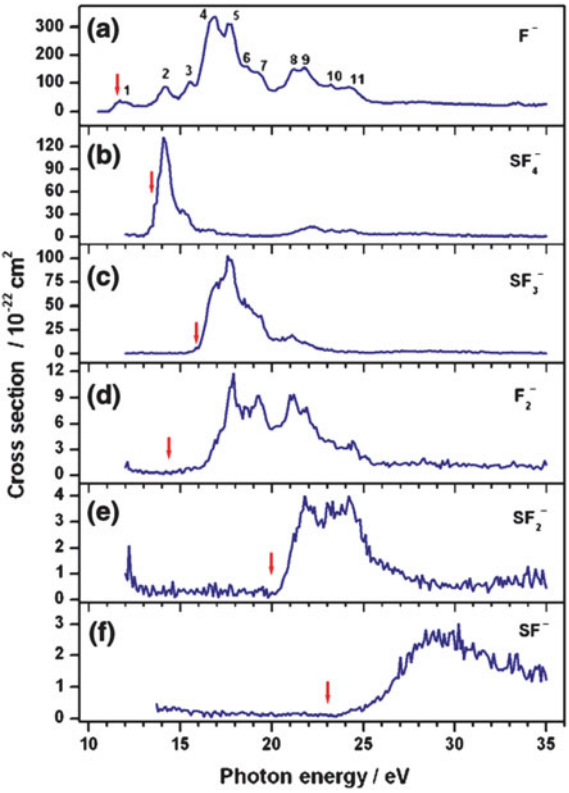

Fig. 3.3 Cross sections for anion production following photoexcitation of SF_5CF_3. Ion yields were recorded as a function of photon energy between 10.5 and 35.0 eV with a step size of 0.1 eV and a wavelength resolution of 6 Å. This resolution is equivalent to 0.05 eV at 10.5 eV and 0.6 eV at 35 eV. Solid *red* arrows in spectra (*a*)–(*f*) show enthalpy values of the thermochemical thresholds calculated for reactions (3.8–3.13), respectively

$$SF_5CF_3 \rightarrow SF_4^- + CF_3^+ + F \tag{3.9}$$

$$SF_5CF_3 \rightarrow SF_3^- + CF_3^+ + F + F \tag{3.10}$$

$$SF_5CF_3 \rightarrow F_2^- + CF_3^+ + SF_3 \tag{3.11}$$

$$SF_5CF_3 \rightarrow SF_2^- + CF_3^+ + 3F \tag{3.12}$$

$$SF_5CF_3 \rightarrow SF^- + CF_3^+ + 4F \tag{3.13}$$

In all cases the cation formed is CF_3^+, the associated anion therefore resulting from the SF_5 part of SF_5CF_3. This is reflected in the results; five different anions containing sulphur are detected compared to one containing carbon, CF^-, which was only just detected above the sensitivity limit of the apparatus.

The S–C bond is most likely to be the weakest in the molecule, the 0 K dissociation energy measured as 3.86 ± 0.45 eV [16]. In addition, Xu et al. [35] have calculated bond dissociation energies in SF_5CF_3, resulting in D^o $(SF_5CF_2 - F) > D^o$ $(F - SF_4CF_3) > D^o$ $(SF_5 - CF_3)$. One cannot say conclusively that reactions (3.8–3.13) are responsible for *all* of the detected anion

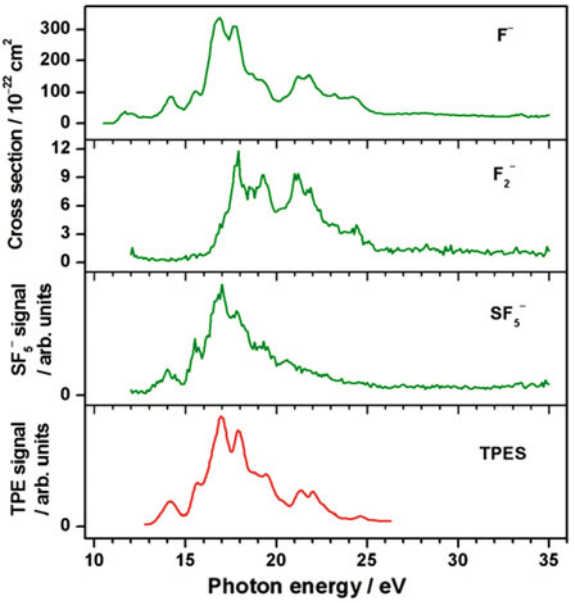

Fig. 3.4 Cross sections for anion production following photoexcitation of SF_5CF_3. Note that the SF_5^- spectrum is not on an absolute scale. Ion yields were recorded as a function of photon energy between 10.5 and 35.0 eV with a step size of 0.1 eV and a wavelength resolution of 6 Å. This resolution is equivalent to 0.05 eV at 10.5 eV, 0.6 eV at 35 eV. The ion yields are compared with the threshold photoelectron spectrum (shown in *red*) of SF_5CF_3 [13]

signals across the complete energy range studied. Certainly, more channels become energetically accessible at higher energies. It is, however, interesting that the thermochemical thresholds for reactions (3.8–3.13) approximately reflect the observed *AE* values (Table 3.1). The only apparent exception is reaction (3.11), F_2^- production, where steric constraints on forming a new bond could be responsible. This trend can be visualised in Fig. 3.3 by vertical arrows representing the enthalpies of the calculated thermochemical thresholds. These values for $\Delta_r H°_{298}$ are 11.5, 13.4, 16.0, 14.3, 20.0 and 23.0 eV for reactions (3.8–3.13), respectively. No errors are given but there is significant uncertainty in some of the $\Delta_f H°_{298}$ values used, which probably explains why the calculated *AE* is sometimes greater than the experimental value (e.g. F^- and SF_4^- in Fig. 3.3a and b).

The formation of F^- and F_2^- over the complete energy range 11–35 eV are unlikely to result exclusively from reactions (3.8) and (3.11) respectively, whereas the channels available to form the sulphur-containing anions are fewer. Indeed, the ion yields for F^- and F_2^- do show structure over a much wider energy range than those of SF_x^- ($x = 1$–4).

The ion yields for F^-, F_2^- and SF_5^- are presented in Fig. 3.4 and compared to the TPES of SF_5CF_3 [13]. SF_5^- is the only anion detected which is *not* associated with ion-pair formation. Three comparisons can be made between the behaviour of SF_5^- formed from SF_5CF_3 and SF_5^- formed from SF_6 (also see Sect. 3.2). First, the SF_5^- signal increases non-linearly with pressure, with the rate of change of signal increasing as the pressure increases. Second, electron attachment to SF_5CF_3 is dissociative forming SF_5^- (and CF_3) as the only significant channel [9–12]

(Hotop H (2007) private communication). Third, the ion yield of SF_5^- shows many similarities to the TPES of SF_5CF_3. It is therefore proposed that the dominant mechanism for the production of SF_5^- from SF_5CF_3 is dissociative electron attachment following photoionisation as the source of low-energy electrons:

$$SF_5CF_3 + h\nu \rightarrow SF_5CF_3^+ + e^- \tag{3.14}$$

$$SF_5CF_3 + e^- \rightarrow SF_5^- + CF_3 \tag{3.15}$$

As shown in Fig. 3.4, the F^- and F_2^- ion yields also show similarities to the TPES of SF_5CF_3. Due to its higher signal-to-noise ratio, it is in the F^- spectrum where these similarities are most obvious. In the photon energy range 13–23 eV the agreement between peak positions is good and the relative signal strengths show only small differences. The resemblance of the F^- ion yield to the TPES could be explained by a process involving electron attachment being significant in F^- formation. This has been the case in the discussion above, explaining the formation of SF_5^- from both SF_6 and SF_5CF_3. However, the F^- signal rises *linearly* with increasing gas pressure. This suggests strongly that a primary process, i.e. ion-pair formation to $F^- + SF_4CF_3^+$ (or $F^- + CF_3^+ + SF_4$), is dominant.

For the purposes of this discussion the features in the F^- ion yield are labelled 1–11 in Fig. 3.3a. The experimental *AE* (F^-) is 11.05 eV, and this anion gives rise to peak 1 centred at 11.7 eV. This peak occurs below the onset of ionisation for SF_5CF_3, reported as 12.9 eV [13], so the presence of photoelectrons from reaction (3.14) is not relevant. The energy of peak 1 is close to peaks observed in the SF_5CF_3 photoabsorption [20] and total fluorescence yield [36] spectra at 11.4 eV. These two studies give different assignments to this transition. Holland et al. [20] assign it to a blend of several valence–valence transitions, whilst Ruiz et al. [36] assign it to a valence-Rydberg transition from the 29a' highest-occupied molecular orbital of SF_5CF_3 to a 4*s* Rydberg orbital. The contribution of fluorescence at this energy was reported to originate from the CF_3 fragment, following dissociation of $SF_5CF_3^*$ and production of an excited electronic state of the CF_3 radical. In addition, this was the most intense band observed within the photon energy range studied of 10−28 eV [36]. It must represent a transition to the same intermediate state which predissociates into states yielding both CF_3^* and F^- anions. The ion-pair quantum yield at the maximum of the peak in the F^- ion yield at 11.7 eV is $\Phi = 1.5 \times 10^{-4}$. This small value, coupled with the fact that fluorescence from $SF_5CF_3^*$ is unlikely to have a large quantum yield, suggests strongly that predissociation into neutral fragments is the favoured process at this energy. A similar conclusion was reached by Shaw et al. [37] in a comparable study of the dissociation dynamics of Rydberg states of some substituted methane molecules. The agreement of peak positions in SF_5CF_3 between the photoabsorption spectrum [20], the total fluorescence yield [36], and the F^- ion yield extends up to 17 eV, but above this energy similarities between the spectra are less clear.

Table 3.3 F^- ion-pair quantum yields (Φ_F-) at energies below and above the onsets of ionisation for SF_6, CF_4 and SF_5CF_3. Cross sections from this work are normalised to photoabsorption cross sections for SF_6 [28], CF_4 [3] and SF_5CF_3 [20] to give values for Φ_F-

Molecule	Φ_F- below onset of ionisation	Φ_F- above onset of ionisation
SF_6	2.4×10^{-4} at 14.2 eV	1.5×10^{-5} at 24.6 eV
CF_4	2.8×10^{-5} at 14.0 eV	9.3×10^{-6} at 21.8 eV
SF_5CF_3	1.5×10^{-4} at 11.7 eV	3.4×10^{-4} at 16.9 eV

It is interesting that the F^- ion-pair quantum yield does not decrease above the onset of ionisation of SF_5CF_3, 12.9 eV. Features 1 and 4 at 11.7 and 16.9 eV, for example, have $\Phi = 1.5 \times 10^{-4}$ and 3.4×10^{-4}, respectively (Table 3.3). As a result of significant photoabsorption leading to ionisation, one would expect the ion-pair quantum yield to decrease, as observed for both SF_6 and CF_4 (Table 3.3). However, above the ionisation energy of SF_5CF_3 the F^- ion yield increases, approximately matching the shape of the TPES. In fact features 2–11 of Fig. 3.3a occur at, or just below, vertical ionisation energies in the TPES of SF_5CF_3 [20]. Only feature 1 does not follow this trend. It seems unlikely that valence states of SF_5CF_3 which predissociate into ion pairs coincidentally lie very close to the ionisation thresholds, certainly across this large energy range. It is much more likely that Rydberg states play an important role. Certainly the F^- ion yield would be explained if coupling to ion-pair states was more significant from Rydberg states close to the ionisation thresholds than from those lower in energy. Contributions to the F^- ion yield from low-lying Rydberg states would then be the dominant cause of peak 1. F^- ions produced via high-lying Rydberg states would be dominant at higher energy, and hence responsible for features 2−11 in the ion yield. If this is true, it negates the generally accepted rule that it is low-*n*, and not high-*n*, Rydberg states which interact most strongly with ion-pair states. However, most of the ion-pair experiments on polyatomics to date have studied halogenated molecules where the lowest ion-pair threshold lies *below* the first ionisation energy [34], so by definition it is the low-*n* states which have been the most widely studied. The difficulties in assigning peaks in the total fluorescence yield spectrum of SF_5CF_3 have already been noted by Ruiz et al. [36], and at our modest resolution there are several valence-Rydberg transitions which could be assigned to peaks 2−11 in Fig. 3.3a. A much higher-resolution spectrum would be needed for such a large molecule in order to give definitive assignments.

An alternative mechanism to reaction (3.8) for production of F^- might be via dissociative electron attachment to SF_5CF_3,

$$e.g. \qquad SF_5CF_3 + e^- \rightarrow F^- + SF_4 + CF_3 \qquad (3.16)$$

This is rejected because it is well known that the only product of low-energy electron attachment to SF_5CF_3 is SF_5^- (reaction 3.15) [9–12] (Hotop H (2007)

private communication), and note the huge signal of the F^- ion yield to the relatively weak signal of SF_5^- (Fig. 3.4).

This analysis also extends to the ion yields for SF_4^-, SF_3^-, F_2^-, SF_2^-, and SF^-; the peak positions and the extent of structure observed for these anions can be explained in the same way as the F^- ion yield. The SF_4^-, SF_3^-, and SF_2^- ion yields show less structure than is seen from F^-. In the energy regions where peaks are observed, their energies agree with those in the F^- ion yield, and hence with vertical ionisation energies. It is suggested here that the number of available ion-pair states reflects the structure seen in the ion yields. SF_4^-, for example, is likely to arise from reaction (3.9) only. It is certainly the most sterically viable channel. Coupling of high-lying Rydberg states to this ion-pair state will give rise to the peaks in the SF_4^- yield at 14 and 15 eV (Fig. 3.3b). Lack of structure above 16 eV represents the point where this ion-pair state no longer couples significantly to Rydberg states. SF_3^- and SF_2^- also arise through coupling of high-lying Rydberg states to an appropriate ion-pair state, and only over a limited energy range above the onset. In contrast, many more dissociation channels will be available to yield the anions F^- and F_2^-. As a result, structure in both ion yields extends extensively from onset up to 25 eV. Finally, it is noted that shape resonances have been observed in the yields of many anions in both SF_6 and CF_4 above 25 eV [23, 29]. There is no obvious evidence for such peaks in our ion yields from SF_5CF_3, but it would be surprising if they were not present.

3.5 Conclusions

The peaks in the F^- yields from both SF_6 and CF_4 have been assigned to Rydberg transitions [21, 22], and the assignments are not repeated here. However, there is some disagreement whether the transitions observed in the VUV absorption spectrum of SF_5CF_3 [7, 20], and indeed the CF_3^* fluorescence excitation spectrum [36], are due to intravalence or Rydberg transitions. Peaks in the absorption and electron energy loss spectra of SF_5CF_3 are assigned by Limao-Vieira et al. [7] to valence-Rydberg transitions, and quantum defects determined. Ruiz et al. [36] also assign peaks in the absorption spectrum that led to CF_3^* fluorescence to valence-Rydberg transitions. Holland et al. [20], however, assign the main peaks in the absorption spectrum to valence–valence transitions. The spectra presented here observe a different exit channel, i.e. photodissociation of excited states of SF_5CF_3 to production of *anions*. However, the primary excitation process in all these experiments is the same, and their assignment to Rydberg transitions is favoured, for two reasons. First, all previous work on ion-pair production from polyatomic molecules has preferred the process of Rydberg state photoexcitation, followed by predissociation into an ion-pair state [34]. Second, apart from the low-energy peak in the F^- yield at 11.7 eV below the ionisation energy of SF_5CF_3, all the F^- peaks have energies very close to peaks in the TPES of this molecule. Since it is Rydberg states that have energies converging on ground and excited electronic states of

$SF_5CF_3^+$, it seems very likely that these F^- peaks correspond to photoexcitation of Rydberg states.

A summary of the numerical information obtained from the ion yields from SF_6, CF_4 and SF_5CF_3 is given in Table 3.1, listing *AE*s of anions, cross sections and quantum yields. The anions observed from SF_5CF_3 were all seen in either the SF_6 or CF_4 study. The signal strengths from the SF_x^- anions, however, are stronger from SF_5CF_3 than from SF_6, allowing their ion yields to be recorded. Unsurprisingly, F^- and F_2^- are observed from all three molecules. The most prominent features in the F^- ion yields from SF_6 and CF_4 occur below the onset of ionisation. This is not the case for F^- from SF_5CF_3. This observation is clearly demonstrated in Table 3.3 when comparing the ion-pair quantum yields of F^- above and below the onset of ionisation for these three molecules.

References

1. Simpson MJ, Tuckett RP, Dunn KF, Hunniford CA, Latimer CJ, Scully SWJ (2008) J Chem Phys 128:124315
2. Sturges WT, Wallington TJ, Hurley MD, Shine KP, Sihra K, Engel A, Oram DE, Penkett SA, Mulvaney R, Brenninkmeijer CAM (2000) Science 289:611
3. Chim RYL, Kennedy RA, Tuckett RP (2003) Chem Phys Lett 367:697
4. Kendall PA, Mason NJ, Buchanan GA, Marston G, Tegeder P, Dawes A, Eden S, Limao-Vieira P, Newnham DA (2003) Chem Phys 287:137
5. Kendall PA, Mason NJ (2001) J Electron Spectrosc Relat Phenom 120:27
6. Nielsen OJ, Nicolaisen FM, Bacher C, Hurley MD, Wallington TJ, Shine KP (2002) Atmos Environ 36:1237
7. Limao-Vieira P, Eden S, Kendall PA, Mason NJ, Giuliani A, Heinesch J, Hubin-Franskin MJ, Delwiche J, Hoffmann SV (2004) Int J Mass Spectrom 233:335
8. Huang L, Zhu L, Pan X, Zhang J, Ouyang B, Hou H (2005) Atmos Environ 39:1641
9. Kennedy RA, Mayhew CA (2001) Int J Mass Spectrom 206:AR1
10. Sailer W, Drexel H, Pelc A, Grill V, Mason NJ, Illenberger E, Skalny JD, Mikoviny T, Scheier P, Märk TD (2002) Chem Phys Lett 351:71
11. Miller TM, Arnold ST, Viggiano AA, Knighton WB (2002) J Chem Phys 116:6021
12. Mayhew CA, Critchley A, Howse DC, Mikhailov V, Parkes MA (2005) Eur Phys J D 35:307
13. Chim RYL, Kennedy RA, Tuckett RP, Zhou W, Jarvis GK, Collins DJ, Hatherly PA (2001) J Phys Chem A 105:8403
14. Chim RYL, Kennedy RA, Tuckett RP, Zhou W, Jarvis GK, Mayhew CA, Collins DJ, Hatherly PA (2002) Surf Rev Lett 9:129
15. Garcia GA, Guyon PM, Powis I (2001) J Phys Chem A 105:8296
16. Tuckett RP (2006) Adv Fluorine Sci 1:89
17. Atterbury C, Kennedy RA, Mayhew CA, Tuckett RP (2001) Phys Chem Chem Phys 3:1949
18. Atterbury C, Critchley A, Kennedy RA, Mayhew CA, Tuckett RP (2002) Phys Chem Chem Phys 4:2206
19. Arnold ST, Miller TM, Viggiano AA, Mayhew CA (2003) Int J Mass Spectrom 223:403
20. Holland DMP, Shaw DA, Walker IC, McEwen IJ, Apra E, Guest MF (2005) J Phys B 38:2047
21. Mitsuke K, Suzuki S, Imamura T, Koyano I (1990) J Chem Phys 93:8717
22. Mitsuke K, Suzuki S, Imamura T, Koyano I (1991) J Chem Phys 95:2398
23. Scully SWJ, Mackie RA, Browning R, Dunn KF, Latimer CJ (2002) J Phys B 35:2703

24. Creasey JC, Jones HM, Smith DM, Tuckett RP, Hatherly PA, Codling K, Powis I (1993) Chem Phys 174:441
25. Christophorou LG, Olthoff JK (2000) J Phys Chem Ref Data 29:267
26. Yencha AJ, Thompson DB, Cormack AJ, Cooper DR, Zubek M, Bolognesi P, King GC (1997) Chem Phys 216:227
27. Parkes MA (2007) Ph.D. thesis, University of Birmingham, (http://etheses.bham.ac.uk/74/)
28. Holland DMP, Shaw DA, Hopkirk A, MacDonald MA, McSweeney SM (1992) J Phys B 25:4823
29. Scully SWJ (2004) Ph.D. thesis, Queen's University Belfast
30. Yencha AJ, Hopkirk A, Hiraya A, Dujardin G, Kvaran A, Hellner L, Besnard-Ramage MJ, Donovan RJ, Goode JG, Maier RRJ, King GC, Spyrou S (1994) J Electron Spectrosc Relat Phenom 70:29
31. Holland DMP, Potts AW, Trofimov AB, Breidbach J, Schirmer J, Feifel R, Richter T, Godehusen K, Martins M, Tutay A, Yalcinkaya M, Al-Hada M, Eriksson S, Karlsson L (2005) Chem Phys 308:43
32. Lee LC, Phillips E, Judge DL (1977) J Chem Phys 67:1237
33. Suits AG, Hepburn JW (2006) Annu Rev Phys Chem 57:431
34. Berkowitz J (1996) VUV and Soft X-Ray Photoionization. In: Becker U, Shirley DA (eds) Plenum Press, New York, Chap. 8
35. Xu W, Xiao C, Li Q, Xie Y, Schaefer HF (2004) Mol Phys 102:1415
36. Ruiz JA, Kivimäki A, Stankiewicz M, Garcia EM, Coreno M, Ali S, Koperski J, Rachlew E, Serrano G, Feyer V, Tuckett RP (2006) Phys Chem Chem Phys 8:5199
37. Shaw DA, Holland DMP, Walker IC (2006) J Phys B 39:3549

Chapter 4
Vacuum Ultraviolet Negative Photoion Spectroscopy of CF_3Cl, CF_3Br and CF_3I

This chapter presents and analyses the data collected for trifluorochloromethane (CF_3Cl), trifluorobromomethane (CF_3Br) and trifluoroiodomethane (CF_3I). This series of molecules will be referred to as the CF_3X series, where X = Cl, Br or I, and the main aim of this study is to compare the data and see the effects and resulting trends of changing substituent X. These results were collected in September 2006 at the Daresbury synchrotron radiation source on beamline 3.1. Many thanks go to Professors Richard Tuckett and Colin Latimer, Drs Ken Dunn, Adam Hunniford, and David Shaw for their individual contributions in the data collection. I also thank Richard Tuckett and Michael Parkes for their part in analysing the data. This work was published in the *Journal of Chemical Physics* in 2009 [1].

4.1 Background Information

CF_3Cl, CF_3Br and CF_3I are all greenhouse gases and potential ozone depleters. The use of these molecules in industrial applications has inevitably led to their release into the atmosphere. For example, CF_3Cl (CFC-13) was used as a refrigerant and CF_3Br (halon 1301) as a fire suppressor, but both are now banned in accordance with the Montreal Protocol [2]. CF_3I is considered less environmentally unfriendly than CF_3Cl or CF_3Br and it is expected to have a relatively low atmospheric lifetime [3]. This increases the potential for CF_3I applications, for example, as a plasma etching gas [4] and as a possible replacement for CF_3Br in fire extinguishing systems [5].

This series of CF_3X molecules have C_{3v} symmetry, and the main effect of a change in the substituent X is the elongation and subsequent weakening of the C–X bond. The effect on the overall electronic structure of the molecule on changing X is not dramatic, since the orbitals of the X atom show little mixing with the CF_3 orbitals. The evidence for this property is best observed from photoelectron

M. J. Simpson, *Two Studies in Gas-Phase Ion Spectroscopy*, Springer Theses,
DOI: 10.1007/978-3-642-23129-2_4, © Springer-Verlag Berlin Heidelberg 2012

spectroscopy, where HeI, HeII, and threshold photoelectron (TPE) spectra have been reported for CF_3Cl, CF_3Br and CF_3I [6–11]. Bands observed in the spectra from ionisation of an *X* lone pair or a C–*X* bonding electron shift to lower energy as *X* gets larger. However, bands observed from ionisation of an F lone pair or a C–F bonding electron are very similar in energy for CF_3Cl, CF_3Br and CF_3I. Absorption data on CF_3Cl have been well studied by photoabsorption spectroscopy [12, 13] and electron energy loss spectroscopy (EELS) [14, 15]. More recent absorption [16] and EELS [17] studies compare data for all three CF_3X molecules. While most of this work is restricted to energies <15 eV, absorption data for CF_3Cl is reported up to 25 eV [13, 18], and for CF_3Br up to 30 eV [18]. Vacuum-UV fluorescence spectroscopy has also been studied for CF_3X molecules, where X = F, H, Cl, and Br [19] and where X = F, H, Cl, Br, and I [18].

The VUV photoion-pair formation of CF_3Cl has been studied previously using a quadrupole mass analyser by Schenk et al. [20], but this is the first report of ion-pair production following photoexcitation of CF_3Br and CF_3I.

4.2 The Anions Observed from CF_3Cl, CF_3Br and CF_3I

The negative ion mass spectra for the three CF_3X (X = Cl, Br, I) molecules recorded with white light at 0 nm all show the presence of the same seven anions; F^-, X^-, F_2^-, FX^-, CF^-, CF_2^- and CF_3^-. F^- and X^- are always the strongest signals. The remaining five anions were detected just above the sensitivity level of the apparatus, the signals being ≤ca. 2% of that of the dominant anion (F^- or X^-). It was observed that the X^- relative signal strengths increased with increasing mass and size of *X*; Cl^- = 18%, Br^- = 37%, and I^- = 100% from CF_3Cl, CF_3Br, and CF_3I, respectively, of the strongest anion signal (F^- from CF_3Cl and CF_3Br, I^- from CF_3I). Of all the anions, only FI^- was too weak to record as a function of photon energy. Negative ion yields for all other anions are presented below.

Of particular relevance to this study is the work of Schenk et al. [20], who also investigated the valence region of CF_3Cl with VUV synchrotron radiation, and comparisons between the two sets of results are detailed in the discussion below. In summary, Schenk et al. were only able to detect F^-, Cl^- and CF_3^-. CF_3^- was detected with low intensity and an ion yield was not recorded. The F^- and Cl^- ion yields are in excellent agreement with the results presented here.

4.3 F^- from CF_3Cl, CF_3Br and CF_3I

The F^- ion yields from CF_3Cl, CF_3Br and CF_3I are presented in Fig. 4.1 in the photon energy range 8–32 eV. For comparative purposes Fig. 4.1 also includes the total photoabsorption spectrum [18], threshold photoelectron spectrum

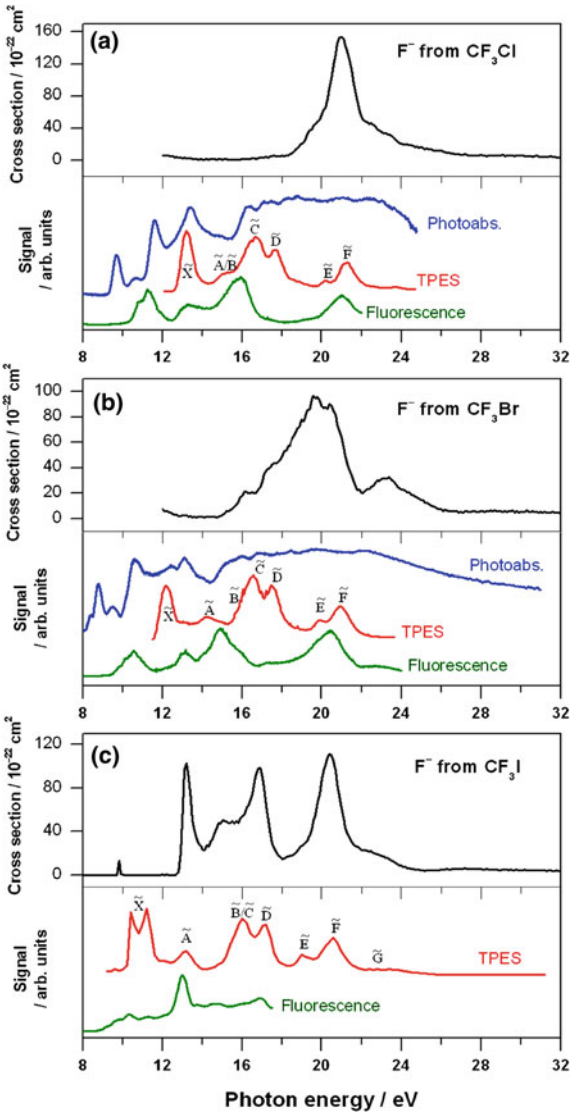

Fig. 4.1 Cross sections for F^- production following photoexcitation of **a** CF_3Cl, and **b** CF_3Br between 12 and 32 eV. The total photoabsorption spectra [18], TPE spectra [10], and total fluorescence yields [18] for CF_3Cl and CF_3Br are included for comparative purposes. **c** Cross section for F^- production following photoexcitation of CF_3I between 8 and 32 eV. The TPES [11] and total fluorescence yield [18] are included. All F^- ion yields were recorded with a step size of 0.1 eV and a wavelength resolution of 6 Å. This resolution is equivalent to 0.2 eV at 20.0 eV

(TPES) [10] and total fluorescence yield [18] for CF_3Cl and CF_3Br, and the TPES [11] and total fluorescence yield [18] for CF_3I. The corresponding numerical data from the F^- ion yields are presented in Table 4.1. The small rise in signal at 12 eV seen in the F^- ion yields from CF_3Cl and CF_3Br is considered to result from second-order radiation, and is exaggerated by normalisation to photon flux which is low at this energy. In all three cases the F^- signal shows a linear rise with gas pressure, indicating that F^- ions are formed by unimolecular ion-pair dissociation.

Table 4.1 Appearance energies, cross sections and quantum yields for anions observed from photoexcitation of CF_3Cl, CF_3Br and CF_3I

Molecule (*IE*[a]/eV)	Anion	*AE*[b]/eV	Cross section[c]/cm^2	Energy[d]/eV	Quantum yield[e]
CF_3Cl (12.4)	F^-	16.0	1.5×10^{-20}	21.0	1.8×10^{-4}
	Cl^-	16.1	2.3×10^{-21}	20.9	2.9×10^{-5}
	F_2^-	~21[f]	6.8×10^{-23}	22.7	8.5×10^{-7}
	FCl^-	~18[f]	6.5×10^{-23}	20.8	8.0×10^{-7}
	CF^-	25.5[g]	1.6×10^{-22}	27.3	–[h]
	CF_2^-	20.2	1.5×10^{-22}	21.3	1.8×10^{-6}
	CF_3^-	15.5	2.8×10^{-22}	18.1	3.5×10^{-6}
CF_3Br (11.5)	F^-	14.7	9.7×10^{-21}	19.6	1.2×10^{-4}
	Br^-	15.1	–[i]	–	–[i]
	F_2^-	~19[f]	2.8×10^{-22}	20.4	3.4×10^{-6}
	FBr^-	~18[f]	5.5×10^{-22}	20.4	6.6×10^{-6}
	CF^-	23.6	3.4×10^{-22}	25.6	5.2×10^{-6}
	CF_2^-	18.2	4.9×10^{-22}	19.5	5.8×10^{-6}
	CF_3^-	13.6	2.5×10^{-22}	14.8	4.0×10^{-6}
CF_3I (10.4)	F^-	9.7	1.1×10^{-20}	20.4	–[j]
	I^-	8.8	–[i]	–	–[i]
	F_2^-	~17[f]	8.5×10^{-23}	20.1	–[j]
	CF^-	21.6	1.1×10^{-22}	23.6	–[j]
	CF_2^-	16.0	4.6×10^{-22}	16.8	–[j]
	CF_3^-	11.0	5.7×10^{-22}	12.7	–[j]

[a] Adiabatic *IE* for CF_3Cl [10], CF_3Br [10], and CF_3I [21] are given in parentheses

[b] Observed *AE* from this work. The error is estimated to be ±0.2 eV, based on the resolution and step size used when recording the ion yields

[c] Cross section for anion production following photoexcitation of the parent molecule

[d] Energy of peak maximum at which cross section and quantum yield measurements are taken

[e] Quantum yields for anion production, obtained by dividing cross sections for anions (column 4) by total photoabsorption cross sections. The photoabsorption cross sections are given for CF_3Cl and CF_3Br [18]

[f] Cannot state *AE* with confidence due to poor signal/noise

[g] There is some ambiguity surrounding the mass of anions detected contributing to the CF^- ion yield from CF_3Cl. The signal observed in the range 16–25 eV is thought to arise from Cl^- ions (see text), and the value of 25.5 eV represents the current interpretation of the true onset to CF^- ions

[h] Quantum yield is not calculated because absolute photoabsorption data for CF_3Cl is not available at this energy

[i] The Br^- and I^- ion yields are significantly influenced by anions arising from dissociative electron attachment and cross sections, and hence quantum yields, cannot be defined

[j] Quantum yields cannot be calculated at this photon energy, because the available absolute photoabsorption data for CF_3I is limited to photon energies <12 eV

The F^- ion yield from CF_3Cl shows a gradual onset. The first indication of a rise in signal above the background is at 16.0 ± 0.2 eV (Fig. 4.1a, Table 4.1). In the earlier work of Schenk et al. the F^- ion yield from CF_3Cl is reported with a wavelength resolution of 2 Å [20]. They report the onset of F^- ions to be 15.9 ± 0.3 eV, correlating this onset to reaction (4.1) using thermochemical calculations:

$$CF_3Cl \rightarrow F^- + CF_2^+ + Cl \quad (4.1)$$

Schenk et al. also report second (16.8 ± 0.1 eV), third (18.2 ± 0.1 eV), and fourth (20.0 ± 0.1 eV) onsets corresponding to the dissociation reactions (4.2), (4.3), and (4.4), respectively:

$$CF_3Cl \rightarrow F^- + CFCl^+ + F \quad (4.2)$$

$$CF_3Cl \rightarrow F^- + CF^+ + F + Cl \quad (4.3)$$

$$CF_3Cl \rightarrow F^- + CCl^+ + 2F \quad (4.4)$$

The thermochemical analysis performed here, as discussed in Chap. 1, agrees with all these assignments. However, the lack of well-defined onsets and features in the F^- ion yield from CF_3Cl, combined with the number of different dissociation channels possible, does not allow these assignments to be made with confidence. For example, the calculated dissociation enthalpies for producing the ion-pairs $F^-/CFCl^+$ (+ F) (reaction 4.2) and F^-/Cl^+ (+ CF_2) are 17.0 and 17.1 eV, respectively. Not only are both these values *higher*, and not lower, in energy than the second onset, but from this analysis alone both are equally valid assignments.

The F^- ion yield from CF_3Br shows the first onset at 14.7 ± 0.2 eV (Fig. 4.1b, Table 4.1) which correlates best to the dissociation enthalpy of 14.9 eV calculated for reaction (4.5):

$$CF_3Br \rightarrow F^- + CF_2^+ + Br \quad (4.5)$$

For the same reasons as discussed above in the thermochemical analysis of F^- from CF_3Cl, even tentative assignments of other unimolecular dissociation reactions to onsets of features in the F^- ion yield from CF_3Br are not suggested here.

Assignments of dissociation processes to onsets in the F^- ion yield from CF_3I can be made more confidently; calculated thresholds for reactions (4.6)–(4.9) coincide with local minima, and hence with onsets to features in the ion yield (Fig. 4.1c).

$$CF_3I \rightarrow F^- + CF_2^+ + I \quad (4.6)$$

$$CF_3I \rightarrow F^- + CF^+ + FI \quad (4.7)$$

$$CF_3I \rightarrow F^- + FI^+ + CF \quad (4.8)$$

$$CF_3I \rightarrow F^- + I^+ + CF + F \quad (4.9)$$

The calculated enthalpy changes for reactions (4.6)–(4.9) are 14.2, 14.3, 15.7 and 18.5 eV, respectively. It is likely that features in the ion yield which occur just after these values represent the 'turning on' of the newly-available dissociation channel(s). In addition, the sharp onset observed at 12.7 ± 0.2 eV can be correlated to formation of the F^-/I^+ (+ CF_2) ion-pair—although this assignment is made more tentatively since the calculated enthalpy is 13.2, 0.5 eV *above* this onset.

The lowest energy ion-pair reaction which yields F^- must be:

$$CF_3X \rightarrow F^- + CF_2X^+ (X = Cl, Br, I) \tag{4.10}$$

Lack of reliable information for $\Delta_f H°_{298}$ (CF_2I^+) prevented a dissociation enthalpy for CF_3I in reaction (4.10) to be calculated. For CF_3Cl and CF_3Br the calculated thresholds for this reaction are 10.2 and ≤10.1 eV, respectively. In both cases these calculated dissociation enthalpies are significantly below the experimentally-observed appearance energy (*AE*) for F^- ions; recall the *AE*s are 16.0 and 14.7 eV for F^- from CF_3Cl and CF_3Br, respectively. There is therefore no evidence, from this thermochemical analysis, that F^- ions produced from CF_3Cl and CF_3Br arise via reaction (4.10). The *AE* for F^- from CF_3I, however, is much lower, at 9.7 eV (Fig. 4.1c, Table 4.1). Even though a threshold energy could not be calculated for reaction (4.10) when $X = I$, it is the only ion-pair channel forming F^- from CF_3I that is likely to occur at energies below ca. 13 eV. The peak at 9.8 eV in the F^- ion yield from CF_3I, albeit very weak, must therefore arise from reaction (4.10).

The photoabsorption spectra of CF_3Cl and CF_3Br, shown in Fig. 4.1 [18], extend over the energy range where F^- ions are observed from the two molecules. Figure 4.1 does not include a photoabsorption spectrum for CF_3I and published data in the energy range of interest (up to 25 eV) is limited. The peak centred at 16.32 eV in the CF_3Cl absorption spectrum has been assigned as a transition to a 3*s* Rydberg orbital coverging on the fifth excited valence state of CF_3Cl^+ ($\tilde{E}^2A_1$) [18]. From EELS of CF_3Cl, King and McConkey [14] have assigned observed features at 16.29, 17.1 and 18.2 eV as transitions to 3*s*, 3*p* and 3*d* Rydberg orbitals, respectively, all converging to CF_3Cl^+ ($\tilde{E}^2A_1$). These features occur in the same energy range where the gradual onset of F^- ions from CF_3Cl is observed. The cross section for F^- ions in this energy range is relatively small (6×10^{-22} cm^2 at 17.6 eV) and well-defined peaks are not observed. As a result, and given the tentative nature of the assignments made from the photoabsorption and EEL spectra, assigning the same transitions to the F^- ion yield is speculative. The one peak that is observed at 21.0 eV has not been clearly seen in the absorption spectrum [18]. It may correspond to a Rydberg state of CF_3Cl converging on either the $\tilde{F}^2E$ or $\tilde{G}^2A_1$ state of the parent ion.

The above discussion assumes the formation mechanism is predissociative, yet direct excitation to the ion-pair state should not be discounted. The gradual onset and small cross section indicate weak Franck–Condon overlap, and therefore direct ion-pair formation is plausible. If this is the case, the *AE* of F^- ions may exceed the thermochemical ion-pair dissociation threshold by a greater amount than that from a predissociation mechanism where these two energies are more likely to be similar.

The feature in the CF_3Br photoabsorption spectrum at 15.96 eV has been assigned as a transition to a 4*d* Rydberg orbital converging on the fourth excited valence state of CF_3Br^+ ($\tilde{D}^2E$) [18]. It is close in energy to the first observable peak in the F^- ion yield at 16.1 eV, and it is possible these two features share the same primary excitation process. The peak at 9.8 eV in the F^- ion yield from CF_3I is very sharp and weak, and appears anomalous by comparison to the rest of the

spectrum. The abrupt nature of this feature points to a predissociative mechanism and the low cross section could indicate the extent of overlap between states is small. It has been suggested, albeit tentatively, that Rydberg states of the *ns* series converging to the $\tilde{X}^2E_{3/2}$ ionisation limit lie in this energy region. Indeed there is a strong absorption band between 9.4 and 9.9 eV showing detailed structure [16].

It is generally accepted that the $\tilde{X}^2E$ electronic states of the CF_3X^+ (X = Cl, Br, I) cations result from ionisation of X lone pair electrons, and the $\tilde{A}^2A_1$ states from ionisation of a C–X bonding electron [6–9]. The $\tilde{B}$, $\tilde{C}$, $\tilde{D}$, $\tilde{E}$ and $\tilde{F}$ electronic states of the cations between 15 and 22 eV are most likely from fluorine lone pair excitations. It is expected that the bonding character of the fluorine lone pair electrons will increase with increasing ionisation energy (*IE*) [8]. Photoexcitation of these electrons leads to the production of F^- anions. Only F^- produced from CF_3I is observed following photoexcitation of an electron associated with the X substituent. Even so, the resulting single peak at 9.8 eV appears isolated and the cross section is very small compared to the rest of the spectrum. The similarities of the photoelectron spectra for the three CF_3X molecules have been highlighted by Cvitaš et al. [6, 8], and they suggest that changing substituent X affects the electronic structure of the CF_3 group very little. Despite this observation, the F^- ion yields from these three molecules differ significantly. The extent of structure and the energy range over which F^- is observed increases as X changes from Cl to I. In addition, the *AE* of F^- ions decreases. These trends appear more significant when substituting Br for I than when substituting Cl for Br. This trend possibly reflects the differing polarisabilities of the halogen atoms; the values are 2.18, 3.05 and 5.35×10^{-24} cm^3 for neutral atomic Cl, Br and I, respectively [22].

4.4 Cl^- from CF_3Cl

The Cl^- ion yield from CF_3Cl is shown in Fig. 4.2 from 12 to 34 eV. For comparative purposes it also includes the total photoabsorption spectrum [18], TPES [10] and total fluorescence yield [18] for CF_3Cl. The numerical information is summarised in Table 4.1. The signal in the Cl^- ion yield observed between 12 and 14 eV is considered to result from second-order effects, which are exaggerated when flux normalising the spectrum. The Cl^- signal changes linearly with CF_3Cl gas pressure, indicating that the mechanism for Cl^- formation is unimolecular ion-pair dissociation.

The lowest energy ion-pair fragmentation leading to Cl^- production must also produce the cation CF_3^+:

$$CF_3Cl \rightarrow Cl^- + CF_3^+ \tag{4.11}$$

The calculated enthalpy for reaction (4.11) is 9.2 eV, however, the experimentally-observed onset to Cl^- production from CF_3Cl is 16.1 ± 0.2 eV. In the earlier work of Schenk et al. [20] a value of 16.0 ± 0.1 eV is reported, in excellent agreement

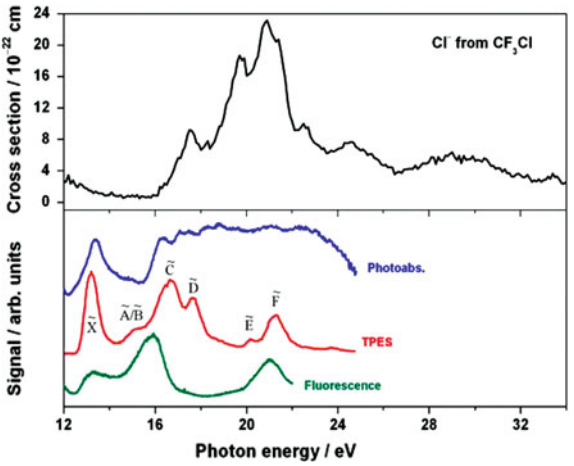

Fig. 4.2 Cross section for Cl^- production following photoexcitation of CF_3Cl in the energy range 12–34 eV. The total photoabsorption spectrum [18], TPES [10], and total fluorescence yield [18] for CF_3Cl are included for comparative purposes. The F^- ion yield was recorded with a step size of 0.1 eV and a wavelength resolution of 6 Å. This resolution is equivalent to 0.2 eV at 20.0 eV

with this work. The observed Cl^- signal at onset may be assigned to the following dissociation reaction:

$$CF_3Cl \rightarrow Cl^- + CF_2^+ + F \tag{4.12}$$

The calculated enthalpy change for reaction (4.12) is 15.4 eV. Other onsets to features in the Cl^- ion yield, observed at 18.4, 21.3, and 23.4 eV (Fig. 4.2), occur where a different fragmentation reaction becomes energetically accessible:

$$CF_3Cl \rightarrow Cl^- + CF^+ + 2F \tag{4.13}$$

$$CF_3Cl \rightarrow Cl^- + F^+ + CF_2 \tag{4.14}$$

$$CF_3Cl \rightarrow Cl^- + F_2^+ + CF \tag{4.15}$$

The calculated enthalpy changes for reactions (4.13)–(4.15) are 18.4, 21.4, and 23.3 eV, respectively.

The production of Cl^- has similarities to that of F^- from CF_3Cl; the fragmentation reaction assumed to occur at onset [reaction (4.12)] is almost identical to that assigned to F^- anions from CF_3Cl [reaction (4.1)]. Both ion yields show a very similar *AE* (Table 4.1) and in both cases this value is much higher than the lowest energy dissociation reaction to form the respective anion as an ion-pair [reactions (4.10) and (4.11)]. In addition, the cross sections for F^- and Cl^- production peak at almost identical energies and in the range 16–18 eV the cross sections are of similar magnitude. For example, at 17.6 eV, $\sigma_{F-} = 5.4 \times 10^{-22}$ cm^2 and $\sigma_{Cl^-} = 9.2 \times 10^{-22}$ cm^2. Above 18 eV F^- formation increases with respect to Cl^- anions; at 21.0 eV, $\sigma_{F-} = 1.5 \times 10^{-20}$ cm^2 and $\sigma_{Cl^-} = 2.2 \times 10^{-21}$ cm^2.

4.5 Br^- from CF_3Br and I^- from CF_3I

The Br^- and I^- ion yields from CF_3Br and CF_3I, respectively, are shown in Fig. 4.3 in the range 8–28 eV. The TPE spectra for CF_3Br [10] and CF_3I [11] are superimposed above the ion yields for comparative purposes. When recorded as a function of gas pressure, both the Br^- and I^- signals change *non*-linearly; the rate of change in anion signal increases pseudo-exponentially with increasing pressure. When this trend has been seen before (e.g. SF_5^- from SF_6 and SF_5CF_3) the anions have been shown to arise from dissociative electron attachment, following photoionisation of the parent molecule as the source of low-energy electrons [23] (also see Chap. 3). The same conclusion is reached in this study for the formation of Br^- and I^- ions from CF_3X (X = Br, I). The two-step mechanism is shown below:

$$CF_3X + h\nu \rightarrow CF_3X^+ + e^- \tag{4.16}$$

$$CF_3X + e^- \rightarrow X^- + CF_3 \tag{4.17}$$

CF_3Br [24, 25] and CF_3I [4, 26] are both known to attach electrons rapidly: the recommended values for the thermal electron attachment rate coefficients are 1.4×10^{-8} cm^3 s^{-1} for CF_3Br [24] and 1.9×10^{-7} cm^3 s^{-1} for CF_3I [4]. In addition, the Br^- and I^- ion yields show similarities to the TPE spectra for CF_3Br and CF_3I, respectively (Fig. 4.3). These similarities are much more obvious between the I^- ion yield and CF_3I TPES, which perhaps reflects the difference in magnitude between the attachment rate coefficients for CF_3Br and CF_3I. The apparent lack of agreement between the two spectra (ion yield vs TPES) at lower photon energies in both molecules is interesting. Only background signal is observed in the Br^- ion yield over the photon energy range, 12–15 eV, where the first two bands can be seen in the CF_3Br TPES.

The first bands in the CF_3I TPES, representing the spin-orbit split ground state of CF_3I^+, $\tilde{X}^2E_{3/2}$ and $\tilde{X}^2E_{1/2}$, are only observed very weakly in the I^- spectrum; in Fig. 4.3 the I^- signal over this energy region has been enlarged by a factor of 30. The ion yields of Fig. 4.3 are unlikely to result from dissociative electron attachment alone; Br^- or I^- anions produced by ion-pair dissociation are also detected. How much of either anion signal is due to dissociative electron attachment, and how much to ion-pair formation is unknown. However, given the evidence above it is clear that dissociative electron attachment is the more dominant mechanism contributing to the Br^- and I^- ion yields.

The agreement between the TPES and the Br^-/I^- yield is slightly better at the higher energies scanned in Fig. 4.3, and the absence of the low-energy bands between 12 and 15 eV in the Br^- channel from CF_3Br, and the relative weakness of the analogous bands in the I^- channel from CF_3I, remain unexplained. Likewise, the reasons why the relative intensities between ion yield and TPES spectra are different, including the relative intensities of the $\tilde{X}^2E_{3/2}$ and $\tilde{X}$ $^2E_{1/2}$ spin-orbit

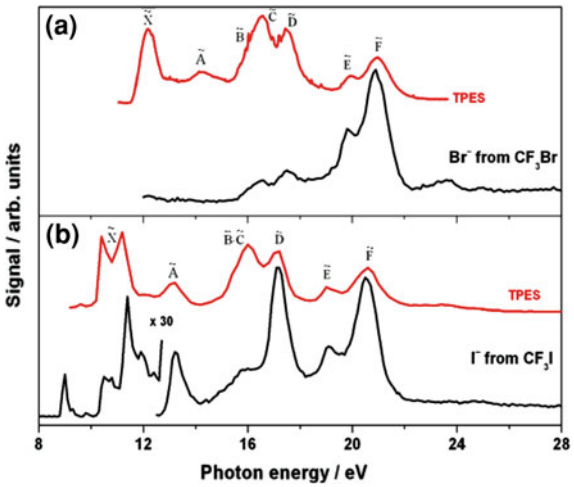

Fig. 4.3 **a** Br^- ion yield recorded following photoexcitation of CF_3Br between 12 and 28 eV. The TPES [10] is superimposed on top of the Br^- ion yield for comparative purposes. **b** I^- ion yield recorded following photoexcitation of CF_3I between 8 and 28 eV. The 8–12 eV range of this spectrum has been blown-up by a factor of 30. The TPES [11] is superimposed on top of the I^- ion yield for comparative purposes. The anion spectra are not put onto an absolute scale because the signals are shown to change non-linearly with pressure. The peak at 9.0 eV in the I^- spectrum, however, results from ion-pair formation and the cross section at this energy is 3.8×10^{-21} cm^2

sub-bands in CF_3I^+, is unclear. Note that the SF_6^- yield from SF_6 and the SF_5^- yield from SF_5CF_3 are both dominated by the two-step electron attachment mechanism over the *whole* of the valence region, and the anion yield and TPES show better agreement over a wider range of energies [23] (also see Chap. 3). There is limited evidence from work on other polyatomic molecules (e.g. *c*-C_5F_8) that the agreement between the two spectra is enhanced if electron attachment is *non*-dissociative [23, 27].

For electron attachment to occur, the parent molecule must first be ionised. Therefore, at energies below the onset to ionisation any anions produced can only arise from ion-pair dissociation. This is observed in the ion yield for I^- from CF_3I. The onset to ionisation in CF_3I is 10.4 eV [21]. However, the experimentally-determined onset to I^- formation is at 8.8 ± 0.2 eV and a discrete peak in the signal results at 9.0 eV (Fig. 4.3). Thermochemical calculations suggest the only possible ion-pair dissociation reaction which produces I^- at this energy is:

$$CF_3I \rightarrow I^- + CF_3^+ \tag{4.18}$$

The calculated enthalpy change for reaction (4.18) is 8.3 eV. The cross section for I^- ion-pair formation at 9.0 eV is 3.8×10^{-21} cm^2. Normalising this value to the total photoabsorption cross section at 9.0 eV [16] gives a quantum yield of ca. 8×10^{-5}. An analysis of the photoabsorption spectrum of CF_3I has suggested that

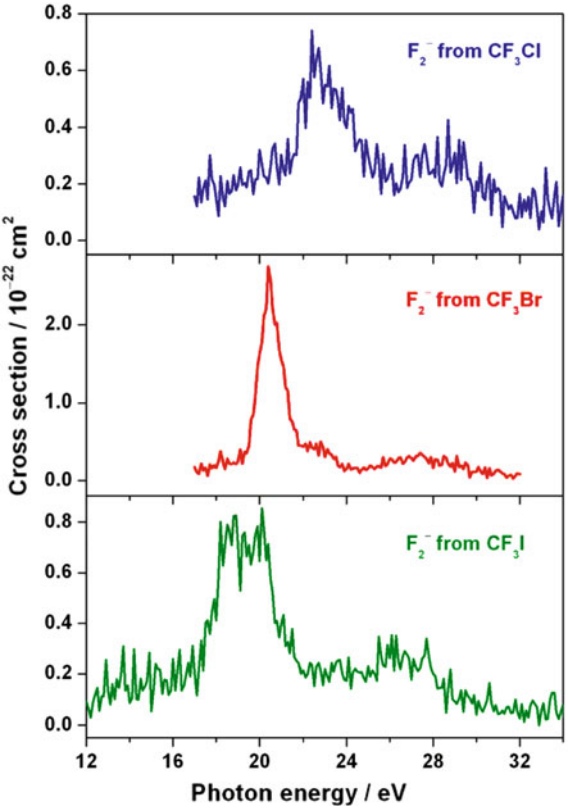

Fig. 4.4 Cross sections for F_2^- production following photoexcitaion of CF_3Cl, CF_3Br and CF_3I in the photon energy range 12–34 eV. The ion yields were recorded with a step size of 0.1 eV and a wavelength resolution of 6 Å. This resolution is equivalent to 0.2 eV at 20.0 eV

Rydberg states of the *ns* series converging to the $\tilde{X}^2E_{3/2}$ ionisation limit lie in this energy region, and absorption features showing vibrational structure have been observed centred at energies 8.8 and 9.5 eV [16].

4.6 F_2^- and FX^- (X = Cl, Br) from CF_3Cl, CF_3Br and CF_3I

The F_2^- ion yields from CF_3X (X = Cl, Br, I) and the FX^- (X = Cl, Br) yields from CF_3Cl and CF_3Br in the range 12–34 eV are shown in Figs. 4.4 and 4.5, respectively. All these anion signals show a linear increase when recorded as a function of gas pressure, indicating that F_2^- and FX^- result from unimolecular photodissociation. The figures report absolute cross sections for these processes and further numerical information is provided in Table 4.1; the cross sections for production of FCl^-, FBr^- and F_2^- from CF_3X are up to three orders of magnitude smaller compared to F^- production.

The onsets for F_2^- production, ca. 21, 19 and 17 eV for X = Cl, Br, I, occur at the thermochemical thresholds for the ion-pair dissociation reaction shown below:

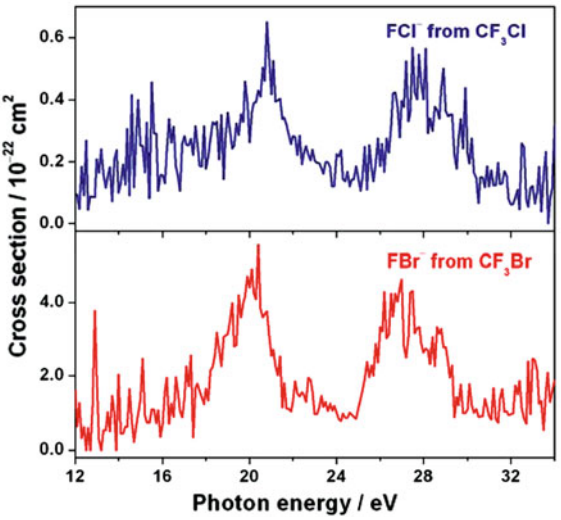

Fig. 4.5 Cross sections for FCl^- and FBr^- production following photoexcitaion of CF_3Cl and CF_3Br, respectively, in the photon energy range 12–34 eV. The ion yields were recorded with a step size of 0.1 eV and a wavelength resolution of 6 Å. This resolution is equivalent to 0.2 eV at 20.0 eV

$$CF_3X \rightarrow F_2^- + X^+ + CF \ (X = Cl, Br, I) \tag{4.19}$$

The calculated dissociation enthalpy changes for this reaction are 21.1, 19.2, and 17.2 eV for $X = Cl$, Br, and I, respectively. Two cautionary points should be made: first, the uncertainty in the values of the experimentally-determined onsets (Table 4.1, Fig. 4.4) is degraded by the poor signal/noise ratio in the ion yields; second, an energy barrier resulting from forming a new F–F bond is likely—if so, the true thermochemical threshold will lie below the experimental onset, and other lower energy dissociation reactions should be considered (e.g. F_2^-/CF^+ ion-pair formation). A similar discussion on the dissociation reactions leading to FCl^- and FBr^- from CF_3Cl and CF_3Br, respectively, is not possible due to the lack of data on the electron affinities of FCl and FBr.

The F_2^- ion yields all show one major feature which most likely represents the presence of a Rydberg state converging to the fifth ($\tilde{E}$) or sixth ($\tilde{F}$) excited valence states of the CF_3X^+ molecules. As discussed in Sect. 4.3, the origin of the excited electron is from a fluorine lone pair with significant C–F bonding character. In all three F_2^- ion yields a tentative correlation can be made between the peak energy and features in the corresponding F^- ion yields. This is unsurprising considering two F atoms must be cleaved preceding the formation of F_2^-.

4.7 CF_n^- (n = 1–3) from CF_3Cl, CF_3Br and CF_3I

The CF^-, CF_2^- and CF_3^- ion yields from CF_3X ($X = Cl$, Br, I) are shown in Fig. 4.6. Numerical information is given in Table 4.1. All these anion signals show a linear rise when recorded as a function of increasing gas pressure, indicating they

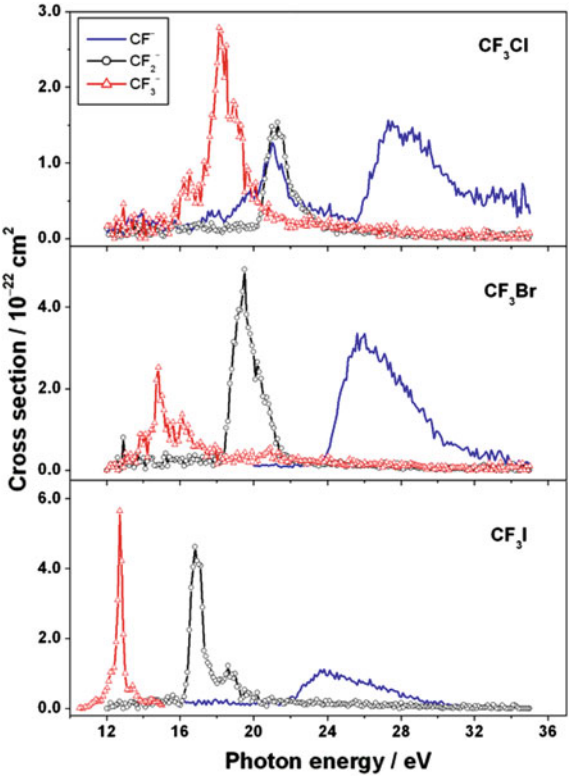

Fig. 4.6 Cross sections for CF^-, CF_2^- and CF_3^- production following photoexcitation of CF_3Cl, CF_3Br and CF_3I in the photon energy range 10–35 eV. The ion yields were recorded with a step size of 0.1 eV and a wavelength resolution of 6 Å. This resolution is equivalent to 0.2 eV at 20.0 eV

result from unimolecular photodissociation. The cross sections for CF_n^- (n = 1–3) production are approximately two orders of magnitude smaller than those determined for F^- production.

Each CF_n^- (n = 1–3) anion from each parent CF_3X molecule shows only one feature in the ion yield, with the exception of CF^- from CF_3Cl which shows more features. It is proposed that the true onset for CF^- from CF_3Cl is 25.5 eV (Table 4.1, Fig. 4.6) and that the observed signal in the energy range 16–25 eV results from detecting Cl^- anions. There are two reasons for this. First, the mass-to-charge ratios (m/z) used when recording ion yields are close in value, 31 for CF^- and 35 for Cl^-. Although the Cl^- signal peaks at m/z 35, *weak* contributions can be detected at m/z values as low as 30. Combined with the fact that the CF^- signal relative to that of Cl^- is very weak, the Cl^- contribution at m/z 31 becomes significant. Second, the ion yield of Cl^- (Fig. 4.2) and that of CF^- (Fig. 4.6) from CF_3Cl appear similar in the 16–25 eV energy range; both ion yields show an onset around 16 eV, with featues at ca. 17.5 and 21.0 eV.

Unimolecular dissociation of CF_3X (X = Cl, Br, I) leading to CF_3^- formation must also produce the cation X^+:

$$CF_3X \rightarrow CF_3^- + X^+ (X = \text{Cl, Br, I}) \tag{4.20}$$

The calculated thermochemical thresholds for reaction (4.20) are 14.9, 13.1, and 11.0 eV when $X = Cl$, Br, and I, respectively; the experimentally-determined onsets for CF_3^- anions are 15.5, 13.6, and 11.0 eV, respectively. A similar dissociation process most likely produces the CF_2^- anions:

$$CF_3X \rightarrow CF_2^- + X^+ + F \ (X = Cl, Br, I) \tag{4.21}$$

The calculated thermochemical thresholds for reaction (4.21) are 20.3, 18.5, and 16.4 eV when $X = Cl$, Br, and I, respectively; the experimentally-determined onsets for CF_2^- anions are 20.2, 18.2, and 16.0 eV, respectively. Dissociation of CF_3X ($X = Cl$, Br, I) to produce the CF_2^-/F^+ ion-pair will only occur at excitation energies several eV *above* the experimental onset, and is therefore not a possible assignment. Dissociation to produce the CF_2^-/FX^+ ion-pair, however, may occur *below* the experimental onset.

$$CF_3X \rightarrow CF_2^- + FX^+ (X = Cl, Br, I) \tag{4.22}$$

The calculated thermochemical thresholds for reaction (4.22) are 17.4, 15.9, and 13.6 eV when $X = Cl$, Br, and I, respectively. If reaction (4.22) occurs, 2–3 eV excess energy must be accounted for. An experimental onset is always considered an upper limit, and small amounts of energy will undoubtedly be converted into translational energy of the fragment species. It should also be considered that an energy barrier to FX^+ formation may exist, given that bonds are both broken and formed. Similar arguments are made in Sect. 4.6 with respect to the anions F_2^- and FX^- ($X = Cl$, Br, I). The more likely process producing CF_2^- from CF_3X is reaction (4.21), rather than reaction (4.22). Low excess energies favour the production of ion-pairs [28], and a bond-breaking-only dissociative reaction is favoured over one where bonds are additionally formed.

The considerations discussed above are also relevant in the discussion of the CF^- fragment anion. The possibilities for the associated fragment cation and neutral species are greater. Several diatomic fragments, F_2, F_2^+, FX or FX^+, could realistically be associated with CF^- ion-pair formation. The thermochemistry suggests all processes pairing CF^- formation with X^+, F^+ or F_2^+ could be contributing to the observed CF^- signal from CF_3X photodissociation as observed in Fig. 4.6. This is perhaps reflected by the broad band which features in all three CF^- ion yields.

From observation of Fig. 4.6 it is clear that interchanging the X substituent in CF_3X with Cl, Br, or I has little effect on the structure of the ion yields of CF^-, CF_2^-, or CF_3^-. There are consistent shifts in the AE values of CF_n^- to lower energy as X increases in size. For example, the shift in AE for each anion is almost exactly the same when substituting Cl for Br as when substituting Br for I (Table 4.1); the AE (CF^-) from CF_3I is 2.0 eV lower in energy than AE (CF^-) from CF_3Br which is 1.9 eV lower than AE (CF^-) from CF_3Cl. This trend is expected because all anions are observed at their thermochemical threshold, whose values decrease as the size of X increases.

The broad nature of the features in the CF^- ion yields does not allow any direct comparisons to be made with other spectra. In addition, the energy required to yield CF^- from photoexciting CF_3X (X = Cl, Br, I) is comparatively large with respect to other negative ions. Intermediate excited Rydberg states at these energies probably converge on the first *inner*-valence excited state of CF_3X^+. Alternatively, these features may represent direct ion-pair formation with no involvement of an intermediate excited state. The energies of peak maxima in all the CF_2^- and CF_3^- ion yields, however, are similar to energies of features observed in other anion spectra, and likely represent common excited intermediate states and hence competing ion-pair dissociation channels.

4.8 Bond Dissociation Energies

As discussed in Chap. 1, the experimental *AE*s for anions determined by this work may be used to calculate upper limits to 298 K bond dissociation energies, D^o [28]. For example, using the *AE* of CF_3^- can provide an upper limit to $D^o(CF_3–X)$ if the *IE* of X and the electron affinity (*EA*) of CF_3 are known, where X = Cl, Br, I:

$$AE(CF_3^-) \geq D^o(CF_3 - X) + IE(X) - -EA(CF_3) \tag{4.23}$$

Note that the *AE* (CF_3^-) correlates to dissociation reaction (4.20). When the unimolecular dissociation involves multiple bond-breaking or the formation of a new bond, calculations performed in this way become over-complicated and too many assumptions are made. Therefore, only *AE* values for anions resulting from *single* bond-breaking ion-pair dissociation are considered here.

The resulting upper limits to bond dissociation energies are presented in Table 4.2 and compared to literature values. In addition, $D^o(CF_3–F)$ is calculated from the *AE* (F^- from CF_4) [23] (also see Chap. 3) and included in Table 4.2. The uncertainty in the D^o upper limits calculated from these data is ±0.2 eV which is taken directly from the estimated error in the *AE* values (Table 4.1). The calculations for these values are explained in more detail below. Note the consistency between upper limit values for $D^o(CF_3–X)$ obtained indirectly from this ion-pair work and the accepted literature values [22]. Furthermore, the upper limit value for D^o tends towards the accurate value as the size of X increases from F to I.

As shown in Eq. 4.23 the *AE* values for CF_3^- from CF_3X (Table 4.1, Fig. 4.6) are used to calculate $D^o(CF_3–X)$. The *EA* of the CF_3 radical is 1.82 ± 0.05 eV [35], and the ionisation energies for Cl (12.970 eV), Br (11.816 eV) and I (10.453 eV) are taken from the JANAF thermochemical tables [36]. The calculation is slightly different for $D^o(CF_3–F)$ because CF_3^- was not observed from CF_4 [23], but the *AE* (F^- from CF_4) can be used to yield the same information if the *EA* (F) = 3.401 eV [37] and *IE* (CF_3) = 9.04 ± 0.04 eV [38] are used instead.

The formation of F^- from CF_3I at onset arises from dissociation reaction (4.10). Unfortunately, because the *IE* (CF_2I) is currently not known, an upper limit to $D^o(CF_2I–F)$ cannot be calculated from the *AE* (F^-) value as described above.

Table 4.2 Upper limits to experimentally-determined bond dissociation energies and comparison with literature values. [#]

Bond	D^o_{298}/ eV	
	This work	Literature value[a]
H–CH_3	4.21 ± 0.11	4.553 ± 0.004
F–CH_3	≤5.84 ± 0.02[b]	4.77 ± 0.09
Cl–CH_3	≤3.81 ± 0.02[b]	3.63 ± 0.02
Br–CH_3	≤2.98 ± 0.02[b]	3.05 ± 0.02
H–CH_2F	$\leq 4.8_4 \pm 0.2^c_7$	4.39 ± 0.04
H–CH_2Cl	$\leq 4.3_3 \pm 0.2^c_6$	4.34 ± 0.02
H–CH_2Br	$\leq 4.2_8 \pm 0.2^c_4$	4.43 ± 0.02
F–CF_3	≤7.4 ± 0.2[d]	5.67 ± 0.02
Cl–CF_3	≤4.4 ± 0.2[e]	3.79 ± 0.04
Br–CF_3	≤3.6 ± 0.2[e]	3.07 ± 0.01
I–CF_3	≤2.4 ± 0.2[e]	2.35 ± 0.01
F–CF_2Cl	≤11.1 ± 0.2	5.30[f]
F–CF_2Br	≤18.1–*IE*(CF_2Br)	5.09[i]
F–CF_2I	≤13.1–*IE*(CF_2I)	5.40[i]
F–SF_5	≤6.3 ± 0.3	4.06[f]
F–CF_3	≤7.4 ± 0.2	5.67 ± 0.02
F_5S–CF_3	–[g]	3.86 ± 0.45[j]
F–SF_4CF_3	≤14.5–*IE*(SF_4CF_3)	N/a
F–SF_4Cl	≤4.8 ± 0.3[h]	3.70[k]
Cl–F_5	≤4.4 ± 0.3	2.54[k]

[#] Note that this version of Table 4.2 is updated from that published in my PhD thesis. I am grateful to Professor Richard Tuckett for his help in expanding this Table. The version shown here is taken from Ref. [29]

[a] Reference [22]

[b] Calculated from the *AE* of Y^- from CH_3Y [30]. The compound errors have contributions from the errors in *AE* (Y^-), typically 0.02 eV, and the error in *IE* (CH_3), 0.01 eV

[c] Calculated from the *AE* of CH_2Y^- from CH_3Y [30]. The errors are dominated by that of the *AE* (CH_2Y^-), typically 0.2 eV

[d] Calculated from the *AE* (F^-) from CF_4 [23]

[e] Calculated from the *AE* of X^- formation from CF_3X

[f] Error not quoted

[g] CF_3^- and SF_5^- are either not observed, or are not formed by ion-pair formation

[h] Uses an enthalpy of formation of SF_4Cl^+ of + 327 kJ mol^{-1} [31]

[i] Calculated assuming the enthalpies of formation at 298 K of the CF_2Br and CF_2I radicals are −238 and −144 kJ mol^{-1}, respectively [32, 33]

[j] Value at 0 K [34]

[k] Calculated assuming the enthalpies of formation of SF_4Cl and SF_5 are − 761 and − 915 kJ mol^{-1}, respectively [31]. Errors are often not quoted and difficult to estimate, but probably an error in the bond energy of ± 0.20 eV is realistic

However, the relevant information is known in order to calculate an upper limit to $D^o(CF_2I^+–F)$ if Eq. 4.24 is considered:

$$AE(F^-) \geq IE(CF_3I) + D(CF_2I^+ - F) - EA(F) \tag{4.24}$$

The *AE* (F^-) is 9.7 ± 0.2 eV, the *IE* (CF_3I) is 10.37 eV [21], and the *EA* (F) is 3.401 eV [37], giving $D^o(CF_2I^+–F) \leq (2.7 \pm 0.2)$ eV or (263 ± 20) kJ mol^{-1}. If $D^o(CF_2I^+–F)$ is simply defined as the enthalpy change for reaction (4.25), then an upper limit to $\Delta_f H^\circ_{298}$ (CF_2I^+) can be determined.

$$CF_3I^+ \rightarrow CF_2I^+ + F \quad \Delta_r H^\circ_{298} \leq (263 \pm 20)\,\text{kJ mol}^{-1} \tag{4.25}$$

Using thermochemistry provided in Appendix I, $\Delta_f H^\circ_{298}$ (CF_2I^+) is calculated as $\leq$(598 ± 22) kJ mol^{-1}.

4.9 Conclusions

Negative ions have been detected following photoexcitation of CF_3Cl, CF_3Br and CF_3I in the photon energy range 8–35 eV. For the fast electron-attaching gases CF_3Br and CF_3I, the Br^- and I^- signals are heavily influenced by dissociative electron attachment. All other anions detected from these three molecules result from ion-pair formation. A collection of the numerical data from this study is compiled in Tables 4.1 and 4.2. It has been shown that experimental *AE* values from ion-pair formation can be used to calculate upper limits for bond dissociation energies. This same point was made by Berkowitz [28], but has rarely been implemented since. New data is reported for $D^o_{298}(CF_2I^+ - F) \leq (2.7 \pm 0.2)$ eV and $\Delta_f H^\circ_{298}(CF_2I^+) \leq (598 \pm 22)\,\text{kJ mol}^{-1}$.

The most surprising observation from this work is the lack of ion-pair formation detected at lower photon energies, particularly at energies below the *IE* of the parent molecule. This anomaly is surprising because ion-pair fragmentation is energetically allowed and because significant structure is observed in the photoabsorption spectra below the *IE*. The best example of this is seen in X^- ion-pair formation from CF_3X (X = Cl, Br, I): a comparatively large cross section for X^- produced by reaction (4.26) would be predicted, but the spectra show no contribution from Cl^- or Br^- anions produced in this way. I^- anions, however, are observed below the *IE* of CF_3I but the signal is surprisingly weak.

$$CF_3X \rightarrow X^- + CF_3{}^+ (X = \text{Cl, Br, I}) \tag{4.26}$$

The total fluorescence yields and photoabsorption spectra correlate very little, and although there will be some contribution from fluorescence, it is not expected to be significant. Therefore, the structure observed in the photoabsorption spectra for CF_3Cl, CF_3Br and CF_3I below the *IE* must almost exclusively result from neutral photodissociation.

It is noted that ion-pair formation from CF_4 (see Chap. 3) shows completely different properties to the CF_3X molecules studied in this paper. This should not be surprising for two reasons: first, the symmetry of the molecule changes from T_d to C_{3v}; second, the substitution of one F by a much heavier halogen atom increases

the polarisability of the molecule, and therefore enhances its propensity to attach low-energy electrons.

Finally, it is noted that the strongest anion observed, F^-, corresponds to cleavage of a strong C–F bond, whereas the anion produced by cleavage of a much weaker C–X bond, X^-, is significantly less intense. This is true for $X = Cl$, Br and I. It appears that the dynamics of the crossing of Rydberg states with the ion-pair continuum determines the relative intensities of the anions that are formed, and not the thermochemistry of the different dissociation channels. This point is revisited in Chaps. 5 and 6.

References

1. Simpson MJ, Tuckett RP, Dunn KF, Hunniford CA, Latimer CJ (2009) J Chem Phys 130:194302
2. United Nations Environment Programme (2008) (http://ozone.unep.org/). Oct 2008
3. Solomon S, Burkholder JB, Ravishankara AR, Garcia RR (1994) J Geophys Res D 99:20929
4. Christophorou LG, Olthoff JK (2000) J Phys Chem Ref Data 29:553
5. Li Y, Patten KO, Youn D, Wuebbles DJ (2006) Atmos Chem Phys 6:4559
6. Cvitaš T, Güsten H, Klasinc L (1977) J Chem Phys 67:2687
7. Jadrny R, Karlsson L, Mattsson L, Siegbahn K (1977) Phys Scr 16:235
8. Cvitaš T, Güsten H, Klasinc L, Novadj I, Vančik H (1978) Z Naturforsch 33A:1528
9. Doucet J, Sauvageau P, Sandorfy C (1972) J Chem Phys 58:3708
10. Creasey JC, Smith DM, Tuckett RP, Yoxall KR, Codling K, Hatherly PA (1996) J Phys Chem 100:4350
11. Powis I, Dutult O, Richard-Viard M, Guyon PM (1990) J Chem Phys 92:1643
12. Gilbert R, Sauvageau P, Sandorfy C (1974) J Chem Phys 60:4820
13. Jochims HW, Lohr W, Baumgärtel H (1976) Ber Bunsen Ges Phys Chem 80:130
14. King GC, McConkey (1978) J Phys B 11:1861
15. Au JW, Burton GR, Brion CE (1997) Chem Phys 221:151
16. Eden S, Limão-Vieira P, Hoffmann SV, Mason NJ (2006) Chem Phys 323:313
17. Hoshino M, Sunohara K, Makochekanwa C, Pichl L, Cho H, Tanaka H (2007) J Chem Phys 126:024303
18. Ali S (2007) Ph.D. thesis, University of Birmingham. http://etheses.bham.ac.uk/897/
19. Biehl H, Boyle KJ, Tuckett RP, Baumgärtel H, Jochims HW (1997) Chem Phys 214:367
20. Schenk H, Oertel H, Baumgärtel H (1979) Ber Bunsen Ges Phys Chem 83:683
21. Macleod NA, Wang S, Hennessy J, Ridley T, Lawley KP, Donovan RJ (1998) J Chem Soc, Faraday Trans 94:2689
22. Lide DR (2007) Handbook of chemistry and physics, 88th edn. Taylor & Francis, London
23. Simpson MJ, Tuckett RP, Dunn KF, Hunniford CA, Latimer CJ, Scully SWJ (2008) J Chem Phys 128:124315
24. Christophorou LG (1996) Z Phys Chem 195:195
25. Marienfield S, Sunagawa T, Fabrikant II, Braun M, Ruf M-W, Hotop H (2006) J Chem Phys 124:154316
26. Marienfield S, Fabrikant II, Braun M, Ruf M-W, Hotop H (2006) J Phys B 39:105
27. Parkes MA (2007) Ph.D. thesis, University of Birmingham. http://etheses.bham.ac.uk/74/
28. Berkowitz J (1996) In: Becker U, Shirley DA (eds) VUV and soft X-ray photoionization. Plenum Press, New York Chap. 8
29. Simpson MJ, Tuckett RP (2011) Int Rev Phys Chem 30:197

30. Rogers NJ, Simpson MJ, Tuckett RP, Dunn KF, Latimer CJ (2010) Phys Chem Chem Phys 12:10971
31. Chim RYL, Cicman C, Märk TD, Mayhew CA, Scheier P, Tuckett RP (2007) Int J Mass Spectrom 261:208
32. Bilde M, Sehested J, Mogelberg TE, Wallington TJ, Nielsen OJ (1996) J Phys Chem 100:7050
33. Gilles MK, Turnipseed AA, Talukdar RK, Rudich Y, Villalta PW, Huey LG, Burkholder JB, Ravishankara AR (1996) J Phys Chem 100:14005
34. Tuckett RP (2006) Adv Fluorine Sci (Elsevier) 1:89 ISBN: 9780444528117
35. Deyerl HJ, Alconcel LS, Continetti RE (2001) J Phys Chem A 105:552
36. Chase MW (1998) J Phys Chem Ref Data, Monograph no. 9
37. Blondel C, Delsart C, Goldfarb F (2001) J Phys B 34:L281
38. Garcia GA, Guyon PM, Powis I (2001) J Phys Chem A 105:8296

Chapter 5
Vacuum Ultraviolet Negative Photoion Spectroscopy of SF_5Cl

The experimental data for SF_5Cl was collected in May 2008 on beamline 3.1 of the Daresbury synchrotron radiation source. Many thanks go to Dr David Shaw, Professor Colin Latimer, Dr Ken Dunn and Professor Richard Tuckett for providing their experimental expertise. This work has been accepted for publication in the *Journal of Physical Chemistry A* (2010) [1].

5.1 Background Information

The anthropogenic gas sulphur chloropentafluoride (SF_5Cl) is used as a reagent in chemical synthesis, but only for the infrequently required application of introducing an SF_5 group into other molecules [2, 3]. Therefore gas-phase studies on this molecule are few and far between, and are generally limited to fundamental investigations where SF_5Cl is compared to its better-known relation sulphur hexafluoride (SF_6). More recently these studies have extended to include another related molecule, trifluoromethyl sulphur pentafluoride (SF_5CF_3). The negative ion spectroscopy of SF_6 and SF_5CF_3 has already been reported in Chap. 3. The structure of SF_5Cl, C_{4v} symmetry in the gas phase, has been established by microwave spectroscopy [4] and electron diffraction [5]. Four equatorial S–F bonds have a slightly shorter length, 0.157 nm, than the S–F axial bond, 0.159 nm, while that of S–Cl is significantly longer, 0.204 nm. Perhaps surprisingly, there are no vacuum ultraviolet photoabsorption spectra of any kind, either below or above the energy of the LiF cutoff (11.8 eV), reported in the literature.

It is the electron scavenging properties of SF_6 which make it such an important gas, and hence several groups have investigated electron attachment to SF_5Cl [6–9]. There have been two measurements of the thermal electron attachment rate coefficient for SF_5Cl are $(4.8 \pm 1.2) \times 10^{-8}$ cm^3 s^{-1} by Van Doren et al. [9] and $(2.0 \pm 0.3) \times 10^{-8}$ cm^3 s^{-1} by Mayhew et al. [6]. In comparison, the generally accepted values for SF_6 and SF_5CF_3 are $(2.38 \pm 0.15) \times 10^{-7}$ cm^3 s^{-1}, and

DOI: 10.1007/978-3-642-23129-2_5,

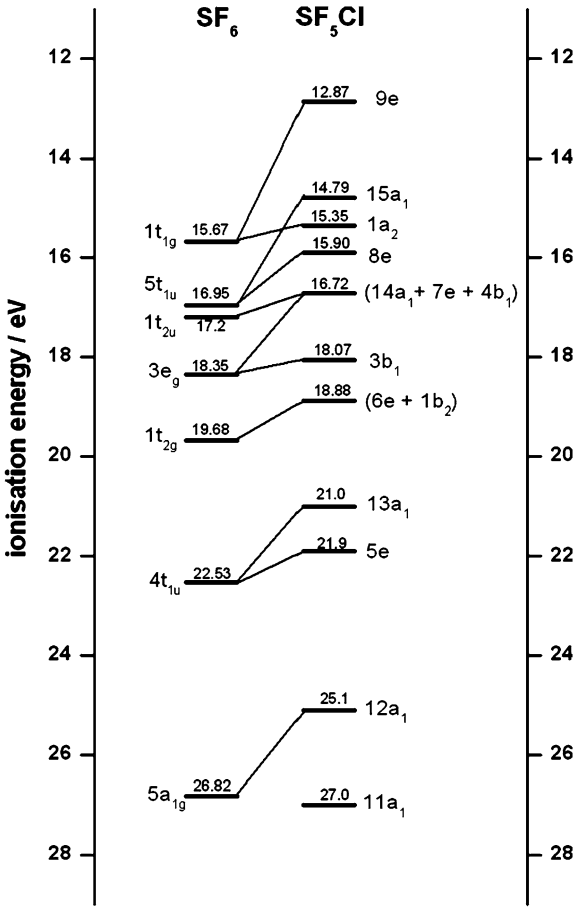

Fig. 5.1 Valence electronic molecular orbitals assigned to energy maxima of features (indicated by solid lines with numeric values, in eV) observed in experimental photoelectron spectra for SF_6 [14] and SF_5Cl [10]. Following increasing ionisation energy the ordering goes from top to bottom, and where applicable, from left to right. Orbitals in parenthesis are thought to lie close in energy but have not been individually resolved in experimental spectra

$(8.0 \pm 0.3) \times 10^{-8}$ cm^3 s^{-1}, respectively [6]. Electron attachment to SF_6 is predominantly non-dissociative, whereas SF_5CF_3 and SF_5Cl attach electrons via dissociative processes: SF_5^- is the major anion product in both instances.

Information on the valence electronic structure of SF_5Cl is limited. Photoelectron spectra reported by DeKock et al. [10] followed up with calculations by Klyagina et al. [11], provided the first ordering for the molecular orbital (MO) configuration of SF_5Cl. A more recently recorded threshold photoelectron spectrum, using synchrotron radiation, has confirmed the experimental work by DeKock in the 12–20 eV range [12]. This publication also reports results from a calculation which supports the MO assignments (to the experimentally observed bands) made by Klyagina et al. Figure 5.1 summarises the combined findings of these three investigations and correlates the MOs for SF_5Cl, of C_{4v} symmetry, with those of SF_6, of O_h symmetry. While the ordering of the valence MOs in Fig. 5.1 (i) for SF_6 is well known [13, 14], it is noted that the ordering and assignments given for SF_5Cl is based on limited evidence.

The sample of SF_5Cl used in this experiment was obtained from *Apollo Scientific* with a quoted purity of 97%. Impurities of SF_4, FCl and Cl_2 have been noted in previous studies using SF_5Cl samples, and small amounts of SF_xO_y species have also been detected—identified as products from the hydrolysis of SF_4 [8, 12]. There is no way of eliminating any potential contributions from these impurities to the anion spectra reported here.

The anions F^-, SF_5^- and Cl^- were detected following VUV photoexcitation of SF_5Cl. The F^- signal was by far the strongest of the three, whilst the other two anions were only just detected above the sensitivity limit of the apparatus.

5.2 F^- from SF_5Cl

The cross section for F^- formation is shown in Fig. 5.2 over the range 12–30 eV. The F^- signal was shown to increase linearly with increasing SF_5Cl gas pressure, thus indicating it is formed via unimolecular ion-pair dissociation. The experimentally determined onset for F^- production is 12.7 ± 0.2 eV (Fig. 5.2a and b). It is noteworthy that this value lies *above* the adiabatic ionisation energy for SF_5Cl, 12.3 eV [10, 12]. The onset is gradual and the cross section increases at a steady gradient up to about 13.6 eV. From this point the gradient appears to increase, leading to the cross section maximum of 6.1×10^{-20} cm^2 at 14.06 eV (Fig. 5.2b).

The 'shoulder', from onset at 12.7 eV to the point of change in gradient at 13.6 eV (labelled '1' in Fig. 5.2b) may arise from one or more of the following three ion-pair dissociation reactions:

$$SF_5Cl \rightarrow F^- + SF_4Cl^+ \tag{5.1}$$

$$SF_5Cl \rightarrow F^- + SF_3^+ + FCl \tag{5.2}$$

$$SF_5Cl \rightarrow F^- + SF_3Cl^+ + F \tag{5.3}$$

There is uncertainty in the enthalpy of formation for SF_4Cl^+: the value used is +327 kJ mol^{-1} which represents an *upper limit* determined from the appearance energy of SF_4Cl^+ ions following the dissociative photoionisation of SF_5Cl [12]. The corresponding upper limit for the enthalpy change of reaction (5.1) is 11.6 eV, whilst the enthalpy change for reaction (5.2) is 11.4 eV. The enthalpy change for reaction (5.3) is also expected to be less than the appearance energy of F^- ions of 12.7 eV, but the value for $\Delta_f H°_{298}$ (SF_3Cl^+) is not known. It is worth noting that the SF_3Cl^+ species has *not* been observed in photon excitation or electron impact excitation experiments [12], casting doubt over the production of F^- ions from reaction (5.3).

The feature in the F^- ion yield between 13.6 and 14.8 eV is labelled '2' in Fig. 5.2b. The increase in gradient of the cross section at 13.6 eV, giving rise to feature 2, correlates to the thermochemical onset of 13.5 eV for the dissociation reaction shown in (5.4).

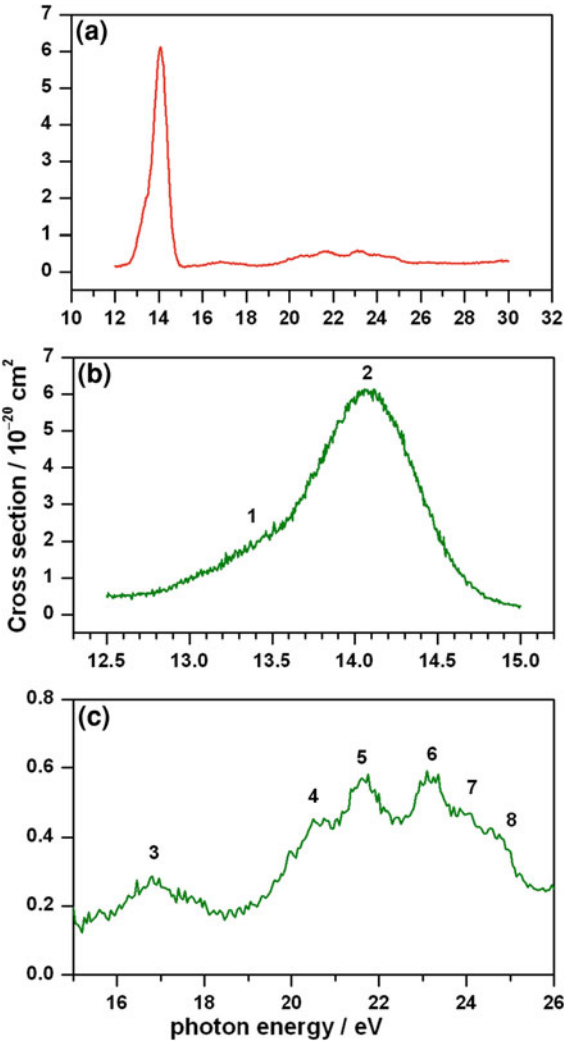

Fig. 5.2 Cross section for F^- formation from SF_5Cl, **a** From 12 to 30 eV recorded with a step size of 0.05 eV and a wavelength resolution of 6 Å, **b** From 12.5 to 15.0 eV recorded with a step size of 0.005 eV and a wavelength resolution of 1.2 Å and **c** A blow-up of spectrum (**a**) between 15 and 26 eV. All of the observable features in the F^- cross section are labelled 1–8 in spectra (**b**) and (**c**) and are referred to in the text

$$SF_5Cl \rightarrow F^- + SF_4^+ + Cl \tag{5.4}$$

This evidence suggests that the most significant contribution to the F^- cross section at 14.06 eV is from the F^-/SF_4^+ ion-pair process in which the S–Cl bond is also broken, and not from dissociation reactions (5.1–5.3).

It is difficult to assign features in ion-pair spectra to specific dissociation reactions with any confidence. This is particularly true at higher photon energies because the number of accessible ion-pair reaction products increases. Some examples of the many reactions which may be occurring at photon energies >14 eV (giving rise to features 3–8 shown in Fig. 5.2c) are listed below:

$$SF_5Cl \rightarrow F^- + Cl^+ + SF_4 \qquad \Delta_r H^\circ = 14.5\,eV \tag{5.5}$$

$$SF_5Cl \rightarrow F^- + SF_2^+ + F + FCl \qquad \Delta_r H^\circ = 15.7\,eV \tag{5.6}$$

$$SF_5Cl \rightarrow F^- + SF^+ + F_2 + FCl \qquad \Delta_r H^\circ = 18.0\,eV \tag{5.7}$$

$$SF_5Cl \rightarrow F^- + SF_2^+ + 2F + Cl \qquad \Delta_r H^\circ = 18.3\,eV \tag{5.8}$$

$$SF_5Cl \rightarrow F^- + Cl^+ + SF_3 + F \qquad \Delta_r H^\circ = 18.7\,eV \tag{5.9}$$

$$SF_5Cl \rightarrow F^- + Cl^+ + SF_2 + F_2 \qquad \Delta_r H^\circ = 19.4\,eV \tag{5.10}$$

$$SF_5Cl \rightarrow F^- + SF^+ + 2F + FCl \qquad \Delta_r H^\circ = 19.7\,eV \tag{5.11}$$

$$SF_5Cl \rightarrow F^- + SF^+ + F_2 + F + Cl \qquad \Delta_r H^\circ = 20.6\,eV \tag{5.12}$$

$$SF_5Cl \rightarrow F^- + Cl^+ + SF_2 + 2F \qquad \Delta_r H^\circ = 21.0\,eV \tag{5.13}$$

$$SF_5Cl \rightarrow F^- + SF^+ + 3F + Cl \qquad \Delta_r H^\circ = 22.3\,eV \tag{5.14}$$

Feature 1 in the F^- ion yield exhibits characteristics often associated with *direct* ion-pair formation; the onset is gradual and the resulting feature is broad and structureless. However, it is not possible to rule out an *indirect* process, identifying feature 1 as a Rydberg state. There is no identifiable maximum to feature 1—it appears in the cross section as a shoulder—and therefore no attempt is made to assign it using the Rydberg formula. Features 2–8 in Fig. 5.2 have been assigned and the results are shown in Table 5.1. In producing this table it is assumed, in most cases, that the given Rydberg state converges towards the excited state of SF_5Cl^+ closest in energy to that of the feature. For example, it is assumed that feature 2 at 14.06 eV converges to SF_5Cl^+ $\tilde{A}\ ^2A_1$ at 14.79 eV and not to SF_5Cl^+ $\tilde{B}\ ^2A_2$ at 15.35 eV. However, this assumption is not made for feature 4 and two potential assignments have been given.

The cross section for F^- formation at its maximum point, at feature 2, is 6.1×10^{-20} cm^2. Features 3–8 are much weaker in comparison and the cross section is approximately an order of magnitude smaller; the cross section at 23.2 eV, corresponding to feature 6, is 5.9×10^{-21} cm^2. This may be due to the nature of the Rydberg state assigned to feature 2. Gaussian 03 calculations have shown the first excited state of SF_5Cl^+ involves the removal of an electron from the $15a_1$ MO which has both S–F_{eq} and S–Cl bonding character [12, 15]. The Rydberg state represented by feature 2 is thought to converge on the first excited state of SF_5Cl^+ and is identified to come from the dissociation reaction (5.4) where a fluorine anion and a chlorine atom are both cleaved from the molecule.

Table 5.1 Rydberg assignments to features observed in the F^- ion yield recorded following the photoexcitation of SF_5Cl

Feature[a]	E/eV[b]	IE[c]	δ[d]	Assignment[e]
2	14.06	14.79 ($\tilde{A}^2A_1$)	1.68	$6p^1A_1$
3	16.80	18.07 ($\tilde{G}^2A_1$)	1.73	$5p^1A_1$
4	20.65	21.0 ($\tilde{J}^2A_1$)	1.80	$8p^1A_1$
		21.9 ($\tilde{K}^2E$)	1.70	$5p^1E$
5	21.65	21.9 ($\tilde{K}^2E$)	1.62	$9p^1E$
6	23.20	25.1 ($\tilde{L}^2A_1$)	1.33	$4p^1A_1$
7	23.95	25.1 ($\tilde{L}^2A_1$)	1.56	$5p^1A_1$
8	24.60	25.1 ($\tilde{L}^2A_1$)	1.78	$7p^1A_1$

[a] The feature in the F^- ion yield as labelled in Fig. 5.2
[b] The photon energy of the feature identified from the spectra in Fig. 5.2. The uncertainty in these values is estimated to be ±0.01 eV for feature 2 and ±0.1 eV for features 3–8
[c] The electronic state of SF_5Cl^+ to which the assigned Rydberg state converges. Vertical ionisation energy values are taken from the work by DeKock et al. [10]
[d] Value of the quantum defect calculated from the Rydberg formula
[e] Rydberg orbital assignment

5.3 Cl^- from SF_5Cl

Cl^- anions were observed following the VUV photoexcitation of SF_5Cl, but the signal was very weak. Only one peak was detected in the range 8–35 eV, shown in Fig. 5.3. This feature was reproducible when scanning over the same energy region with a LiF window in place and so it is not an artefact arising from higher-order radiation. The appearance energy for Cl^- anions is 10.6 ± 0.2 eV and the maximum of the resulting single peak is 10.9 eV. Now, these energies lie *below* the adiabatic ionisation energy of SF_5Cl, 12.3 eV [10, 12]; therefore, Cl^- can only form from an ion-pair dissociation. The only energetically accessible ion-pair dissociation reaction at this energy is:

$$SF_5Cl \rightarrow Cl^- + SF_5^+ \qquad \Delta_r H^\circ = 8.7 \text{ eV} \tag{5.15}$$

The experimental onset therefore occurs 1.9 eV above the thermochemical threshold. This feature may be assigned as the initial transition from the highest occupied MO to an excited Rydberg state, $9e \rightarrow 4p$, converging on SF_5Cl^+ $\tilde{X}\ ^2E$ which then predissociates into the Cl^-/SF_5^+ ion-pair state. The spectrum in Fig. 5.3 has not been put onto an absolute scale because the signal detected was so weak.

5.4 SF_5^- from SF_5Cl

SF_5^- anions were also detected from SF_5Cl. A spectrum was recorded in the range 12–35 eV which is presented in Fig. 5.4. The SF_5^- signal was very weak and the spectrum is noisy as a result. There is only one distinct feature in the spectrum, at

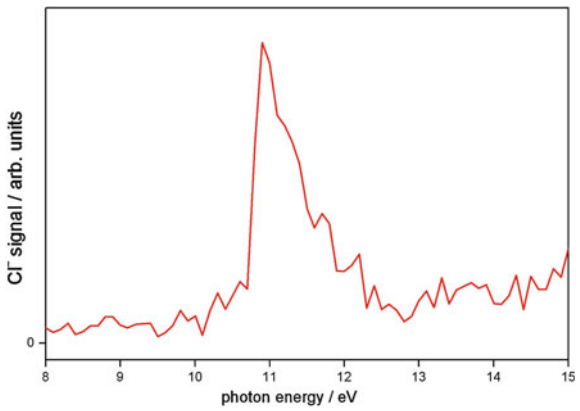

Fig. 5.3 The observation of Cl^- anions following the photoexcitation of SF_5Cl in the range 8–15 eV. The spectrum was recorded with a step size of 0.1 eV and a wavelength resolution of 6 Å

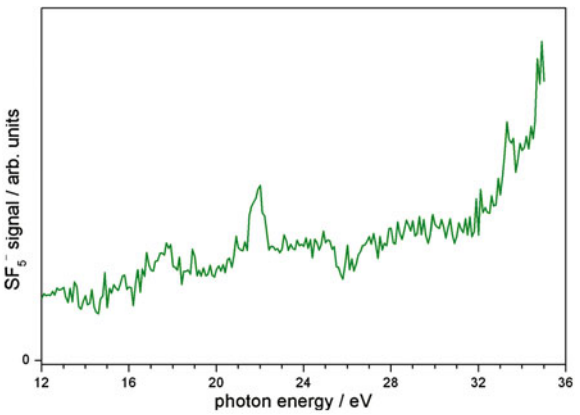

Fig. 5.4 SF_5^- ion yield recorded following the photoexcitation of SF_5Cl in the range 12–35 eV. The spectrum was recorded with a step size of 0.1 eV and a wavelength resolution of 6 Å

22.0 eV, and when the excitation source was fixed at this energy the SF_5^- signal was shown to increase *non*-linearly with increasing SF_5Cl gas pressure. It is concluded, therefore, that the SF_5^- anions are produced by the dissociative electron attachment process outlined below, where photoionisation provides the source of low-energy electrons:

$$SF_5Cl + e^- \rightarrow SF_5^- + Cl \tag{5.16}$$

It is noted that this anion is the dominant species from studies of thermal electron attachment to SF_5Cl [6].

As discussed in Sect. 5.1 the thermal electron attachment rate coefficient for SF_5Cl is in the region of (2–5) $\times$ 10^{-8} cm^3 s^{-1}. This value is of a similar magnitude to that of other molecules such as SF_5CF_3 ($k_a = 8.0 \times 10^{-8}$ cm^3 s^{-1}, see Chap. 3) and CF_3Br ($k_a = 1.4 \times 10^{-8}$ cm^3 s^{-1}, see Chap. 4). In the photon experiments reported in this thesis, the anions SF_5^- and Br^- from SF_5CF_3 and CF_3Br, respectively, are observed and identified as products from electron

attachment reactions rather than from ion-pair dissociation. Thus, SF_5Cl is following the same pattern. It is predicted that an anion spectrum resulting from an electron attachment process will mimic, at least to some extent, a threshold photoelectron spectrum. The feature in Fig. 5.4 at 22.0 eV matches the vertical ionisation energy for the band observed from photoelectron spectroscopy at 21.9 eV (see Fig. 5.1). This is, however, the *only* such similarity between the two different types of spectra and the reasons for this is not known.

5.5 Conclusions

The anions F^-, Cl^-, and SF_5^- have been observed following the VUV photoexcitation of SF_5Cl. The F^- and Cl^- anions arise from ion-pair dissociation but SF_5^- is produced from dissociative electron attachment. Only the production of F^- can be put onto an absolute cross section scale, but the quantum yield for its production cannot be determined since photoabsorption cross section data are not available. Indeed, the analysis of the results is limited by the lack of other complimentary spectroscopic investigations, e.g. fluorescence excitation as well as photoabsorption spectra.

It is an apparent coincidence that the *AE* for F^- from both SF_5Cl and SF_6 takes the same value, 12.7 ± 0.2 eV (Table 5.2): there is no reasonable explanation for their equality. It is the relative position of the *AE* to the adiabatic *IE* of the parent molecule which is more interesting. The most significant features in the F^- spectrum from SF_6 appear below the *IE* (Fig. 3.1a), yet for SF_5Cl the *AE* (F^-) exceeds the *IE*. In fact, the same comment is made when comparing F^- from CF_4 (Fig. 3.2i) with F^- from CF_3Cl (Fig. 4.1): for CF_4 the *AE* (F^-) < *IE*, for CF_3Cl the *AE* (F^-) > *IE* (Table 5.2).

SF_6 and CF_4 follow the 'expected' trend that the probability for an excited electronic state to predissociate into ion pairs is greater in the absence of a competing autoionisation process. It is possible, therefore, that the change in symmetry on substituting a F for a Cl atom (e.g. $SF_6 \rightarrow SF_5Cl$) suppresses the formation of ion pairs below the ionisation energy—or rather *increases* the probability of a competing process, such as neutral dissociation (e.g. $SF_5Cl \rightarrow SF_5 + Cl$). With respect to SF_5Cl this idea is only speculative because data from other VUV experiments, such as fluorescence excitation spectra, let alone photoabsorption spectra, are not available. However, when comparing the data for ion-pair formation from CF_3Cl with total photoabsorption and fluorescence excitation spectra, the evidence suggested that photoexcitation below the *IE* must almost exclusively result from neutral photodissociation [19] (also see Sect. 4.1).

The lack of ion-pair formation processes from SF_5Cl producing Cl^- anions cannot be explained. Indeed, perhaps the most interesting aspect of this work is the observation that the F^- cross sections are orders of magnitude greater than the Cl^- cross sections, yet the S–Cl bond is significantly weaker than the S–F bond; the bond dissociation energies are 2.5 and 3.7 eV, respectively (calculated from

Table 5.2 Comparisons of data obtained for the ion-pair formation of F^- from SF_5Cl, SF_6 and SF_5CF_3. The separate comparison of CF_3Cl vs CF_4 is also included. The complete data for SF_6, SF_5CF_3, and CF_4 are presented and discussed in Chap. 3, and those for CF_3Cl in Chap. 4

Molecule	IE[a]/eV	AE (F^-)[b]/eV	Reaction at AE[c]	E (σ_{max})[d]/eV	Reaction at σ^c_{max}
SF_5Cl	12.3	12.7 ± 0.2	Not known	14.06	$SF_5Cl \rightarrow F^- + SF_4^+ + Cl$
SF_6	15.1	12.7 ± 0.2	$SF_6 \rightarrow F^- + SF_5^+$	14.2	$SF_6 \rightarrow F^- + SF_5^+$
SF_5CF_3	12.9	11.05 ± 0.05	$SF_5CF_3 \rightarrow F^- + CF_3^+ + SF_4$	16.9	Not known
CF_3Cl	12.4	16.0 ± 0.2	$CF_3Cl \rightarrow F^- + CF_2^+ + Cl$	21.0	Not known
CF_4	15.4	13.0 ± 0.2	$CF_4 \rightarrow F^- + CF_3^+$	14.0	$CF_4 \rightarrow F^- + CF_3^+$

[a] Adiabatic ionisation energy for SF_5Cl [10], SF_6 [13], SF_5CF_3 [16], CF_3Cl [17] and CF_4 [18]
[b] Experimentally observed appearance energy for F^- anions
[c] The ion-pair dissociation reactions are assigned by comparing calculated reaction enthalpies with onsets to features observed in the anion spectra
[d] The energy position of the maximum point in the cross section

$\Delta_f H°_{298}$ values provided in Appendix I). These and other generic issues on ion-pair dissociation reactions are addressed in Chap. 6.

References

1. Simpson MJ, Tuckett RP (2010) J Phys Chem A 114:8043
2. Tullock CW, Coffman DD, Muetterties EL (1964) J Am Chem Soc 86:357
3. Jonethal U, Kuschel R, Seppelt K (1998) J Fluorine Chem 88:3
4. Bellet J, Jurek R, Chanussot J (1979) J Mol Spectrosc 78:16
5. Marsden CJ, Bartell LS (1976) Inorg Chem 15:3004
6. Mayhew CA, Critchley A, Howse DC, Mikhailov V, Parkes MA (2005) Eur Phys J D 35:307
7. Mayhew CA, Critchley A, Jarvis GK (2004) Int J Mass Spectrom 233:259
8. Braun M, Ruf M-W, Hotop H, Cicman C, Scheier P, Märk TD, Illenberger E, Tuckett RP, Mayhew CA (2006) Int J Mass Spectrom 252:234
9. Van Doren JM, Miller TM, Viggiano AA, Spanel P, Smith D, Bopp C, Troe J (2008) J Chem Phys 128:094309
10. DeKock RL, Higginson BR, Lloyd DR (1972) J Chem Soc Faraday Discuss 54:84
11. Klyagina AP, Levin AA, Gutzev GL (1981) Chem Phys Lett 77:365
12. Chim RYL, Cicman C, Märk TD, Mayhew CA, Scheier P, Tuckett RP (2007) Int J Mass Spectrom 261:208
13. Yencha AJ, Thompson DB, Cormack AJ, Cooper DR, Zubek M, Bolognesi P, King GC (1997) Chem Phys 216:227
14. Holland DMP, MacDonald MA, Baltzer P, Karlsson L, Lundqvist M, Wannberg B, Von Niessen W (1995) Chem Phys 192:333
15. Tuckett RP, Parkes MA (2010) Private communication
16. Chim RYL, Kennedy RA, Tuckett RP, Zhou W, Jarvis GK, Collins DJ, Hatherly PA (2001) J Phys Chem A 105:8403
17. Creasey JC, Smith DM, Tuckett RP, Yoxall KR, Codling K, Hatherly PA (1996) J Phys Chem 100:4350
18. Creasey JC, Jones HM, Smith DM, Tuckett RP, Hatherly PA, Codling K, Powis I (1993) Chem Phys 174:441
19. Simpson MJ, Tuckett RP, Dunn KF, Hunniford CA, Latimer CJ (2009) J Chem Phys 130:194302

Chapter 6
Vacuum Ultraviolet Negative Photoion Spectroscopy of Small Polyatomic Molecules

6.1 Summary of Results

A total of 24 small polyatomic molecules have been studied by the Chemical Physics groups in Birmingham and Belfast from 2005 to 2008 using VUV negative photoion spectroscopy: the data for SF_5CF_3, SF_6 and CF_4 were published in 2008 in the *Journal of Chemical Physics* [1], and updated here in Chap. 3; the data for CF_3Cl, CF_3Br and CF_3I were published in 2009 in the *Journal of Chemical Physics* [2], and are also presented here in Chap. 4; the data for SF_5Cl were published in 2010 in the *Journal of Physical Chemistry A* [3], and are also presented here in Chap. 5; the data for CH_4, CH_3F, CH_3Cl and CH_3Br were published in 2010 by Rogers et al. [4, 5]; the data recorded for the remaining 13 molecules (C_2H_4, C_2H_6, C_3H_8, C_2F_4, C_2F_6, C_3F_8, CH_2F_2, CHF_3, CH_2Cl_2, $CHCl_3$, CCl_4, CF_2Cl_2, $CFCl_3$) are presented here in Appendix II. Specific data for *all* of these molecules [such as anions observed, appearance energies (*AE*s), cross sections (σ) and quantum yields (Φ)] are compiled in Table 6.1. This forms the most comprehensive collection of information about ion-pair formation from polyatomic molecules since the 1996 Berkowitz review [6].

Of these 24 molecules, several have been studied previously, by other research groups, using VUV anion spectroscopy. These data are available in the literature for CF_4 [41], SF_6 [42, 43], CH_4 [44], CH_3X (X = F, Cl, Br) [45], C_2H_4 [46], C_2H_6 [47, 48], C_3H_8 [47], and the chlorofluoromethanes ($CFCl_3$, CF_2Cl_2, CF_3Cl) [49]. The present work is in excellent agreement with these earlier studies and in most cases the quality and quantity of data obtained have improved. For example, anion spectra have been recorded over a larger photon energy range (typically from onset up to 35 eV) and new anions have been observed. Indeed the apparatus used to collect these data provides excellent sensitivity which is crucial when detecting negative ions. New results are presented here for SF_5CF_3, SF_5Cl, CF_3X, the perfluorocarbons, the fluoromethanes and the chloromethanes.

M. J. Simpson, *Two Studies in Gas-Phase Ion Spectroscopy*, Springer Theses,
DOI: 10.1007/978-3-642-23129-2_6, © Springer-Verlag Berlin Heidelberg 2012

Table 6.1 A summary of data collected for anion production following the VUV photoexcitation of twenty-four gas-phase polyatomic molecules

Molecule 1	IE[a]/eV 2	Anion 3	AE^{b}_{298}/eV 4	Reaction at AE[c] 5	$\Delta_r H^{\circ d}_{298}$/eV 6	σ^{e}_{max}/cm^2 7	$E(\sigma_{max})$[f]/eV 8	$\Phi(\sigma_{max})$[g] 9
CH_4[h]	12.61	H^-	13.30 ± 0.10	$CH_4 \rightarrow H^- + CH_3^+$	13.7	1.4×10^{-22}	20.6	4.4×10^{-6}
C_2H_4[i]	10.51	H^-	13.06 ± 0.10	$C_2H_4 \rightarrow H^- + C_2H_3^+$	12.5	8.3×10^{-22}	18.0	1.4×10^{-5}
C_2H_6[i]	11.52	H^-	12.00 ± 0.10	$C_2H_6 \rightarrow H^- + C_2H_5^+$	11.9	1.7×10^{-21}	19.3	2.7×10^{-5}
C_3H_8[i]	10.9	H^-	13.2 ± 0.2	$C_3H_8 \rightarrow H^- + C_3H_7^+$	11.7	3.3×10^{-21}	18.6	3.3×10^{-5}
CF_4[j]	15.4	F^-	13.0 ± 0.2	$CF_4 \rightarrow F^- + CF_3^+$	11.3	1.4×10^{-21}	14.0	2.8×10^{-5}
		F_2^-	20.1 ± 0.2	$CF_4 \rightarrow F_2^- + CF^+ + F$	19.3	4.0×10^{-23}	21.6	5.6×10^{-7}
C_2F_4[i]	10.12	F^-	13.17 ± 0.05	$C_2F_4 \rightarrow F^- + C_2F_3^+$	12.4	1.7×10^{-20}	16.5	-[m]
		CF^-	22.4 ± 0.5	$C_2F_4 \rightarrow CF^- + CF^+ + 2F$	19.7	2.4×10^{-22}	27.5	-[m]
C_2F_6[i]	13.4	F^-	13.62 ± 0.10	$C_2F_6 \rightarrow F^- + C_2F_5^+$	11.5	7.4×10^{-21}	14.7	-[n]
C_3F_8[i]	13.0	F^-	13.1 ± 0.2	$C_3F_8 \rightarrow F^- + C_3F_7^+$	12.2	4.7×10^{-21}	23.4	-[m]
		CF_2^-	20.4 ± 0.2	-[k]	–	4.9×10^{-22}	21.8	-[m]
CH_3F[L]	12.53	H^{-p}	–	–	–	–	–	–
		F^-	12.28 ± 0.02	$CH_3F \rightarrow F^- + CH_3^+$	11.2	1.2×10^{-19}	13.4	2.3×10^{-3}
		CF^-	24.4 ± 0.2	$CH_3F \rightarrow CF^- + H^+ + 2H$	22.1	4.2×10^{-23}	27.2	1.5×10^{-6}
		CHF^-	21.5 ± 0.2	$CH_3F \rightarrow CHF^- + H^+ + H$	21.7	8.8×10^{-23}	22.4	2.2×10^{-6}
		CH_2F^-	18.2 ± 0.2	$CH_3F \rightarrow CH_2F^- + H^+$	17.7	4.1×10^{-23}	19.7	8.9×10^{-7}
CH_2F_2[i]	12.729	H^{-q}	12.08 ± 0.05[r]	$CH_2F_2 \rightarrow H^- + CHF_2^+$	12.5[r]	–	–	–
		F^-	11.86 ± 0.05	$CH_2F_2 \rightarrow F^- + CH_2F^+$	10.7	6.6×10^{-21}	18.8	1.4×10^{-4}
		F_2^-	17.20 ± 0.05	$CH_2F_2 \rightarrow F_2^- + CH_2^+$	15.9	3.3×10^{-22}	18.5	6.9×10^{-6}
CHF_3[i]	13.8	H^{-q}	12.82 ± 0.05[r]	$CHF_3 \rightarrow H^- + CF_3^+$	12.9[r]	–	–	–
		F^-	≤ 12.4 [s]	$CHF_3 \rightarrow F^- + CHF_2^+$	11.0	4.5×10^{-21}	23.1	8.2×10^{-5}
		CF_3^-	16.6 ± 0.2	$CHF_3 \rightarrow CF_3^- + H^+$	16.5	2.7×10^{-20}	18.0	4.4×10^{-4}
CH_3Cl[L]	11.29	H^{-p}	–	–	–	–	–	–
		Cl^-	10.04 ± 0.02	$CH_3Cl \rightarrow Cl^- + CH_3^+$	9.9	1.2×10^{-19}	11.3	2.3×10^{-3}
		CH_2Cl^-	17.2 ± 0.2	$CH_3Cl \rightarrow CH_2Cl^- + H^+$	17.2	7.6×10^{-21}	18.2	1.0×10^{-4}
CH_2Cl_2[i]	11.326	H^{-q}	11.5 ± 0.2[r]	$CH_2Cl_2 \rightarrow H^- + CHCl_2^+$	11.7[r]	–	–	–
		Cl^-	9.31 ± 0.05	$CH_2Cl_2 \rightarrow Cl^- + CH_2Cl^+$	8.6	6.6×10^{-20}	10.1	1.0×10^{-3}
		Cl_2^-	13.74 ± 0.10	$CH_2Cl_2 \rightarrow Cl_2^- + CH_2^+$	13.0	1.4×10^{-21}	16.0	1.5×10^{-5}

(continued)

Table 6.1 (continued)

Molecule 1	IE^{a}/eV 2	Anion 3	AE^{b}_{298}/eV 4	Reaction at AE^{c} 5	$\Delta_r H^{\circ d}_{298}$/eV 6	σ^{e}_{max}/cm^2 7	$E(\sigma_{max})^{f}$/eV 8	$\Phi(\sigma_{max})^{g}$ 9
$CHCl_3$[i]	11.30	H^{-q}	11.2 ± 0.2	$CHCl_3 \rightarrow H^- + CCl_3^+$	11.2	–	–	–
		Cl^-	9.26 ± 0.05	$CHCl_3 \rightarrow Cl^- + CHCl_2^+$	7.9	7.0×10^{-21}	20.3	5.4×10^{-5}
		CH^-	22.7 ± 0.2	$CHCl_3 \rightarrow CH^- + Cl^+ + 2Cl$	22.8	3.7×10^{-22}	24.8	5.7×10^{-6}
		CCl^-	19.3 ± 0.5	-[T]	–	5.7×10^{-22}	20.3	4.4×10^{-6}
CCl_4[i]	11.30	Cl^{-u}	11.35 ± 0.05	$[CCl_4 + e^- \rightarrow CCl_3 + Cl^-]$	–	–	–	–
		CCl^-	21.2 ± 0.2	-[T]	–	1.6×10^{-21}	23.8	1.7×10^{-5}
CF_3Cl[w]	12.4	F^-	16.0 ± 0.2	$CF_3Cl \rightarrow F^- + CF_2^+ + Cl$	15.6	1.5×10^{-20}	21.0	1.8×10^{-4}
		Cl^-	16.1 ± 0.2	$CF_3Cl \rightarrow Cl^- + CF_2^+ + F$	15.4	2.3×10^{-21}	20.9	2.9×10^{-5}
		F_2^-	21 ± 2	$CF_3Cl \rightarrow F_2^- + Cl^+ + CF$	21.1	6.8×10^{-23}	22.7	8.5×10^{-7}
		FCl^-	18 ± 2	-[T]	–	6.5×10^{-23}	20.8	8.0×10^{-7}
		CF^-	25.5 ± 0.2	-[k]	–	1.6×10^{-22}	27.3	-[m]
		CF_2^-	20.2 ± 0.2	$CF_3Cl \rightarrow CF_2^- + Cl^+ + F$	20.3	1.5×10^{-22}	21.3	1.8×10^{-6}
		CF_3^-	15.5 ± 0.2	$CF_3Cl \rightarrow CF_3^- + Cl^+$	14.9	2.8×10^{-22}	18.1	3.5×10^{-6}
CF_2Cl_2[i]	11.734	F^-	12.2 ± 0.1	$CF_2Cl_2 \rightarrow F^- + CFCl_2^+$	9.8	1.1×10^{-20}	19.1	1.0×10^{-4}
		Cl^-	10.35 ± 0.1	$CF_2Cl_2 \rightarrow Cl^- + CF_2Cl^+$	8.2	1.3×10^{-20}	20.0	1.2×10^{-4}
		CF^-	23.5 ± 0.5	-[k]	–	2.2×10^{-22}	25.6	-[m]
$CFCl_3$[i]	11.53	F^-	14.4 ± 0.2	$CFCl_3 \rightarrow F^- + CCl_2^+ + Cl$	13.7	1.2×10^{-21}	18.3	1.0×10^{-5}
		Cl^{-u}	11.54 ± 0.10	$[CFCl_3 + e^- \rightarrow CFCl_2 + Cl^-]$	–	–	–	–
CH_3Br[L]	10.54	H^{-q}	12.1 ± 0.2	$CH_3Br \rightarrow H^- + CH_2Br^+$	11.6	–	–	–
		Br^-	9.46 ± 0.02	$CH_3Br \rightarrow Br^- + CH_3^+$	9.5	2.5×10^{-20}	10.0	4.1×10^{-4}
		$CHBr^-$	20 ± 2	$CH_3Br \rightarrow CHBr^- + H^+ + H$	20.9	1.3×10^{-22}	22.4	3.3×10^{-6}
		CH_2Br^-	17.1 ± 0.2	$CH_3Br \rightarrow CH_2Br^- + H^+$	17.0	5.6×10^{-22}	17.8	8.1×10^{-6}
CF_3Br[w]	11.5	F^-	14.7 ± 0.2	$CF_3Br \rightarrow F^- + CF_2^+ + Br$	14.9	9.7×10^{-21}	19.6	1.2×10^{-4}
		Br^{-u}	15.1 ± 0.2	$[CF_3Br + e^- \rightarrow CF_3 + Br^-]$	–	–	–	–
		F_2^-	19 ± 0.2	$CF_3Br \rightarrow F_2^- + Br^+ + CF$	19.2	2.8×10^{-22}	20.4	3.4×10^{-6}
		FBr^-	18 ± 2	-[T]	–	5.5×10^{-22}	20.4	6.6×10^{-6}
		CF^-	23.6 ± 0.2	-[k]	–	3.4×10^{-22}	25.6	5.2×10^{-6}
		CF_2^-	18.2 ± 0.2	$CF_3Br \rightarrow CF_2^- + Br^+ + F$	18.5	4.9×10^{-22}	19.5	5.8×10^{-6}
		CF_3^-	13.6 ± 0.2	$CF_3Br \rightarrow CF_3^- + Br^+$	13.1	2.5×10^{-22}	14.8	4.0×10^{-6}

(continued)

Table 6.1 (continued)

Molecule 1	IE[a]/eV 2	Anion 3	AE^{b}_{298}/eV 4	Reaction at AE[c] 5	$\Delta_r H^{o d}_{298}$/eV 6	σ^{e}_{max}/cm^2 7	$E(\sigma_{max})$[f]/eV 8	$\Phi(\sigma_{max})$[g] 9
CF_3I[w]	10.37	F^-	9.7 ± 0.2	$CF_3I \rightarrow F^- + CF_2I^+$	-[T]	1.1×10^{-20}	20.4	-[m]
		I^-[x]	8.8 ± 0.2	$CF_3I \rightarrow I^- + CF_3^+$	8.3	–	–	-[x]
		F_2^-	17 ± 2	$CF_3I \rightarrow F_2^- + I^+ + CF$	17.2	8.5×10^{-23}	20.1	-[m]
		CF^-	21.6 ± 0.2	-[k]	–	1.1×10^{-22}	23.6	-[m]
		CF_2^-	16.0 ± 0.2	$CF_3I \rightarrow CF_2^- + I^+ + F$	16.4	4.6×10^{-22}	16.8	-[m]
		CF_3^-	11.0 ± 0.2	$CF_3I \rightarrow CF_3^- + I^+$	11.0	5.7×10^{-22}	12.7	-[m]
SF_6[j]	15.116	F^-	12.7 ± 0.2	$SF_6 \rightarrow F^- + SF_5^+$	10.4	7.1×10^{-21}	14.2	2.4×10^{-4}
		F_2^-	16.3 ± 0.2	$SF_6 \rightarrow F_2^- + SF_3^+ + F$	14.1	1.4×10^{-22}	18.3	1.9×10^{-6}
		SF_5^-[u]	15.1 ± 0.2	$[SF_6 + e^- \rightarrow F + SF_5^-]$	–	–	–	–
		SF_6^-[u]	15.1 ± 0.2	$[SF_6 + e^- \rightarrow SF_6^-]$	–	–	–	–
SF_5Cl[y]	12.3	F^-	12.7 ± 0.2	-[k]	–	6.1×10^{-20}	14.1	-[m]
		Cl^-	10.6 ± 0.2	$SF_5Cl \rightarrow Cl^- + SF_5^+$	8.7	–	10.9	–
		SF_5^-	–	$[SF_5Cl + e^- \rightarrow Cl + SF_5^-]$	–	–	–	–
SF_5CF_3[j]	12.9	F^-	11.05 ± 0.2	$SF_5CF_3 \rightarrow F^- + CF_3^+ + SF_4$	11.5	3.4×10^{-20}	16.9	3.4×10^{-4}
		F_2^-	16.1 ± 0.2	$SF_5CF_3 \rightarrow F_2^- + CF_3^+ + SF_3$	14.3	1.2×10^{-21}	17.9	1.1×10^{-5}
		SF^-	24.0 ± 0.2	$SF_5CF_3 \rightarrow SF^- + CF_3^+ + 4F$	23.0	2.8×10^{-22}	28.8	2.4×10^{-6}
		SF_2^-	20.2 ± 0.2	$SF_5CF_3 \rightarrow SF_2^- + CF_3^+ + 3F$	20.0	3.9×10^{-22}	24.2	2.5×10^{-6}
		SF_3^-	15.4 ± 0.2	$SF_5CF_3 \rightarrow SF_3^- + CF_3^+ + 2F$	16.0	1.0×10^{-20}	17.6	1.0×10^{-4}
		SF_4^-	13.0 ± 0.2	$SF_5CF_3 \rightarrow SF_4^- + CF_3^+ + F$	13.4	1.3×10^{-20}	14.1	1.7×10^{-4}
		SF_5^-	13.0 ± 0.2	$[SF_5CF_3 + e^- \rightarrow CF_3 + SF_5^-]$	–	–	–	–

[a] Adiabatic ionisation energy (IE) values are taken from the following sources: CH_4 [7, 8]; C_2H_4 [9]; C_2H_6 [10]; C_3H_8 [11]; CF_4 [12]; C_2F_4 [13]; C_2F_6 [14]; C_3F_8 [14]; CH_3F [15]; CH_2F_2 [16]; CHF_3 [17]; CH_3Cl [15]; CH_2Cl_2 [18]; $CHCl_3$ [19]; CCl_4 [JN Harvey, NJ Rogers, RP Tuckett, A Bodi, TPES of CCl4 recorded at SLS, PSI Villigen, unpublished data]; CF_3Cl [20]; CF_2Cl_2 [16]; $CFCl_3$ [19]; CH_3Br [21]; CF_3Br [20]; CF_3I [22]; SF_6 [23]; SF_5Cl [24, 25]; SF_5CF_3 [26]

[b] Experimentally determined appearance energy (AE)

[c] Reaction occurring at onset

[d] The enthalpy change at 298 K for the reaction in column 5, calculated from enthalpies of formation (listed in Appendix I)

[e] Absolute value for the ion-pair formation cross section (σ) at its maximum point

[f] Energy (E) at which the ion-pair formation cross section reaches its maximum point

(continued)

Table 6.1 (continued)

[g] Quantum yield (Φ) for ion-pair formation at E (σ_{max}). The ion-pair cross section is divided by the total photoabsorption cross section (σ_{abs}), from the following sources (for molecules not listed here see references in column 1): C_2H_4 [27]; C_2H_6 [28]; C_3H_8 [28]; CH_2F_2 [29]; CHF_3 [30]; CH_2Cl_2 [31]; $CHCl_3$ [D. P. Seccombe and R. P. Tuckett, *Absorption cross section for* $CHCl_3$ and $CFCl_3$, unpublished data]; CCl_4 [30]; CF_2Cl_2 [29]; $CFCl_3$ [D. P. Seccombe and R. P. Tuckett, *Absorption cross section for* $CHCl_3$ and $CFCl_3$, unpublished data]

[h] Data in columns 3–9 taken, with permission, from Rogers et al. [5]

[i] Preliminary results for this molecule are presented in Appendix II, from which the anion data (columns 3, 4, 7 and 8) are taken

[j] Data in columns 3–9 for CF_4, SF_6 and SF_5CF_3 are taken from Chap. 3

[k] The reaction occurring at the *AE* for this anion is not known due to the many different thermochemically available dissociation channels

[L] Data in columns 3–9 taken, with permission, from Rogers et al. [4]

[m] Total photoabsorption cross section is absent in the literature *or* not available over the required energy range, thus the ion-pair quantum yield cannot be calculated

[n] Total photoabsorption cross section for C_2F_6 is reported from 16–62 eV and so $\Phi(\sigma_{max})$, at 14.7 eV, cannot be calculated. However, $\Phi_{17.7\ eV}$ for F^- formation from C_2F_6 is 4.8×10^{-5} [σ_{abs} (C_2F_6, 17.7 eV) = 7.3×10^{-17} cm^2] [32]

[p] H^- detected at *m/z* 1, but signal was significantly weaker than the dominant anion. The H^- ion yield matches that of the dominant anion, presumably because of the *zero blast* effect [33] in the quadrupole mass spectrometer, and therefore cannot be trusted

[q] H^- detected at *m/z* 1, and the signal was of similar intensity to that of other anions. The H^- ion yield is unique, but may contain contributions from other anions due to the *zero blast* effect [33]. As a result, only limited information is presented here. For example, absolute cross sections cannot be determined for H^- ion-pair formation unless it is the only detected anion [4]

[r] The fact that $\Delta_r H°_{298}$ exceeds the AE_{298} may result from other anions being detected due to the *zero blast* effect (see notes [p] and [q]), giving an *AE* lower than it should be. Alternatively, thermal effects (i.e. hotbands) could cause the AE_{298} to preceed $\Delta_r H°_{298}$; the AE_{298} for H^- from CH_4, where the zero blast effect from other anions does not affect the spectrum, preceeds the calculated $\Delta_r H°_{298}$ value by 0.4 eV [5]

[s] Uncertainty in the AE_{298} arises from contributions to the cross section from absorptions of second order radiation over the energy range of interest (see Appendix II)

[T] $\Delta_f H°_{298}$ is not known for CCl^-, FCl^-, FBr^- and CF_2I^+

[u] Anion signal was shown to increase non-linearly with increasing parent gas pressure and electron attachment to the parent molecule is well documented; anion production is dominated by a two-step electron attachment process where photoionisation provides the source of electrons. The thermal electron attachment rate coefficients, k_a, in units of cm^3 s^{-1} are: CCl_4 [3.6×10^{-7}] [34]; $CFCl_3$ [2.4×10^{-7}] [35, 36]; CF_3Br [1.4×10^{-8}] [36]; CF_3I [1.9×10^{-7}] [37]; SF_6 [2.4×10^{-7}] [38]; SF_5Cl [(2–5) $\times 10^{-8}$] [38, 39]; SF_5CF_3 [8.0×10^{-8}] [38]

[w] Data in columns 3–9 for CF_3X molecules (X = Cl, Br, I) are taken from Chap. 4

[x] The I^- ion yield at $E \geq 10.4$ eV is dominated by dissociative electron attachment to CF_3I (see note [u]). However, below 10.4 eV the observed I^- signal must arise by unimolecular ion-pair dissociation; the cross section for I^- formation at 9.0 eV is 3.8×10^{-21} cm^2 with a corresponding quantum yield of 8×10^{-5} (photoabsorption cross section reported by Eden et al.) [40]

[y] Data in columns 3–9 for SF_5Cl are taken from Chap. 5

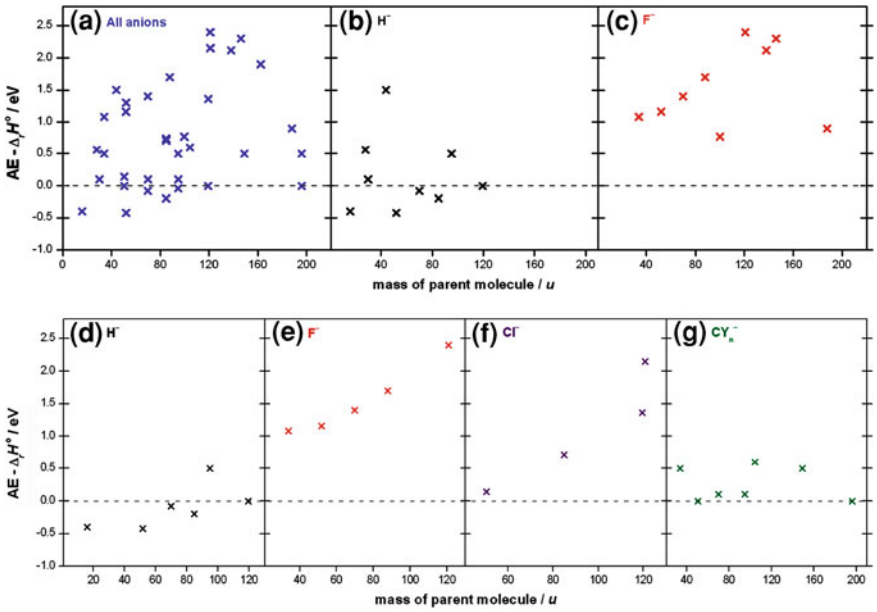

Fig. 6.1 (**a**–**c**) The distribution of AE_{298}—$\Delta_r H°_{298}$ for anions produced from a single bond-breaking ion-pair dissociation reaction (see Table 6.1). (**d**–**g**) Data extracted from graph (**a**) for methane and the halo-substituted methanes only. CY_n^- includes data for CF_3^-, CH_2F^-, CH_2Cl^- and CH_2Br^- ions

6.2 Ion-pair Appearance Energies and Thermochemical Thresholds

Consider the comparison between the experimental appearance energy (*AE*) for ion-pair formation and the thermochemically determined threshold (Table 6.1, columns 4 and 6, respectively). The former quantity must be greater than or equal to the latter. This is true for the majority of results shown in Table 6.1. For the few instances where this inequality is disobeyed (e.g. H^- from CH_4), thermal effects and/or uncertainty in the calculated $\Delta_r H°_{298}$ values are expected to be responsible. In most cases, when only one dissociation process is thermodynamically accessible, the reaction occurring at the *AE* can be unambiguously identified. These are *single* bond-breaking ion-pair dissociation reactions. *Multiple* bond-breaking ion-pair dissociation reactions are assigned more tentatively, assuming the process yielding the least amount of excess energy prevails (e.g. $CF_3Cl \rightarrow Cl^- + CF_2^+ + F$ rather than $CF_3Cl \rightarrow Cl^- + CF_3^+$). This assumption is justified by experimental observations: it is common for the appearance of a feature in an ion-pair spectrum to correlate with a possible dissociation threshold.

The difference between AE_{298} and $\Delta_r H°_{298}$ is plotted in Fig. 6.1a for all anions listed in Table 6.1 that result from *single* bond-breaking ion-pair dissociation. The apparently random distribution of points in this plot is expected. However, if the

points for H^- and F^- ions are plotted separately (Fig. 6.1b and c, respectively), the distributions show an interesting trend: the points for H^- ions are clustered around $AE - \Delta_r H^\circ = 0$, whilst those for F^- take larger values. This indicates the dynamics for H^- ion-pair formation allow for a tendancy for this anion to 'turn on' at the thermochemical threshold, favouring dissociation with low excess energy.

It is also interesting that the anion is H^- for four out of five instances in Fig. 6.1a where $AE - \Delta_r H^\circ < 0$ (the other is for Br^- with a value of −0.04 eV). In contrast, F^- ion pairs are formed with relatively larger excess energies. These trends become even clearer when the dataset is limited to methane and the halo-substituted methanes (Fig. 6.1d–g). Now, the data for Cl^- and CY_3^- (i.e. CF_3^-, CH_2F^-, CH_2Cl^- and CH_2Br^-) anions are also isolated and plotted. Low excess energies are also observed for CY_3^- anion formation; all points in graph (g) have values for $AE - \Delta_r H^\circ$ between 0 and 0.6 eV. In graphs (e) and (f) of Fig. 6.1, for F^- and Cl^- ions from halo-substituted methanes, a positive correlation between ($AE - \Delta_r H^\circ$) and mass of the parent molecule is observed. This is surprising given that the data were plotted against mass for no particular reason, the primary aim always being to observe the scattering about the *y* axis. Indeed, the same correlation is observed if the *x* axis represents the total number of electrons in the molecule, or the molecular polarisability. There is no explaination for this observation and ideally more data points are required if this trend is to be confirmed.

6.3 Ion-pair Formation Below the Ionisation Energy

From an experimental point of view it is advantageous to look for ion pairs below the ionisation energy (*IE*); there will be zero background signal, and anions or cations can be detected with the confidence that they must originate from ion-pair formation.

It is energetically possible for ion-pair formation to occur below the *IE* of the parent molecule if, for the generic reaction $AB \rightarrow A^- + B^+$, the electron affinity (*EA*) of A exceeds the bond dissociation energy (D°) of $A - B^+$ (discussed in Chap. 1). This condition is most likely satisfied when A is a halogen atom and its *EA* is large. Indeed, *theoretically*, this is true for every halogen-containing molecule in Table 6.1, with one exception: F^- from C_2F_4. Thus, D° ($F–C_2F_3^+$) > *EA* (F), where *EA* (F) is 3.401 eV [50]. Tetrafluoroethene is an unsaturated perfluorinated molecule and is a classic example of the 'perfluoro effect'; the C–F bonds in C_2F_4 are strengthened by the combined inductive effect of the fluorine atoms at the expense of a significantly weakened C = C bond (also the corresponding discussion in Chap. 8). Bond dissociation energies for ionised and neutral molecules of interest can be found in Appendix III.

The observation of ion-pair formation below the *IE* is not always restricted to instances where A is a halogen. Despite the small *EA* of the hydrogen atom, 0.754 eV [50], H^- ions may be observed below the *IE* from three out of the eleven

hydrogen-containing molecules listed in Table 6.1: CH_2F_2, CHF_3 and $CHCl_3$. For these three molecules $D°(H - CY_3^+) < 0.754$ eV (see Appendix III).

From all of the data in Table 6.1, there are only four instances where the cross section maximum, σ_{max}, was observed below the *IE* of the parent molecule: F^- from CF_4, Cl^- from CH_2Cl_2, Br^- from CH_3Br and F^- from SF_6. In all other cases, σ_{max} was recorded at photon energies above the *IE*. It is also worth noting that, for the majority of molecules, σ_{max} for producing *atomic* anions occurs between 16 and 22 eV—enough energy to access multiple bond-breaking ion-pair dissociation channels. Exceptions to this are for CF_4, C_2F_6, SF_6, SF_5Cl, CH_3F, CH_3Cl, CH_2Cl_2 and CH_3Br, where the lowest-energy ion-pair dissociation reaction occurs at the cross section maximum.

6.4 Quantum Yields

The quantum yield values, Φ, in Table 6.1 are probabilities for the formation of a given anion (via an ion-pair reaction) following the absorption of a photon by the parent molecule. The quantum yield is calculated by dividing the anion cross section by the total photoabsorption cross section. A quantum yield value is always quoted at a given energy. Each quantum yield listed in column 9 of Table 6.1 represents the maximum value calculated within the energy range studied. The largest quantum yield value is 2.3×10^{-3} or 0.23% (for both F^- from CH_3F *and* Cl^- from CH_3Cl). The smallest value is 5.6×10^{-7} or 0.000056% (for F_2^- from CF_4). The majority of quantum yields, however, lie between 5×10^{-4} and 1×10^{-6} (i.e. 0.05–0.0001%).

Some interesting observations are made based on the quantum yield data in column 9 in Table 6.1. By comparing these data between all of the listed molecules the following general statements are made:

1. Quantum yields for the production of an *atomic* anion are greater than quantum yields for the production of a *molecular* anion. There are some exceptions to this statement (e.g. CF_3^- formation from CHF_3).
2. Quantum yields for the production of an atomic halogen anion are greater than quantum yields for the production of H^- anions. Note that for instances where the H^- cross section (and hence quantum yield) was not determined (footnotes p and q in Table 6.1), its intensity was always similar to, or weaker than that for the halogen anion.
3. The quantum yield at E (σ_{max}) for F^- formation from the fluoromethanes increases as the number of fluorine atoms decreases: Φ (F^- from CH_3F) > Φ (F^- from CH_2F_2) > Φ (F^- from CHF_3) > Φ (F^- from CF_4). The opposite trend is observed for F^- anions produced from the chlorofluoromethanes: Φ (F^- from CF_3Cl) > Φ (F^- from CF_2Cl_2) > Φ (F^- from $CFCl_3$).
4. The quantum yield at E (σ_{max}) for Cl^- formation from the chloromethanes increases as the number of chlorine atoms decreases: Φ (Cl^- from CH_3Cl) > Φ

(Cl^- from CH_2Cl_2) > Φ (Cl^- from $CHCl_3$). The opposite trend is observed for Cl^- anions produced from the chlorofluoromethanes: Φ (Cl^- from CF_2Cl_2) > Φ (Cl^- from CF_3Cl). Note that Cl^- spectra recorded for $CFCl_3$ and CCl_4 were dominated by dissociative electron attachment; the contribution from Cl^- anions produced by ion-pair formation is not known.

5. The quantum yield at E (σ_{max}) for H^- formation from the hydrocarbons increases as the number of hydrogen atoms increases: Φ (H^- from C_3H_8) > Φ (H^- from C_2H_6) > Φ (H^- from C_2H_4) > Φ (H^- from CH_4).

These statements may be understood better if one considers the *electronegativity* of the individual atoms, and therefore the overall polarisation of the electron density across the molecule. Pauling electronegativities for relevant atoms are: F (3.98), Cl (3.16), Br (2.96), I (2.66), S (2.58), C (2.55) and H (2.20) [51]. For example, the bond polarisation in CH_4 can be represented by $C^{\delta-}$–$H^{\delta+}$, and in CF_4 by $C^{\delta+}$–$F^{\delta-}$. The effects of fluorine substitution in methane have been studied in great detail by Brundle et al. [17], and the following extract from their publication is particularly relevant:

> As expected, the protons in CH_4 are positively charged, while the carbon atom assumes a rather large negative charge. Upon the substitution of fluorine for hydrogen, the charges on the remaining protons are calculated to be very much what they are in CH_4, whereas the fluorines drain charge from the carbon and very quickly make it electropositive. In going from CH_4 to CF_4, the carbon atom surrenders over 1.6 electrons to the fluorines, mostly through the polarisation of the C–X bonds.

Qualitatively, one can therefore appreciate how F^- formation from CF_4 is more probable than H^- from CH_4. Also consider statement 3 for the fluoromethanes. Although the carbon atom gives up more charge as more H atoms are substituted for F atoms, the electron density on any *one* given F atom will be reduced when the total number of F atoms within the molecule increases. The same logic is followed for the chloromethanes and statement 4. For any chlorofluoromethane, however, the central carbon is always bonded to four highly electronegative species—the difference between electronegativities for F and Cl is relatively small. Now perhaps a statistical factor plays a part, whereby the number of F or Cl atoms determines which anion is formed in preference to the other; indeed the quantum yields at E (σ_{max}) for F^- and Cl^- from CF_2Cl_2 are almost identical (Table 6.1).

It is incorrect to attempt to understand any of the above statements by considering absolute energetic quantities such as electron affinites or bond dissociation energies; these values simply determine the asymptotic dissociation energy for the ion-pair state. Assuming indirect formation of ion pairs via an excited neutral state, it is the dynamics of the crossing between states which is important, and indeed the probability for the excited state to decay by a different process. Therefore, the position of the ion-pair state along the reaction coordinate (i.e. the value for r_e) and its shape are significant.

6.5 Competing ion-pair Reactions

It is observed from many ion-pair studies that different anions from the same molecule display peaks in their spectrum at the same energy. These peaks most likely identify the same excited intermediate state, and this is further evidence that ion pairs are commonly formed by the indirect mechanism. Specific examples for CH_2F_2 and CF_3Cl are discussed below.

The spectra for anions produced from CH_2F_2 are presented in Appendix II. The first band in the H^- spectrum shows vibrational structure consistent with that observed by photoelectron spectroscopy for the ground state of $CH_2F_2^+$, $\tilde{X}^2B_2$ [16]. The peaks in this band are assigned using the Rydberg formula to overlapping members of the $np\ ^1B_2$ Rydberg series ($n = 5$–7). The first peak in the F^- spectrum, however, is assigned to the $5p\ ^1B_2$ Rydberg member only. It is clear that two different ion-pair dissociation channels are competing following excitation to the $5p$ Rydberg state ($CH_2F_2^* \rightarrow F^- + CH_2F^+$ and $CH_2F_2^* \rightarrow H^- + CHF_2^+$). However, the F^- channel no longer competes following excitation to higher-n Rydberg members; the first peak in the F^- spectrum spans between 11.8 and 13.1 eV only. These high-lying np Rydberg states overlap with the ground state of $CH_2F_2^+$, $\tilde{X}^2B_2$; the adiabatic IE is 12.73 eV and the vertical IE is 13.28 eV [16]. At 13.08 eV, $CH_2F_2^+$ becomes unstable with respect to $H + CHF_2^+$ [52]. Certainly, this dissociation is complementary to the $CH_2F_2^* \rightarrow H^- + CHF_2^+$ ion-pair dissociation, and *not* to the $CH_2F_2^* \rightarrow F^- + CH_2F^+$ reaction. This may explain why the F^- dissociation channel diminishes at 13.1 eV, while that for H^- continues. Although a cross section for H^- formation was not determined, its signal strength at ca. 12.6 eV was comparable to, if not weaker than the F^- signal.

Ion-pair formation from CF_3Cl has been discussed in detail in Chap. 4. The F^- and Cl^- spectra (Figs. 4.1a and 4.2, respectively) share some common features. For the benefit of the discussion below, these two spectra are compared directly and plotted on the same axis in Fig. 6.2. F^- and Cl^- anions were both detected at 17.6 eV, but only the Cl^- ion yield displays a true peak at this energy. Clearly shown in Fig. 6.2, this is the only region across the two spectra where the Cl^- cross section is larger than that for F^-. The two spectra cross at 18.4 and 28.2 eV and between these energies the F^- cross section is significantly larger than that for Cl^-. The fact that features are observed in both spectra at similar energies suggests these do indeed represent competing decay channels from the same Rydberg states. Vertical ionisation energies for CF_3Cl^+ $\tilde{D}^2E$, $\tilde{E}^2A_1$, $\tilde{F}^2E$ and $\tilde{G}^2A_1$ are 17.71, 20.20, 21.20 and 23.80 eV, respectively [53]. The features in the spectra at 17.6, 19.7 and 20.9 eV are assigned to high-lying Rydberg states ($n > 5$) converging on the $\tilde{D}$, $\tilde{E}$ and $\tilde{F}$ ionisation limits, respectively. The feature at 22.5 eV is assigned as either the $3p\ ^1A_1$ or $4s\ ^1A_1$ Rydberg state.

Section 6.4 addressed *general* trends in quantum yield and cross section values, only comparing those in Table 6.1 quoted at E_{max}. The data for F^- and Cl^- from CF_3Cl, however, is one example showing that cross section and quantum yield values should be compared at the same energy. This point is perhaps obvious,

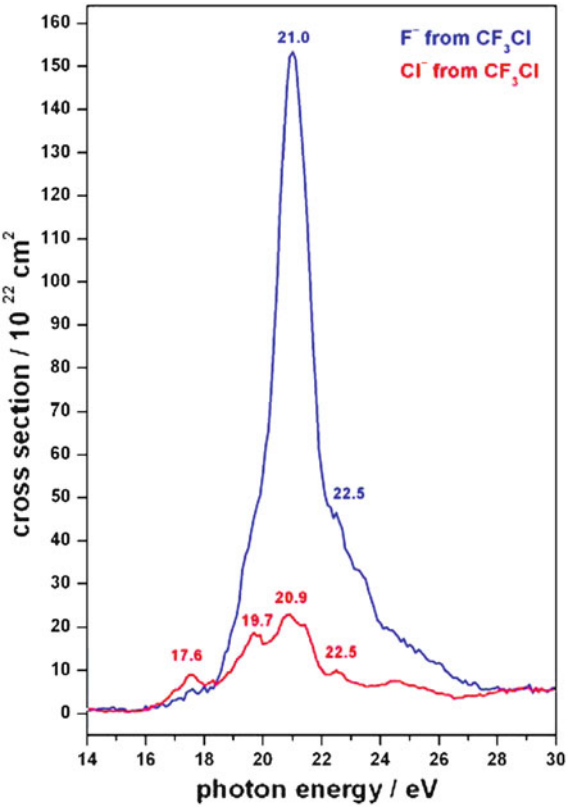

Fig. 6.2 F^- and Cl^- cross sections recorded following the VUV photoexcitation of CF_3Cl. Only the 14–30 eV range is shown here. The complete spectra are presented and discussed in Chap. 4

but it serves to highlight the challenges in understanding why one particular anion has a higher probability for formation than another.

6.6 Electron Attachment

For a molecule under study by negative photoion spectroscopy, below the *IE* any anion produced must result from an ion-pair reaction. Above the *IE*, however, photoelectrons are produced and negative ions resulting from electron attachment processes can be detected. Examples where this has been observed include: SF_5^- and SF_6^- from SF_6, SF_5^- from SF_5CF_3 (Chap. 3); Br^- from CF_3Br and I^- from CF_3I (Chap. 4); SF_5^- from SF_5Cl (Chap. 5); Cl^- from $CFCl_3$ and Cl^- from CCl_4 (Appendix II). The electron attachment process observed may be generically described by the following two reactions:

$$AB + h\nu \rightarrow AB^+ + e^- \tag{6.1}$$

$$AB + e^- \rightarrow AB^- or\ A^- + B \quad (6.2)$$

Four points are made when identifying such electron attachment processes:

1. A plot of the anion signal as a function of gas pressure will be linear for ion-pair formation, but non-linear (with the rate of change in signal increasing with increasing pressure) if electron attachment is detected. Fig. 3.1b shows examples for F^- and SF_5^- from SF_6. Following reactions 6.1 and 6.2, $[A^-]$ is proportional to $[AB]^2$, and these two quantities may be indirectly measured in the experiment as the A^- signal and pressure of AB, respectively.
2. It is evident that the molecule must have an electron attachment rate coefficient, k_a, of sufficient magnitude in order for this process to be observed. The molecules listed above have thermal k_a values between 1×10^{-8} and 4×10^{-7} cm^3 molecule^{-1} s^{-1} (refer to footnote u in Table 6.1). Molecules with slightly lower k_a values were also studied [e.g. $CHCl_3$ and CF_2Cl_2 ($k_a = 4.7 \times 10^{-9}$ and 1.9×10^{-9} cm^3 molecule^{-1} s^{-1}, respectively) [34]], but the anion signals were all attributed to ion-pair formation.
3. There is usually only one anion produced by electron attachment from any given molecule which is detected by negative photoion spectroscopy (the exception being SF_6^- *and* SF_5^- from SF_6). This anion always matches the dominant species identified from independent thermal electron attachment experiments.
4. The spectrum of an anion produced by electron attachment matches, to varying extent depending on the molecule and signal strength, the threshold photoelectron spectrum (TPES) for that molecule. In most cases peak positions are the same, but relative intensities of peaks can vary significantly.

The most interesting of these points is number 4. The similarities/differences between anion spectrum and TPES have already been discussed for the molecules SF_6, SF_5CF_3, CF_3Br, CF_3I and SF_5Cl in Chaps. 3–5. There is no general trend and the reasons for any differences cannot be explained. New data for Cl^- from $CFCl_3$ and CCl_4 are shown in Appendix II. Both spectra show a remarkable tendancy for the relative anion signal to increase with increasing photon energy, especially above ca. 22 eV. It is even possible that some of the features observed above 22 eV identify ionisation potentials which are very weak or absent in the TPES. Furthermore, signal vs pressure plots recorded at these peak energies show a non-linear dependence as discussed in point 1. For the Cl^- from CCl_4 example, a close examination of the TPES does reveal weak and partially resolved features between 22 and 27 eV.

6.7 Concluding Remarks

The formation of ion pairs from polyatomic molecules is a weak process. Quantum yield values are less than or equal to ca. 0.2%. The detection of ion-pair formation therefore requires a sensitive experimental apparatus, and most spectra could only be recorded at a modest resolution.

Ion-pair formation is most commonly formed by the indirect mechanism via an initially excited Rydberg state. Many peaks in ion-pair spectra occur between adiabatic and vertical ionisation energy values. Indeed many of the strongest anion signals result following the predissociation of high-lying Rydberg states ($n > 5$). It can be difficult to resolve these overlapping excited states, let alone assign them, especially when the resolution of the experiment is limited.

One of the most interesting questions raised is: why is one anion produced preferentially to another? This question can be asked when comparing the same anion from different molecules (e.g. Cl^- from CF_3Cl and CF_2Cl_2), different anions from different molecules (e.g. H^- from CH_4 and F^- from CF_4), and different anions from the same molecule (e.g. F^- and Cl^- from CF_3Cl). Some trends are apparent when comparing a series of similar molecules [e.g. the methyl halides [4], the fluoromethanes or the chloromethanes (Sect. 6.4)], but there is no common explanation. Another unanswered question is: why are some anions not observed at all? Examples include the absence of Cl^- anions from CF_3Cl below 16 eV (Chap. 4), and the absence of Cl^- anions from SF_5Cl above 12 eV (Chap. 5).

Thermochemistry is a useful tool to identify the cation and neutral dissociation fragments accompanying the detected anion. However, conclusive assignments are only made at the onset for ion-pair formation when only one dissociation reaction is energetically allowed. The ideal experiment would detect anion and cation fragments above the ionisation energy in coincidence [54], and perhaps this is where the future of ion-pair spectroscopy lies. Such coincidence experiments would identify both the anion *and* cation fragments, allowing for a more detailed analysis of ion-pair dissociation dynamics.

Little information is known about ion-pair potential energy surfaces in polyatomic molecules and I am convinced that the vast collection of experimental data collected in this thesis would provide interest and direction for a theoretical study. For example, one can use Eq. 1.8 to model the potential energy function of an ion-pair state if constants A and α can be derived using experimental results [for example, r can be estimated at known values for $V(r)$].

Finally, it is noted that much of the data collected during my time at Birmingham has not been fully analysed. The spectra recorded from these experiments are presented in Appendix II.

References

1. Simpson MJ, Tuckett RP, Dunn KF, Hunniford CA, Latimer CJ, Scully SWJ (2008) J Chem Phys 128:124315
2. Simpson MJ, Tuckett RP, Dunn KF, Hunniford CA, Latimer CJ (2009) J Chem Phys 130:194302
3. Simpson MJ, Tuckett RP (2010) J Phys Chem A 114:8043
4. Rogers NJ, Simpson MJ, Tuckett RP, Dunn KF, Latimer CJ (2010) Phys Chem Chem Phys 12:10971
5. Rogers NJ, Simpson MJ, Tuckett RP, Dunn KF, Latimer CJ (2010) Mol Phys 108:895

6. Berkowitz J (1996) In: Becker U, Shirley DA (eds) VUV and Soft X-Ray Photoionization. Plenum Press, New York Chapter 8
7. Rabalais JW, Bergmark T, Werme LO, Karlsson L, Siegbahn K (1971) Physica Scripta 3:13
8. Potts AW, Price WC (1972) Proc Royal Soc Lond A 326:165
9. Williams BA, Cool TA (1991) J Chem Phys 94:6358
10. Berkowitz J (2002) Atomic and molecular photoabsorption: absolute total cross sections. Academic, London
11. Bieri G, Åsbrink L (1980) J Electron Spectrosc Relat Phenom 20:149
12. Creasey JC, Jones HM, Smith DM, Tuckett RP, Hatherly PA, Codling K, Powis I (1993) Chem Phys 174:441
13. Eden S, Limao-Vieira P, Kendall PA, Mason NJ, Delwiche J, Hubin-Franskin MJ, Tanaka T, Kitajima M, Tanaka H, Cho H, Hoffmann SV (2004) Chem Phys 297:257
14. Jarvis GK, Boyle KJ, Mayhew CA, Tuckett RP (1998) J Phys Chem A 102:3219
15. Karlsson L, Jadrny R, Mattsson L, Chau FT, Siegbahn K (1977) Physica Scripta 16:225
16. Pradeep T, Shirley DA (1993) J Electron Spectrosc Relat Phenom 66:125
17. Brundle CR, Robin MB, Basch H (1970) J Chem Phys 53:2196
18. Lago AF, Kercher JP, Bödi A, Sztáray B, Miller B, Wurzelmann D, Baer T (2005) J Phys Chem A 109:1802
19. Seccombe DP, Chim RYL, Jarvis GK, Tuckett RP (2000) Phys Chem Chem Phys 2:769
20. Creasey JC, Smith DM, Tuckett RP, Yoxall KR, Codling K, Hatherly PA (1996) J Phys Chem 100:4350
21. Locht R, Leyh B, Dehareng D, Hottmann K, Jochims HW, Baumgärtel H (2006) Chem Phys 323:458
22. Macleod NA, Wang S, Hennessy J, Ridley T, Lawley KP, Donovan RJ (1998) J Chem Soc, Faraday Trans 94:2689
23. Yencha AJ, Thompson DB, Cormack AJ, Cooper DR, Zubek M, Bolognesi P, King GC (1997) Chem Phys 216:227
24. DeKock RL, Higginson BR, Lloyd DR (1972) J Chem Soc Faraday Discuss 54:84
25. Chim RYL, Cicman P, Märk TD, Mayhew CA, Scheier P, Tuckett RP (2007) Int J Mass Spectrom 261:208
26. Chim RYL, Kennedy RA, Tuckett RP, Zhou W, Jarvis GK, Collins DJ, Hatherly PA (2001) J Phys Chem A 105:8403
27. Berkowitz J (2002) Atomic and molecular photoabsorption: absolute total cross sections. Academic, London
28. Kameta K, Machida S, Kitajima M, Ukai M, Kouchi N, Hatano Y, Ito K (1996) J Electron Spectrosc Relat Phenom 79:391
29. Seccombe DP, Chim RYL, Tuckett RP, Jochims HW, Baumgärtel H (2001) J Chem Phys 114:4058
30. Ali S (2007) Ph.D. thesis, University of Birminghamhttp://etheses.bham.ac.uk/897/
31. Chim RYL (2003) Ph.D. thesis, University of Birminghamhttp://etheses.bham.ac.uk/1526/
32. Lee LC, Phillips E, Judge DL (1977) J Chem Phys 67:1237
33. Dawson PH (1995) Quadrupole mass spectrometry and its applications. American Institute of Physics, New York
34. Burns SJ, Matthews JM, McFadden DL (1996) J Phys Chem 100:19436
35. Klar D, Ruf M-W, Fabrikant II, Hotop H (2001) J Phys B 34:3855
36. Christophorou LG (1996) Z Phys Chem 195:195
37. Christophorou LG, Olthoff JK (2000) J Phys Chem Ref Data 29:553
38. Mayhew CA, Critchley A, Howse DC, Mikhailov V, Parkes MA (2005) Eur Phys J D 35:307
39. Van Doren JM, Miller TM, Viggiano AA, Spanel P, Smith D, Bopp C, Troe J (2008) J Chem Phys 128:094309
40. Eden S, Limão-Vieira P, Hoffmann SV, Mason NJ (2006) Chem Phys 323:313
41. Mitsuke K, Suzuki S, Imamura T, Koyano I (1991) J Chem Phys 95:2398
42. Mitsuke K, Suzuki S, Imamura T, Koyano I (1990) J Chem Phys 93:8717
43. Scully SWJ, Mackie RA, Browning R, Dunn KF, Latimer CJ (2002) J Phys B 35:2703

44. Mitsuke K, Suzuki S, Imamura T, Koyano I (1991) J Chem Phys 94:6003
45. Suzuki S, Mitsuke K, Imamura T, Koyano I (1992) J Chem Phys 96:7500
46. Mackie RA, Scully SWJ, Sands AM, Browning R, Dunn KF, Latimer CJ (2003) Int J Mass Spectrom 223–224:67
47. Mitsuke K, Hattori H, Yoshida H (1993) J Chem Phys 99:6642
48. Mackie RA, Sands AM, Scully SWJ, Holland DMP, Shaw DA, Dunn KF, Latimer CJ (2002) J Phys B 35:1061
49. Schenk H, Oertel H, Baumgärtel H (1979) Berichte Bunsenges-Gesellschaft für Physikalische Chemie 83:683
50. Rienstra-Kiracofe JC, Tschumper GS, Schaefer HF, Nandi S, Ellison B (2002) Chem Rev 102:231
51. Shriver DF, Atkins PW (1999) Inorganic chemistry, 3rd edn. Oxford University Press, Oxford
52. Seccombe DP, Tuckett RP, Fisher BO (2001) J Chem Phys 114:4074
53. Cvitaš T, Güsten H, Klasinc L (1977) J Chem Phys 67:2687
54. Yoshida H, Mitsuke K (1996) J Electron Spectrosc Relat Phenom 79:487

Chapter 7
The Reactions of CF_n^+ (n = 1–3) with C_2H_4, C_2H_3F, $C_2H_2F_2$ and C_2HF_3

This chapter reports a fundamental study which investigates on two fronts the effects of fluorination on the reactivity of small molecules. First, how increasing fluorine substitution in neutral ethene affects its reactivity, and second how using different fluorocarbon cation species in the reactions changes the outcome. These data were collected by myself, Dr Michael Parkes, Dr Victor Mikhailov and Dr Chris Mayhew in the Department of Physics and Astronomy at The University of Birmingham between Spring 2007 and Autumn 2009.

7.1 Background Information

A consequence of the 1987 Montreal Protocol, and the many amendments made to it since, has been the significant reduction over the last two decades in the use and production of many ozone-depleting substances. These substances include chlorofluorocarbons (CFCs) and halons, commonly used in applications such as fire protection, refrigeration and aerosols. Many hydrofluorocarbons (HFCs) are considered to be *less* environmentally unfriendly alternatives to CFCs. This is because HFCs are greenhouse gases, whereas CFCs and halons are both greenhouse and ozone-depleting gases. It is therefore important to study these HFCs in order to learn more about their fundamental properties.

The main aim of this study is to investigate the effects on reactivity as the degree of fluorine substitution in ethene increases. This extends other earlier studies by the *Molecular Physics* group at Birmingham, for which the reactions of a series of cations with a number of *chloro*ethenes, including the three isomers of dichloroethene, were investigated [1, 2]. This present study focuses on the reactions of ethene (C_2H_4), monofluoroethene (C_2H_3F), 1,1-difluoroethene (CH_2CF_2), and trifluoroethene (C_2HF_3) with the cations CF^+, CF_2^+, and CF_3^+ using a Selected Ion Flow Tube (SIFT). Unfortunately, owing to expense and hence non-availability, the two 1, 2-difluoroethene isomers have not been investigated.

The results presented here are compared with previous work, where available, on the reactions of the CF_n^+ (n = 1–3) ions with tetrafluoroethene (C_2F_4) and the

M. J. Simpson, *Two Studies in Gas-Phase Ion Spectroscopy*, Springer Theses,
DOI: 10.1007/978-3-642-23129-2_7, © Springer-Verlag Berlin Heidelberg 2012

chlorinated ethenes. The aim of these comparisons is to give a more complete account on the effects of fluorination, and to aid the explanation of any trends observed. This is the first SIFT study on the reactions of CF^+, CF_2^+, and CF_3^+ with C_2H_3F, CH_2CF_2, and C_2HF_3. The reactions of CF_n^+ with C_2F_4 have been investigated by several groups [3–5]. Of these investigations, the work by Morris et al. [5], who also use a SIFT apparatus, is particularly relevant when making comparisons. Some of the reactions presented have also been studied previously by different techniques. The reaction of CF_3^+ with C_2H_4 has been investigated by SIFT Mass Spectrometry [6] and using an ion beam apparatus [7]. The reactions of CF^+ with C_2HF_3 [4], and CF^+ and CF_3^+ with CH_2CF_2 [8] have also been observed previously using ion cyclotron resonance mass spectrometry (ICR-MS).

The adiabatic ionisation energies (*IE*) for C_2H_4, C_2H_3F, CH_2CF_2 and C_2HF_3 are 10.51, 10.36, 10.29 and 10.14 eV, respectively [9, 10]. Comparisons of these values with the recombination energy (*RE*) of the reagent ion (equal in magnitude to the adiabatic *IE* of the corresponding neutral) determines if charge transfer is energetically possible; the *RE* values are 9.11 [11], 11.44 [12] and 9.04 eV [13] for CF^+, CF_2^+, and CF_3^+, respectively, and so charge transfer is only exothermic for the reactions with CF_2^+.

7.2 The Reactions of CF^+

A summary of the results for the reactions of CF^+ with C_2H_4, C_2H_3F, CH_2CF_2, and C_2HF_3 is presented in Table 7.1. The experimental results identify the product cations, their branching ratios (BRs) and the bimolecular reaction rate coefficient, k_{exp}. In addition, neutral products are proposed, the corresponding reaction enthalpies calculated and collisional rate coefficients, k_c, are also included.

First, the reactions of the *fluorinated* ethenes will be considered. The summary of results in Table 7.1 reveals that only two different types of reaction mechanism are occurring involving CF^+. One is F^- transfer from the neutral species:

$$CF^+ + C_2H_xF_y \rightarrow C_2H_xF_{y-1}^+ + CF_2 \tag{7.1}$$

As the degree of fluorination increases, reaction 7.1 becomes *less* favourable. For C_2H_3F this reaction represents the major product channel (88%). However, for CH_2CF_2 the BR falls to just 7%, and for C_2HF_3 this reaction is not observed at all, presumably because it is endothermic. The second type of reaction involves either HF or F_2 abstraction:

$$CF^+ + C_2H_xF_y \rightarrow CHF_2^+/CF_3^+ + C_2H_{x-1}F_{y-1}/C_2H_xF_{y-2}. \tag{7.2}$$

For C_2H_3F reaction 7.2 represents the minor product channel (12%), although it is more exothermic than the F^- abstraction channel. However, it has often been noted that energetics alone do not necessarily dictate the reaction pathway. Now,

Table 7.1 A summary of results for the gas-phase reactions of CF^+ with ethene and the fluorinated ethenes

Reaction[a]		$\Delta_r H°_{298}$ [b]/ kJ mol^{-1}	Product branching ratio (%)	Rate coefficient [c]/10^{-9} cm^3 molecule^{-1} s^{-1} (%)
$CF^+ + C_2H_4$	$\rightarrow CH_2F^+ + C_2H_2$	−141	80	1.1 [1.3] 85
	$\rightarrow C_3H_3^+ + HF$	−295	20	
$CF^+ + C_2H_3F$	$\rightarrow C_2H_3^+ + CF_2$	−81	88	2.1 [2.0] 100
	$\rightarrow CHF_2^+ + C_2H_2$	−172	12	
$CF^+ + CH_2CF_2$	$\rightarrow CF_3^+ + C_2H_2$	−170	88	1.4 [1.9] 74
	$\rightarrow C_2H_2F^+ + CF_2$	−35	7	
	$\rightarrow CHF_2^+ + C_2HF$	−86	5	
$CF^+ + C_2HF_3$	$\rightarrow CF_3^+ + C_2HF$	−145	100	1.0 [1.7] 59

[a] Note that the neutral products in these reactions are not detected in the experiment, but are proposed as the most likely candidate species

[b] The reaction enthalpy calculated from 298 K enthalpies of formation

[c] The experimentally determined rate coefficient, k_{exp}. In square brackets are the collisional values, k_c. The third number gives the rate efficiency, expressed as the percentage of k_{exp} with respect to k_c

as the degree of fluorination increases the BR associated with reaction 7.2 increases; the BR for CH_2CF_2 is (88 + 5)%, and for C_2HF_3, 100%.

F^- abstraction (as in reaction 7.1) suggests that the CF^+ cation attacks the electron rich fluorine in $C_2H_xF_y$ rather than the carbon–carbon double bond. Thus, it is the decrease in dipole moment as fluorination increases (Table 1.1) which is responsible for the trend noted; the larger the dipole moment, the more concentrated the electron density is on an individual fluorine atom, and so it becomes more nucleophilic.

For reaction 7.2, there is no obvious mechanism to explain the observed products, but a tight transition state is expected to be formed. It is also unclear if this mechanism involves breaking the carbon–carbon double bond or not. The reaction of CF^+ with CH_2CF_2 produces two different outcomes resulting from reaction 7.2; $CF_3^+ + C_2H_2$ and $CHF_2^+ + C_2HF$, the former being significantly more favourable. It is also worth noting that H_2 abstraction is not observed in either the reaction with C_2H_3F or CH_2CF_2. For CH_2CF_2, H_2 abstraction is *endo*thermic by 56 kJ mol^{-1}, but H_2 abstraction from C_2H_3F is *exo*thermic by 64 kJ mol^{-1}. Although the competition between reactions 7.1 and 7.2 is not considered to be energetically driven, when considering reaction 7.2 alone, F_2 abstraction is more exothermic than HF abstraction, which is more exothermic than H_2 abstraction—and this is reflected in the results. It is also considered, however, that there will be a preference for CF^+ to attack one side of the fluorinated ethene in preference to another; again it is the dipole moment of these molecules which is likely to dictate the products, and CF^+ will attack the side of the molecule with more fluorine substituents.

The reaction of CF^+ with C_2F_4 has been reported by Morris et al. [5], and this reaction fits in with the trends observed from the present study; F_2 abstraction described by reaction 7.2 is observed as the major product ($CF^+ + C_2F_4 \rightarrow CF_3^+ + C_2F_2$) and reaction 7.1 is not observed at all. However, the reaction with C_2F_4 also produces the minor products $C_3F_5^+$ and $C_2F_4^+$ by association and charge transfer reactions, respectively [5]. The adiabatic *IE* of C_2F_4 is 10.12 eV [14], and so charge transfer is endothermic; its observation is attributed to the reaction with excited-state CF^+ (produced from electron impact ionisation of CF_3Br). It is noted that in the present experiment CF^+ ions are produced by electron impact ionisation from C_3F_8. Charge transfer products from the reaction of CF^+ with C_2H_3F, CH_2CF_2 and C_2HF_3 have not been observed.

The results from the reaction with C_2H_4 (Table 7.1) also fit into the general trend. C_2H_4 has no fluorine substituent nor dipole moment and reaction 7.1 is not observed. The analogous outcome of reaction 7.2, producing $CH_2F^+ + C_2H_2$, is the dominant channel. It is, however, interesting that HF elimination *is* observed in this reaction, but not in those of the fluorinated ethenes.

In summary, it is proposed that the reactions between CF^+ and C_2H_3F, CH_2CF_2 and C_2HF_3 are largely dictated by the dipole moments of these neutral species. The outcome of competition between reactions 7.1 and 7.2 is down to the *magnitude* of the dipole moment; the larger the value the more preference there is for reaction 7.1 to dominate. The outcome of reaction 7.2, i.e. F_2 *vs* HF abstraction, is favoured towards F_2 abstraction because CF^+ attacks the molecule preferentially where more fluorine substituents are present. For C_2H_4 and C_2F_4 there is no dipole moment and the outcome is the equivalent to reaction 7.2, i.e. H_2 and F_2 abstraction, respectively.

The reactions of CF^+ with the chlorinated ethenes have also been performed by Mayhew et al. using the Birmingham SIFT apparatus [1, 2], and some similarities can be drawn when comparing the two studies. Comparisons show that the reactions of CF^+ with C_2H_3Cl, CH_2CCl_2, C_2HCl_3 and C_2Cl_4 all follow the same general trend as discussed above for the fluorinated ethene study. That is, the equivalent of reactions 7.1 and 7.2 can be used to describe all of the observed products, with the dominance of reaction 7.1, i.e. Cl^- transfer, decreasing with decreasing dipole moment. The results from the chlorinated ethenes reveal information about reaction 7.2 which is not possible from this fluorinated ethene study. For example, the reaction of CF^+ with C_2HCl_3 produces 23% $CHCl_2^+ + C_2FCl$, and it is interesting that the neutral substituted ethyne product contains the fluorine atom. In the analogous reaction with C_2HF_3 it could easily be assumed that the atoms in the neutral ethyne product, C_2HF, all originate from the C_2HF_3 reactant, and that CF^+ simply strips two fluorine atoms from it. The chlorinated ethene study shows that this may not be the case and a more complicated mechanism needs to be considered. The study of the three isomers of dichloroethene also reveals additional information [2]. Most significantly, the reaction of *cis*-1,2-dichloroethene shows no products from the equivalent of reaction 7.1 whereas in the reactions of C_2H_3Cl and CH_2CCl_2 reaction 7.1 dominates. This is interesting because of these three chlorinated ethenes it is the

Table 7.2 A summary of results for the gas-phase reactions of CF_2^+ with ethene and the fluorinated ethenes

Reaction[a]		$\Delta_r H°_{298}$ [b]/kJ mol^{-1}	Product branching ratio (%)	Rate coefficient [c]/10^{-9} cm^3 molecule^{-1} s^{-1} (%)
$CF_2^+ + C_2H_4$	$\rightarrow C_3H_3F_2^+ + H$	?	55	1.1 [1.1] 100
	$\rightarrow C_2H_4^+ + CF_2$	−109	45	
$CF_2^+ + C_2H_3F$	$\rightarrow C_2H_3F^+ + CF_2$	−124	88	1.8 [1.8] 100
	$\rightarrow C_2H_3^+ + CF_3$	−161	12	
$CF_2^+ + CH_2CF_2$	$\rightarrow CH_2CF_2^+ + CF_2$	−131	100	1.6 [1.6] 100
$CF_2^+ + C_2HF_3$	$\rightarrow C_2HF_3^+ + CF_2$	−146	100	1.5 [1.5] 100

[a] Note that the neutral products in these reactions are not detected in the experiment, but are proposed as the most likely candidate species

[b] The reaction enthalpy calculated from 298 K enthalpies of formation

[c] The experimentally determined rate coefficient, k_{exp}. In square brackets are the collisional values, k_c. The third number gives the rate efficiency, expressed as the percentage of k_{exp} with respect to k_c

cis-1,2 isomer which has the largest dipole moment. In fact, of the complete series of chlorinated ethenes reacting with CF^+, only C_2H_3Cl and CH_2CCl_2 show products from reaction 7.1—all others show products from reaction 7.2 only. It could be significant that these two species are the only ones where the chlorine substituents are only on one of the carbon atoms. If this is indeed important in determining if reaction 7.1 or 7.2 dominates, it is not easy to explain why from CH_2CF_2 it is reaction 7.2 which is dominant (88% $CF_3^+ + C_2H_2$), but from CH_2CCl_2 reaction 7.1 dominates (69% $C_2H_2Cl^+ + CFCl$).

Clearly similar mechanisms are involved in the reactions of CF^+ with both the fluorinated and chlorinated series of ethenes. It is, however, difficult to explain the relative trends observed in *both* sets of results with the same arguments. Some similarities in the results suggest there should be a common explanation, but the difference in the chemistry of fluorine and chlorine could easily explain otherwise.

7.3 The Reactions of CF_2^+

A summary of the results for the reactions of CF_2^+ with C_2H_4, C_2H_3F, CH_2CF_2 and C_2HF_3 are presented in Table 7.2. The equality between experimental and collisional rate coefficients indicates all reactions occur with 100% efficiency. Non-dissociative charge transfer is the only channel observed for the reaction of CF_2^+ with CH_2CF_2 and C_2HF_3. The reaction of CF_2^+ with C_2H_3F, however, yields two different ionic products, although the major product still arises from non-dissociative charge transfer. The minor product is $C_2H_3^+$, which can only arise from an intimate chemical reaction involving F^- abstraction:

Table 7.3 A summary of results for the gas-phase reactions of CF_3^+ with ethene and the fluorinated ethenes

Reaction[a]		$\Delta_r H°_{298}$ [b]/ kJ mol^{-1}	Product branching ratio (%)	Rate coefficient [c]/10^{-9} cm^3 molecule^{-1} s^{-1} (%)
$CF_3^+ + C_2H_4$	$\rightarrow C_3H_3F_2^+ + HF$	?	60	0.7 [1.1] 64
	$\rightarrow C_2H_3^+ + CHF_3$	−43	40	
$CF_3^+ + C_2H_3F$	$\rightarrow C_2H_3^+ + CF_4$	−88	75	1.3 [1.6] 81
	$\rightarrow CHF_2^+ + CH_2CF_2$ [d]	−1	25	
$CF_3^+ + CH_2CF_2$	$\rightarrow C_2H_2F^+ + CF_4$	−43	50	0.7 [1.5] 47
	$\rightarrow C_3H_2F_5^+$ (adduct)	?	44	p(He) = 0.5 Torr
	$\rightarrow C_3HF_4^+ + HF$	?	6	
$CF_3^+ + C_2HF_3$	$\rightarrow C_3HF_6^+$ (adduct)	?	100	0.2 [1.3] 15
				p(He) = 0.5 Torr

[a] Note that the neutral products in these reactions are not detected in the experiment, but are proposed as the most likely candidate species

[b] The reaction enthalpy calculated from 298 K enthalpies of formation. Absence of a value indicates the $\Delta_f H°$ for the product cation is not known

[c] The experimentally determined rate coefficient, k_{exp}. In square brackets are the collisional values, k_c. The third number gives the rate efficiency, expressed as the percentage of k_{exp} with respect to k_c

[d] The (Z) and (E)—1,2 isomers give endothermic reaction enthalpies, and so it is proposed 1,1-difluorethene is the neutral product species formed

$$CF_2^+ + C_2H_3F \rightarrow C_2H_3^+ + CF_3 \quad (7.3)$$

It is noted that dissociative charge transfer, $CF_2^+ + C_2H_3F \rightarrow (C_2H_3F^+)* + CF_2 \rightarrow C_2H_3^+ + F + CF_2$, is endothermic by 206 kJ mol^{-1}.

The results from the reaction with C_2H_4 are anomalous with respect to the other reactions; charge transfer is observed, but it is not the major channel. In addition, the product $C_3H_3F_2^+$ (formed by H-atom elimination) is surprising. On the other hand, this product has also been observed in the reactions of ethene with CF_3^+ and $C_2F_4^+$, and from the reaction of $C_2F_4^+$ with C_2H_3F (see Tables 7.3 and 8.1). The exact structure of this species is unknown, but its frequent observation suggests it is a relatively stable species. Unfortunately its $\Delta_f H°$ value is unknown, so $\Delta_r H°$ values for the reactions where it is produced cannot be calculated.

The adiabatic *IE* of C_2F_4 is 10.12 eV [14] and so charge transfer in its reaction with CF_2^+ is exothermic. The reaction of CF_2^+ with C_2F_4 has been reported by Morris et al. [5], and unsurprisingly, this reaction proceeds exclusively by charge transfer at the collisional rate.

7.4 The Reactions of CF_3^+

A summary of the results for the reactions of CF_3^+ with C_2H_4, C_2H_3F, CH_2CF_2, and C_2HF_3 are presented in Table 7.3. Where an association reaction is observed the He buffer gas pressure is quoted due to its involvement in collisionally stabilising the energised intermediate formed. The data in Table 7.3 highlights some trends in the reactions of the *fluorinated* ethenes with CF_3^+. F^- abstraction from the neutral appears *less* favourable as the degree of fluorine substitution increases; in the reaction with C_2H_3F the BR is 75%, CH_2CF_2 only 50% and for C_2HF_3 this reaction is not observed. Recall the discussion in Sect. 7.2 where the same trend is apparent in the analogous reaction with CF^+, and the larger the dipole moment of the fluorinated ethene, the more likely F^- abstraction is to occur. Three points need to be made regarding F^- transfer to CF_3^+, in comparison with the CF^+ reactions. First, only the reaction of CF_3^+ with C_2H_3F can be *directly* compared with CF^+ because the same two product cations are observed with similar BRs. Second, as the BR for F^- abstraction decreases there is no common mechanism in all three reactions taking its place, i.e. there is no significant competition to the F^- abstraction reaction. Third, although the value for $\Delta_f H°_{298}$ ($C_2HF_2^+$) is not known, F^- abstraction in the reaction with C_2HF_3 is expected to be endothermic.

Note the trend in the reaction enthalpies in Table 7.3, and that the reaction $CF_3^+ + C_2F_4 \rightarrow C_2F_3^+ + CF_4$ is endothermic by 111 kJ mol^{-1}. Considering these points, the energetics *are* likely to be important in interpreting the results from the reactions of CF_3^+ with the fluorinated ethenes. Key supporting evidence is that adduct formation is observed, and the BR increases with *increasing* fluorine substitution; no adduct is formed in the reaction with C_2H_3F, the BR for adduct formation is 44% with CH_2CF_2, and with C_2HF_3 the BR is 100%. As F^- abstraction becomes energetically less favourable, the results suggest that the lifetime of the reaction complex increases and it is more likely to be collisionally stabilised and hence observed.

There are also other interesting reactions occurring which do not lead to F^- abstraction or association; for example, the observation of CHF_2^+ as the minor product (25%) from the reaction with C_2H_3F:

$$CF_3^+ + C_2H_3F \rightarrow CHF_2^+ + CH_2CF_2 \tag{7.4}$$

The proposed neutral product species is 1,1-difluoroethene because this is the only exothermic outcome, based on thermochemical calculations. (The *cis* and *trans* isomers for 1,2-difluoroethene give reaction enthalpies endothermic by 47 and 51 kJ mol^{-1}, respectively.) Another interesting reaction which does not fit the general trend is that of CF_3^+ with CH_2CF_2:

$$CF_3^+ + CH_2CF_2 \rightarrow C_3HF_4^+ + HF \tag{7.5}$$

The BR for this reaction, elimination of HF, is only 6%. Reactions 7.4 and 7.5 represent thermodynamically favourable exit channels from the adduct complex

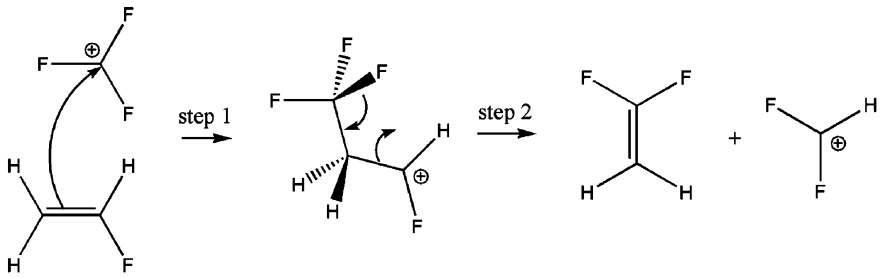

Fig. 7.1 A proposed mechanism for the reaction $CF_3^+ + C_2H_3F \rightarrow CHF_2^+ + CH_2CF_2$

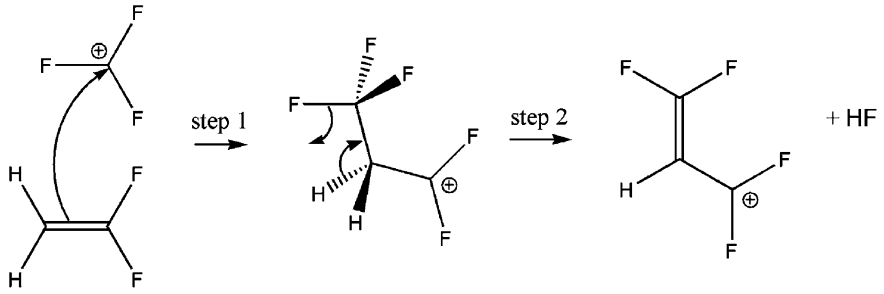

Fig. 7.2 A proposed mechanism for the reaction $CF_3^+ + CH_2CF_2 \rightarrow C_3HF_4^+ + HF$

which is formed. It is expected that the adduct species in this series of reactions is covalently bonded, rather than involving intramolecular forces, because reactions 7.4 and 7.5 are expected to result from a covalently-bonded complex (proposed mechanisms for these reactions are presented in Figs. 7.1 and 7.2, respectively), and previous work has shown that CF_3^+ reacts with neutral C_2F_4 to produce $C_3F_7^+$ [5].

In the reaction of CF_3^+ with C_2H_4, H^- abstraction is observed, which is not observed in the reactions with the fluorinated ethenes because it cannot compete with F^- abstraction. Recall the comparisons made above between F^- abstraction in the reactions of both CF^+ and CF_3^+ with the fluorinated ethenes, and it should be noted that the same comment cannot be made regarding H^- abstraction in ethene because this outcome in the reaction with CF^+ is endothermic by 36 kJ mol^{-1}. The other product from the reaction of CF_3^+ with C_2H_4 is $C_3H_3F_2^+$, a product of HF elimination with a BR of 60%. HF elimination is also observed from the reaction with CH_2CF_2, but as the *minor* product, further demonstrating the dominance of the F^- abstraction channel in the fluorinated ethenes and the comparatively less dominant H^- abstraction reaction from C_2H_4. Another SIFT study has also reacted CF_3^+ with ethene, and the results are in excellent agreement with this work [6]; the dominant product is $C_3H_3F_2^+$, the minor product is $C_2H_3^+$, and the rate coefficient at 300 K is 0.98×10^{-9} cm^3 $molecule^{-1}$ s^{-1}.

The previous work on ion–molecule reactions with the chlorinated ethenes report their gas-phase reactions with CF_3^+ [1, 2]. Similarities are noted in the reaction with C_2H_3Cl and CH_2CCl_2, particularly the former. CF_3^+ reacting with C_2H_3Cl produces $C_2H_3^+ + CF_3Cl$ (65%), and $CHFCl^+ + C_2H_2F_2$ (35%). Note the similarities here with the reaction of C_2H_3F in Table 7.3. It is inferred that in *both* reactions, the $C_2H_2F_2$ neutral product is the 1,1-difluoroethene isomer, because the *cis*-1,2 and *trans*-1,2 isomers give endothermic reaction enthalpies. The similarities in the reaction of CH_2CF_2 and CH_2CCl_2 are less striking; $CF_3^+ + CH_2CCl_2$ exclusively produces $C_2H_2Cl^+ + CF_3Cl$ via Cl^- abstraction, whereas the analogous F^- abstraction reaction with CH_2CF_2 forms only 50% of the observed products (Table 7.3). Also note that Cl^- abstraction *is* observed in the reactions of C_2HCl_3 and C_2Cl_4, but the analogous F^- abstraction reaction is *not* observed from C_2HF_3 (this work) or C_2F_4 [5]. Recall from the discussion above that the latter two reactions are expected to be endothermic, whereas the former two reactions are clearly exothermic. In fact all other reactions observed in the chlorinated ethene series, which are not equivalently observed in the fluorinated ethene series, are simply because of the new atom involved—chlorine. For example, $CF_3^+ + C_2HCl_3$ produces 24% $CFCl_2^+ + C_2HClF_2$, whereas this reaction for C_2HF_3 would have a thermoneutral outcome, i.e. it will revert back to the reactants. So, although it might appear that the differences in the reactions of CF_3^+ with the fluorinated and chlorinated series of ethenes appear significant, they are actually explained by two simple statements. First, Cl^- abstraction is energetically more favourable than the equivalent F^- abstraction reactions. Second, reactions with the chlorinated ethenes involve the atoms C, H, F *and* Cl, allowing for a larger number of viable (both dynamically and energetically) exit channels to be available to the reaction complex.

7.5 Conclusions

The gas-phase reactions of CF^+, CF_2^+ and CF_3^+ with C_2H_4, C_2H_3F, CH_2CF_2 and C_2HF_3 have been studied using a SIFT. For energetic reasons, the reactions with CF_2^+ can proceed by non-dissociative charge transfer, whereas those with CF^+ and CF_3^+ only produce products from a reaction complex where bonds break and new ones form. The discussion has focused on the reactions of CF^+ and CF_3^+ with ethene and the three fluorinated ethenes, and some similarities are noted between these and a previous study on the chlorinated ethenes [1, 2].

The dipole moment of the fluorinated ethene is significant because it is a measure of how nucleophilic a fluorine atom in the molecule is. This has been highlighted when analysing the results for the CF^+ and CF_3^+ reactions. The dynamics involved for an F^- abstraction reaction are favoured when the dipole moment is large. The branching into this channel decreases as the dipole moment of the fluorinated ethene decreases. It is unclear if this trend is due to dynamics alone, or if energetics play a part. It is noted that as branching into F^- abstraction

decreases, so does the exothermicity of the reaction—in both CF^+ and CF_3^+ reactions with C_2HF_3, this channel is expected to be endothermic. However, the reaction of CF^+ with C_2H_3F provides an example where dynamics are more important than energetics; F^- abstraction is competing with HF abstraction, and the former mechanism dominates despite the latter being significantly more exothermic, and it is C_2H_3F which has the largest dipole moment of the three fluoroethenes studied here. It is also unclear if dynamics or energetics are responsible for the apparent preference for F_2 abstraction over HF abstraction in the reactions with CF^+.

The comparisons of the fluorinated ethene reactions with those of ethene show how the reaction mechanisms, and hence the products and their branching ratios, often differ due to the significance of the dipole moment. It has been observed that adding one or two fluorine substituents can increase the reactivity of ethene, but adding three or four fluorine atoms can then have the opposite effect, resulting in stabilising the molecule and/or the reaction complex.

References

1. Mikhailov V, Parkes MA, Simpson MJ, Tuckett RP, Mayhew CA (2008) J Phys Chem A 112:9012
2. Mikhailov V, Parkes MA, Tuckett RP, Mayhew CA (2006) J Phys Chem A 110:5760
3. Derwish GAW, Galli A, Giardini-Guidoni A, Volpi GG (1964) J Am Chem Soc 86:4563
4. Anicich VG, Bowers MT, O'Malley RM, Jennings KR (1973) Int J Mass Spectrom Ion Phys 11:99
5. Morris RA, Viggiano AA, Paulson JF (1993) J Phys Chem 97:6208
6. Morris RA, Brown ER, Viggiano AA, Van Doren JM, Paulson JF, Motevalli V (1992) Int J Mass Spectrom Ion Processes 121:95
7. Tsuji M, Aizawa M, Nishimura Y (1995) J Phys Chem 99:3195
8. O'Malley RM, Jennings KR, Bowers MT, Anicich VG (1973) Int J Mass Spectrom 11:89
9. Williams BA, Cool TA (1991) J Chem Phys 94:6358
10. Bieri G, Von Niessen W, Åsbrink L, Svensson A (1981) Chem Phys 60:61
11. Dyke JM, Lewis AE, Morris A (1984) J Chem Phys 80:1382
12. National Institute of Standards and Technology website (http://webbook.nist.gov/chemistry/)
13. Garcia GA, Guyon PM, Powis I (2001) J Phys Chem A 105:8296
14. Eden S, Limao-Vieira P, Kendall PA, Mason NJ, Delwiche J, Hubin-Franskin MJ, Tanaka T, Kitajima M, Tanaka H, Cho H, Hoffmann SV (2004) Chem Phys 297:257

Chapter 8
The Reactions of $C_2F_4^+$ with C_2H_4, C_2H_3F, $C_2H_2F_2$ and C_2HF_3

This chapter continues the investigation on the effects of fluorination in ethene, but the reactant ion is now a fluorinated ethene itself, the tetrafluoroethene cation, $C_2F_4^+$. In the original study of the reactions with CF^+, CF_2^+ and CF_3^+ (Chap. 7) a new source gas was used, perfluoropropane (C_3F_8). This gas was used simply out of curiosity to see if it yielded the ions in question more efficiently than the usual choice of source gases—either tetrafluoromethane (CF_4) or hexafluoroethane (C_2F_6). It was then discovered, albeit unintentionally, that C_3F_8 can be used to produce $C_2F_4^+$ ions and the decision was made to include this reactant in the fluorinated ethene investigation. These data were collected by myself and Dr Chris Mayhew using the SIFT apparatus in the University of Birmingham Department of Physics and Astronomy in the spring and summer of 2009.

8.1 Background Information

A general introduction into the fluorinated ethene series of molecules including the motivations for undertaking these studies has been given in Chap. 7, and the same comments are not repeated here. Ion Cyclotron Resonance Mass Spectrometry (ICR-MS) has been used previously to observe ion–molecule reactions of $C_2F_4^+$ with ethane [1, 2], and all possible neutral fluorinated ethene molecules [3, 4]. This is thought to be the first study of this set of reactions using the SIFT technique. The reaction between $C_2F_4^+$ and C_2F_4, which is not investigated here, has been studied by Morris et al. also using a SIFT apparatus [5], and provides a useful comparison when looking at trends in how the results change with increasing fluorine substitution.

8.2 Results and Discussion

The results for the reactions of $C_2F_4^+$ with ethene (C_2H_4), monofluoroethene (C_2H_3F), 1,1-difluoroethene (CH_2CF_2), and trifluoroethene (C_2HF_3) are presented in Table 8.1. The experimental results identify the product cations, their branching

M. J. Simpson, *Two Studies in Gas-Phase Ion Spectroscopy*, Springer Theses,
DOI: 10.1007/978-3-642-23129-2_8, © Springer-Verlag Berlin Heidelberg 2012

Table 8.1 A summary of results for the gas-phase reactions of $C_2F_4^+$ with ethene and the fluorinated ethenes

Reaction[a]		$\Delta_r H°_{298}$[b]/ kJ mol^{-1}	Product branching ratio (%)	Rate coefficient[c]/ 10^{-9} cm^3 mol^{-1} s^{-1}
$C_2F_4^+ + C_2H_4$	$\rightarrow C_2H_2F_2^+ + C_2H_2F_2$[d]	−65[e]	95	0.7 [1.0] 70%
	$\rightarrow C_3H_3F_2^+ + CHF_2$	?	5	
$C_2F_4^+ + C_2H_3F$	$\rightarrow C_2HF_3^+ + CH_2CF_2$[f]	−35	45	0.6 [1.5] 40%
	$\rightarrow C_3H_3F_2^+ + CF_3$	?	40	p(He) = 0.5 Torr
	$\rightarrow C_3H_2F_3^+ + CHF_2$	?	10	
	$\rightarrow CH_2CF_2^+ + C_2HF_3$	−20	3	
	$\rightarrow C_4H_3F_5^+$ (adduct)	?	2	
$C_2F_4^+ + CH_2CF_2$	$\rightarrow C_4H_2F_6^+$(adduct)	?	60	0.7 [1.4] 50%
	$\rightarrow C_3H_2F_3^+ + CF_3$	?	30	p(He) = 0.5 Torr
	$\rightarrow C_3HF_4^+ + CHF_2$	?	10	
$C_2F_4^+ + C_2HF_3$	$\rightarrow C_2HF_3^+ + C_2F_4$	+ 2	72	0.2 [1.2] 17%
	$\rightarrow C_3HF_4^+ + CF_3$	?	28	

[a] Note that the neutral products in these reactions are not detected in the experiment, but are proposed as the most likely candidate species

[b] The reaction enthalpy calculated from 298 K enthalpies of formation. Absence of a value indicates the $\Delta_f H°$ for the product cation is not known

[c] The experimentally determined rate coefficient, k_{exp}. In square brackets are the collisional values, k_c, and the rate efficiency is given as the percentage of k_{exp} with respect to k_c

[d] The isomeric forms of these two product species are not known, however, it is proposed that both the cation and neutral are the 1,1- isomers of difluoroethene

[e] The calculated $\Delta_r H°$ value if the two product species are *both* the 1,1-isomers

[f] The (Z) and (E)-1,2 isomers give endothermic reaction enthalpies, and so we propose 1,1-difluorethene is the neutral product species formed

ratios (BRs) and the bimolecular reaction rate coefficient, k_{exp}. Where an association reaction is observed the helium buffer gas pressure is given due to its involvement in collisionally stabilising the energised intermediate formed. In addition, neutral reaction products are proposed, the corresponding reaction enthalpies calculated, and collisional rate coefficients, k_c, are also included. The adiabatic ionisation energies for ethene and the fluoroethenes are 10.51, 10.36, 10.29, and 10.14 eV for C_2H_4, C_2H_3F, CH_2CF_2 and C_2HF_3, respectively [6, 7]. The recombination energy for $C_2F_4^+$, defined as the adiabatic ionisation energy for neutral C_2F_4, is 10.12 eV [8]. Charge transfer in this set of reactions is therefore endothermic, and indeed as is seen from the results in Table 8.1, interesting intimate chemical reactions are occurring.

All of the reactions with $C_2F_4^+$ are relatively slow: $k_{exp} < k_c$. Many of the ionic products detected are relatively large species containing three or four carbon atoms. This complicates the data analysis for two reasons. First, it is difficult to assign a mechanism to these reactions, or to suggest confidently a particular isomeric structure for these product ions. Second, many $\Delta_f H°_{298}$ values are not known which prevents $\Delta_r H°_{298}$ being calculated in these instances. As a result,

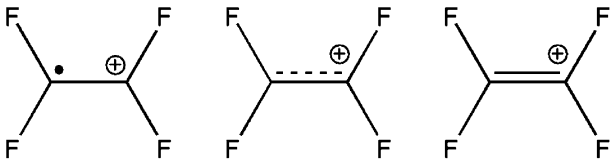

Fig. 8.1 Three examples of how the tetrafluoroethene cation, $C_2F_4^+$, can be pictorially represented for the use in reaction mechanisms

the structures and/or mechanisms assigned to some of the reactions in the discussion below are made tentatively.

First the structure of the reagent ion, $C_2F_4^+$, is discussed. It is perhaps inaccurate to assume this species will have a generic double bond as in neutral C_2H_4, for example, and given the importance of double bonds in the reactive behaviour of a species this point will be addressed. Figure 8.1 shows various ways which $C_2F_4^+$ can be pictorially represented, showing differing degrees of double-bonding character. Species 1 and 2 are preferred because both give an indication of the effects perfluorination and ionisation will have on the double bond. Certainly, species 3 is misleading. Perfluorination of ethene significantly weakens the double bond; a calculation of $\Delta_r H°_{298}$ for reactions 8.1 and 8.2 clearly shows this:

$$C_2H_4 \rightarrow CH_2 + CH_2 \quad \Delta_r H^\circ_{298} = +720 \text{ kJ mol}^{-1} \tag{8.1}$$

$$C_2F_4 \rightarrow CF_2 + CF_2 \quad \Delta_r H^\circ_{298} = +295 \text{ kJ mol}^{-1} \tag{8.2}$$

The ionised species will be even further destabilised with respect to the C=C bond. It has been observed both from this work, and by Su and Kevan [9], that $C_2F_4^+$ is metastable and will produce CF_3^+ by collision induced dissociation. This of course involves some rearrangement, and breaking of the carbon–carbon bond. Of the three species in Fig. 8.1, species 1 will be used to represent $C_2F_4^+$ when using arrow-pushing mechanisms to explain some of the observed reactions.

All of the reaction products shown in Table 8.1 can be divided into three different categories. The first is the observation of the adduct species; the second is the observation of a fluorinated ethene cation which is *different* to the neutral ethene-type reactant; the third is the observation of a cation containing three carbon atoms, with the corresponding neutral species as either CHF_2 or CF_3. The third category is generically shown below:

$$C_2F_4^+ + C_2X_4 \rightarrow C_3X_5^+ + CX_3 (X = \text{H or F}) \tag{8.3}$$

In fact, all product species from any of the three categories described above may be explained by one common reaction mechanism. This involves a branched, 4-carbon chain adduct being formed, which may subsequently fragment to either eliminate CX_3, as in reaction 8.3, or produce two fluorinated ethenes with one retaining the positive charge. Figure 8.2 shows this mechanism for the reaction

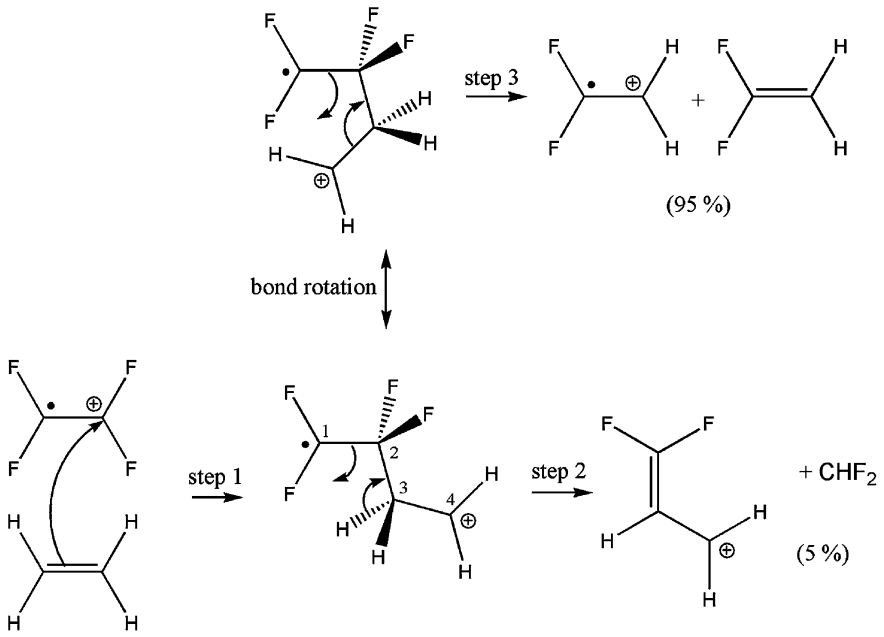

Fig. 8.2 The proposed mechanism for the reaction between the tetrafluoroethene cation ($C_2F_4^+$), and ethene (C_2H_4)

between $C_2F_4^+$ and C_2H_4. It shows how both observed product channels can be produced from the same 4-carbon chain intermediate formed by step 1 (see Table 8.1). Note that this mechanism suggests the observed product channel $C_2H_2F_2^+ + C_2H_2F_2$ produces both species as the 1,1-difluoroethene isomers, and thermochemistry also suggests this is the most exothermic outcome. There is also a preference for step 3 to follow step 1, rather than step 2, and the reasons for this are not entirely clear from analysing this mechanism alone. It does, however, follow the same trend as is seen in the reactions of $C_2F_4^+$ with the fluorinated ethenes (see Table 8.1 and discussion). The reaction channel eliminating CHF_2 is always a minor one, and the product channels analogous to that in step 3, where possible, are all significant ones. It is suggested that step 2 in Fig. 8.2 is unfavourable and relatively slow which allows for bond rotation to occur in the intermediate species, thus allowing step 3 to dominate. It would perhaps shed some light on this argument if the heat of formation of $C_3H_3F_2^+$ was known; $\Delta_r H°$ for producing this product could then be calculated and compared to that for producing $C_2H_2F_2^+$.

Figure 8.3 shows the proposed mechanism for the reaction between $C_2F_4^+$ and C_2H_3F. Note how all products from this reaction shown in Table 8.1 are produced by the mechanism in the Figure. Steps 1a and 1b show that there are two isomerically different intermediate adduct species which can be formed, depending on which carbon in C_2H_3F forms the bond with a carbon in $C_2F_4^+$. Step 1a followed by 2a will always produce $C_3H_2F_3^+$ and CHF_2; both substituents on

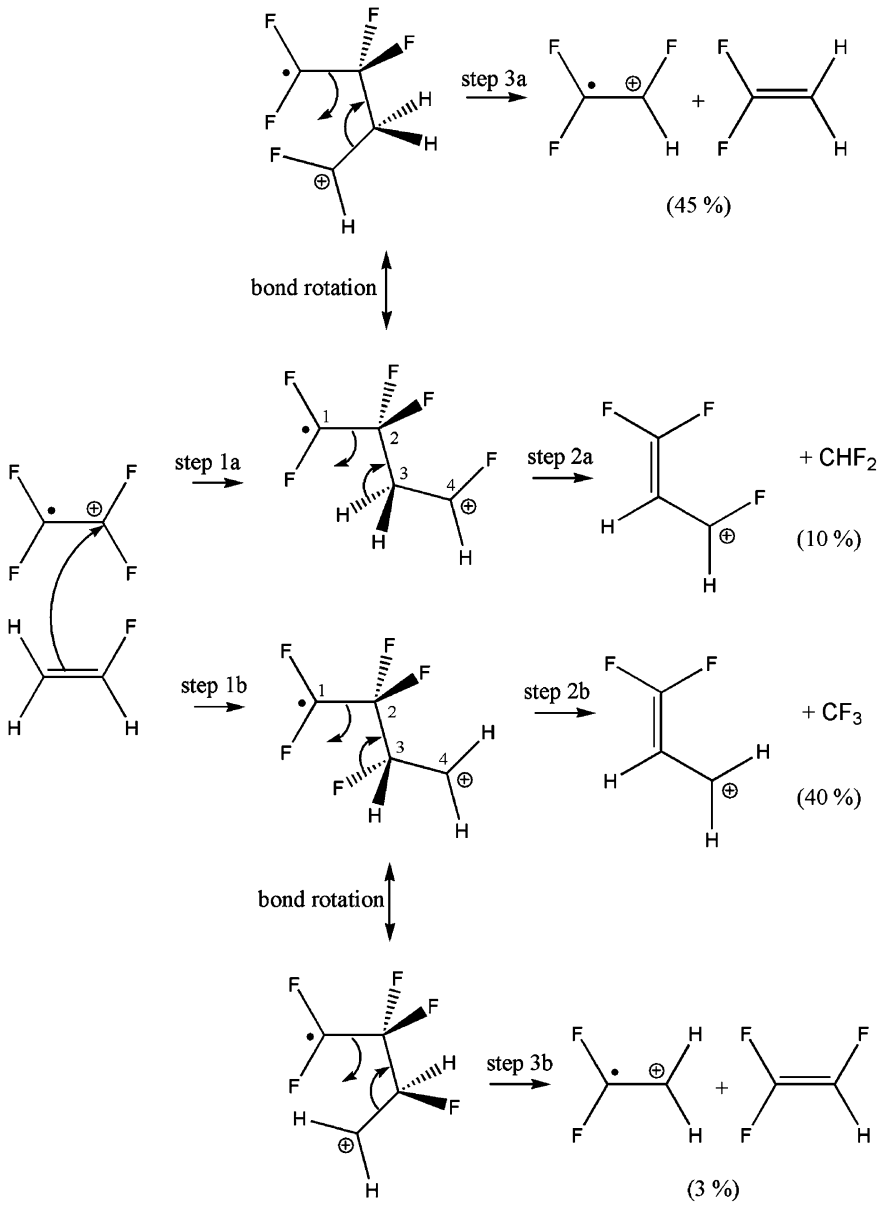

Fig. 8.3 The proposed mechanism for the reaction between the tetrafluoroethene cation ($C_2F_4^+$) and monofluoroethene (C_2H_3F)

carbon 3 in the intermediate adduct are hydrogens. If one considers step 1b followed by 2b, however, carbon 3 now has a hydrogen and a fluorine substituent, so a product mixture of $C_3H_2F_3^+$ (+CHF_2) and $C_3H_3F_2^+$ (+CF_3) would be expected

(note, Figure 8.3 only shows the latter outcome). It is clear from the product branching ratios that there is a preference to eliminate CF_3 over CHF_2. Indeed fluorine is a larger and more polarisable substituent than hydrogen, and the C–F bond distance will be greater. Perhaps this may qualitatively explain how step 2b will preferably eliminate CF_3 rather than CHF_2, and also how step 2b may occur more readily than step 2a.

The other products shown in Fig. 8.3 are $C_2HF_3^+$ and $CH_2CF_2^+$, resulting from steps 3a and 3b, respectively. Again, it is clear which of these products is preferred; $C_2HF_3^+$ is the major product of the reaction (BR = 45%), whereas $CH_2CF_2^+$ is only a minor product (BR = 3%). A bond rotation is required for either step 3a or 3b to occur, which is sterically unfavourable, and so the more favourable step 2b is, the less likely step 3b will be. Likewise, the same comment is made with respect to steps 2a and 3a. This then explains why, following step 1a, formation of $C_2HF_3^+$ by step 3a is the dominant outcome, whereas following step 1b, elimination of CF_3 by step 2b is the dominant outcome. A previous ICR-MS study of the reaction $(C_2H_3F + C_2F_4)^+$ revealed the products $C_2HF_3^+$ (62%), $C_3H_3F_2^+$ (32%), and $C_3H_2F_3^+$ (7%) [4], which is in agreement with the dominant products observed in this SIFT study (Table 8.1). If *only* the mechanism in Fig. 8.3 is considered, then the adduct species, observed as the minor product with BR = 2%, is the detection of either intermediate species produced by steps 1a or 1b. Given the number of hydrogen and fluorine atoms in the two reactants, it should also be considered that the observed adduct may be a hydrogen-bonded species.

Figure 8.4 shows how the same mechanism can be used to explain the products observed from the reaction of $C_2F_4^+$ with CH_2CF_2. In particular, how elimination of CF_3 and CHF_2 *are* observed, yet fluorinated ethene cation products (from steps 3a or 3b) are *not* observed; in the Figure, step 3a will revert back to the reactants and step 3b is endothermic. Again, a preference to eliminate CF_3 over CHF_2 is observed. The major difference in the reaction of $C_2F_4^+$ with CH_2CF_2 compared to that with C_2H_4, C_2H_3F or C_2HF_3 is the large BR recorded for the adduct species (60% compared to 0, 2, and 0%, respectively). There is no obvious explanation. It is also worth noting that in the reaction of $C_2F_4^+$ with C_2F_4, no adduct species is observed, and the only product is $C_3F_5^+$ (+CF_3) [5]. In addition, the ICR-MS study by Anicich and Bowers showed the *only* product in the reaction $(CH_2CF_2 + C_2F_4)^+$ was $C_3H_2F_3^+$ (+CF_3) [4].

Figure 8.5 shows the same mechanism when applied to the reaction of $C_2F_4^+$ with C_2HF_3. Consistent with the results discussed above, the preference for the intermediate species to eliminate CF_3 rather than CHF_2 is observed, but now CHF_2 elimination is not observed at all. In the reaction $C_2F_4^+ + C_2HF_3$, Anicich and Bowers observed 92% $C_3HF_4^+$ (+CF_3) and 8% $C_3F_5^+$ (+CHF_2) [4]. In Fig. 8.5, step 2a shows how CHF_2 elimination is possible, but this step could also lead to CF_3 elimination given that carbon 3 in the intermediate species has both hydrogen and fluorine substituents. It is therefore proposed that the channel leading to 28% CF_3 elimination is a contribution from steps 2a and 2b.

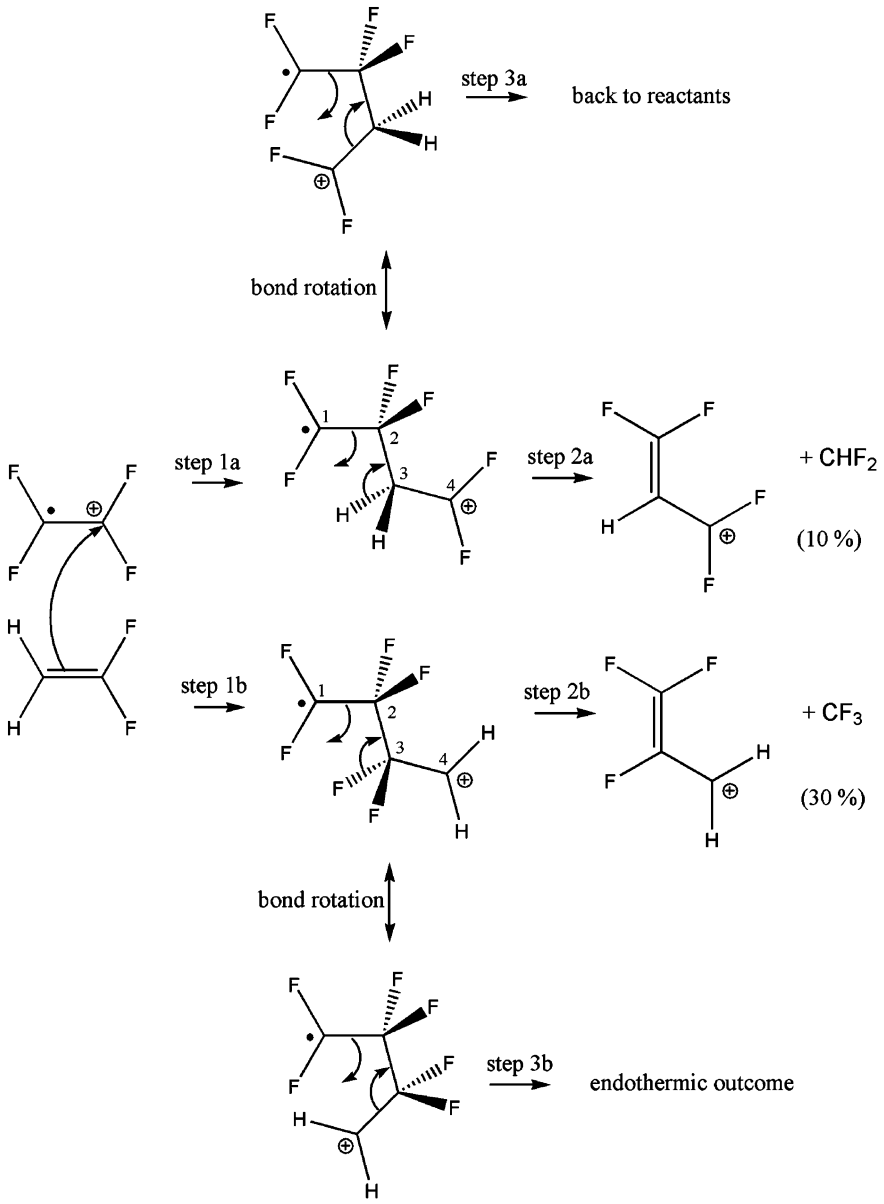

Fig. 8.4 The proposed mechanism for the reaction between the tetrafluoroethene cation ($C_2F_4^+$) and 1,1-difluoroethene (CH_2CF_2)

$C_2HF_3^+$ is detected with a BR of 72% (Table 8.1). Figure 8.5 shows how this can arise from step 3b, however, a charge transfer mechanism could also be the origin of this species. Certainly in ion–molecule reactions when charge transfer is

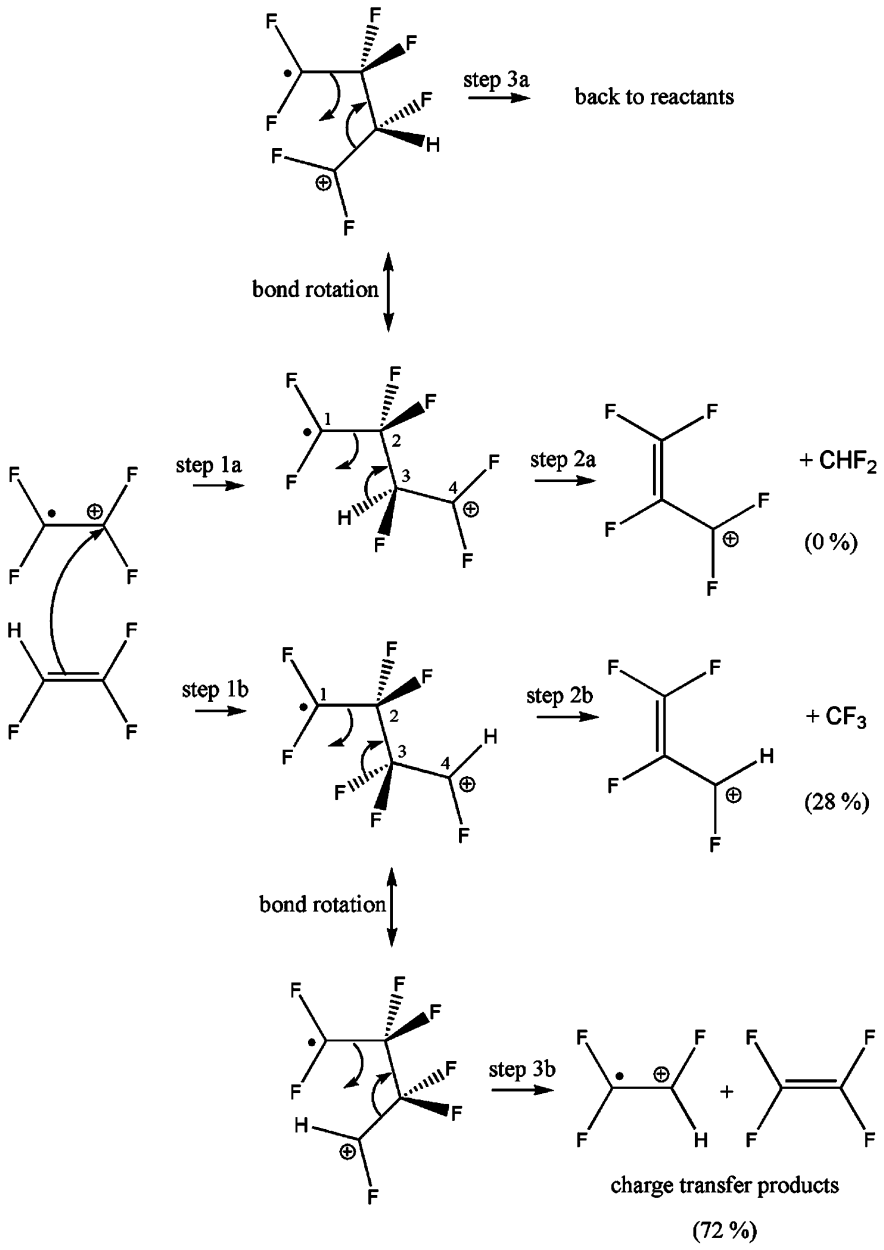

Fig. 8.5 The proposed mechanism for the reaction between the tetrafluoroethene cation ($C_2F_4^+$) and trifluoroethene (C_2HF_3)

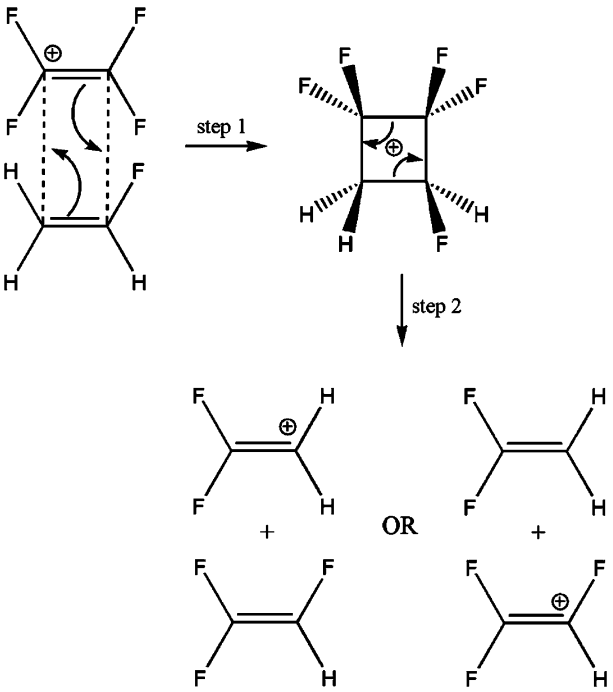

Fig. 8.6 An example of the reaction between $C_2F_4^+$ and C_2H_3F showing the production of two fluorinated ethene products which are different to the reactant species, using a cycloaddition mechanism

observed, it is commonly the dominant product channel. As discussed above, however, this reaction is endothermic, albeit by only +2 kJ mol^{-1}. Therefore, the observation of $C_2HF_3^+$ is perhaps unsurprising, and could result from vibrationally-excited $C_2F_4^+$ present in the flow tube, or by considering thermal energy in overcoming the reaction endothermicity. Also, when the magnitude of the endothermicity is so small, errors in the thermochemical values used to calculate this enthalpy could mean that the reaction is actually exothermic. The *IE* of C_2F_4 is 10.12 eV [8], that of C_2HF_3 is 10.14 eV [7], but experimental errors are not quoted for these values. A 'charge transfer' reaction does not imply the two species react intimately, but rather an electron from the neutral molecule 'hops' over a given distance to combine with the cation. These reactions are usually fast and occur at the collisional rate.

The intimate chemical reaction shown by step 3b in Fig. 8.5, in which the two species come into contact and form/break bonds, does also explain the observation of $C_2HF_3^+$ from the reaction of C_2HF_3 with $C_2F_4^+$. Evidence in support of this mechanism can be found in the values for k_{exp} and k_c for this reaction (Table 8.1); if 72% of products formed were from a fast charge transfer reaction, it is unlikely that the rate efficiency would be as low as 17%. In addition, this efficiency in the

reaction of $C_2F_4^+$ with C_2HF_3 is lower than that for $C_2F_4^+$ with C_2H_4 (70%), C_2H_3F (40%) or with CH_2CF_2 (50%). None of the products from the latter three reactions are expected to arise from 'fast' processes, and so it becomes difficult to explain the relatively low rate efficiency when $C_2F_4^+$ reacts with C_2HF_3 if 72% of products occur by charge transfer. On the other hand, the slight endothermicity of this reaction might explain why a charge transfer reaction might not occur at a collisional rate. Another reason to consider the reaction shown in Figure 8.5 is that all other products observed in the four reactions with $C_2F_4^+$ can be explained if a similar reaction mechanism is considered (see discussion above).

In Figs. 8.2, 8.3, 8.4 and 8.5, steps 3, 3a, and 3b show the proposed mechanism to explain the formation of two substituted ethene products different to the reacting species. In similar ion–molecule reactions of substituted ethene species it has been suggested that a cycloadduct intermediate is formed, rather than a 4-carbon chain, which then dissociates to form products [1, 4]. The cycloaddition reaction is shown in Fig. 8.6 for the example of C_2H_3F reacting with $C_2F_4^+$. Note that in these earlier studies a 4-carbon chain intermediate is still suggested to explain the $C_3X_5^+$ products (X = H or F), shown in Figs. 8.2, 8.3, 8.4 and 8.5 by steps 2, 2a, and 2b. The 4-carbon chain intermediate is considered a preferable mechanism to the cycloaddition intermediate for the following reasons. First, the cycloaddition reaction requires $C_2F_4^+$ to be represented as species 3, when in fact species 1 is much more realistic (see discussion above and Fig. 8.1). If species 1 was used to represent $C_2F_4^+$ in Fig. 8.6, it becomes more difficult to rationalise the formation of a cycloadduct in step 1. Second, the relative BRs in the observed products (excluding the adduct) are better explained by one mechanism, rather than by two different mechanisms; for example in Fig. 8.3 step 3a is more likely to occur than step 3b because step 2b is considered a more favourable outcome than step 2a (see discussion above).

8.3 Conclusions

The reactions between $C_2F_4^+$ and C_2H_4, C_2H_3F, CH_2CF_2, and C_2HF_3 have been performed using a Selected Ion Flow Tube. Some interesting intimate chemical reactions have been observed, and the product channels have been explained using arrow-pushing mechanisms. The same generic mechanism can be used to explain all products observed from each of the reactions studied.

The proposed mechanisms suggest that there are two major reaction pathways competing which both arise from the same 4-carbon branched intermediate species. In one instance, CF_3 or CHF_2 is eliminated from the intermediate [generically described by reaction 8.4], and in the other case the intermediate dissociates to yield two fluorinated ethene products [generically described by reaction 8.5].

$$C_2F_4^+ + C_2X_4 \rightarrow C_3X_5^+ + CX_3 \quad (X = \text{H or F}) \tag{8.4}$$

$$C_2F_4^+ + C_2X_4 \rightarrow C_2X_4^+ + C_2X_4 \quad (X = \text{H or F}) \tag{8.5}$$

In reaction 8.4, a clear preference for CF_3 elimination *vs* CHF_2 elimination is observed. Other trends in the results are less clear-cut but arguments, albeit suggested tentatively, are proposed in an attempt to explain them. This work shows how common organic chemistry-type arrow-pushing mechanisms can help to explain seemingly complex gas-phase reactions.

References

1. Ferrer-Correia AJ, Jennings KR (1973) Int J Mass Spectrom and Ion Phys 11:111
2. Anicich VG, Bowers MT (1974) Int J Mass Spectrom Ion Phys 13:351
3. Anicich VG, Bowers MT, O'Malley RM, Jennings KR (1973) Int J Mass Spectrom Ion Phys 11:99
4. Anicich VG, Bowers MT (1974) Int J Mass Spectrom Ion Phys 13:359
5. Morris RA, Viggiano AA, Paulson JF (1993) J Phys Chem 97:6208
6. Williams BA, Cool TA (1991) J Chem Phys 94:6358
7. Bieri G, Von Niessen W, Åsbrink L, Svensson A (1981) Chem Phys 60:61
8. Eden S, Limao-Vieira P, Kendall PA, Mason NJ, Delwiche J, Hubin-Franskin MJ, Tanaka T, Kitajima M, Tanaka H, Cho H, Hoffmann SV (2004) Chem Phys 297:257
9. Su T, Kevan L (1973) Int J Mass Spectrom Ion Phys 11:57

Chapter 9
The Reactions of OH^-, O^-, CF_3^-, F^-, and O_2^- with C_2H_4, C_2H_3F, $C_2H_2F_2$, C_2HF_3 and C_2F_4

This chapter takes a new approach in the investigation of fluorination in ethene by looking at some *anion*-molecule reactions. The data presented were collected by Drs Richard Kennedy and Chris Mayhew many years ago. The raw data was given to me for a project which I started in the fourth year of my undergraduate MSci degree, and continued over the first few years of my Ph.D. The discussion and interpretation of the results presented here is almost entirely my own work, but I would like to thank Dr Liam Cox for many helpful discussions about organic chemistry reaction mechanisms, and Dr Michael Parkes and Professor Richard Tuckett for continued guidance during these early stages of my research.

9.1 Background Information

The reactions of ethene (C_2H_4), monofluoroethene (C_2H_3F), 1,1-difluoroethene (CH_2CF_2), trifluoroethene (C_2HF_3) and tetrafluoroethene (C_2F_4) with some cations have been discussed in Chaps. 7 and 8. The electron density around the fluorine atom(s), and the dipole moment are important factors in understanding how the molecule interacts with the cation. It is now *anions* which are being reacted with this same group of substituted ethene molecules, and so it is the *acidity* of the molecule and the *electropositivity* of the carbon atoms which becomes important. It has been discussed by Sullivan and Beauchamp that single fluorine substitution in both ethene [1] and ethane [2] increases the acidity of the molecule by approximately 100 kJ mol^{-1}, and that additional fluorine substitution will increase the acidity further, but to a much lesser extent.

Some of the reactions presented here have been studied previously by other groups. The gas-phase reaction of O^- with C_2H_4 has been studied by Drift Tube mass spectrometry [3, 4], and using a SIFT [5]. Ion Cyclotron Resonance Mass Spectrometry (ICR-MS) has been used to study the reaction of O^- with C_2H_4, C_2H_3F and CH_2CF_2 [6], and a Flowing Afterglow apparatus used to study O^- and OH^- reactions with C_2H_4 [7]. Some anions reacting with C_2F_4 have also been

M. J. Simpson, *Two Studies in Gas-Phase Ion Spectroscopy*, Springer Theses,
DOI: 10.1007/978-3-642-23129-2_9, © Springer-Verlag Berlin Heidelberg 2012

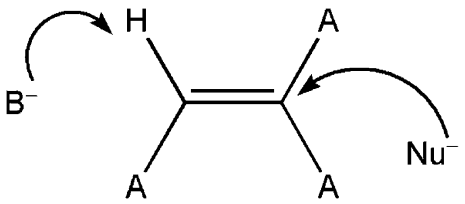

Fig. 9.1 A pictoral representation of the differences in the initial reaction step depending if the anion acts as a base (B^-) or as a nucleophile (Nu^-). A represents either H or F

investigated by SIFT mass spectrometry; O^- and O_2^- by Morris [8], and F^- and CF_3^- by Su et al. [9].

The data presented here forms the continuation of a study into the gas-phase reactions of anions with halogen substituted ethenes by the Molecular Physics group in Birmingham, and the reactions of OH^-, O^-, CF_3^-, F^- and O_2^- with the *chlorinated* ethenes have already been investigated [10].

The discussion below often refers to the reactant anion species either acting as a *base*, or as a *nucleophile*. Figure 9.1 clarifies what is meant by these two terms, and the intended differentiation between them: when the anion acts as a base it will attack a hydrogen atom, and when acting as a nucleophile it will attack a carbon atom.

9.2 Results

In this section the results are presented and some general comments are made. In particular, comparisons are made to previous studies, and some ambiguous details regarding some of the observed anion species are discussed.

The results for the reactions of OH^-, O^-, CF_3^-, F^- and O_2^- with ethene (C_2H_4), monofluoroethene (C_2H_3F), 1,1-difluoroethene (CH_2CF_2), trifluoroethene (C_2HF_3) and tetrafluoroethene (C_2F_4) are presented in Table 9.1. These include the product anions, their branching ratios (BRs) and the bimolecular reaction rate coefficient, k_{exp}. Collisional rate coefficients, k_c, are also included. Where an association reaction is observed the helium buffer gas pressure is given due to its involvement in collisionally stabilising the energised intermediate formed.

The reactions of C_2H_4 provide a useful comparison to those of the fluorinated ethenes. As seen from Table 9.1 only O^- and F^- react with C_2H_4, and the experimental rate coefficients are significantly below the corresponding collisional values. For the reaction with F^- an association product is observed, but the depletion in F^- signal was too small to determine the value for k_{exp}, and the value of 1.0×10^{-13} cm^3 mol^{-1} s^{-1} represents the lowest value which can be measured by the Birmingham SIFT apparatus.

The fluorinated ethenes show a much higher level of reactivity, highlighting the effect electronegative fluorine atoms have on the molecule; a fluorine substituent on ethene will generate electropositivity in carbon (making it more susceptible to nucleophilic attack), and increase the acidity of the molecule (increasing susceptibility to attack from a base).

Table 9.1 A summary of results for the gas-phase reactions of some anions with ethene and the fluorinated ethenes. All reaction rate coefficients, k, are given in units of cm^3 $molecule^{-1}$ s^{-1} and branching ratios are expressed as percentages

	C_2H_4	C_2H_3F	CH_2CF_2	C_2HF_3	C_2F_4
OH^-	No reaction	$k_{exp} = 3.1 \times 10^{-9}$ $k_c = 2.5 \times 10^{-9}$ $H_2O.F^-$ (53%) $C_2H_2F^-$ (40%) F^- (5%) $C_2H_3O^-$ (2%)	$k_{exp} = 1.8 \times 10^{-9}$ $k_c = 2.4 \times 10^{-9}$ $C_2HF_2^-$ (97%) $H_2O.F^-$ (3%)	$k_{exp} = 2.8 \times 10^{-9}$ $k_c = 2.2 \times 10^{-9}$ $C_2F_3^-$ (100%)	$k_{exp} = 1.2 \times 10^{-9}$ $k_c = 1.3 \times 10^{-9}$ CF_3^- (48%) FCO^- (18%) $C_2F_3O^-$ (15%) F^- (10%) HF_2^- (9%)
O^-	$k_{exp} = 6.3 \times 10^{-10}$ $k_c = 1.5 \times 10^{-9}$ $C_2H_2^-$ (71%) e^- (26%)[a] $C_2H_3O^-$ (3%)	$k_{exp} = 3.9 \times 10^{-9}$ $k_c = 2.5 \times 10^{-9}$ e^- (72%)[a] C_2HF^- (24%) $C_2H_2O^-$ (4%)	$k_{exp} = 2.0 \times 10^{-9}$ $k_c = 2.4 \times 10^{-9}$ e^- (80%)[a] $C_2F_2^-$ (20%)	$k_{exp} = 2.2 \times 10^{-9}$ $k_c = 2.2 \times 10^{-9}$ e^- (65%)[a] $C_2F_3^-$ (35%)	$k_{exp} = 1.0 \times 10^{-9}$ $k_c = 1.3 \times 10^{-9}$ F^- (68%) e^- (18%)[a] $C_2F_3O^-$ (6%) CF_3^- (4%) FCO^- (4%)
CF_3^-	No reaction	No reaction	No reaction	$k_{exp} = 8.5 \times 10^{-10}$ $k_c = 1.3 \times 10^{-9}$ $C_2F_3^-$ (100%)	$k_{exp} = 2.6 \times 10^{-10}$ $k_c = 7.6 \times 10^{-10}$ F^- (100%)
F^-	$k_{exp} < 1.0 \times 10^{-13}$ $k_c = 1.4 \times 10^{-9}$ $p(He) = 0.6$ Torr $C_2H_4F^-$ (100%)	$k_{exp} = 5.6 \times 10^{-12}$ $k_c = 2.4 \times 10^{-9}$ $p(He) = 0.6$ Torr $C_2H_3F_2^-$ (100%)	$k_{exp} = 1.1 \times 10^{-11}$ $k_c = 2.3 \times 10^{-9}$ $p(He) = 0.5$ Torr $C_2H_2F_3^-$ (100%)	$k_{exp} = 2.3 \times 10^{-10}$ $k_c = 2.1 \times 10^{-9}$ $p(He) = 0.6$ Torr $C_2HF_4^-$ (95%) $C_2F_3^-$ (5%)	$k_{exp} = 3.0 \times 10^{-10}$ $k_c = 1.2 \times 10^{-9}$ $p(He) = 0.5$ Torr $C_2F_5^-$ (100%)

(continued)

Table 9.1 (continued)

	C_2H_4	C_2H_3F	CH_2CF_2	C_2HF_3	C_2F_4
O_2^-	No reaction	$k_{exp} = 1.1 \times 10^{-12}$ $k_c = 2.0 \times 10^{-9}$ $p(He) = 0.65$ Torr $C_2H_3FO_2^-$ (100%)	$k_{exp} = 2.0 \times 10^{-11}$ $k_c = 1.9 \times 10^{-9}$ e^- (100%)[a]	$k_{exp} = 4.8 \times 10^{-10}$ $k_c = 1.7 \times 10^{-9}$ F^- (100%)	$k_{exp} = 1.0 \times 10^{-9}$ $k_c = 1.0 \times 10^{-9}$ F^- (46%) e^- (35%)[a] F_2^- (8%) $C_2F_4O^-$ (8%) FCO^- (3%)

[a] The production of electrons, e^-, from a reaction is monitored in the experiment by observing a drop in the current across the Faraday plate (see Chap. 2 for experimental details)

Several other groups have studied the gas-phase reaction of O^- with C_2H_4. In agreement with this study, using a SIFT Viggiano and Paulson observe three anion products: e^-, $C_2H_2^-$ and a minor product, $C_2H_3O^-$ [5]. The major difference between these studies is the difference in BRs for the two major products: $C_2H_2^-$ and electrons. This work suggests $C_2H_2^-$ is the dominant product (BR = 71%), whereas Viggiano and Paulson record it as e^- detachment (BR = 68%). Using a drift tube apparatus, Parkes [3] and Lindinger et al. [4] not only observe $C_2H_2^-$ and $C_2H_3O^-$, but also OH^- and C_2HO^- which are not seen in either SIFT study. Lindinger et al. did not monitor electrons in their study, however, Parkes also reports electron detachment as the major channel. In a Flowing Afterglow experiment, O^- was found to react with C_2H_4 by electron detachment only [7]. Using ICR-MS, $C_2H_2^-$ was the only observed reaction, although electron detachment was not monitored [6]. Given the differences in techniques used to study the reaction of O^- with C_2H_4, it is difficult to compare and explain all these results, but it is clear that when electron detachment was monitored it was found to be the dominant reaction in all experiments except this SIFT study.

The reaction of OH^- with C_2H_4 has also been studied previously, and in agreement with the results of this study, these species were found not to react [7]. This is not surprising, as the expected H^+ abstraction reaction forming water is endothermic by 71 kJ mol^{-1}.

The reactions of C_2H_3F and CH_2CF_2 show few trends when comparing the data of each individual neutral as the reactant anion changes. For C_2H_3F only association is observed in the reactions with F^- and O_2^-, whereas the reactions with OH^- and O^- afford a wider range of product anions. Similarly for CH_2CF_2, an equally diverse range of products are detected; exclusive electron detachment results from the reaction with O_2^-, with F^- only association is observed, but the reactions with OH^- and O^- produce products such as $C_2HF_2^-$ and $C_2F_2^-$, respectively. These basic observations from Table 9.1 show that the reactant anion probably holds the key to interpreting the outcome from these reactions, and when looking at *all* of the results shown, trends are more obviously identified when comparing results from all the reactions with one single anion (i.e. observing left to right in Table 9.1). In Sects. 9.3–9.7 the discussion focuses on this, looking at how the reaction of one anion with the series of ethenes changes as the degree of fluorination increases.

The exception to the comment made above is perhaps in the reactions with C_2HF_3. Its reactions with OH^-, O^-, CF_3^- and F^- all yield a common product: $C_2F_3^-$. Certainly C_2HF_3 is expected to be the most acidic of the neutral reactants, which favours proton abstraction reactions being dominant:

$$B^- + C_2HF_3 \rightarrow C_2F_3^- + BH \tag{9.1}$$

where B^- represents the reactant anion acting as a base. It is also noted that $C_2F_3^-$ is a relatively stable anion and the negative charge is delocalised by the electronegative fluorine atoms. Simmonett et al. [11] performed theoretical calculations for the fluorinated vinyl anion series, attributing the greater relative stability of

$C_2F_3^-$ to inductive and negative hyperconjugative effects. The thermochemical tabulations of Lias et al. [12] contain three quite different values for the enthalpy of formation of $C_2F_3^-$: -391 ± 19 [13], -637 ± 58 [14] and -420 ± 42 kJ mol^{-1} [15]. The first value comes from an experiment in which $C_2F_3^-$ was observed as a product of dissociative electron attachment to C_3F_8:

$$e^- + C_3F_8 \rightarrow C_2F_3^- + CF_4 + F \tag{9.2}$$

The value extracted from this work by Lias et al. comes from the estimated $\Delta_r H°$ for reaction 9.2, and assumes the structure of $C_2F_3^-$ to be $CF_2{=}CF^-$. The second value comes from the threshold for formation of $C_2F_3^-$ from CF_3CHO:

$$e^- + CF_3CHO \rightarrow CF_3C^- + O + H \tag{9.3}$$

Note the isomeric form of $C_2F_3^-$ in reaction 9.3 has all fluorines bonded to *one* of the carbon atoms. The third and preferred value, -420 kJ mol^{-1}, was derived from the observed threshold for reaction 9.4:

$$e^- + C_2F_4 \rightarrow C_2F_3^- + F \tag{9.4}$$

Clearly there is uncertainty in all of the values discussed above, but when calculating initial enthalpy changes for reactions 9.5–9.9,[1] the value of -420 ± 42 kJ mol^{-1} is used.

The only reaction of C_2HF_3 which does not yield $C_2F_3^-$ as a product is that with O_2^-. The thermochemistry for the expected H^+ abstraction resulting in $C_2F_3^-$ is endothermic:

$$O_2^- + C_2HF_3 \rightarrow C_2F_3^- + HO_2 \quad \Delta_r H° = +122 \text{ kJ mol}^{-1} \tag{9.5}$$

This can then be compared to the thermochemistry for the other anion reactions with C_2HF_3, where $C_2F_3^-$ *is* a common product:

$$OH^- + C_2HF_3 \rightarrow C_2F_3^- + H_2O \quad \Delta_r H° = -29 \text{ kJ mol}^{-1} \tag{9.6}$$

$$O^- + C_2HF_3 \rightarrow C_2F_3^- + OH \quad \Delta_r H° = +8 \text{ kJ mol}^{-1} \tag{9.7}$$

$$CF_3^- + C_2HF_3 \rightarrow C_2F_3^- + CHF_3 \quad \Delta_r H° = +15 \text{ kJ mol}^{-1} \tag{9.8}$$

$$F^- + C_2HF_3 \rightarrow C_2F_3^- + HF \quad \Delta_r H^o = +48 \text{ kJ mol}^{-1} \tag{9.9}$$

The calculated enthalpies are positive for reactions 9.7–9.9, yet the product $C_2F_3^-$ is observed. It is very likely that uncertainty in the value for $\Delta_f H°$ ($C_2F_3^-$), as

[1] The enthalpy changes for reactions 9.5–9.9 are considered incorrect, because of uncertainty in the value of $\Delta_f H°$ ($C_2F_3^-$) used, -420 kJ mol^{-1}. A new value, -504 kJ mol^{-1}, is evaluated from recent theoretical calculations, and from the presented experimental observations shown by reactions 9.5–9.9. The updated reaction enthalpies are +38, -113, -76, -69, and -36 kJ mol^{-1}, respectively. See text for a more detailed discussion.

discussed above, when used to calculate the $\Delta_r H°$ values is responsible for this inconsistency. If it is assumed that reaction 9.5 *is* endothermic because the $C_2F_3^-$ product is not observed, then the true value for $\Delta_f H°$ ($C_2F_3^-$) should lie between −468 and −543 kJ mol^{-1} (the actual value used is −420 ± 42 kJ mol^{-1}). Reactions 9.6–9.9 then all become exothermic—a much better reflection of the results.

Since the tabulations of Lias et al. [12], theoretical calculations on the electron affinity (*EA*) and $\Delta_f H°$ of C_2F_3 have been performed. Thus, a new value for $\Delta_f H°$ ($C_2F_3^-$) can be determined. The calculations by Bauschlicher and Ricca [16] give a value for $\Delta_f H°$ (C_2F_3) = −224 kJ mol^{-1}, and data collected for the *EA* (C_2F_3) is summarised in a review article [17]. The values for the *EA* range from 2.06 to 2.90 eV. As discussed above, it is expected that $\Delta_f H°$ ($C_2F_3^-$) takes the values between −468 and −543 kJ mol^{-1}, which corresponds to the *EA* being between 2.53 and 3.31 eV, respectively. This clearly suggests the *EA* (C_2F_3) is towards the higher end of the values given. Therefore, for the purposes of this thesis, a value for the *EA* of 2.90 eV (280 kJ mol^{-1}) and the $\Delta_f H°$ of −224 kJ mol^{-1} for C_2F_3 are used to give $\Delta_f H°_{298}$ ($C_2F_3^-$) = −504 kJ mol^{-1}, with an estimated ± 20 kJ mol^{-1} uncertainty. Using this new value, the updated enthalpy changes for reactions 9.5–9.9 are +38, −113, −76, −69 and −36 kJ mol^{-1}, respectively.

Absence of hydrogens in C_2F_4 eliminates any possibility of the reactant anions acting as bases in their reactions. Attack of an anionic species on electron-rich fluorine is unlikely, and it is therefore expected to see anions only acting as nucleophiles in their reactions with C_2F_4.

The reactions of OH^-, O^- and O_2^- with C_2F_4 proceed at, or close to the collisional rate. Inspection of Table 9.1 shows the diversity of anion products observed from these reactions. Morris also studied the reactions of O^- and O_2^- with C_2F_4 [8]. An equally broad range of anion products was observed, and Morris rationalised this by comparing the weak double bond in C_2F_4 with the strong C=O bonds which can form, concluding that specific mechanisms to account for all the products are difficult to propose.

F^- reacts with C_2F_4 to produce $C_2F_5^-$ by association, and this same result was observed by Su et al. [9].

$$F^- + C_2F_4 \rightarrow C_2F_5^- \quad \Delta_r H° = -159 \text{ kJ mol}^{-1} \tag{9.10}$$

This association reaction fits into the trend of the other reactions with F^-, and it is discussed in detail in Sect. 9.6.

F^- anions were detected as the major product species (>95%) from the reaction of CF_3^- with C_2F_4. The only thermochemically viable reaction is the addition of CF_3^-, followed by the elimination of F^- to produce hexafluoropropene:

$$CF_3^- + C_2F_4 \rightarrow F^- + C_3F_6 \quad \Delta_r H° = -74 \text{ kJ mol}^{-1} \tag{9.11}$$

In addition to F^- ions, $C_2F_5^-$ was also observed but as a minor product (<5%). The BR studies for this reaction, however, showed that $C_2F_5^-$ is a *secondary* product. It must be that F^- anions produced from reaction 9.11 react with C_2F_4 by

association, which has already been shown to occur independently. Su et al. [9] report $C_2F_5^-$ is the *only* product from the reaction of CF_3^- with C_2F_4 suggesting it is produced by F^- transfer:

$$CF_3^- + C_2F_4 \rightarrow C_2F_5^- + CF_2 \quad \Delta_r H^\circ = +51 \text{ kJ mol}^{-1} \tag{9.12}$$

It is more likely that they are observing $C_2F_5^-$ from the secondary reaction as discussed above, and *not* that shown in reaction 9.12 which is endothermic.

9.3 The Reactions of OH^-

Inspection of Table 9.1 shows that the large majority of the observed anionic products from the reactions of OH^- can be explained with the anion acting as a base. However, the minor products F^- and $C_2H_3O^-$ from the reaction with C_2H_3F result from OH^- acting as a nucleophile. The proposed addition–elimination mechanisms for producing these two anions are shown in Fig. 9.2. A stepwise addition–elimination mechanism is suggested rather than a concerted S_N2 (bimolecular nucleophilic substitution) mechanism because the former allows for the carbanion intermediate to eliminate F^- *or* HF (i.e. step 2a vs. step 2b). The only expected anionic product from an S_N2 reaction would be F^-. The elimination of F^- following step 2a forms neutral C_2H_4O, presumably the isomeric form CH_2=CHOH. The change in enthalpy for this reaction is -91 kJ mol^{-1}. Step 3a, however, shows how CH_2=CHOH could rearrange to form CH_3CHO, a possibility given that $\Delta_f H^\circ_{298}$ (CH_2=CHOH) $= -125$ and $\Delta_f H^\circ_{298}$ (CH_3CHO) $= -166$ kJ mol^{-1}. The competing mechanism, elimination of HF following step 2b, suggests the isomeric form of the observed $C_2H_3O^-$ anion is in fact CH_2=CHO^-, and the enthalpy change for this reaction is -155 kJ mol^{-1}. This anion has two resonance forms, which are also shown in Fig. 9.2, where the negative charge is delocalised across the oxygen and carbon atoms—the likely reason for the relative stability of this species, and hence its observation as a product.

In the reactions with C_2H_3F, CH_2CF_2 and C_2HF_3, it is OH^- acting as a base which accounts for the majority of the products detected. The products $C_2H_2F^-$, $C_2HF_2^-$ and $C_2F_3^-$ are produced from H^+ abstraction reactions:

$$OH^- + C_2H_3F \rightarrow C_2H_2F^- + H_2O \quad \Delta_r H^\circ = 41 + \Delta_f H^\circ(C_2H_2F^-) \text{ kJ mol}^{-1} \tag{9.13}$$

$$OH^- + CH_2CF_2 \rightarrow C_2HF_2^- + H_2O \quad \Delta_r H^\circ = 247 + \Delta_f H^\circ\left(C_2HF_2^-\right) \text{ kJ mol}^{-1} \tag{9.14}$$

$$OH^- + C_2HF_3 \rightarrow C_2F_3^- + H_2O \quad \Delta_r H^\circ = -113 \text{ kJ mol}^{-1} \tag{9.15}$$

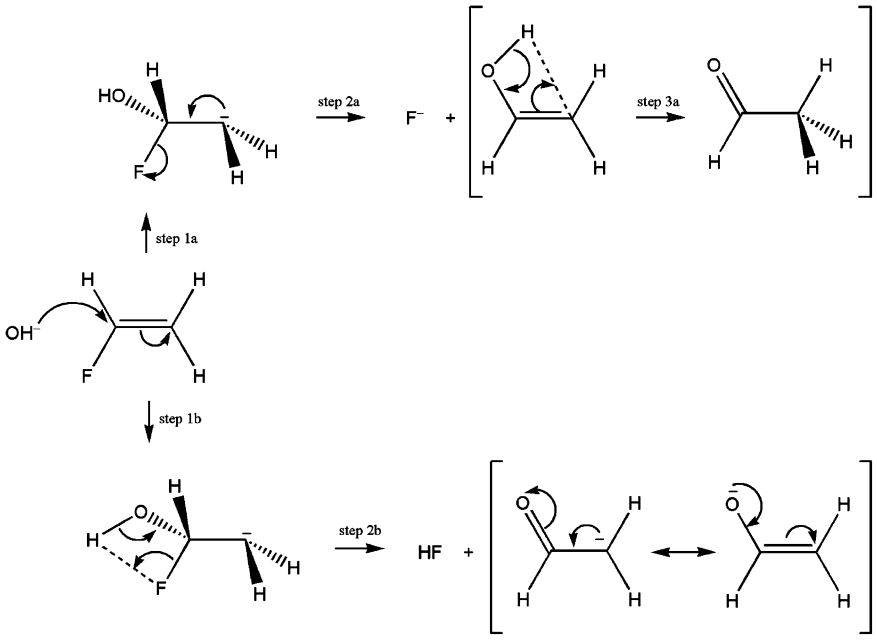

Fig. 9.2 Addition–elimination mechanisms showing the formation of F^- and $C_2H_3O^-$ in the reaction of OH^- with C_2H_3F. The *dotted lines* represent bonds between atoms which are formed following the next reaction step

Unfortunately no values for $\Delta_f H°$ ($C_2H_2F^-$ *or* $C_2HF_2{}^-$) have been found in the literature or thermochemical databases. Reactions 9.13 and 9.14 are expected to be exothermic, and so upper limits to these $\Delta_f H°$ values can be calculated: $\Delta_f H°_{298}$ ($C_2H_2F^-$) ≤ -41 kJ mol^{-1}, and $\Delta_f H°_{298}$ ($C_2HF_2{}^-$) ≤ -247 kJ mol^{-1}. There has been much discussion surrounding the structure of these two anionic species because of the potential for hydrogen-bonding to occur [11, 18–21].

The two different suggested structures are shown in Fig. 9.3. The general conclusion is that the hydrogen-bonded structure for $C_2H_2F^-$ is in the region of 50 kJ mol^{-1} *lower* in energy than the vinyl anion [11, 18], but for $C_2HF_2{}^-$ the difference in energies of the two structures is negligible [11].

In the reactions of OH^- with C_2H_3F and CH_2CF_2, the structures of the anion products $C_2H_2F^-$ and $C_2HF_2{}^-$, respectively, are not known. The mechanism for H^+ abstraction is straightforward, as shown by mechanism 1 in Fig. 9.4, and suggests it is the vinyl anion structure which is being observed. On the other hand, mechanism 2 in Fig. 9.4 shows a possible way for rearrangement to occur where the hydrogen-bonded species is formed—essentially the elimination of F^-. The elimination of F^-, and it forming the hydrogen bond, are shown to occur in a concerted fashion because reactions 9.16 and 9.17 are endothermic.

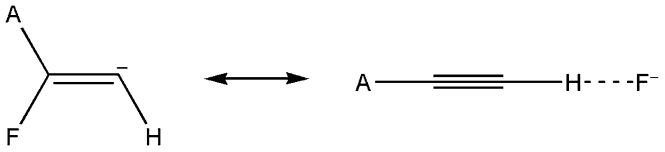

Fig. 9.3 The two different structures suggested for $C_2H_2F^-$ (when A = H) and $C_2HF_2^-$ (when A = F). Here, the dotted line represents hydrogen-bonding

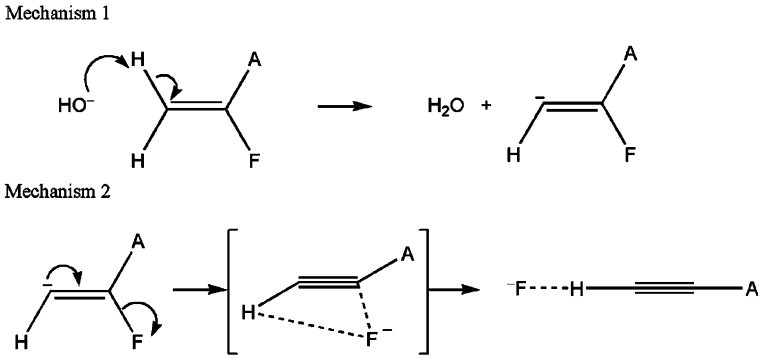

Fig. 9.4 *Mechanism 1* showing H^+ abstraction by OH^- forming water and the corresponding vinyl anion. *Mechanism 2* shows the rearrangement of the vinyl anion to form a hydrogen-bonded ethyne structure via the elimination of F^-. In both mechanisms A = H showing the reaction with C_2H_3F, and A = F showing the reaction with CH_2CF_2

$$OH^- + C_2H_3F \rightarrow F^- + H_2O + C_2H_2 \quad \Delta_r H^\circ = +20 \text{ kJ mol}^{-1} \tag{9.16}$$

$$OH^- + CH_2CF_2 \rightarrow F^- + H_2O + C_2HF \quad \Delta_r H^\circ = +105 \text{ kJ mol}^{-1} \tag{9.17}$$

$$OH^- + C_2HF_3 \rightarrow F^- + H_2O + C_2F_2 \quad \Delta_r H^\circ = +165 \text{ kJ mol}^{-1} \tag{9.18}$$

Thus, the energy gained on forming the hydrogen bond is required to drive the elimination of F^-. Indeed the endothermicity of the elimination reactions above supports the suggestion made earlier that F^- from the reaction with C_2H_3F is produced by an addition–elimination mechanism (Fig. 9.2), with OH^- acting as a nucleophile.

The formation of $H_2O.F^-$ (H_2O and F^- hydrogen-bonded to one another) is the abstraction by OH^- of HF:

$$OH^- + C_2H_3F \rightarrow H_2O.F^- + C_2H_2 \quad \Delta_r H^\circ = -98 \text{ kJ mol}^{-1} \tag{9.19}$$

$$OH^- + CH_2CF_2 \rightarrow H_2O.F^- + C_2HF \quad \Delta_r H^\circ = -13 \text{ kJ mol}^{-1} \tag{9.20}$$

$$OH^- + C_2HF_3 \rightarrow H_2O.F^- + C_2F_2 \quad \Delta_r H^\circ = +48 \text{ kJ mol}^{-1} \tag{9.21}$$

The thermochemistry of reactions 9.19–9.21 reflect the products which are observed; the production of $H_2O.F^-$ in reactions with C_2H_3F (53%) and CH_2CF_2 (3%), but not with C_2HF_3. Energetics alone are unlikely to explain why the BR is much larger in the reaction of C_2H_3F than in that of CH_2CF_2; for HF to be abstracted from CH_2CF_2 the hydrogen and fluorine must come from different ends of the double bond, which is not the case for C_2H_3F.

The reaction of OH^- with C_2F_4 is more complicated. It seems fair to assume OH^- will be drawn towards the electropositive carbon atoms in C_2F_4, and acts as a nucleophile. The range of products observed show that the resulting reaction complex will readily rearrange, break bonds and form new ones. Some exothermic reactions are listed below which show how the stable neutral products which can be formed are the likely driving force in this reaction:

$$OH^- + C_2F_4 \rightarrow CF_3^- + HFCO \quad \Delta_r H^\circ = -220 \text{ kJ mol}^{-1} \tag{9.22}$$

$$OH^- + C_2F_4 \rightarrow CF_3^- + HF + CO \quad \Delta_r H^\circ = -227 \text{ kJ mol}^{-1} \tag{9.23}$$

$$OH^- + C_2F_4 \rightarrow FCO^- + CHF_3 \quad \Delta_r H^\circ = -335 \text{ kJ mol}^{-1} \tag{9.24}$$

$$OH^- + C_2F_4 \rightarrow FCO^- + CF_2 + HF \quad \Delta_r H^\circ = -92 \text{ kJ mol}^{-1} \tag{9.25}$$

$$OH^- + C_2F_4 \rightarrow C_2F_3O^- + HF \quad \Delta_r H^\circ = 530 + \Delta_f H^\circ(C_2F_3O^-) \text{ kJ mol}^{-1} \tag{9.26}$$

$$OH^- + C_2F_4 \rightarrow F^- + CHF_3 + CO \quad \Delta_r H^\circ = -259 \text{ kJ mol}^{-1} \tag{9.27}$$

$$OH^- + C_2F_4 \rightarrow F^- + HF + CF_2 + CO \quad \Delta_r H^\circ = -16 \text{ kJ mol}^{-1} \tag{9.28}$$

$$OH^- + C_2F_4 \rightarrow F^- + CF_2 + HFCO \quad \Delta_r H^\circ = -10 \text{ kJ mol}^{-1} \tag{9.29}$$

$$OH^- + C_2F_4 \rightarrow F^- + CF_2CFOH \quad \Delta_r H^\circ = 554 + \Delta_f H^\circ(CF_2CFOH) \text{ kJ mol}^{-1} \tag{9.30}$$

$$OH^- + C_2F_4 \rightarrow F^- + CF_3CHO \quad \Delta_r H^\circ = -224 \text{ kJ mol}^{-1} \tag{9.31}$$

$$OH^- + C_2F_4 \rightarrow HF_2^- + CF_2 + CO \quad \Delta_r H^\circ = -173 \text{ kJ mol}^{-1} \tag{9.32}$$

The formation of F^- and $C_2F_3O^-$ from C_2F_4 are analogous to the products F^- and $C_2H_3O^-$ from C_2H_3F, and so the suggested mechanism in Fig. 9.2 is also considered to describe reactions 9.26 and 9.30. Reactions 9.30 and 9.31 show different isomeric forms of the neutral product C_2HF_3O. The product CF_2CFOH would be the expected species following a substitution reaction, whereas the product CF_3CHO would require additional rearrangement. Unfortunately, $\Delta_f H^\circ$ (CF_2CFOH) is not known.

9.4 The Reactions of O^-

The first observation noted from this set of reactions is the production of the anion product following H_2^+ abstraction by O^- to form water:

$$O^- + C_2H_4 \rightarrow C_2H_2^- + H_2O \quad \Delta_r H^\circ = -11 \text{ kJ mol}^{-1} \tag{9.33}$$

$$O^- + C_2H_3F \rightarrow C_2HF^- + H_2O \quad \Delta_r H^\circ = -113 \text{ kJ mol}^{-1} \tag{9.34}$$

$$O^- + CH_2CF_2 \rightarrow C_2F_2^- + H_2O \quad \Delta_r H^\circ = -74 \text{ kJ mol}^{-1} \tag{9.35}$$

The isomeric forms of the anion products are $H_2C{=}C^-$, $HFC{=}C^-$ and $F_2C{=}C^-$ for reactions 9.33–9.35, respectively. Note that there is some uncertainty in the $\Delta_f H^\circ$ values for these species (see Appendix I). It is therefore assumed that the reaction mechanism leads to both hydrogen atoms being abstracted from the same carbon atom, and certainly this *must* be the case for $C_2F_2^-$ production with CH_2CF_2.

These reaction products have been observed previously by Dawson and Jennings [6] when performing reactions of O^- with a variety of molecules using ICR-MS, and the same conclusion regarding the structure of the product anion was reached. It seems very likely that H_2^+ abstraction is energetically more favourable than H^+ abstraction in the reactions of O^- with C_2H_3F and CH_2CF_2; it is certainly the case for C_2H_4. In the case of C_2HF_3, H_2^+ abstraction is no longer possible and H^+ abstraction is observed instead. Consider the reactions below:

$$O^- + C_2H_4 \rightarrow C_2H_3^- + OH \quad \Delta_r H^\circ = +106 \text{ kJ mol}^{-1} \tag{9.36}$$

$$O^- + C_2H_3F \rightarrow C_2H_2F^- + OH \quad \Delta_r H^\circ = 76 + \Delta_f H^\circ(C_2H_2F^-) \text{ kJ mol}^{-1} \tag{9.37}$$

$$O^- + CH_2CF_2 \rightarrow C_2HF_2^- + OH \quad \Delta_r H^\circ = 282 + \Delta_f H^\circ\left(C_2HF_2^-\right) \text{ kJ mol}^{-1} \tag{9.38}$$

The values for $\Delta_f H^\circ(C_2H_2F^-)$ and $\Delta_f H^\circ(C_2HF_2^-)$ have been discussed in Sect. 9.3 (see reactions 9.13–9.15), and upper-limit values of ≤ -41, and ≤ -247 kJ mol^{-1}, respectively, were evaluated. Also recall the discussion in Sect. 9.2 about H^+ abstraction reactions with C_2HF_3. It is difficult to predict if reactions 9.37 and 9.38 are exothermic or not, and given that Dawson and Jennings observed these two reactions [6], albeit as minor product channels, it is unclear why they are not observed in the present SIFT study.

It is very interesting that electron ejection is observed in the reactions of O^- with ethene and the fluorinated ethenes. The fact that O^- is a radical anion with an odd number of electrons is the likely cause. This represents the major product channel in the reactions of C_2H_3F (72%), CH_2CF_2 (80%), and C_2HF_3 (65%), but

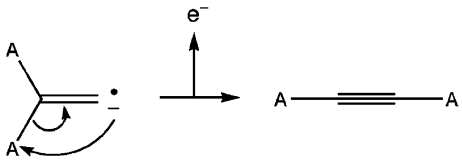

Fig. 9.5 A possible mechanism to account for electron ejection in the reactions of O^- with C_2H_4, C_2H_3F and CH_2CF_2. The radical carbene structure results from the abstraction of H_2^+ by O^-. A represents either H or F

the BRs are less in the case of C_2H_4 (26%) and C_2F_4 (18%). The reason for these differences in BRs is unclear, but it may be no coincidence that C_2H_4 and C_2F_4 are the only two of the five molecules with no dipole moment. Understanding the mechanism for the electron ejection reaction is not easy, and it is not even obvious if it is initiated by O^- acting as a base or as a nucleophile.

One possibility arises from the radical anion species produced following H_2^+ abstraction, shown in Fig. 9.5, where a rearrangement to generate a carbon–carbon triple bond will result in electron ejection. This seems reasonable given that neutral carbenes, e.g. CF_2=C, are known to convert into the corresponding ethyne, e.g. CFCF, by a Fritsch-Buttenberg-Wiechell rearrangement [22, Cox LR, private communication]. The mechanism in Fig. 9.5 can only be applied to the reactions of C_2H_4, C_2H_3F and CH_2CF_2, because the radical carbene is produced following H_2^+ abstraction. It seems reasonable to assume a similar mechanism is responsible for electron ejection from *all* of the neutral ethenes, C_2HF_3 and C_2F_4 included, and so this possibility is not convincing.

Another possibility is if O^- acts as a nucleophile, forming an intermediate complex with the neutral ethene and ejecting an electron to form an oxirane species (Fig. 9.6). Heats of formation for the *fluorinated* oxirane species are not available, but the reaction in Fig. 9.6 is exothermic when all A substituents are hydrogen (i.e. for ethene):

$$O^- + C_2H_4 \rightarrow e^- + c - CH_2(O)CH_2 \quad \Delta_r H^\circ = -207 \text{ kJ mol}^{-1} \qquad (9.39)$$

This mechanism for nucleophilic attack seems reasonable, and certainly other anion products observed in the reactions with O^- surely arise from the same initial step. These include $C_2H_3O^-$ from C_2H_4, $C_2H_2O^-$ from C_2H_3F, and all of the products in the reaction with C_2F_4. Suggested arrow-pushing mechanisms for the formation of these anions are shown in Fig. 9.7. All of these mechanisms follow the same initial step: the nucleophilic addition of O^- to the neutral ethene. Figure 9.7 only presents the subsequent step, which shows how the resulting carbanion intermediate may rearrange and/or dissociate to generate the observed products.

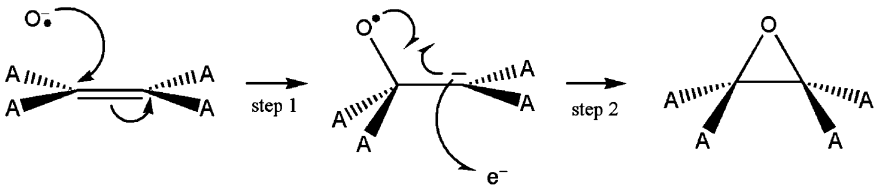

Fig. 9.6 A possible mechanism to explain electron ejection observed from the reactions of O^- with ethene and the fluorinated ethenes. It shows the formation of a neutral oxirane species following step 2. A represents either H or F

9.5 The Reactions of CF_3^-

Only C_2HF_3 and C_2F_4 react with CF_3^-, and in each of these reactions only one anion product is detected (Table 9.1). $C_2F_3^-$ produced in the reaction with C_2HF_3 arises following H^+ abstraction, as discussed in Sect. 9.2 and shown in reaction 9.8. F^- is produced in the reaction with C_2F_4 by addition–elimination (or substitution):

$$CF_3^- + C_2F_4 \rightarrow F^- + C_3F_6 \quad \Delta_r H^\circ = -74 \text{ kJ mol}^{-1} \tag{9.40}$$

These are the two most likely reactions for CF_3^- acting as a base or as a nucleophile, respectively, and it is no coincidence that C_2HF_3 is the most acidic of the neutral ethenes, and C_2F_4 is the most susceptible to attack from a nucleophile.

The likely reason for the overall low reactivity of CF_3^- is its relative stability, having a large negative enthalpy of formation (-641 kJ mol^{-1}), but reaction dynamics must also play a part because, for example, the addition–elimination reaction with C_2H_3F is not observed despite it being an exothermic channel:

$$CF_3^- + C_2H_3F \rightarrow F^- + CH_2CHCF_3 \quad \Delta_r H^\circ = -83 \text{ kJ mol}^{-1} \tag{9.41}$$

The analogous reactions with CH_2CF_2 and C_2HF_3 are also expected to be exothermic, but $\Delta_f H^\circ$ values for the neutral product species CH_2CFCF_3 and $CHFCFCF_3$, respectively, are not known:

$$CF_3^- + CH_2CF_2 \rightarrow F^- + CH_2CFCF_3 \quad \Delta_r H^\circ = 738 + \Delta_f H^\circ(CH_2CFCF_3) \text{ kJ mol}^{-1} \tag{9.42}$$

$$CF_3^- + C_2HF_3 \rightarrow F^- + CHFCFCF_3 \quad \Delta_r H^\circ = 884 + \Delta_f H^\circ(CHFCFCF_3) \text{ kJ mol}^{-1} \tag{9.43}$$

These reactions occur by CF_3^- acting as a nucleophile and attacking the electron deficient carbon atoms. The size of CF_3^- may hinder this type of reaction and only with C_2F_4 when the electrophilicity of the carbon is relatively large, will a reaction occur. Evidence for this suggestion can be found in the efficiency of the $CF_3^- + C_2F_4$ reaction, which is only 34%.

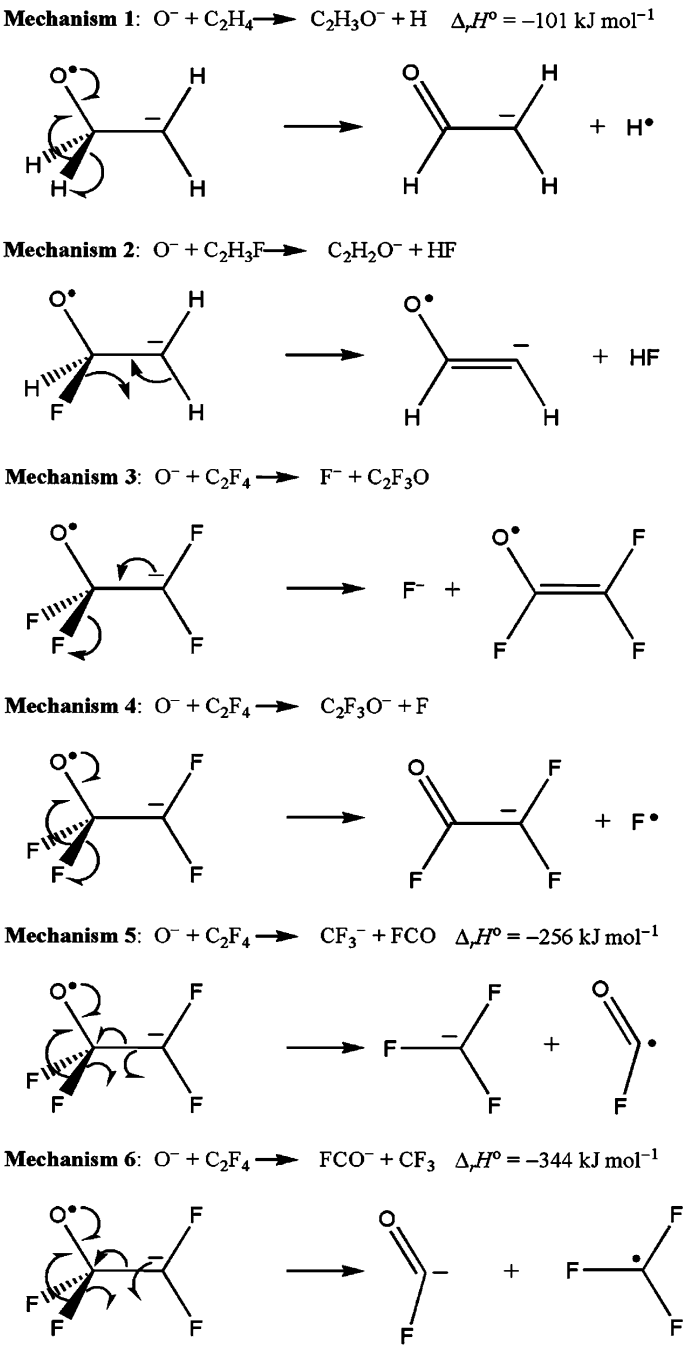

Fig. 9.7 Reaction mechanisms showing how the carbanion intermediate formed following the nucleophilic addition of O^- may rearrange and/or dissociate to yield some of the observed anion products in the reactions of ethene and the fluorinated ethenes. Reaction enthalpies are included where $\Delta_f H°$ values are available for all reactants and products

The hindering effect that the size of CF_3^- has on its reactivity is still apparently present, but to a lesser degree, when it attacks a hydrogen substituent (acting as a base); the rate efficiency of the $CF_3^- + C_2HF_3$ reaction is 65%. Note that the rates show no evidence of inefficiency in H^+ abstraction reactions of the other anions with C_2HF_3 (see Table 9.1). Nevertheless, the reason for the absence of H^+ abstraction in the reactions of CF_3^- with C_2H_4, C_2H_3F, and CH_2CF_2 is most likely an energetic one:

$$CF_3^- + C_2H_4 \rightarrow C_2H_3^- + CHF_3 \quad \Delta_r H^\circ = +113 \text{ kJ mol}^{-1} \tag{9.44}$$

$$CF_3^- + C_2H_3F \rightarrow C_2H_2F^- + CHF_3 \quad \Delta_r H^\circ = 83 + \Delta_f H^\circ(C_2H_2F^-) \text{ kJ mol}^{-1} \tag{9.45}$$

$$CF_3^- + CH_2CF_2 \rightarrow C_2HF_2^- + CHF_3 \quad \Delta_r H^\circ = 289 + \Delta_f H^\circ\left(C_2HF_2^-\right) \text{ kJ mol}^{-1} \tag{9.46}$$

The values for $\Delta_f H^\circ(C_2H_2F^-)$ and $\Delta_f H^\circ(C_2HF_2^-)$ have been discussed in Sect. 9.3, and upper-limit values of ≤ -41 and ≤ -247 kJ mol^{-1}, respectively, have been evaluated. Reactions 9.45 and 9.46 are likely therefore to be endothermic.

9.6 The Reactions of F^-

F^- reacts with ethene and the fluorinated ethenes by association, and the experimental rate coefficient increases as the fluorination on ethene increases (Table 9.1). This demonstrates the preference F^- has to act as a nucleophile rather than a base, and it is only in the reaction with C_2HF_3—the most acidic of the neutral ethenes—where H^+ abstraction is observed, albeit only with a BR of 5% (also see reaction 9.9 and the discussion in Sect. 9.2).

The expected reaction following nucleophilic attack on carbon is addition–elimination (or substitution), but in this instance the nucleophile and leaving group are both the same: F^-. Thus, the relative stability of the adduct carbanion must be considered to explain the observations in this set of reactions. Consider the resonance scheme illustrated in Fig. 9.8. It shows how the geometry of a carbanion is dependent on orbital interactions between the carbon atoms and a substituent X. This is essentially describing *anionic hyperconjugation* [18]. Geometry 1 is considered to have large hyperconjugative effects because the X^- lone-pair orbital is in the same plane as the adjacent carbon π orbital. In geometry 2 these effects are less because the negative charge is on the β carbon with respect to the X substituent, and the carbon lone-pair orbital is slightly out-of-plane with the X *p*-orbitals. The effects of anionic hyperconjugation are significant when X is an electronegative species.

In this set of reactions X is fluorine and each A substituent is either hydrogen or fluorine. In the reaction of F^- with C_2H_4, all A substituents in Fig. 9.8 are

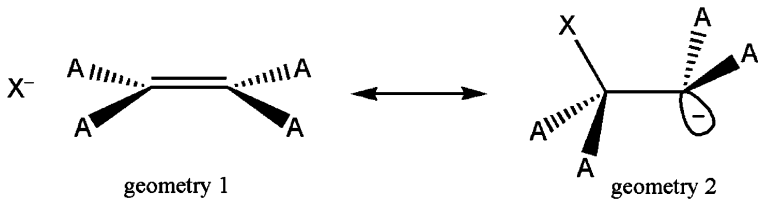

Fig. 9.8 Resonance effects reflecting the degree of anionic hyperconjugation, essentially the delocalisation of negative charge, in the adduct between X^- and either ethene or a fluorinated ethene, where A represents H or F

hydrogen atoms, and the negative charge in the adduct can only be delocalised by anionic hyperconjugation, so the configuration of this species is expected to be more like geometry 1 than geometry 2. In the other extreme, in the reaction of F^- with C_2F_4, all A substituents are fluorines. The resulting adduct may delocalise the negative charge across the whole molecule through the σ network, and so geometry 2 is expected to be more stable than geometry 1. The general trend therefore, is that the greater the degree of fluorine substitution in ethene, the better representative geometry 2 is for the structure of its adduct with F^-. Indeed the strength of the bond formed between X (reactant F^-) and the ethene will be stronger in geometry 2 than geometry 1. This point has also been made by Sullivan and Beauchamp [1], after calculating binding energies of F^- to the fluorinated ethenes. The value increased with increasing fluorine substitution. This trend also matches that observed in the rate coefficients for the reactions of F^- with ethene and the fluorinated ethenes (Table 9.1).

From another point of view, the scheme in Fig. 9.8 can be considered as an equilibrium between reactants (geometry 1) and the formation of the adduct (geometry 2). When more A substituents are fluorines, the adduct is more stable with respect to eliminating F^- and regenerating the reactants. Thus, the rate of forming the adduct increases as the degree of fluorine substitution increases.

9.7 The Reactions of O_2^-

The superoxide anion, O_2^-, has been described as an excellent gas-phase nucleophile [23]. Indeed the results in Table 9.1 show product anions which must arise following initial nucleophilic attack, and O_2^- is the only reactant ion which does not react with C_2HF_3 by proton abstraction.

The reactivity of O_2^- towards the fluorinated ethenes increases as the degree of fluorine substitution increases; there is no reaction with C_2H_4, association with C_2H_3F, electron and F^- ejection is observed with CH_2CF_2 and C_2HF_3, respectively, and a diverse range of products are detected with C_2F_4. In addition, the rate coefficient increases as fluorine substitution in ethene increases.

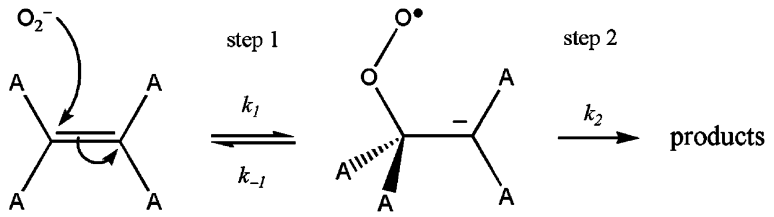

Fig. 9.9 A generic schematic showing the addition of O_2^- to the fluorinated ethenes by nucleophilic attack. A represents either hydrogen or fluorine

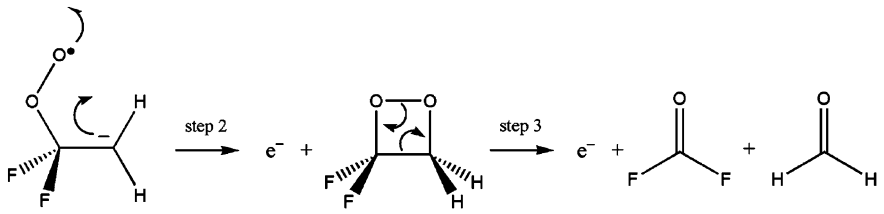

Fig. 9.10 A possible mechanism for electron ejection following the nucleophilic addition of O_2^- to CH_2CF_2

Given that C_2H_4 does not react with O_2^-, fluorines are important in stabilising the adduct species which is formed after initial nucleophilic addition. More substituted fluorine atoms allow a better delocalisation of the negative charge, leading to a more stable adduct (with respect to the *reactants*). Recall a similar discussion in Sect. 9.6 on the trend in k_{exp} values in the reactions of F^-. Consider Fig. 9.9, where the rate determining step is represented by the ratio of k_1/k_{-1}. This ratio is expected to increase when more A substituents are fluorines. If the second step, represented by k_2, is expected to be fast in comparison, the observed trend in the reaction rate coefficients, k_{exp}, is explained.

It is interesting that O_2^- with CH_2CF_2 reacts exclusively by electron ejection. Reactions 9.47 and 9.48 show the two most likely outcomes for this reaction: formation of a dioxetane, or dissociation into two aldehydes, respectively:

$$O_2^- + CH_2CF_2 \rightarrow e^- + CH_2(O_2)CF_2 \quad \Delta_r H^\circ = 394 + \Delta_f H^\circ(CH_2(O_2)CF_2)\ \text{kJ mol}^{-1} \tag{9.47}$$

$$O_2^- + CH_2CF_2 \rightarrow e^- + CH_2O + CF_2O \quad \Delta_r H^\circ = -361\ \text{kJ mol}^{-1} \tag{9.48}$$

Arrow-pushing mechanisms can explain reactions 9.47 and 9.48, which are shown in Fig. 9.10. The former is explained by step 2 only, and the latter by steps 2 and 3 taking place. The same mechanism can also be applied to the reaction with C_2F_4, where electron ejection is also observed with a BR of 35%:

$$O_2^- + C_2F_4 \rightarrow e^- + CF_2(O_2)CF_2 \quad \Delta_r H^\circ = 707 + \Delta_f H^\circ(CF_2(O_2)CF_2) \text{ kJ mol}^{-1} \tag{9.49}$$

$$O_2^- + C_2F_4 \rightarrow e^- + 2\ CF_2O \quad \Delta_r H^\circ = -571 \text{ kJ mol}^{-1} \tag{9.50}$$

The reactions of O_2^- with C_2HF_3 and C_2F_4 to produce F^- are likely to follow the same reaction mechanism of nucleophilic substitution:

$$O_2^- + C_2HF_3 \rightarrow F^- + C_2HF_2O_2 \quad \Delta_r H^\circ = 291 + \Delta_f H^\circ(C_2HF_2O_2) \text{ kJ mol}^{-1} \tag{9.51}$$

$$O_2^- + C_2F_4 \rightarrow F^- + C_2F_3O_2 \quad \Delta_r H^\circ = 458 + \Delta_f H^\circ(C_2F_3O_2) \text{ kJ mol}^{-1} \tag{9.52}$$

It is unclear how stable the neutral products are in reactions 9.49, 9.51 and 9.52. It is entirely possible that these products may rearrange and/or fragment, and there are other reasonable exothermic outcomes (see below). Indeed many potential oxygen-containing product species are not well documented in the literature, and some desired $\Delta_f H^\circ$ values are therefore unavailable (e.g. $C_2F_4O^-$, $C_2F_3O_2$, CHF_2O). In addition there are different isomeric forms of many of these species, further preventing any conclusive product assignments. The product assignments discussed so far (reactions 9.47–9.52) are based on reasonable or likely reaction mechanisms, but many more exothermic possibilities exist. These are presented below in reactions 9.53–9.67. Possibilities are also given for the anions F_2^-, $C_2F_4O^-$, and FCO^- observed in the reaction of O_2^- with C_2F_4 which have not yet been discussed (reactions 9.68–9.72).

$$O_2^- + CH_2CF_2 \rightarrow e^- + CO_2 + CH_2F_2 \quad \Delta_r H^\circ = -451 \text{ kJ mol}^{-1} \tag{9.53}$$

$$O_2^- + CH_2CF_2 \rightarrow e^- + 2\ CO + 2\ HF \quad \Delta_r H^\circ = -372 \text{ kJ mol}^{-1} \tag{9.54}$$

$$O_2^- + CH_2CF_2 \rightarrow e^- + 2\ HFCO \quad \Delta_r H^\circ = -360 \text{ kJ mol}^{-1} \tag{9.55}$$

$$O_2^- + C_2HF_3 \rightarrow F^- + CO_2 + CHF_2 \quad \Delta_r H^\circ = -340 \text{ kJ mol}^{-1} \tag{9.56}$$

$$O_2^- + C_2HF_3 \rightarrow F^- + HC(O)O + CF_2 \quad \Delta_r H^\circ = -24 \text{ kJ mol}^{-1} \tag{9.57}$$

$$O_2^- + C_2HF_3 \rightarrow F^- + FCO + HF + CO \quad \Delta_r H^\circ = -264 \text{ kJ mol}^{-1} \tag{9.58}$$

$$O_2^- + C_2HF_3 \rightarrow F^- + FCO + HFCO \quad \Delta_r H^\circ = -257 \text{ kJ mol}^{-1} \tag{9.59}$$

$$O_2^- + C_2HF_3 \rightarrow F^- + FCOCOF + H \quad \Delta_r H^\circ = -219 \text{ kJ mol}^{-1} \tag{9.60}$$

$$O_2^- + C_2F_4 \rightarrow e^- + CO + CF_3OF \quad \Delta_r H^\circ = -188 \text{ kJ mol}^{-1} \tag{9.61}$$

$$O_2^- + C_2F_4 \rightarrow e^- + CO_2 + CF_4 \quad \Delta_r H^\circ = -620 \text{ kJ mol}^{-1} \tag{9.62}$$

$$O_2^- + C_2F_4 \rightarrow e^- + FCO + CF_3O \quad \Delta_r H^\circ = -95 \text{ kJ mol}^{-1} \tag{9.63}$$

$$O_2^- + C_2F_4 \rightarrow F^- + CO_2 + CF_3 \quad \Delta_r H^\circ = -401 \text{ kJ mol}^{-1} \tag{9.64}$$

$$O_2^- + C_2F_4 \rightarrow F^- + CO + CF_3O \quad \Delta_r H^\circ = -283 \text{ kJ mol}^{-1} \tag{9.65}$$

$$O_2^- + C_2F_4 \rightarrow F^- + FCO + CF_2O \quad \Delta_r H^\circ = -352 \text{ kJ mol}^{-1} \tag{9.66}$$

$$O_2^- + C_2F_4 \rightarrow F^- + FCOCOF + F \quad \Delta_r H^\circ = -190 \text{ kJ mol}^{-1} \tag{9.67}$$

$$O_2^- + C_2F_4 \rightarrow F_2^- + CO_2 + CF_2 \quad \Delta_r H^\circ = -169 \text{ kJ mol}^{-1} \tag{9.68}$$

$$O_2^- + C_2F_4 \rightarrow F_2^- + FCOCOF \quad \Delta_r H^\circ = -322 \text{ kJ mol}^{-1} \tag{9.69}$$

$$O_2^- + C_2F_4 \rightarrow C_2F_4O^- + O \quad \Delta_r H^\circ = 956 + \Delta_f H^\circ(C_2F_4O^-) \text{ kJ mol}^{-1} \tag{9.70}$$

$$O_2^- + C_2F_4 \rightarrow FCO^- + CF_3O \quad \Delta_r H^\circ = -359 \text{ kJ mol}^{-1} \tag{9.71}$$

$$O_2^- + C_2F_4 \rightarrow FCO^- + CF_2O + F \quad \Delta_r H^\circ = -287 \text{ kJ mol}^{-1} \tag{9.72}$$

9.8 Conclusions

The gas-phase reactions of the anions OH^-, O^-, CF_3^-, F^- and O_2^- with the neutral ethenes C_2H_4, C_2H_3F, CH_2CF_2, C_2HF_3 and C_2F_4 have been investigated using the SIFT technique. The results are shown in Table 9.1. Arrow-pushing reaction mechanisms have been used to help explain the reaction products observed, and to attempt to assign neutral products. This type of analysis, however, has its limitations and many reactions have been observed where significant rearrangement and/or fragmentation of the reaction complex must occur. Using enthalpies of formation for the reactant and product species to calculate reaction enthalpy changes, a thorough account of the thermochemistry in this set of reactions is presented.

The reaction products are dictated by a combination of the properties of the reactant anion and the reactant neutral. For example, the reactions of C_2F_4 show a wide variety of products, many of which result from significant rearrangement and fragmentation of the reaction complex. However, this is not a property of C_2F_4 alone and it is only in the reactions with oxygen-containing anions where this is particularly evident. Another example is in the reactions with C_2HF_3 which show a preference for H^+ abstraction. This preference is also limited by the properties of the reactant anion, O_2^- for example, which is not basic enough to abstract a proton—even from C_2HF_3. The investigation into these reactions with C_2HF_3 has lead to the evaluation of a new value for $\Delta_f H^\circ$ ($C_2F_3^-$), -504 ± 20 kJ mol^{-1}.

Table 9.2 Proton affinities of the reactant anions

Anion	PA[a]/kJ mol^{-1}
OH^-	1,634
O^-	1,599
CF_3^-	1,592
F^-	1,560
O_2^-	1,486

[a] The proton affinity (PA), defined as the enthalpy change for the reaction $BH \rightarrow B^- + H^+$, where B^- is the anion in question. Therefore, the more positive the value, the higher the affinity B^- has for a proton. Values were calculated using enthalpies of formation listed in Appendix I

Electron ejection is observed in several reactions with the anions O^- and O_2^-, and attempts have been made to uncover the reaction mechanisms involved. It is most likely the radical properties of these two anions which are responsible for these interesting reactions.

A general trend can be uncovered when considering the proton affinity (PA) values of the reactant anions. The PAs for OH^-, O^-, CF_3^-, F^- and O_2^- are listed in Table 9.2. Generally speaking, the type of reaction observed correlates to the relative PAs of the reactant anion. The anion is more likely to act as a base (i.e. attack a hydrogen atom) the higher its proton affinity value. The majority of reactions with OH^- are thought to be initiated in this way (i.e. H^+ and HF abstraction reactions). With the exception of electron ejection, for which the mechanism is unknown, H_2^+ abstraction is a significant outcome in the reactions with O^-. By contrast, almost all of the reactions involving F^- or O_2^-, with a lower PA, are initiated by the anion acting as a nucleophile.

The rate coefficients for the reactions with F^- and O_2^- increase as the degree of fluorination in ethene increases. This trend has been rationalised by resonance and inductive effects influencing the initially formed adduct anion, following nucleophilic addition of the anion to the ethene molecule. There is no obvious trend for the reactions of OH^-, O^- and CF_3^-.

References

1. Sullivan SA, Beauchamp JL (1976) J Am Chem Soc 98:1160
2. Sullivan SA, Beauchamp JL (1977) J Am Chem Soc 99:5017
3. Parkes DA (1972) J Chem Soc Faraday Trans 68:613
4. Lindinger W, Albritton DL, Fehsenfeld FC, Ferguson EE (1975) J Chem Phys 63:3238
5. Viggiano AA, Paulson JF (1983) J Chem Phys 79:2241
6. Dawson J, Jennings KR (1976) J Chem Soc Faraday Trans 72:700
7. Bohme DK, Brewster Young L (1970) J Am Chem Soc 92:3301
8. Morris RA (1992) J Chem Phys 97:2372
9. Su T, Su A, Viggiano AA, Paulson JF (1987) J Phys Chem 91:3683

10. Kennedy RA, Mayhew CA, Peverall R, Watts P (2000) Phys Chem Chem Phys 2:3145
11. Simmonett AC, Wheeler SE, Schaefer HF (2004) J Phys Chem 108:1608
12. Lias SG, Bartmess JE, Liebman JF, Holmes JL, Levin RD, Mallard WG (1988) J Phys Chem Ref Data 17:1
13. Spyrou S, Sauers I, Christophorou LG (1983) J Chem Phys 78:7200
14. Harland PW, Thynne JCJ (1975) Int J Mass Spectrom 18:73
15. Lifshitz C, Grajower R (1972) Int J Mass Spectrom 10:25
16. Bauschlicher CW, Ricca A (2000) J Phys Chem A 104:4581
17. Rienstra-Kiracofe JC, Tschumper GS, Schaefer HF, Nandi S, Ellison B (2002) Chem Rev 102:231
18. Schleyer PVR, Kos A (1983) Tetrahedron 39:1141
19. Bach RD, Evans C (1986) J Am Chem Soc 108:1374
20. Roy M, McMahon TB (1985) Can J Chem 63:708
21. Rabasco JJ, Kass SR (1992) J Am Soc Mass Spectrom 3:91
22. Knorr R (2004) Chem Rev 104:3795
23. McDonald RN, Kasem Chowdhury A (1985) J Am Chem Soc 107:4123

Appendix I
Standard Enthalpies of Formation at 298 K of Gas-Phase Species Relevant to this Thesis[#]

a.m.u	Species	$\Delta_f H°_{298}$ (kJ mol^{-1})	Source(s)
Neutrals			
1	H	+217.99 ± 0.006	Ref. [1]
13	CH	+594.1 ± 17.5	Ref. [1]
14	CH_2	+386.4 ± 4.2	Ref. [1]
16	CH_4	−74.87 ± 0.34	Ref. [1]
16	O	+249.17 ± 0.10	Ref. [1]
17	OH	+38.99 ± 1.21	Ref. [1]
18	H_2O	−241.83 ± 0.04	Ref. [1]
19	F	+79.4 ± 0.3	Ref. [1]
20	HF	−272.5 ± 0.8	Ref. [1]
26	C_2H_2	+228 ± 1	Ref. [2]
28	CO	−110.5 ± 0.2	Ref. [1]
28	C_2H_4	+52.47 ± 0.29	Ref. [1]
30	C_2H_6	−84.0 ± 0.2	Ref. [2]
30	CH_2O	−115.90 ± 6.3	Ref. [1]
31	CF	+255.2 ± 8	Ref. [1]
32	CHF	+125.5 ± 29	Ref. [1]
33	HO_2	+2.09 ± 8.4	Ref. [1]
34	CH_3F	−247	Ref. [2]
35	OF	+109.9	Ref. [3]
35.5	Cl	+121.30 ± 0.01	Ref. [1]
44	C_3H_8	−104.5 ± 0.3	Ref. [2]
44	CO_2	−393.52 ± 0.05	Ref. [1]
44	C_2HF	+107	Ref. [2]
44	CH_2=CHOH	−125	Ref. [2]
44	CH_3CHO	−165.8 ± 0.4	Ref. [2]
44	*c*-$CH_2(O)CH_2$	−52.6 ± 0.6	Ref. [2]
45	HC(O)O	−132.98	Ref. [3]
46	C_2H_3F	−138.8 ± 1.7	Ref. [2]

(continued)

M. J. Simpson, *Two Studies in Gas-Phase Ion Spectroscopy*, Springer Theses,
DOI: 10.1007/978-3-642-23129-2, © Springer-Verlag Berlin Heidelberg 2012

(continued)

a.m.u	Species	$\Delta_f H°_{298}$ (kJ mol^{-1})	Source(s)
47	FCO	−171.5 ± 63	Ref. [1]
47.5	CCl	+502.1 ± 20	Ref. [1]
48	HFCO	−376.56	Ref. [1]
50	CF_2	−182 ± 6.3	Ref. [1]
50.5	CH_3Cl	−83.68	Ref. [1]
51	CHF_2	−237 ± 5	Ref. [2]
51	SF	+3.0	Ref. [4]
52	CH_2F_2	−450.66 ± 1.7	Ref. [1]
54.5	FCl	−50.292 ± 0.42	Ref. [1]
62	C_2F_2	+20.9 ± 21	Ref. [1]
64	$C_2H_2F_2$ (1,1)	−345 ± 10	Ref. [2]
64	$C_2H_2F_2$ (*Z* -1,2)	−297	Ref. [2]
64	$C_2H_2F_2$ (*E*-1,2)	−293	Ref. [2]
66	CF_2O	−638.9 ± 1.7	Ref. [1]
69	CF_3	−465.7 ± 2.1	Ref. [5]
70	CHF_3	−697.1 ± 3.3	Ref. [1]
70	SF_2	−295.2	Ref. [4]
78	CF_2CO	−290.3 ± 13.2	Ref. [6]
80	Br	+111.86 ± 0.06	Ref. [1]
82	C_2HF_3	−491 ± 8	Ref. [2]
83	CCl_2	+238.5 ± 21	Ref. [1]
85	CH_2Cl_2	−95.52	Ref. [1]
85	CF_3O	−630.56	Ref. [3]
88	CF_4	−933.2 ± 1.3	Ref. [1]
89	SF_3	−441.6	Ref. [4]
94	FCOCOF	−728	Ref. [2]
95	CH_3Br	−34.3 ± 0.8	Ref. [7]
97	CF_3CO	−608.68	Ref. [3]
98	CF_3CHO	−778.47	Ref. [3]
99	FBr	−58.463 ± 1.7	Ref. [1]
100	C_2F_4	−658.6 ± 2.9	Ref. [1]
101	CF_3OO	−635.02	Ref. [3]
104	CF_3OF	−785	Ref. [2]
104.5	CF_3Cl	−709.2 ± 3	Ref. [5]
108	SF_4	−768.4	Ref. [4]
119.5	$CHCl_3$	−103.18 ± 1.3	Ref. [1]
121	CF_2Cl_2	−491.6 ± 8	Ref. [1]
127	SF_5	−908	Ref. [1]
127	I	+106.76 ± 0.04	Ref. [1]
137.5	$CFCl_3$	−288.7 ± 6.3	Ref. [1]
138	C_2F_6	−1343	Ref. [2]
143.5	SF_4Cl	−761	Ref. [8]
146	SF_6	−1220.47 ± 0.8	Ref. [1]

(continued)

(continued)

a.m.u	Species	$\Delta_f H°_{298}$ (kJ mol^{-1})	Source(s)
146	FI	−94.76	Ref. [7]
149	CF_3Br	−649.8 ± 2	Ref. [5]
150	C_3F_6	−1125	Ref. [2]
154	CCl_4	−95.98 ± 2.1	Ref. [1]
162.5	SF_5Cl	−1038.9 ± 10.5	Ref. [1]
188	C_3F_8	−1783 ± 7	Ref. [2]
196	SF_5CF_3	−1717.1 ± 63	Ref. [1]
196	CF_3I	−586.2 ± 2	Ref. [5]
Cations			
1	H^+	+1536.25	Ref. [1]
13	CH^+	+1622	Ref. [2]
14	CH_2^+	+1386	Ref. [2]
15	CH_3^+	+1098	Ref. [2]
19	F^+	+1760.6	Ref. [1]
27	$C_2H_3^+$	+1112	Ref. [2]
28	$C_2H_4^+$	+1066	Ref. [2]
29	$C_2H_5^+$	+914 ± 4	Ref. [2]
31	CF^+	+1149.4 ± 5	Ref. [1]
33	CH_2F^+	+833	Ref. [2]
35.5	Cl^+	+1372.6	Ref. [1]
38	F_2^+	+1514	Ref. [7][a]
39	$C_3H_3^+$	+1179	Ref. [2]
43	n-$C_3H_7^+$	+881	Ref. [2]
45	$C_2H_2F^+$	+951	Ref. [2]
46	$C_2H_3F^+$	+861.1	Ref. [2]
47.5	CCl^+	+1311	Ref. [9]
49.5	CH_2Cl^+	+959	Ref. [2]
50	CF_2^+	+941.8 ± 12.6	Ref. [1]
51	CHF_2^+	+611	Ref. [2]
51	SF^+	+998.3	Ref. [4]
54.5	FCl^+	+1171 ± 2	Ref. [1, 7][b]
64	$C_2H_2F_2^+$ (1,1)	+648	Ref. [2]
64	$C_2H_2F_2^+$ (Z -1,2)	+690	Ref. [2]
64	$C_2H_2F_2^+$ (E-1,2)	+692	Ref. [2]
66.5	$CFCl^+$	+1101	Ref. [9]
69	CF_3^+	+406	Ref. [10]
70	SF_2^+	+693.4	Ref. [4]
80	Br^+	+1250.9	Ref. [1]
81	$C_2F_3^+$	+791	Ref. [2]
82	$C_2HF_3^+$	+487	Ref. [2]
83	CCl_2^+	+1163	Ref. [2]
84	$CHCl_2^+$	+887	Ref. [2]
85.5	CF_2Cl^+	+526	Ref. [11]
89	SF_3^+	+361.1	Ref. [4]
94	CH_2Br^+	+937	Ref. [2]

(continued)

(continued)

a.m.u	Species	$\Delta_f H°_{298}$ (kJ mol^{-1})	Source(s)
99	FBr^+	+1086 ± 2	Ref. [1, 7][c]
100	$C_2F_4^+$	+316	Ref. [2]
102	$CFCl_2^+$	+703	Ref. [2]
108	SF_4^+	+389.3	Ref. [4]
118.5	CCl_3^+	+831	Ref. [2]
119	$C_2F_5^+$	15.0	Ref. [12]
127	SF_5^+	+29	Ref. [13]
127	I^+	+1115.2	Ref. [1]
130	CF_2Br^+	≤ +570	Ref. [14]
138	$C_2F_6^+$	−99.9	Ref. [12]
146	FI^+	+922.1	Ref. [7][d]
143.5	SF_4Cl^+	≤ +327	Ref. [13]
169	$C_3F_7^+$	−358.1	Ref. [12]
177	CF_2I^+	≤ +598 ± 22	Ref. [15][e]
196	CF_3I^+	+414.5 ± 2	Ref. [5, 16][f]
Anions			
1	H^-	+145	Ref. [2]
13	CH^-	+477 ± 27	Ref. [2]
16	O^-	+101.85	Ref. [1]
17	OH^-	−143.6 ± 3.8	Ref. [1]
19	F^-	−248.7 ± 0.3	Refs. [1, 17][g]
26	$H_2C{=}C^-$	+385 ± 15	Ref. [7]
27	$C_2H_3^-$	+221 ± 9	Ref. [2]
31	CF^-	−63 ± 106	Refs. [1, 18][h]
32	O_2^-	−48.59	Ref. [1]
35.5	Cl^-	−227.27 ± 0.01	Refs. [1, 19][i]
37	$F^-{\cdot}H_2O$	−605.8	Ref. [7]
38	F_2^-	−301 ± 7	Ref. [20][j]
39	HF_2^-	−683 ± 11	Ref. [2]
43	$CH_2{=}CHO^-$	−165 ± 13	Ref. [2]
43	CH_3CO^-	−60 ± 11	Ref. [2]
44	$HFC{=}C^-$	+92 ± 21	Refs. [7, 21]
47	FCO^-	−435	Ref. [2]
50	CF_2^-	−199 ± 6	Refs. [1, 19][k]
51	SF^-	−224.4	Ref. [4]
62	$F_2C{=}C^-$	−75 ± 50	Refs. [7, 21]
69	CF_3^-	−641.3 ± 5.2	Refs. [5, 22][l]
70	Cl_2^-	−229.6 ± 9.7	Ref. [19][m]
70	SF_2^-	−431.7	Ref. [4]
80	Br^-	−212.68 ± 0.06	Refs. [1, 19][n]
81	$C_2F_3^-$	−504	Refs. [12, 19][o]
89	SF_3^-	−742.7	Ref. [4]

(continued)

(continued)

a.m.u	Species	$\Delta_f H°_{298}$ (kJ mol^{-1})	Source(s)
108	SF_4^-	−907.2	Ref. [4]
119	$C_2F_5^-$	−1067 ± 23	Ref. [2]
127	I^-	−188.39 ± 0.04	Refs. [1, 19][p]

[#] Note that Ref. [1] uses the thermal electron convertion for cations and anions, ref. [2] the stationary electron convertion. At 298 K, $\Delta_f H°_{298}$ (thermal) = $\Delta_f H°_{298}$ (stationary) ± 6.2 kJ mol^{-1}, where the positive sign refers to cations and the negative sign for anions

[a] This value is taken directly as the $IE(F_2)$, 15.697 ± 0.003 eV (Ref. [7])

[b] This value combines $\Delta_f H°_{298}(FCl) = -50.292 \pm 0.42$ kJ mol^{-1} from Ref. [1] with $IE(FCl)$ = 12.66 ± 0.01 eV (1221.5 kJ mol^{-1}) from Ref. [7]

[c] This value combines $\Delta_f H°_{298}$ (FBr) = −58.463 ± 1.7 kJ mol^{-1} from Ref. [1] with $IE(FBr)$ = 11.86 eV (1144.3 kJ mol^{-1}) from Ref. [7]

[d] This value uses $\Delta_f H°_{298}(FI) = -94.76$ kJ mol^{-1} and $IE(FI)$ = 10.54 eV (+1017 kJ mol^{-1}) from Ref. [7]

[e] This value is derived from the experimental appearance energy of F^- anions following photoexcitation of CF_3I. In addition to the reference provided, the derivation of this value can be found in Chap. 4

[f] This value combines $\Delta_f H°_{298}(CF_3I) = -586.2 \pm 2$ kJ mol^{-1} from Ref. [5] with $IE(CF_3I)$ = 83652 ± 2 cm^{-1} (10.37 eV or 1000.7 kJ mol^{-1}) from Ref. [16]

[g] The value of −248.7 ± 0.3 kJ mol^{-1} uses $\Delta_f H°_{298}(F)$ = +79.4 ± 0.3 kJ mol^{-1} from Ref. [1] and $EA(F)$ = +3.401 eV (+328.1 kJ mol^{-1}) from Ref. [17]

[h] This value uses $\Delta_f H°_{298}(CF)$ = +255.2 ± 8 kJ mol^{-1} from Ref. [1] and $EA(CF)$ = +3.3 ± 1.1 eV (+318 ± 106 kJ mol^{-1}) from Ref. [18]

[i] This value uses $\Delta_f H°_{298}(Cl)$ = +121.3 ± 0.01 kJ mol^{-1} from Ref. [1] and $EA(Cl)$ = +3.612724 ± 0.00003 eV (+348.57 ± 0.005 kJ mol^{-1}) from Ref. [19]

[j] The value of −301 kJ mol^{-1} is taken directly from the value for $EA(F_2)$, 3.12 ± 0.07 eV, reported in Ref. [20]

[k] The value of −199 ± 6 kJ mol^{-1} uses $\Delta_f H°_{298}(CF_2) = -182 \pm 6.3$ kJ mol^{-1} from Ref. [1] and $EA(CF_2)$ = +0.179 ± 0.005 eV (+17.3 kJ mol^{-1}) from Ref. [19]

[l] The value of −641.3 ± 5.2 kJ mol^{-1} uses $\Delta_f H°_{298}(CF_3) = -465.7 \pm 2.1$ kJ mol^{-1} from Ref. [5] and $EA(CF_3)$ = +1.82 ± 0.05 eV (+175.6 ± 4.8 kJ mol^{-1}) from Ref. [22]

[m] Taken directly from the value for $EA(Cl_2)$, 2.38 ± 0.10 eV, reported in Ref. [19]

[n] This value uses $\Delta_f H°_{298}(Br)$ = +111.86 ± 0.06 kJ mol^{-1} from Ref. [1] and $EA(Br)$ = +3.363588 ± 0.000006 eV (+324.54 ± 0.0006 kJ mol^{-1}) from Ref. [19]

[o] This value uses $\Delta_f H°(C_2F_3) = -224$ kJ mol^{-1} from Ref. [12] and $EA(C_2F_3)$ = 2.90 eV (+280 kJ mol^{-1}) from Ref. [19]. Both values were chosen from a range of available data based on experimental results from proton abstraction reaction with C_2HF_3 (see Chap. 9)

[p] This value uses $\Delta_f H°_{298}(I)$ = +106.76 ± 0.04 kJ mol^{-1} from Ref. [1] and $EA(I)$ = +3.059038 ± 0.00001 eV (+295.15 ± 0.001 kJ mol^{-1}) from Ref. [19]

Appendix II
Cross Sections for Anion Production Following Vacuum Ultraviolet Photoexcitation of Gas-Phase Molecules which have not yet been Analysed in Detail

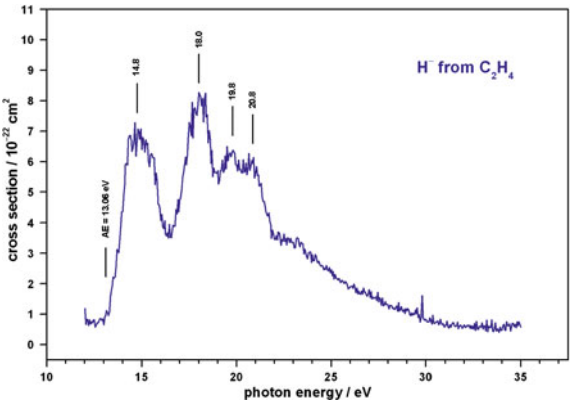

A.II.(1) H^- detected following the unimolecular photodissociation of C_2H_4. The scan was recorded on beamline 3.1 at the Daresbury SRS in April 2008, with a wavelength resolution of 6 Å and a step size of 0.05 eV. The appearance energy (*AE*) was determined from a different scan, recording the onset region with better statistics: a wavelength resolution of 2 Å and a step size of 0.02 eV. The *solid lines* and corresponding numbers show energy positions of features in the spectrum

M. J. Simpson, *Two Studies in Gas-Phase Ion Spectroscopy*, Springer Theses,
DOI: 10.1007/978-3-642-23129-2, © Springer-Verlag Berlin Heidelberg 2012

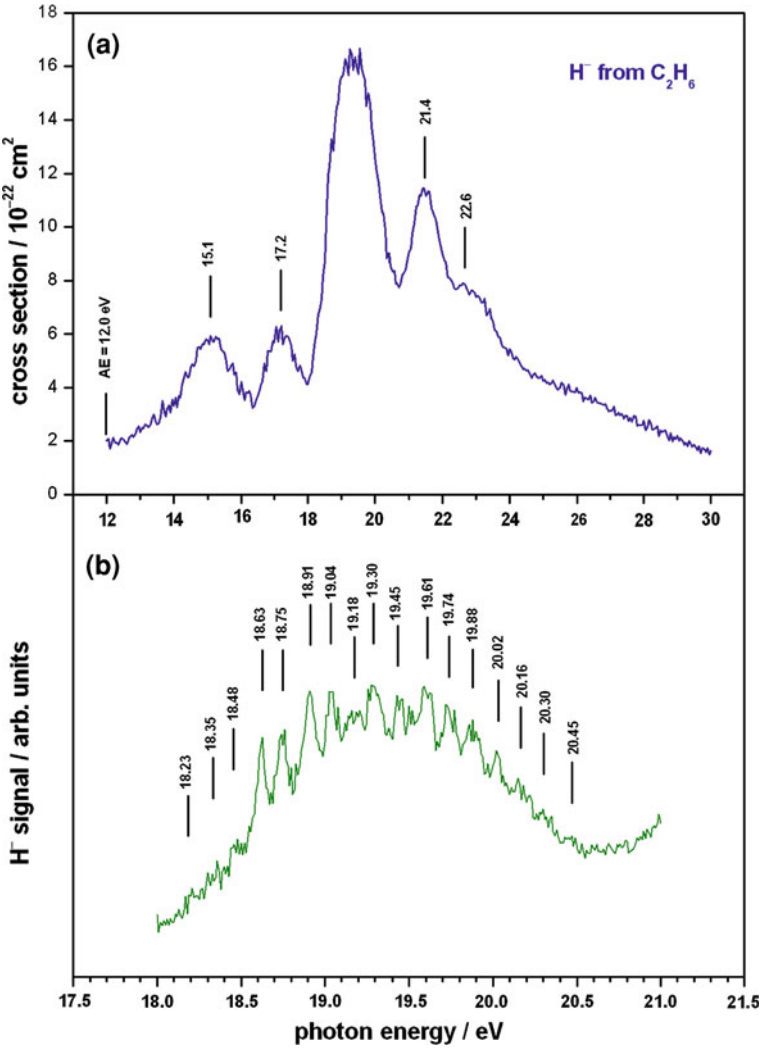

A.II.(2) Data recorded on beamline 3.1 at the Daresbury SRS in June 2008 for H^- detected following the unimolecular photodissociation of C_2H_6: **a** in the photon energy range 12–30 eV with a step size of 0.05 eV and a wavelength resolution of 6 Å; **b** in the range 18–21 eV with a step size of 0.01 eV and a wavelength resolution of 1.2 Å. The appearance energy (*AE*) was determined from a different scan, not shown here, recording the onset region with a wavelength resolution of 3 Å and a step size of 0.02 eV. The *solid lines* and corresponding numbers show energy positions of features in the spectra

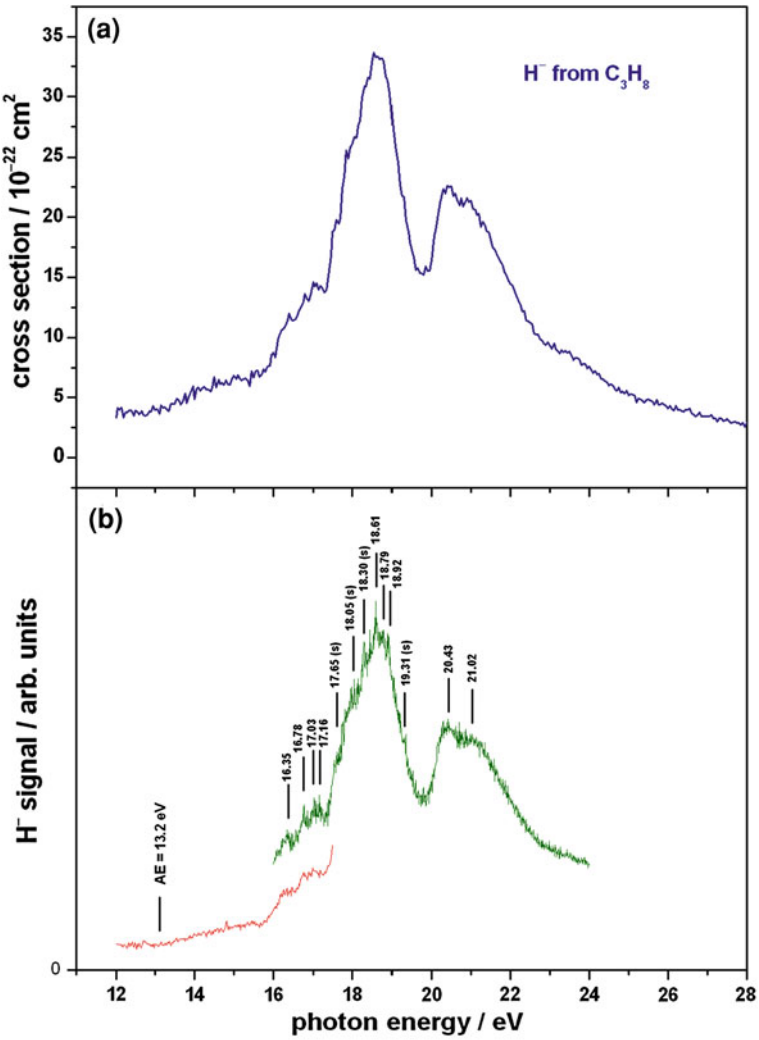

A.II.(3) H^- detected following the unimolecular photodissociation of C_3H_8: **a** in the photon energy range 12–28 eV with a step size of 0.05 eV and a wavelength resolution of 6 Å; **b** two separate scans covering the 12–24 eV range with better statistics, from 12–17.5 eV recorded with a step size of 0.02 eV and a wavelength resolution of 2 Å, and from 16–24 eV recorded with a step size of 0.01 eV and a wavelength resolution of 1.2 Å. The data were recorded on beamline 3.1 at the Daresbury SRS in May 2008. The appearance energy (*AE*) is indicated and *solid lines* (with corresponding numbers) show energy positions of features in the spectra, where '(s)' indicates a shoulder feature

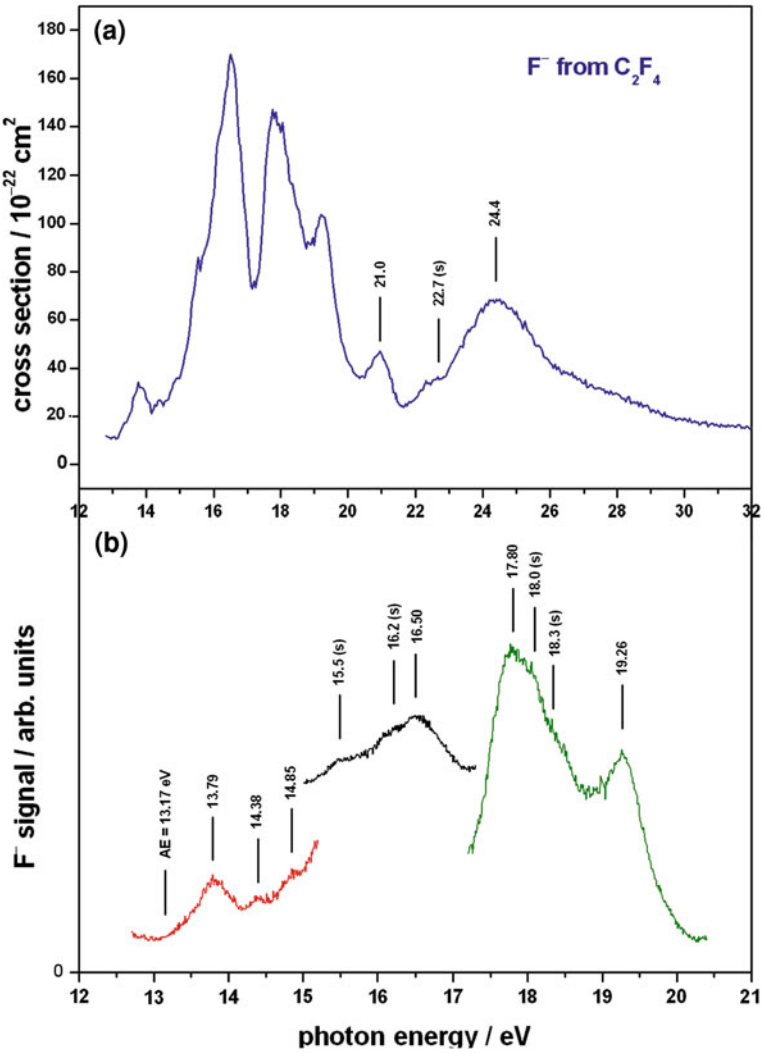

A.II.(4) F^- detected following the unimolecular photodissociation of C_2F_4: **a** in the photon energy range 13–32 eV with a step size of 0.05 eV and a wavelength resolution of 6 Å; **b** three separate scans covering the 12.7–20.4 eV range with better statistics, all with a step size of 0.01 eV and a wavelength resolution of 2 Å. The data for C_2F_4 were recorded on beamline 3.1 at the Daresbury SRS in May 2008. The appearance energy (*AE*) is indicated and *solid lines* (with corresponding numbers) show energy positions of features in the spectra, where '(s)' indicates a shoulder feature

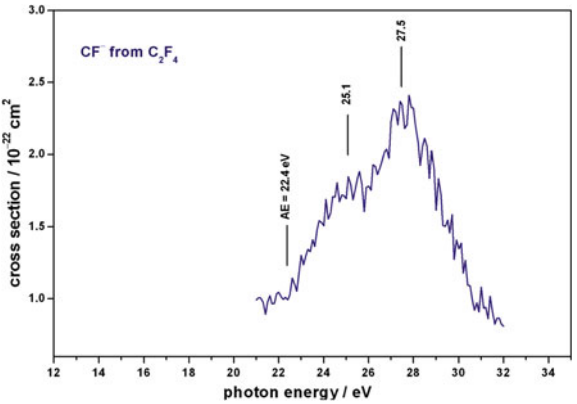

A.II.(5) CF^- detected following the unimolecular photodissociation of C_2F_4 in the photon energy range 21–32 eV with a step size of 0.1 eV and a wavelength resolution of 6 Å. Only background signal was observed from 12–21 eV, and only the 21–32 eV range was scanned to minimise data acquisition time due to the weak CF^- signal

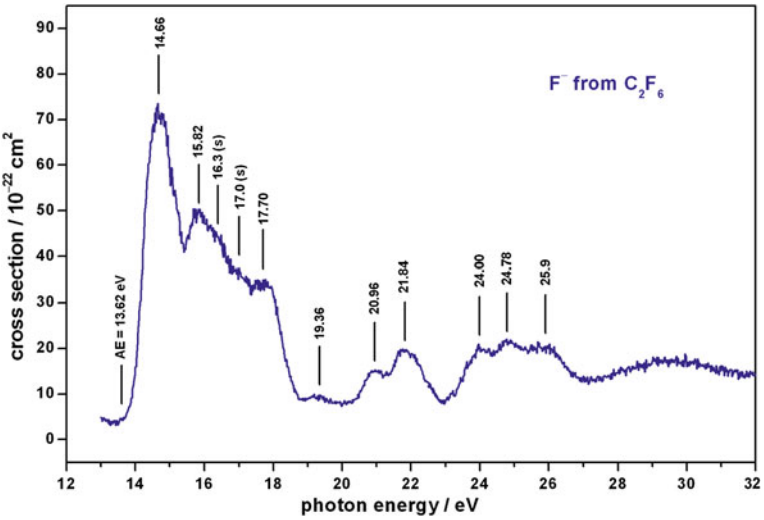

A.II.(6) F^- detected following the unimolecular photodissociation of C_2F_6 in the photon energy range 13–32 eV with a step size of 0.02 eV and a wavelength resolution of 2 Å. This scan was recorded on beamline 3.1 at the Daresbury SRS in May 2008. The appearance energy (*AE*) is indicated and *solid lines* (with corresponding numbers) show energy positions of features in the spectrum, where '(s)' indicates a shoulder feature

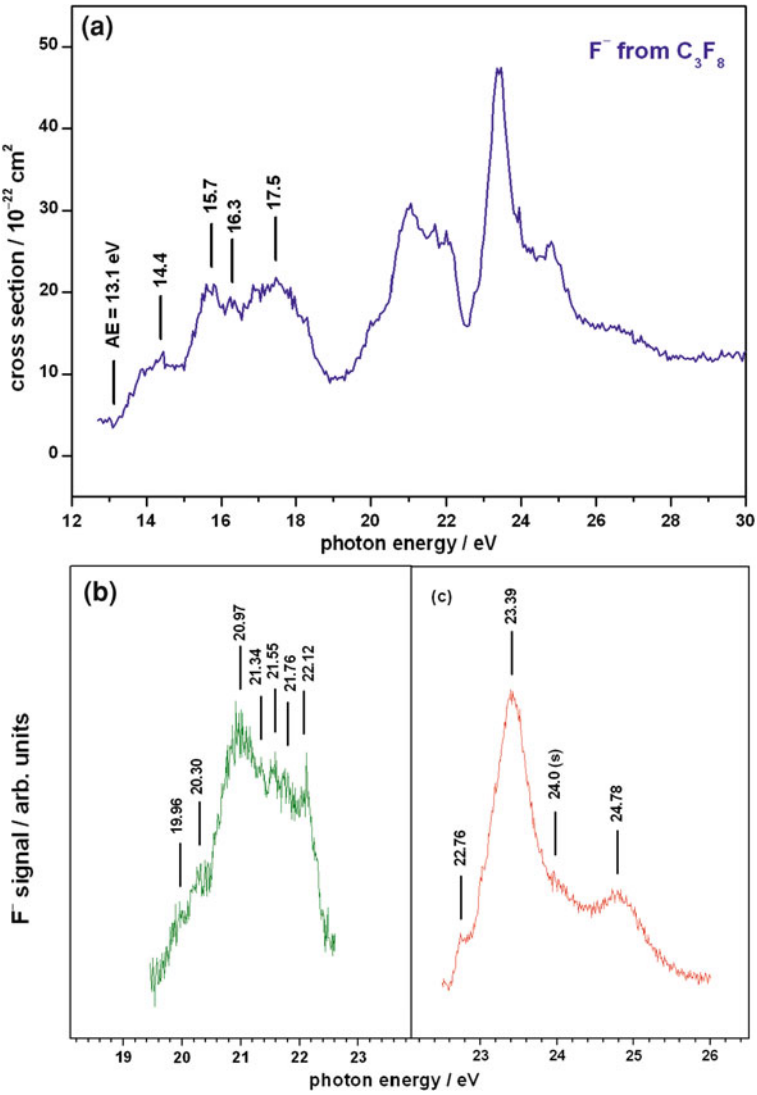

A.II.(7) F^- detected following the unimolecular photodissociation of C_3F_8: **a** in the photon energy range 12.7–30 eV with a step size of 0.05 eV and a wavelength resolution of 6 Å; **b** covering the 19.5–22.5 eV range with better statistics, using a step size of 0.01 eV and a wavelength resolution of 1.2 Å, **c** covering the 22.5–26 eV range with better statistics, using a step size of 0.01 eV and a wavelength resolution of 1.2 Å. The data for C_3F_8 were recorded on beamline 3.1 at the Daresbury SRS in May 2008. The appearance energy (*AE*) is indicated and *solid lines* (with corresponding numbers) show energy positions of features in the spectra, where '(s)' indicates a shoulder feature

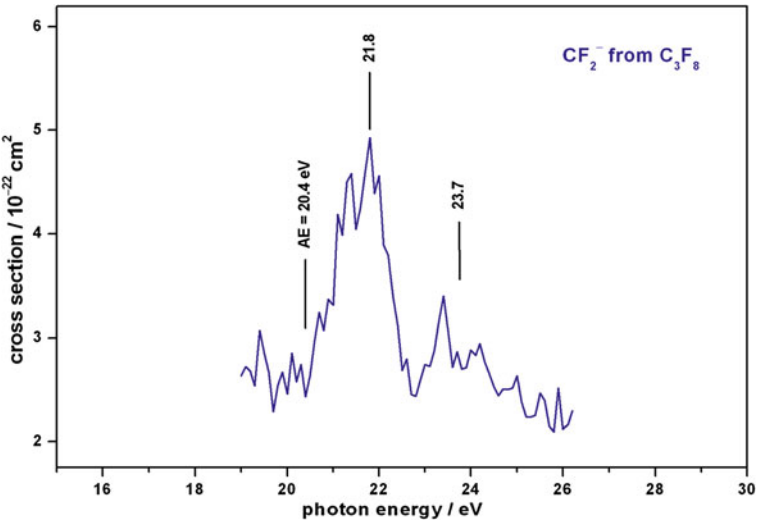

A.II.(8) CF_2^- detected following the unimolecular photodissociation of C_3F_8 in the photon energy range 19–26 eV with a step size of 0.1 eV and a wavelength resolution of 6 Å. Only background signal was observed from 12–19, and from 26–35 eV, and only the 19–26 eV range was scanned to minimise data acquisition time due to the weak signal

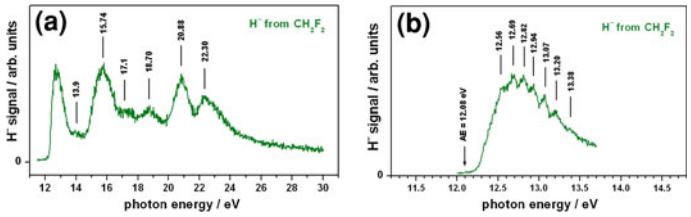

A.II.(9) Ion yields for anions observed following the photoexcitation of CH_2F_2. All scans were recorded on beamline 3.2 at the Daresbury SRS in July 2007. **a** H^- ion yield in the photon energy range 11.5−30.0 eV recorded with a step size of 0.02 eV and a wavelength resolution of 2 Å. Due to the *zero blast* effect in the quadrupole mass spectrometer, the ion signal detected at *m/z* 1 (i.e. H^-) may also contain contributions from other ions present (i.e. F^- and F_2^-). Thus, an absolute cross section cannot be determined for the H^- spectra and it is possible that the observed features do not result exclusively from H^- anions. **b** A separate H^- scan covering the 12.0–13.7 eV region with better statistics: a step size of 0.005 eV and a wavelength resolution of 1 Å. It should be noted that a similar scan of the feature at 12.56 eV in the F^- spectrum was structureless and did *not* reproduce that in (b) for H^-. **c** F^- cross section in the photon energy range 11.5–30.0 eV recorded with a step size of 0.02 eV and a wavelength resolution of 2 Å. **d** F_2^- cross section in the photon energy range 16.5–25.5 eV recorded with a step size of 0.02 eV and a wavelength resolution of 2 Å. The appearance energies (*AE*) are indicated and *solid lines* (with corresponding numbers) show energy positions of features in the spectra, where '(s)' indicates a shoulder feature

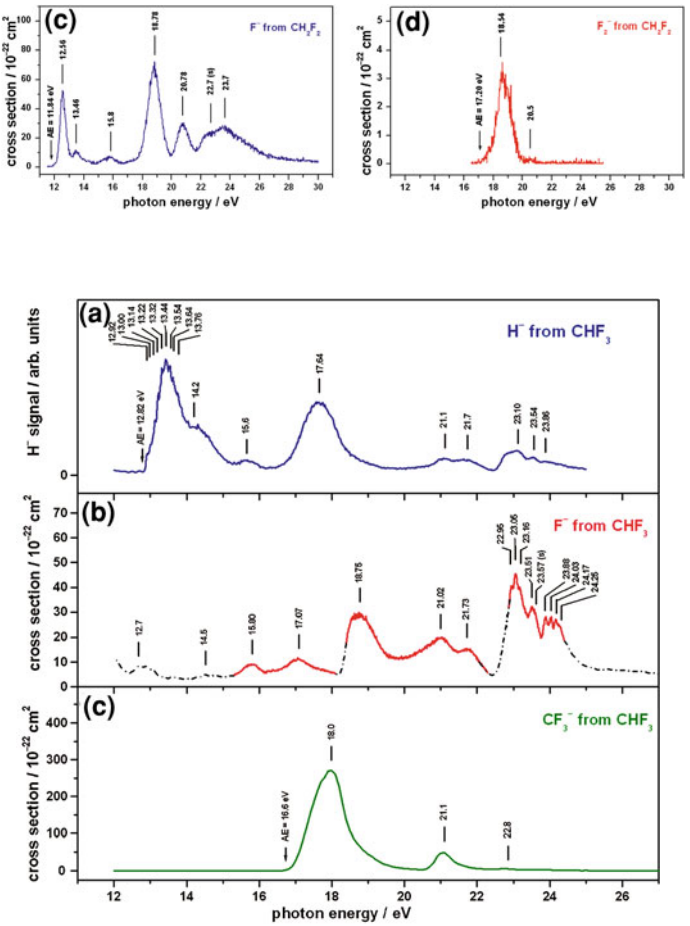

A.II.(10) Ion yields for anions observed following the photoexcitation of CHF_3. All scans were recorded on beamline 3.1 at the Daresbury SRS in April 2007. The appearance energies (*AE*) are indicated (where possible) and *solid lines* (with corresponding numbers) show energy positions of features in the spectra, where '(s)' indicates a shoulder feature. **a** H^- ion yield in the photon energy range 12–25 eV recorded with a step size of 0.02 eV and a wavelength resolution of 3 Å. Due to the *zero blast* effect in the quadrupole mass spectrometer, the ion signal detected at *m/z* 1 (i.e. H^-) may also contain contributions from other ions present (i.e. F^- and F_2^-). Thus, an absolute cross section cannot be determined for the H^- spectra and it is possible that the observed features do not result exclusively from H^- anions. **b** F^- cross section in the photon energy range 12–25 eV constructed by merging four different scans: the *dotted line* is from a scan recorded with a step size of 0.1 eV and a wavelength resolution of 6 Å; the *solid line* from 15.3–18.1 eV was recorded with a step size of 0.01 eV and a wavelength resolution of 2 Å; the *solid line* from 18.4–22.3 eV was recorded with a step size of 0.01 eV and a wavelength resolution of 1.6 Å; the *solid line* from 22.86–24.40 eV was recorded with a step size of 0.005 eV and a wavelength resolution of 1.2 Å. The rise in signal at $h\nu < 12.4$ eV is suspected to arise from second order radiation, and a separate scan from 8–11.8 eV, using a LiF window, showed only background signal. **c** CF_3^- cross section in the photon energy range 12–27 eV recorded with a step size of 0.1 eV and a wavelength resolution of 6 Å

A.II.(11) Ion yields for anions observed following the photoexcitation of CH_2Cl_2. All scans were recorded on beamline 3.2 at the Daresbury SRS in July 2007. **a** H^- ion yield in the photon energy range 11.5–30.0 eV recorded with a step size of 0.02 eV and a wavelength resolution of 2 Å. Due to the *zero blast* effect in the quadrupole mass spectrometer, the ion signal detected at *m/z* 1 (i.e. H^-) may also contain contributions from other ions present (i.e. Cl^- and Cl_2^-). Thus, an absolute cross section cannot be determined for the H^- spectrum and it is possible that the observed features do not result exclusively from H^- anions. **b** Cl^- cross section from 9–30 eV recorded with a step size of 0.02 eV and a wavelength resolution of 2 Å. **c** A separate Cl^- scan, covering the 9.0–12.5 eV region with better statistics: a step size of 0.01 eV and a wavelength resolution of 2 Å. **d** Cl_2^- cross section in the photon energy range 12.5–18.0 eV recorded with a step size of 0.02 eV and a wavelength resolution of 2 Å. A separate scan from 18–30 eV showed only background signal, and is not included here. The appearance energies (*AE*) are indicated and *solid lines* (with corresponding numbers) show energy positions of features in the spectra, where '(s)' indicates a shoulder feature

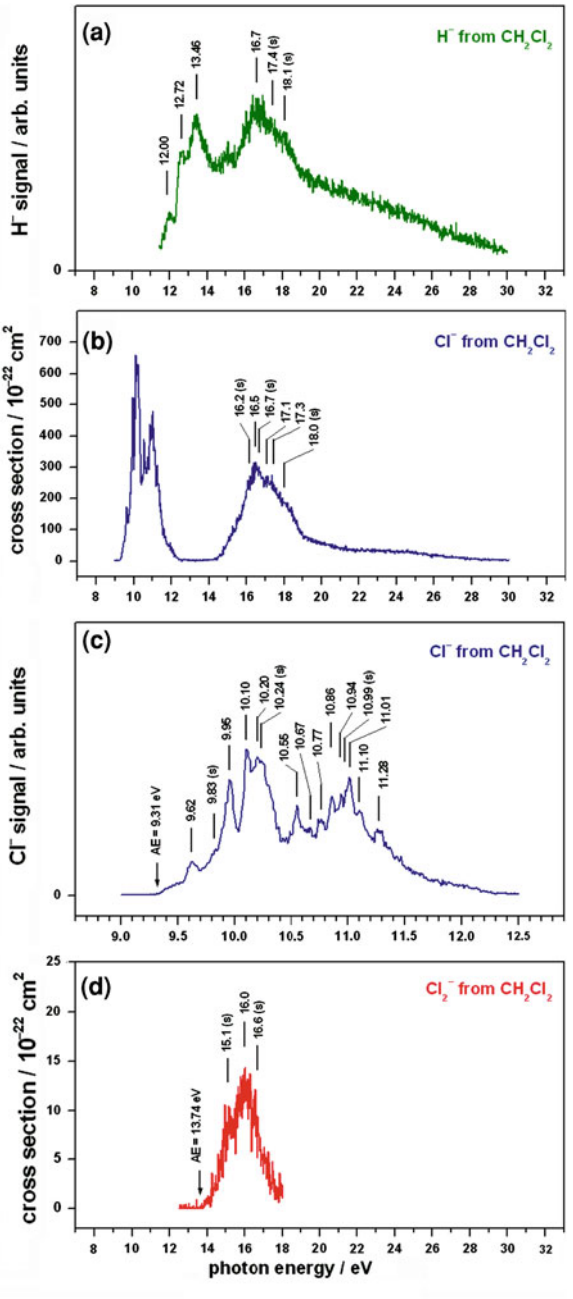

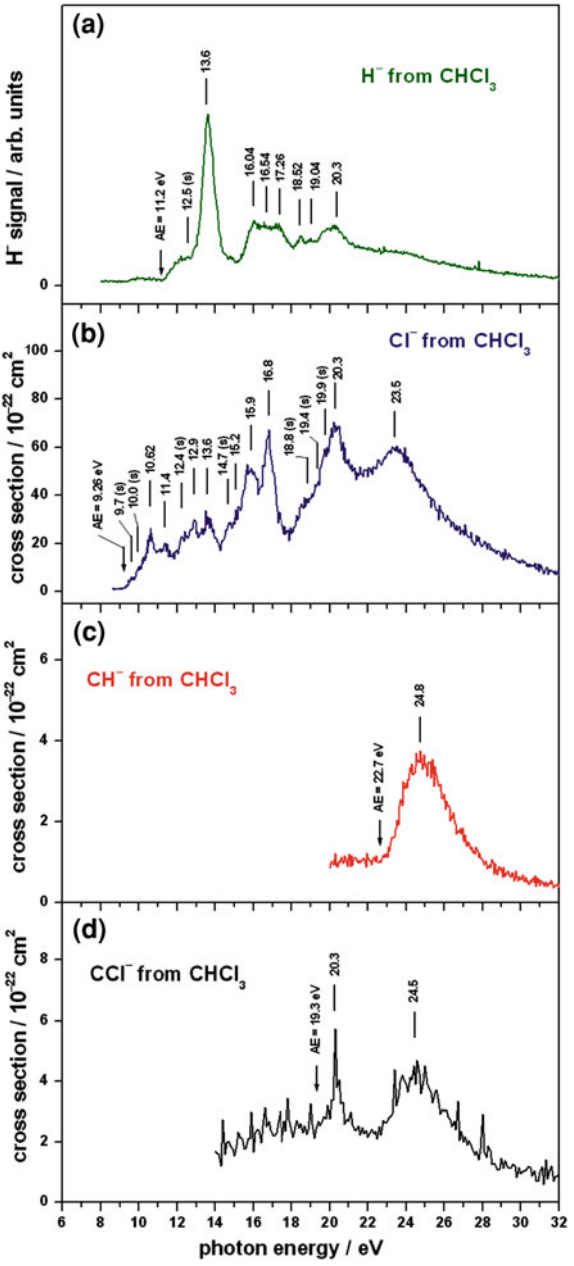
(a)
H⁻ from CHCl3
H⁻ signal / arb. units
AE = 11.2 eV
12.5 (e)
13.6
16.04
16.54
17.26
18.52
19.04
20.3
(b)
Cl⁻ from CHCl3
cross section / 10⁻²² cm²
AE = 9.26 eV
9.7 (e)
10.0 (e)
10.62
11.4
12.4 (e)
12.9
13.6
14.7 (e)
15.2
15.9
16.8
18.8 (e)
19.4 (e)
19.9 (e)
20.3
23.5
(c)
CH⁻ from CHCl3
cross section / 10⁻²² cm²
AE = 22.7 eV
24.8
(d)
CCl⁻ from CHCl3
cross section / 10⁻²² cm²
AE = 19.3 eV
20.3
24.5
photon energy / eV

◀ **A.II.(12)** Ion yields for anions observed following the photoexcitation of $CHCl_3$. All scans were recorded on beamline 3.1 at the Daresbury SRS in April 2008. **a** Three separate scans have been merged to generate the H^- ion yield: from 8–15 eV with a step size of 0.05 eV and a wavelength resolution of 6 Å; 15–19.5 eV with a step size of 0.02 eV and a wavelength resolution of 2 Å; 19.5–32 eV with a step size of 0.05 eV and a wavelength resolution of 6 Å. Due to the *zero blast* effect in the quadrupole mass spectrometer, the ion signal detected at *m/z* 1 (i.e. H^-) may also contain contributions from other ions present (e.g. Cl^-). Thus, an absolute cross section cannot be determined for the H^- spectrum and it is possible that the observed features do not result exclusively from H^- anions. **b** Cl^- cross section from 8–32 eV generated by merging three separate scans: from 8.60–10.64 eV with a step size of 0.02 eV and a wavelength resolution of 4 Å; 10.65–16.80 eV with a step size of 0.05 eV and a wavelength resolution of 6 Å; 16.85–32.00 eV with a step size of 0.05 eV and a wavelength resolution of 6 Å. **c** CH^- cross section in the photon energy range 20–32 eV recorded with a step size of 0.05 eV and a wavelength resolution of 6 Å. **d** CCl^- cross section in the photon energy range 14–32 eV recorded with a step size of 0.1 eV and a wavelength resolution of 6 Å. The appearance energies (*AE*) are indicated and *solid lines* (with corresponding numbers) show energy positions of features in the spectra, where '(s)' indicates a shoulder feature. *Note added after submission of thesis*: the ion yield of Cl^- from $CHCl_3$ has very recently been published by Chen et al. (J. Phys. Chem. A., (2011) 115:4248. Their spectrum shows little resemblance to that we observe in (b). Furthermore, Chen et al. do not report observation of H^-, CH^- or CCl^-

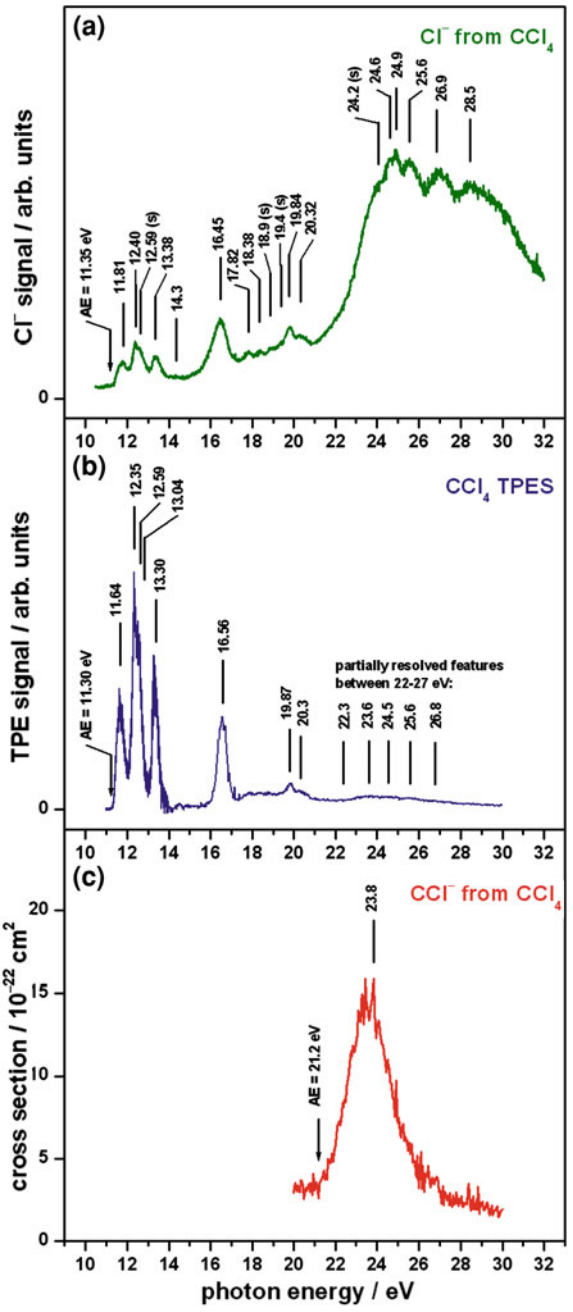

A.II.(13) Ion yields for anions observed following the photoexcitation of CCl_4. **a** Three separate scans have been merged to generate the Cl^- ion yield: from 10.5–17.2 eV with a step size of 0.01 eV and a wavelength resolution of 2 Å; 17.2–22.0 eV with a step size of 0.02 eV and a wavelength resolution of 2 Å; 22–32 eV with a step size of 0.02 eV and a wavelength resolution of 2 Å. The Cl^- signal at 16.45 *and* 24.9 eV was shown to increase non-linearly with increasing gas pressure and an absolute cross section cannot be determined; the formation of Cl^- is dominated by the dissociative electron attachment to CCl_4. **b** CCl_4 threshold photoelectron spectrum (TPES) included to compare with the Cl^- ion yield (shown with permission from J. N. Harvey, R. P. Tuckett, N. J. Rogers and A. Bodi, unpublished data recorded in 2009 at the Swiss Light Source). **c** CCl^- ion-pair formation cross section in the photon energy range 20–32 eV recorded with a step size of 0.05 eV and a wavelength resolution of 6 Å. The appearance energies (*AE*) are indicated and *solid lines* (with corresponding numbers) show energy positions of features in the spectra, where '(s)' indicates a shoulder feature

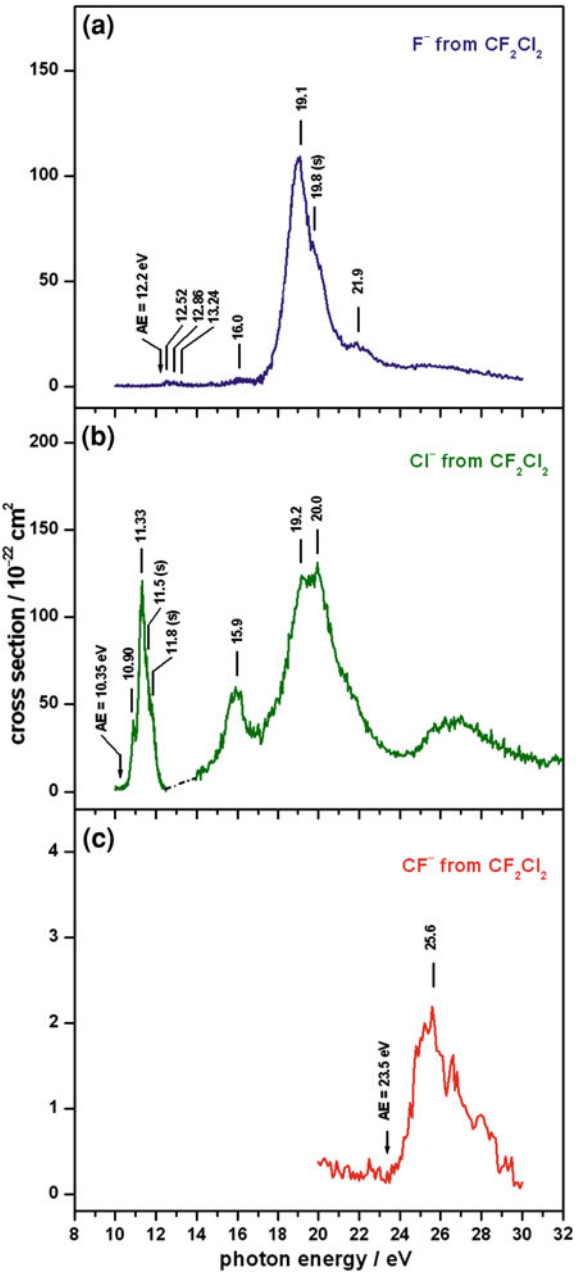

A.II.(14) Ion yields for anions observed following the photoexcitation of CF_2Cl_2. **a** Two scans are merged to generate the F^- ion-pair cross section: from 10.0–17.7 eV recorded with a step size of 0.02 eV and a wavelength resolution of 2 Å; from 17.7–30.0 eV recorded with a step size of 0.05 eV and a wavelength resolution of 6 Å. **b** Two separate scans, put on the same absolute scale, forming the Cl^- cross section: from 10.0–12.5 eV recorded with a step size of 0.01 eV and a wavelength resolution of 2 Å; from 13.9–32.0 eV recorded with a step size of 0.05 eV and a wavelength resolution of 6 Å. **c** CF^- ion-pair formation cross section in the photon energy range 20–30 eV recorded with a step size of 0.1 eV and a wavelength resolution of 6 Å. The appearance energies (*AE*) are indicated and *solid lines* (with corresponding numbers) show energy positions of features in the spectra, where '(s)' indicates a shoulder feature

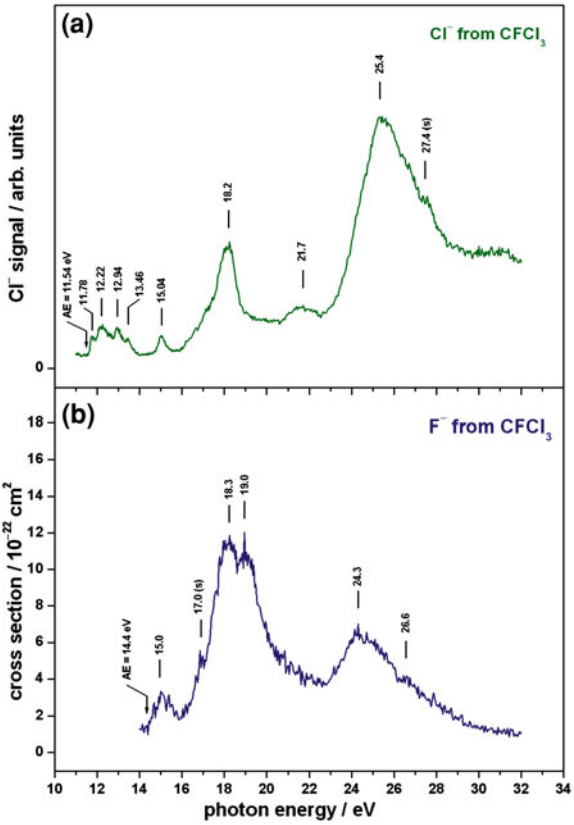

A.II.(15) Ion yields for anions observed following the photoexcitation of $CFCl_3$. **a** Two scans are merged to generate the Cl^- ion yield 11–16 eV recorded with a step size of 0.02 eV and a wavelength resolution of 3 Å, and from 16–32 eV recorded with a step size of 0.05 eV and a wavelength resolution of 6 Å. The Cl^- signal at 12.2, 18.2, 21.7 *and* 25.4 eV was shown to increase non-linearly with increasing gas pressure and an absolute cross section cannot be determined; electron attachment processes are significant in the formation of Cl^- from $CFCl_3$. **b** F^- ion-pair cross section from 14–32 eV recorded with a step size of 0.05 eV and a wavelength resolution of 6 Å

Appendix III: Bond Dissociation Energies of Cations, D^{o+}, and Neutral Polyatomic Molecules, D^{o}, at 298 K

Cation	$D^{o+}_{therm.}$ [a] / eV	$D^{o+}_{expt.}$ [b] / eV	Neutral	$D^{o}_{lit.}$ [c] / eV
H – $C_2H_3^+$	2.7 ± 0.3	≤(3.3 ± 0.2)	H – C_2H_3	4.81 ± 0.03
H – $C_2H_5^+$	1.1 ± 0.1	≤(1.2 ± 0.2)	H – C_2H_5	4.36 ± 0.01
H – $C_3H_7^+$	1.6 ± 0.4	≤(3.1 ± 0.3)	H – C_3H_7	4.38 ± 0.02
H – CH_3^+	1.8 ± 0.2	≤(1.4 ± 0.1)	H – CH_3	4.553 ± 0.004
H – CH_2F^+	0.9 ± 0.4	–[d]	H – CH_2F	4.39 ± 0.04
H – CH_2Cl^+	1.8 ± 0.4	–[d]	H – CH_2Cl	4.34 ± 0.02
H – CH_2Br^+	1.8 ± 0.4	≤(2.3 ± 0.2)	H – CH_2Br	4.43 ± 0.02
H – CHF_2^+	0.4 ± 0.3	≤(0.1 ± 0.1)	H – CHF_2	4.48 ± 0.04
H – $CHCl_2^+$	1.1 ± 0.4	≤(0.9 ± 0.2)	H – $CHCl_2$	4.15 ± 0.02
H – CF_3^+	−0.1 ± 0.4	≤(−0.2 ± 0.2)	H – CF_3	4.61 ± 0.03
H – CCl_3^+	0.7 ± 0.3	≤(0.7 ± 0.3)	H – CCl_3	4.07 ± 0.03
F – CH_3^+	2.1 ± 0.3	≤(3.2 ± 0.1)	F – CH_3	4.77 ± 0.09
F – CH_2F^+	1.4 ± 0.2	≤(2.5 ± 0.1)	F – CH_2F	5.14 ± 0.09
F – CHF_2^+	0.6 ± 0.3	≤(2.0 ± 0.4)	F – CHF_2	5.53 ± 0.06
F – $CFCl_2^+$	1.5 ± 0.2	≤(3.9 ± 0.1)	F – $CFCl_2$	5.00 ± 0.11
F – CF_2Cl^+	1.2 ± 0.3	–[e]	F – CF_2Cl	5.30
F – CF_2Br^+	2.0 ± 0.3	–[e]	F – CF_2Br	5.09[h]
F – CF_2I^+	2.7 ± 0.2 [g]	≤(2.7 ± 0.2)	F – CF_2I	5.40[h]
F – CF_3^+	−0.7 ± 0.3	≤(1.0 ± 0.3)	F – CF_3	5.67 ± 0.02
F – CCl_3^+	0.9 ± 0.2	–[e]	F – CCl_3	4.55 ± 0.04
F – SF_5^+	−1.4 ± 0.3	≤ (1.0 ± 0.2)	F – SF_5	4.06
F – SF_4Cl^+	2.7 ± 0.3	–[e]	F – SF_4Cl	3.70[j]
F – $SF_4CF_3^+$	?	–[e]	F – SF_4CF_3	?
F – $C_2F_3^+$	5.7 ± 0.2	≤(6.5 ± 0.1)	F – C_2F_3	5.66 ± 0.13
F – $C_2F_5^+$	1.5 ± 0.3	≤(3.6 ± 0.2)	F – C_2F_5	5.52 ± 0.07
F – $C_3F_7^+$	2.6 ± 0.3	≤(3.5 ± 0.3)	F – C_3F_7	6.15
Cl – CH_3^+	2.2 ± 0.2	≤(2.4 ± 0.1)	Cl – CH_3	3.63 ± 0.02
Cl – CH_2Cl^+	0.9 ± 0.2	≤(1.6 ± 0.1)	Cl – CH_2Cl	3.50 ± 0.03

(continued)

M. J. Simpson, *Two Studies in Gas-Phase Ion Spectroscopy*, Springer Theses,
DOI: 10.1007/978-3-642-23129-2, © Springer-Verlag Berlin Heidelberg 2012

(continued)

Cation	$D^{o+}_{therm.}$ [a] / eV	$D^{o+}_{expt.}$ [b] / eV	Neutral	$D^{o}_{lit.}$ [c] / eV
$Cl - CHCl_2^+$	0.2 ± 0.2	≤(1.6 ± 0.1)	$Cl - CHCl_2$	3.22 ± 0.02
$Cl - CFCl_2^+$	0.0 ± 0.2	–[f]	$Cl - CFCl_2$	3.33 ± 0.09
$Cl - CF_2Cl^+$	0.1 ± 0.2	≤(2.2 ± 0.1)	$Cl - CF_2Cl$	3.46 ± 0.11
$Cl - CF_3^+$	0.4 ± 0.3	–[e]	$Cl - CF_3$	3.79 ± 0.04
$Cl - CCl_3^+$	−0.4 ± 0.2	–[f]	$Cl - CCl_3$	3.07
$Cl - SF_5^+$	0.0 ± 0.2	≤(1.9 ± 0.3)	$Cl - SF_5$	2.54
$Br - CH_3^+$	2.3 ± 0.1	≤(2.3 ± 0.1)	$Br - CH_3$	3.05 ± 0.02
$Br - CF_3^+$	0.6 ± 0.1	–[e]	$Br - CF_3$	3.07 ± 0.01
$I - CF_3^+$	1.0 ± 0.1	≤(1.5 ± 0.2)	$I - CF_3$	2.35 ± 0.01
$H_2FC - H^+$	5.4 ± 0.2	≤(5.9 ± 0.3)	$H_2FC - H$	4.39 ± 0.04
$H_2ClC - H^+$	6.7 ± 0.2	≤(6.6 ± 0.3)	$H_2ClC - H$	4.34 ± 0.02
$H_2BrC - H^+$	7.5 ± 0.2	≤(7.3 ± 0.3)	$H_2BrC - H$	4.43 ± 0.02
$F_3C - H^+$	4.5 ± 0.1	≤(4.6 ± 0.3)	$F_3C - H$	4.61 ± 0.03
$F_3C - Cl^+$	4.4 ± 0.1	≤(4.9 ± 0.3)	$F_3C - Cl$	3.79 ± 0.04
$F_3C - Br^+$	3.4 ± 0.1	≤(3.9 ± 0.3)	$F_3C - Br$	3.07 ± 0.01
$F_3C - I^+$	2.4 ± 0.1	≤(2.4 ± 0.3)	$F_3C - I$	2.35 ± 0.01
$F_5S - F^+$	6.3 ± 0.3	–[f]	$F_5S - F$	4.06
$F_5S - CF_3^+$	−0.4 ± 0.4	–[f]	$F_5S - CF_3$	3.86 ± 0.45[k]
$F_5S - Cl^+$	3.0 ± 0.3	–[f]	$F_5S - Cl$	2.54[j]

Note that this version of Appendix III is updated from that published in my Ph.D. thesis. I am grateful to Professor Richard Tuckett for his help in expanding this Table. The version shown here is taken from Ref. [23]

[a] Thermochemical ionic bond dissociation energy at 298 K (D^{o+}_{therm}) for the bond shown in the first column. This value is calculated from the equation $D^{o+}_{therm} = \Delta_r H°_{298} - IE(ABC) + EA(A)$, where $\Delta_r H°_{298}$ is the enthalpy change for the reaction $ABC \rightarrow A^- + BC^+$, *IE* is an ionisation energy and *EA* an electron affinity. $\Delta_r H°_{298}$ and *IE* values are included in Table 10. The *EA* values for H, F, Cl, Br and I are 0.754, 3.401, 3.613 eV, 3.364 and 3.059 eV, respectively [19]

[b] Experimental ionic bond dissociation energy at 298 K (D^{o+}_{expt}) for the bond shown in the first column. This value is calculated from $D^{o+}_{expt} \leq AE(A^-) - IE(ABC) + EA(A)$, where *AE* is the appearance energy of A^- detected from the reaction $ABC \rightarrow A^- + BC^+$, *IE* is an ionisation energy and *EA* an electron affinity. The *AE* and *IE* values are included in Chap. 6, Table 6.1

[c] Neutral bond dissociation energy at 298 K for the bond shown in the fourth column, data from Ref. [24]

[d] Experimental data not available because an accurate value for $AE(H^-)$ could not be obtained in either case due to the zero-blast effect [25]

[e] Experimental data not available because ion-pair formation involves production of a neutral species in addition to the anion–cation pair

[f] Experimental data not available because production of the the anion is probably dominated by dissociative electron attachment, and not by ion-pair formation

[g] Assumes F^- turns on at the thermochemical threshold for $CF_3I \rightarrow F^- + CF_2I^+$ (see Chap. 4)

[h] Not quoted in Ref. [24]. Calculated from $\Delta_r H^o_{298}$ for the neutral dissociation reaction $ABC \rightarrow A + BC$. Data for $\Delta_f H^o_{298}$ of CF_2Br and CF_2I radicals are indirect values taken from Refs. [26, 27]

[j] Not quoted in Ref. [24]. Calculated from $\Delta_r H^o_{298}$ for the neutral dissociation reaction $ABC \rightarrow A + BC$. Data for $\Delta_f H^o_{298}$ of SF_4Cl and SF_5 radicals are taken from Ref. [13]

[k] Value at 0 K [28]

Appendix IV: Measuring the Neutral Reactant Concentration in a Selected Ion Flow Tube Experiment

The neutral reactant gas, B, is passed through a capillary prior to it entering the flow tube. The flow of B through the capillary is viscous, and the corresponding flow rate of B can therefore be determined by applying Poiseulle's law:

$$Q_B = \frac{\pi a^4}{8\eta_{He} L} p_c \Delta p \qquad \text{(A.IV.(1))}$$

where Q_B is the flow rate of reactant gas B in units of Pa m^3 s^{-1}, a and L are the radius and length of the capillary in m, respectively, η_{He} is the viscosity of helium in Pa s, p_c is the pressure in Pa at the centre of the capillary, and Δp is the pressure drop across the capillary, in Pa. The pressure into the capillary, p_{in}, and Δp are measured directly by transducers, and so p_c can be calculated as follows:

$$p_c = p_{in} - \frac{\Delta p}{2} \qquad \text{(A.IV.(2))}$$

Different gases have different viscosities, which is taken into account by dividing the flow rate, Q_B, by the ratio of the viscosity of B with that of helium. This viscosity ratio is defined as η_r. After passing through the capillary the reactant B enters the flow tube and will be diluted, so the fraction of the bulk gas in the flow tube which reactant B contributes must be calculated. Q_B is therefore divided by the helium carrier gas flow rate, Q_{He}, as measured by a flowmeter. Thus, the amount of B as a fraction of the total bulk gas in the flow tube is given by:

$$\frac{Q_B}{\eta_r Q_{He}} \cdot \frac{293.2}{T_B} \qquad \text{(A.IV.(3))}$$

where T_B is the absolute temperature of reactant gas B, and 293.2 is the absolute temperature at which the flowmeter measuring Q_{He} is calibrated. Essentially, Q_B is divided by T_B and Q_{He} is divided by 293.2, allowing for temperature normalisation.

Using the ideal gas law, 1 Pa of gas pressure at 273.2 K is shown to be equivalent to 2.651×10^{14} molecules cm^{-3}. Knowing the pressure in the flow

M. J. Simpson, *Two Studies in Gas-Phase Ion Spectroscopy*, Springer Theses,
DOI: 10.1007/978-3-642-23129-2, © Springer-Verlag Berlin Heidelberg 2012

tube, p_{tube}, and adding an additional temperature normalisation term, the absolute concentration in molecules cm^{-3}, $[B]$, can be calculated:

$$[B] = \frac{Q_B}{\eta_r Q_{He}} \cdot \frac{293.2}{T_B} \cdot 2.651 \times 10^{14} \cdot p_{tube} \cdot \frac{273.2}{T_{tube}} \qquad \text{(A.IV.(4))}$$

Appendix V: Results Obtained from the Reactions of Cations (not Described in Chaps. 7 and 8) with the Fluorinated Ethenes using a Selected Ion Flow Tube at 298 K

Cation[a]	C_2H_3F[b]	CH_2CF_2[b]	C_2HF_3[b]
Ne^+ (21.56)	$k_{exp} = 2.2 \times 10^{-9}$	$k_{exp} = 2.0 \times 10^{-9}$	$k_{exp} = 2.0 \times 10^{-9}$
		$k_c = 2.2 \times 10^{-9}$	$k_c = 2.0 \times 10^{-9}$
	$k_c = 2.3 \times 10^{-9}$	CF^+ (34%)	CF^+ (60%)
		C_2HF^+ (25%)	$C_2HF_2^+$ (13%)
	$C_2H_2^+$ (60%)	$C_2H_2^+$ (18%)	CF_2^+ (11%)
	C_2HF^+ (13%)	CH_2^+ (13%)	C_2HF^+ (7%)
	$C_2H_3^+$ (11%)	$C_2H_2F^+$ (8%)	CHF^+ (7%)
	CF^+ (4%)	CF_2^+ (2%)	CHF_2^+ (1%)
	CHF^+ (4%)		C_2F^+ (1%)
	$C_2H_2F^+$ (3%)		
	$C_2H_3F^+$ (2%)		
	C_2H^+ (2%)		
	CH_2F^+ (1%)		
F^+ (17.42)	No data collected	$k_{exp} = 2.4 \times 10^{-9}$	$k_{exp} = 2.5 \times 10^{-9}$
		$k_c = 2.3 \times 10^{-9}$	$k_c = 2.1 \times 10^{-9}$
		$C_2H_2F^+$ (45%)	Products not identified
		CH_2F^+ (28%)	
		CF^+ (18%)	
		$C_2HF_2^+$ (5%)	
		$C_2H_2F_2^+$ (4%)	
Ar^+ (15.76)	$k_{exp} = 1.8 \times 10^{-9}$	$k_{exp} = 1.8 \times 10^{-9}$	$k_{exp} = 1.6 \times 10^{-9}$
	$k_c = 1.9 \times 10^{-9}$	$k_c = 1.8 \times 10^{-9}$	$k_c = 1.6 \times 10^{-9}$
	$C_2H_3^+$ (57%)	$C_2H_2F^+$ (44%)	CHF_2^+ (51%)
	$C_2H_2F^+$ (18%)	CH_2F^+ (22%)	CHF^+ (20%)
	$C_2H_2^+$ (12%)	C_2HF^+ (19%)	$C_2HF_2^+$ (13%)
	C_2HF^+ (7%)	CF^+ (12%)	CF^+ (8%)
	CF^+ (5%)	$C_2H_2F_2^+$ (3%)	$C_2HF_3^+$ (4%)
	$C_2H_3F^+$ (1%)		$C_2F_2^+$ (4%)

(continued)

M. J. Simpson, *Two Studies in Gas-Phase Ion Spectroscopy*, Springer Theses,
DOI: 10.1007/978-3-642-23129-2, © Springer-Verlag Berlin Heidelberg 2012

(continued)

Cation[a]	C_2H_3F[b]	CH_2CF_2[b]	C_2HF_3[b]
N_2^+ (15.58)	$k_{exp} = 1.7 \times 10^{-9}$ $k_c = 2.1 \times 10^{-9}$ $C_2H_3^+$ (40%) $C_2H_2F^+$ (29%) $C_2H_2^+$ (15%) C_2HF^+ (12%) $C_2H_3F^+$ (4%)	$k_{exp} = 2.0 \times 10^{-9}$ $k_c = 2.0 \times 10^{-9}$ $C_2H_2F^+$ (33%) CH_2F^+ (28%) C_2HF^+ (20%) CF^+ (11%) $C_2H_2F_2^+$ (8%)	$k_{exp} = 1.8 \times 10^{-9}$ $k_c = 1.8 \times 10^{-9}$ CHF_2^+ (66%) CF^+ (16%) CHF^+ (12%) $C_2HF_3^+$ (6%)
N^+ (14.53)	$k_{exp} = 1.8 \times 10^{-9}$ $k_c = 1.9 \times 10^{-9}$ $C_2H_3F^+$ (52%) $C_2H_2F^+$ (21%) $C_2H_3^+$ (20%) C_2HF^+ (6%) $C_2H_2^+$ (1%)	$k_{exp} = 2.4 \times 10^{-9}$ $k_c = 2.6 \times 10^{-9}$ $C_2H_2F_2^+$ (82%) $C_2H_2F^+$ (16%) C_2HF^+ (2%)	$k_{exp} = 2.3 \times 10^{-9}$ $k_c = 2.3 \times 10^{-9}$ $C_2HF_3^+$ (100%)
CO^+ (14.01)	$k_{exp} = 2.2 \times 10^{-9}$ $k_c = 2.1 \times 10^{-9}$ $C_2H_3F^+$ (39%) $C_2H_2^+$ (27%) $C_2H_2F^+$ (16%) $C_2H_3^+$ (16%) C_2HF^+ (2%)	$k_{exp} = 2.2 \times 10^{-9}$ $k_c = 2.0 \times 10^{-9}$ $C_2H_2F_2^+$ (84%) $C_2H_2F^+$ (16%)	$k_{exp} = 1.8 \times 10^{-9}$ $k_c = 1.8 \times 10^{-9}$ CHF_2^+ (50%) $C_2HF_3^+$ (41%) CF^+ (9%)
Kr^+ (14.00)	$k_{exp} = 1.6 \times 10^{-9}$ $k_c = 1.6 \times 10^{-9}$ $C_2H_3F^+$ (39%) $C_2H_2^+$ (25%) $C_2H_2F^+$ (23%) C_2HF^+ (7%) $C_2H_3^+$ (6%)	$k_{exp} = 1.2 \times 10^{-9}$ $k_c = 1.4 \times 10^{-9}$ Products not identified	$k_{exp} = 1.2 \times 10^{-9}$ $k_c = 1.3 \times 10^{-9}$ $C_2HF_3^+$ (86%) CHF_2^+ (14%)
CO_2^+ (13.76)	$k_{exp} = 1.9 \times 10^{-9}$ $k_c = 1.8 \times 10^{-9}$ $C_2H_3F^+$ (90%) $C_2H_2^+$ (9%) $C_2H_3^+$ (1%)	$k_{exp} = 1.4 \times 10^{-9}$ $k_c = 1.7 \times 10^{-9}$ $C_2H_2F_2^+$ (100%)	$k_{exp} = 1.2 \times 10^{-9}$ $k_c = 1.5 \times 10^{-9}$ $C_2HF_3^+$ (100%)
O^+ (13.62)	$k_{exp} = 2.5 \times 10^{-9}$ $k_c = 2.5 \times 10^{-9}$ $C_2H_3F^+$ (100%)	$k_{exp} = 2.0 \times 10^{-9}$ $k_c = 2.4 \times 10^{-9}$ Products not identified	k_{exp} not measured $k_c = 2.2 \times 10^{-9}$ $C_2HF_3^+$ (100%)
OH^+ (13.25)	$k_{exp} = 2.4 \times 10^{-9}$ $k_c = 2.5 \times 10^{-9}$ Products not identified	No data collected	$k_{exp} = 2.2 \times 10^{-9}$ $k_c = 2.2 \times 10^{-9}$ Products not identified
N_2O^+ (12.89)	$k_{exp} = 1.5 \times 10^{-9}$ $k_c = 1.8 \times 10^{-9}$ $C_2H_3F^+$ (100%)	$k_{exp} = 1.4 \times 10^{-9}$ $k_c = 1.7 \times 10^{-9}$ $C_2H_2F_2^+$ (100%)	$k_{exp} = 1.1 \times 10^{-9}$ $k_c = 1.5 \times 10^{-9}$ $C_2HF_3^+$ (100%)
H_2O^+ (12.62)	$k_{exp} = 2.4 \times 10^{-9}$ $k_c = 2.4 \times 10^{-9}$ Products not identified	No data collected	$k_{exp} = 2.0 \times 10^{-9}$ $k_c = 2.1 \times 10^{-9}$ Products not identified

(continued)

(continued)

Cation[a]	C_2H_3F[b]	CH_2CF_2[b]	C_2HF_3[b]
Xe^+ (12.13)	$k_{exp} = 1.4 \times 10^{-9}$ $k_c = 1.5 \times 10^{-9}$ $C_2H_3F^+$ (100%)	$k_{exp} = 8.0 \times 10^{-10}$ $k_c = 1.3 \times 10^{-9}$ $C_2H_2F_2^+$ (100%)	$k_{exp} = 8.0 \times 10^{-10}$ $k_c = 1.1 \times 10^{-9}$ $C_2HF_3^+$ (100%)
O_2^+ (12.07)	$k_{exp} = 2.1 \times 10^{-9}$ $k_c = 2.0 \times 10^{-9}$ $C_2H_3F^+$ (100%)	$k_{exp} = 1.8 \times 10^{-9}$ $k_c = 1.9 \times 10^{-9}$ $C_2H_2F_2^+$ (100%)	$k_{exp} = 1.9 \times 10^{-9}$ $k_c = 1.7 \times 10^{-9}$ $C_2HF_3^+$ (100%)
SF_4^+ (11.99)	$k_{exp} = 1.1 \times 10^{-9}$ $k_c = 1.5 \times 10^{-9}$ Products not identified	$k_{exp} = 1.5 \times 10^{-9}$ $k_c = 1.4 \times 10^{-9}$ $C_2H_2F_2^+$ (100%) or $CHSF^+$	$k_{exp} = 1.2 \times 10^{-9}$ $k_c = 1.2 \times 10^{-9}$ $C_2HF_3^+$ (100%)
SF^+ (10.31)	$k_{exp} = 1.6 \times 10^{-9}$ $k_c = 1.8 \times 10^{-9}$ Products not identified	$k_{exp} = 1.4 \times 10^{-9}$ $k_c = 1.6 \times 10^{-9}$ CH_2SF^+ (80%)[c] or 2° $C_2H_3F_2^+$ $C_2H_2F_2^+$ (20%) or $CHSF^+$	$k_{exp} = 1.4 \times 10^{-9}$ $k_c = 1.4 \times 10^{-9}$ $C_2HF_3^+$ (100%)
SF_2^+ (10.24)	No reaction	No reaction	No reaction
SF_5^+ (9.78)	$k_{exp} = 6.4 \times 10^{-10}$ $k_c = 1.5 \times 10^{-9}$ Products not identified	$k_{exp} = 1.0 \times 10^{-10}$ $k_c = 1.3 \times 10^{-9}$ SF_3^+ (53%) $C_2H_2F_3^+$ (32%) or $CHSF_2^+$ $C_2H_2F_2^+$ (15%) or $CHSF^+$	No reaction
NO^+ (9.26)	No reaction	No reaction	No reaction
SF_3^+ (8.32)	No reaction	No reaction	No reaction
H_3O^+ (6.27)	$k_{exp} = 2.3 \times 10^{-9}$ $k_c = 2.4 \times 10^{-9}$ $[C_2H_3F + H]^+$ (100%)	$k_{exp} = 2.3 \times 10^{-9}$ $k_c = 2.3 \times 10^{-9}$ $[C_2H_2F_2 + H]^+$ (100%)	No data collected

[a] Reactant cation and the value, in eV, of its recombination energy (*RE*). For example, the *RE* of A^+ is defined as the ionisation energy of neutral A. All values are taken from the NIST Chemistry Database: webbook.nist.gov/chemistry/, Ref. [7]

[b] The results include the product cation species, their branching ratios in %, and the experimental reaction rate coefficient, k_{exp}. In addition, values for the calculated collisional rate coefficient, k_c, are also included. All values for k are in cm^3 $molecule^{-1}$ s^{-1}

[c] *m/z* 65 detected which could be a primary product CH_2SF^+, or a secondary product $C_2H_3F^+$. If *m/z* 65 is actually a secondary product then the branching ratio for *m/z* 64 ($C_2H_2F_2^+$ or $CHSF^+$) will be 100%

References

1. Chase MW (1998) J Phys Chem Ref Data Monogr 9:1
2. Lias SG, Bartmess JE, Liebman JF, Holmes JL, Levin RD, Mallard WG (1988) J Phys Chem Ref Data 17:1
3. Janoschek R, Rossi M (2004) Int J Chem Kinet 36:661
4. Bauschlicher CW, Ricca A (1998) J Phys Chem A 102:4722
5. Ruscic B, Michael J, Redfern P, Curtiss L, Raghavachari K (1998) J Phys Chem A 102:10889
6. Dawson DF, Holmes JL (1999) J Phys Chem A 103:5217
7. NIST Chemistry webbook. http://webbook.nist.gov/chemistry/
8. Braun M et al (2006) Int J Mass Spectrom 252:234
9. Schenk H, Oertel H, Baumgärtel H (1979) Ber Bunsenges Phys Chem 83:683
10. Garcia GA, Guyon PM, Powis I (2001) J Phys Chem A 105:8296
11. Creasey JC, Smith DM, Tuckett RP, Yoxall KR (1996) J Phys Chem 100:4350
12. Bauschlicher CW, Ricca A (2000) J Phys Chem A 104:4581
13. Chim RYL, Cicman P, Märk TD, Mayhew CA, Scheier P, Tuckett RP (2007) Int J Mass Spectrom 261:208
14. Seccombe DP, Tuckett RP, Fisher BO (2001) J Chem Phys 114:4074
15. Simpson MJ, Tuckett RP, Dunn KF, Hunniford CA, Latimer CJ (2009) J Chem Phys 130:194302
16. Macleod NA, Wang S, Hennessy J, Ridley T, Lawley KP, Donovan RJ (1998) J Chem Soc Faraday Trans 94:2689
17. Blondel C, Delsart C, Goldfarb F (2001) J Phys B At Mol Opt Phys 34:L281
18. Thynne JCJ, MacNeil KAG (1970) Int J Mass Spectrom Ion Phys 5:329
19. Rienstra-Kiracofe JC, Tschumper GS, Schaefer HF, Nandi S, Ellison B (2002) Chem Rev 102:231
20. Artau A, Nizzi KE, Hill BT, Sunderlin LS, Wenthold PG (2000) J Amer Chem Soc 122:10667
21. Heni M, Illenberger E (1986) J Elec Spec Relat Phen 41:453
22. Deyerl H-J, Alconcel L, Continetti R (2001) J Phys Chem A 105:552
23. Simpson MJ, Tuckett RP (2011) Int Rev Phys Chem 30:197
24. Lide DR (2008) Handbook of chemistry and physics, 88th edn. CRC Press, Boca Raton
25. Dawson PH (1995) Quadrupole mass spectrometry and its applications. American vacuum society Classics. American Institute of Physics, New York
26. Bilde M, Sehested J, Mogelberg TE, Wallington TJ, Nielsen OJ (1996) J Phys Chem 100:7050
27. Gilles MK, Turnipseed AA, Talukdar RK, Rudich Y, Villalta PW, Huey LG, Burkholder JB, Ravishankara AR (1996) J Phys Chem 100:14005
28. Tuckett RP (2006) Adv Fluor Sci 1:89